Strategies towards the design and realisation of amide-derived porous organic cages

Andrew Marsh

Department of Chemistry

Supervisors: Prof. Andrew Cooper,

Dr Rebecca Greenaway

Thesis submitted in accordance with the requirements of the University of Liverpool for the degree of Doctor of Philosophy

June 2022

For my Grandma

Table of Contents

Acknowledgements

First, I want to extend huge thanks to Prof. Andy Cooper for the opportunity to study for my PhD in his group. Enormous thanks go to Dr Becky Greenaway, without who's guidance, support, and friendship I know I would not be in this position today. I've been fortunate enough to meet a number of fantastic people during my time in the group, but particular thanks go to Dr Michael Briggs for his early stewardship on my project, Mike Brand for his friendship and assistance on more lab techniques than I can count, Nicola Rankin for her continued friendship and support, and Rob Clowes for his equipment knowledge and technical wizardry.

It's lucky enough to work with great people, but it's luckier still to gain so many friends. To you all: Rach, Duncan, Cath, Mike, Nicola, Rich, Ben, Megan, and a huge list of names I am clearly forgetting as I write this — thank you. Whilst this time has no doubt been one of the more stressful and, at times, painful experiences in my life, it is without a doubt also one of the most gratifying, laugh-filled, joyful times I could wish to experience. This is in no small part due to you all. Your humour, friendship, guidance, and support has meant the world to me. Massive thanks as well go to the extended families of the Greenaway and Jelfs group, whose members I must thank for their help and support during the latter stages of my studies.

To my mum and dad, thank you for your love, constant encouragement, and belief in me — I am eternally grateful. To my family, thank you all for your support over the period I've been studying — I finally have a new answer for "where are you up to now then?". Someone I wish I could share this with is my grandma, who sadly passed away before its completion. While I feel the pain of her loss every day, she remains with me always; this is for her.

Last, but by no means least, thank you to my wonderful girlfriend Sarah. Your love and unwavering support have kept me aloft throughout this entire PhD, but especially during recent times. Words cannot adequately express my gratitude for everything you do, I could not have done this without you.

Abstract

Porous organic cages (POCs) are a class of materials favoured for their discrete nature, solution processability, and inherent porosity. The most popular synthetic route for making POCs rely on dynamic covalent chemistry (DCvC), allowing for error-correction, higher yields, and more straightforward synthesis. However, the POCs formed can often have issues with stability due to the reversible nature of bonding. An ideal POC would incorporate the robustness of irreversible bond-formation, with the syntheses of DCvC. This thesis outlines efforts to form amide-derived cages, with the aim to impart improved stability and robustness into POCs. Initially, studies focused on the use of transamidation, optimising reaction conditions to access dynamic transamidation for a model system. These conditions were then applied in the attempted synthesis of small amide cages. Following this, attempts were made to oxidise existing **CC** (covalent cage) series cages using a known method for imine oxidation. It was hoped that this could potentially be applied to quickly form a new family of amide-derived POCs. Finally, amide-functionalised precursors were used in the formation of new POCs using social self-sorting. These Janus cages contained regions of amide and imine bonding and were based on the prototypical cage **CC3**.

Abbreviations

BET – Brunauer-Emmett-Teller

DCvC – Dynamic covalent chemistry

COSY – Correlated spectroscopy

GC – Gas chromatography

GPC – Gel permeation chromatography

HPLC – High-performance liquid chromatography

IR – Infrared

LC – Liquid chromatography

MS – Mass spectrometry

MW – Microwave

MWR – Microwave reactor

NMR – Nuclear magnetic resonance

Prep-HPLC – Preparative high-performance liquid chromatography

PXRD – Powder X-ray diffraction

QTOF– Quadrupole time-of-flight

rt – Room temperature

SA – Surface area

SCXRD – Single crystal X-ray diffraction

TGA – Thermogravimetric analysis

TSE – Twin-screw extrusion

UPLC – Ultra-performance liquid chromatography

Chemical Abbreviations

Boc – *tert*-Butoxycarbonyl

CC – Covalent cage

COF – Covalent organic framework

CHDA – *trans*-1,2-Cyclohexyldiamine

DBA – 3,5-Dibromobenzoic acid

DCM – Dichloromethane

DMSO – Dimethylsulfoxide

DPT – *N,N'*-diphenylterephthalamide

EDA – 1,2-Ethylenediamine

MeOH – Methanol

m-CPBA - *meta*-Chloroperoxybenzoic acid

MOF – Metal-organic framework

PCP – Hexachloropropene

PBNP – (1*E*,1'*E*)-1,1'-(1,4-phenylene)bis(*N*-phenylmethanimine)

POC – Porous organic cage

PL – Porous liquid

R,R-CHDA – 1*R*,2*R*-Cyclohexyldiamine

S,S-CHDA – 1*S*,2*S*-Cyclohexyldiamine

TBTQ – Tribenzotriquinacene

TCC – Tubular covalent cage

TEA - Triethylamine

TFA – Trifluoroacetic acid

TFB – 1,3,5-Triformylbenzene

THF – Tetrahydrofuran

TMS – Tetramethylsilane

Chapter 1

Introduction

1.1 Porous Materials

Porous materials are defined by IUPAC as "a solid with pores (*i.e.* cavities, channels, or interstices), which are deeper than they are wide".[1] Additionally, the pores themselves can be classified based on their size: 2 nm and below – micropores; 2 nm to 50 nm – mesopores; and 50 nm and above – macropores.[1] The size of the pores and the way they are structured influences how a porous material can perform in a particular role or application. Microporous materials are of interest as the pore dimensions can correspond well to small molecules, potentially allowing favourable interactions in a specific or cooperative manner.[2] Porosity can also be defined as either intrinsic, *i.e.* inherent to the discrete molecule in isolation, or extrinsic, *i.e.* porosity arisen from molecules packing together in the solid state, but not intrinsic to the structure.[2]

In addition to classic porous structures such as zeolites,[3] a number of new porous solids have seen development in recent decades.[4] A number of these are extended structures such as metal-organic frameworks (MOFs),[5,6] covalent organic frameworks (COFs),[7,8] and porous organic polymers,[9–11] linked together by "strong covalent or coordinative bonds".[9,12] As well as these extended structures, a number of porous molecules have also been developed. These can be defined as molecules that pack in the solid state to produce pores.[4,13] Many examples of these porous molecules have been reported, with varying structures, including calix[n]arenes,[14,15] cucurbit[6]urils,[16] pillar[n]arenes,[17] cryptophanes,[18] hemicarcerands,[19] and Noria[20] (Figure 1.1). A number of these structures have an opening, or window, that is as wide as the intrinsic cavity.[13] Another class of intrinsically porous molecules that have seen increasing development in recent years are porous organic cages.[21]

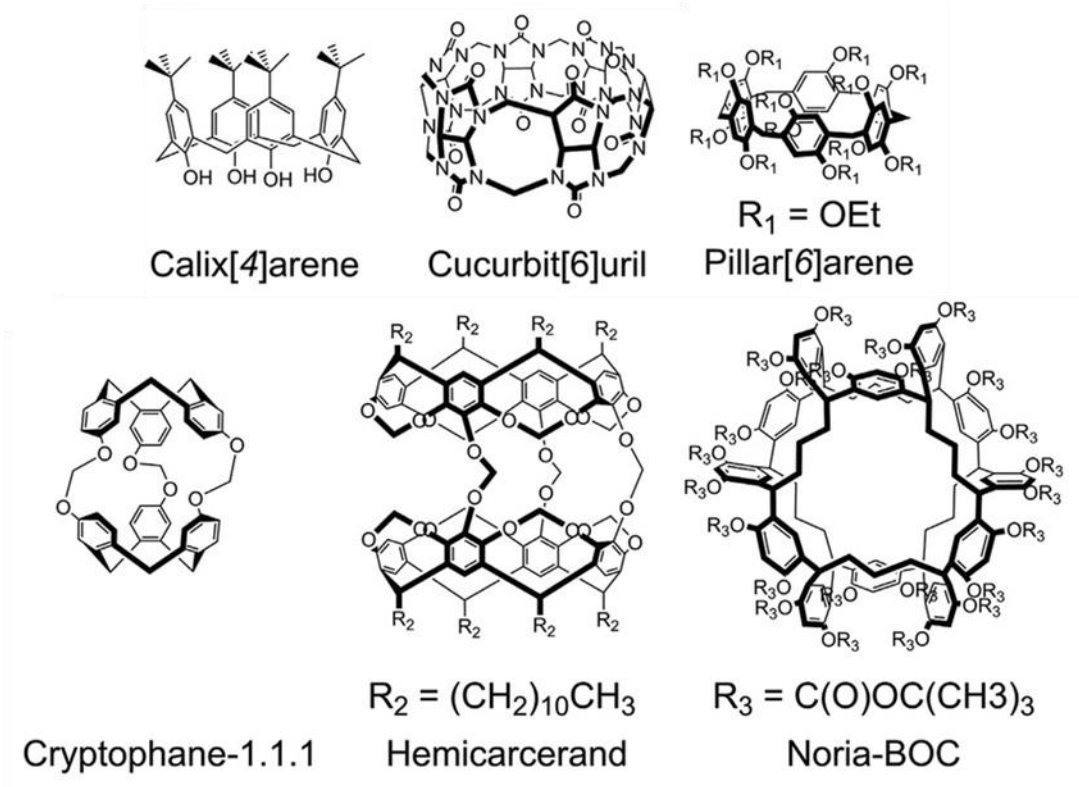

Figure 1.1 – Different classes of porous molecule: calix[n]arenes,[14,15] cucurbit[6]urils,[16] pillar[n]arenes,[17] cryptophanes,[18] hemicarcerands,[19] and Noria[20] (reproduced with permissions from Ref. 13).[13]

1.1.1 Porous Organic Cages (POCs)

Porous organic cages (POCs) are a class of porous molecule that have seen much interest following their initial report by Cooper and co-workers in 2009.[21] POCs are formed by the assembly of small organic precursors to produce three-dimensional discrete molecules. A key feature of these cages is a permanent void accessible *via* gaps, or "windows", within the cage structure.[4] These cage windows can also aid interactions between individual POCs to direct the packing and form larger supramolecular architectures, such as 1D nanotubes and extended 3D networks.[21,22] The molecular nature of POCs means that they are often solution processable — this is a major advantage over the less-soluble framework materials discussed previously. Solution processability allows for characterisation and purification methods unavailable for framework materials, such as solution NMR spectroscopy, chromatography, and recrystallisation.[23] It also allows cages to be used in applications where less-soluble alternatives are not feasible.

The use of porous organic cages as functional materials is based on the inherent properties of the cages *i.e.,* porosity *via* the accessible cavity within the structure; and how this function can be used in various applications. However, a major factor in determining the properties is the synthesis of the cages. The choice of reaction methodology, precursor choice, and bond-forming chemistry can all play a major role in the final properties of the cage — the latter of these is of relevance to the work outlined in later chapters of this thesis. As such, this chapter first discusses the synthesis of POCs. Additionally, it should be noted that for general considerations of cage synthesis, discussions generally focus on cages formed using reversible bond-forming chemistry, as most reported cages utilise reversible methods. Reversible and irreversible bond-formation are both discussed further later in this chapter

1.2 Synthetic approaches to porous organic cages

1.2.1 General considerations for the synthesis of POCs

The synthesis of POCs presents a number of challenges, whether in the formation of novel structures or derivatives of existing cages.[23] Often, descriptions of cage synthesis use the notation [X+Y], where X and Y represent the number of each building block that react to form a cage structure. However, this can often be misleading as the topicity (*i.e.*, number of reactive functional groups) of the precursors is not included, and X and Y are often used to differentiate the functionality on the building blocks but are interchanged between different research groups. Jelfs and co-workers outlined an alternative naming system which includes the topicity of the precursors, avoiding ambiguity when comparing between different structures.[24] The relative ratio/equivalents of each building block required depends on the topology of the target structure, and the topicity of the precursor itself. This can be exemplified using the prototypical cage **CC3**. First reported in 2008,[25] and investigated as a POC in 2009,[21] **CC3** is described as a [4+6] cage, where 4 equivalents of 1,3,5-triformylbenzene (TFB) react with 6 equivalents cyclohexyldiamine (CHDA), to afford **CC3** with 12 imine groups in the cage structure (Figure 1.2). Using the more recent nomenclature, this POC would be described as **Tri^{4}Di^{6}**.[24]

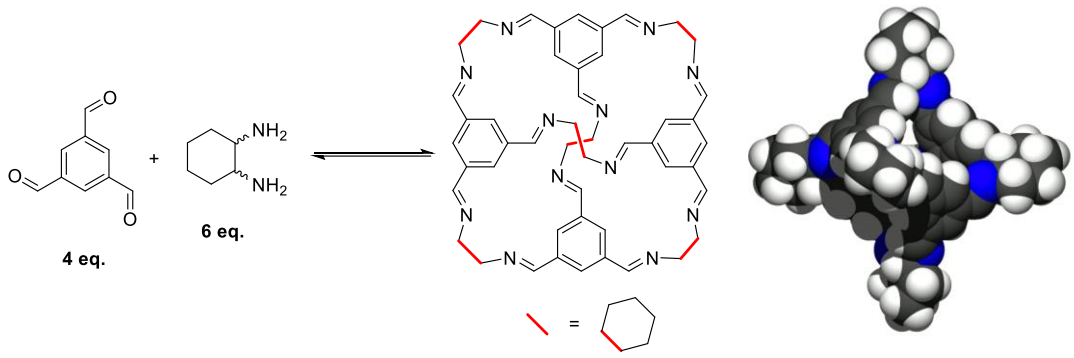

*Figure 1.2 – **Tri^{4}Di^6** imine cage **CC3**, formed by the reaction of 4 equivalents of TFB and 6 equivalents of CHDA; also shown is a model of **CC3** to exhibit the 3D nature of the POC structure.*

The selection of suitable precursors is pivotal, not only in terms what cage topology will be accessed, but also in determining whether cage formation will be successful. For a cage to be produced, at least one of the precursors must link in more than 2 directions, with a majority of cages reported built from combinations of two-way and three-way linkers.[4] In addition, the precursors need to be able to configure into the correct geometry to form a cage. The bond angles between the functionalities of the precursor used can have a large effect on the final topology of the desired cage (Figure 1.3) — narrower angles tend to produce smaller cages while wider angles can produce larger cages .[4] However even small changes to these angles can have a dramatic effect on the reaction outcome.[26,27]

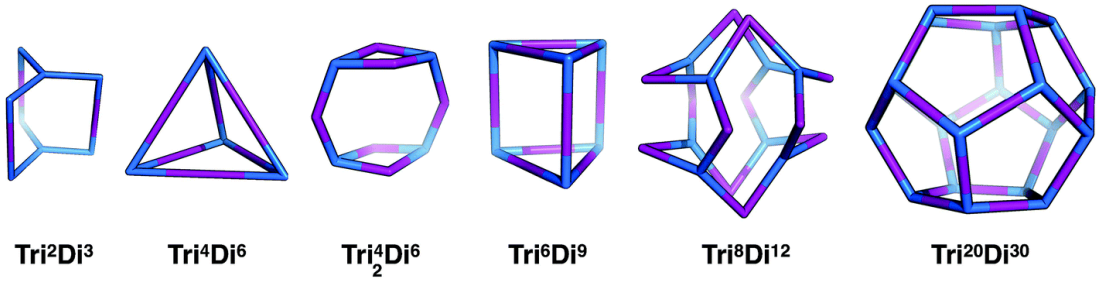

Figure 1.3 – The range of topologies available for a combination of tritopic and ditopic building blocks; tritopic vertices are in blue, ditopic linkers are in purple (reproduced from Ref. 24 with permission from the Royal Society of Chemistry).[24]

Even when chosen carefully, essentially any combination of precursors could form a polymeric network rather than a cage.[23] The use of pre-configured precursors, *i.e.*, where the reactive groups are arranged such to promote cage formation, can be beneficial in biasing the system towards the desired product by reducing the chance for misaligned reactions to occur. High-throughput investigations completed by Greenaway *et al.* varied the inherent flexibility of three triamine precursors by the use of directing alkyl groups (Figure 1.4a).[28] Overall, clean formation of cages with the expected topology was in general more likely when using one of the two more pre-configured triamines.[28] A similar effect was observed by Lauer *et al.* using triamines the unsubstituted and ethyl-substituted triamines in the synthesis of truncated tetrahedron cages (Figure 1.4b).[29] The absence of the ethyl groups on the triamine allow for more free rotation of the amine units, encouraging the system towards polymer formation over discrete cage assembly. Important to note for this system is that it was it was theorised the synthesis of the cages was under kinetic control, meaning "…the geometrical pre-organisation is crucial".[29] A similar effect is seen for **CC3**, with the rigidity and homochirality of CHDA ensuring that intermediates are partially preconfigured to form the cage species.[23]

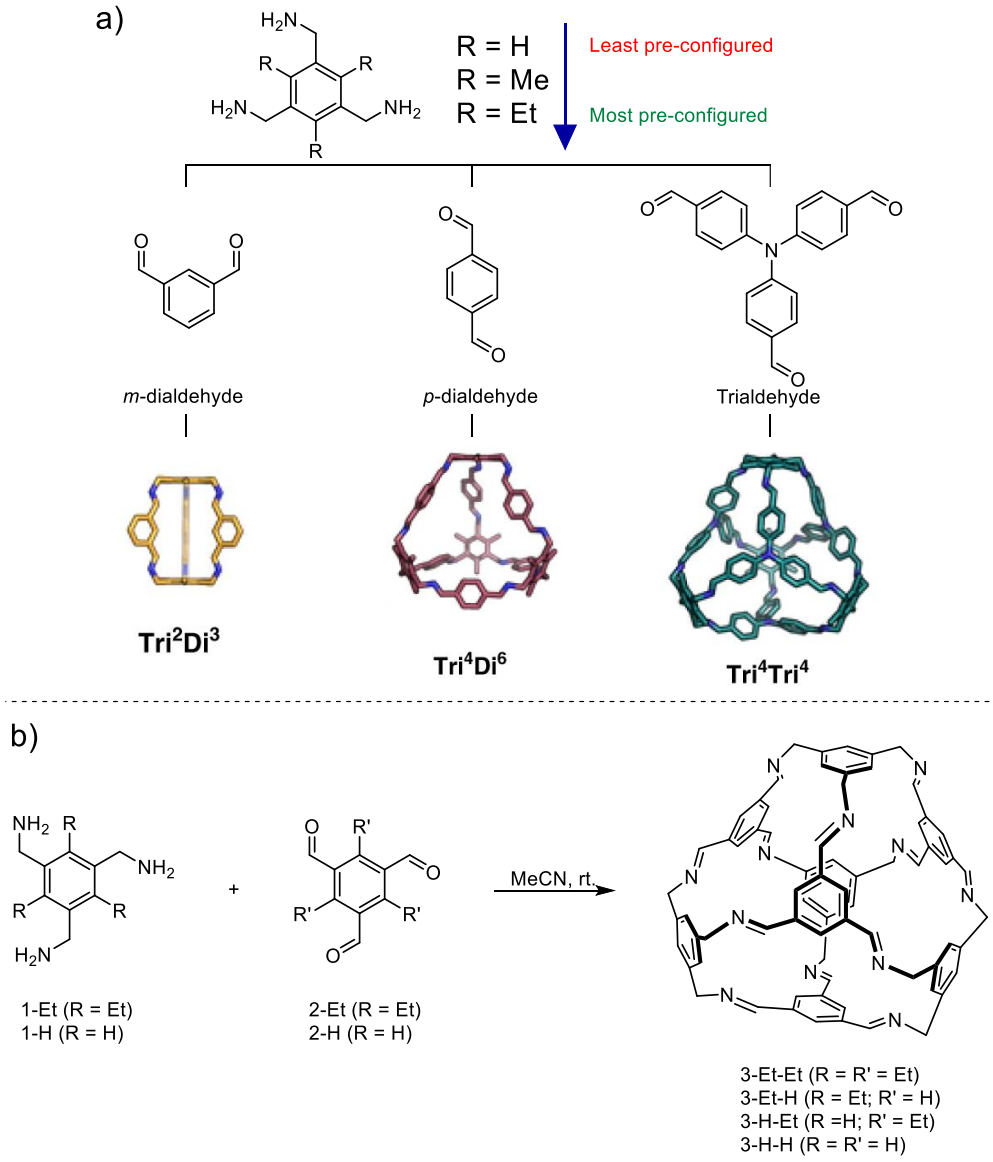

Figure 1.4 – a) The three triamines used in high-throughput cage formation studies by Greenaway et al.[28] — cage formation was successful in more cases where one of the more preorganised trimethyl- or triethyl- triamines was used as a precursor (reproduced with permissions from Ref. 28); b) the report of Lauer et al.[29] into ***Tri⁴Tri⁴*** *cage synthesis found the use of triamines 1-Et and 1-H directed more towards cage and polymer synthesis, respectively, due to the relative flexibility/pre-configuration of the triamines (reproduced with permissions from Ref. 29).[29]*

Directly linked is the relationship between precursor rigidity and the shape-persistence of the resulting cage, which subsequently has a direct impact on the porosity of the cage. If a cage structure is too flexible, it will not retain its shape on desolvation (*i.e.,* on the removal of the solvent molecules which may be acting as a

scaffold) and the structure may “collapse”, leading to loss of porosity – these cages are said to lack shape-persistence,[23] which can be caused by the use of flexible or freely rotatable precursors in the synthesis.[23] Mastalerz and co-workers investigated the effect of precursor flexibility on the formation of cages when using linear aldehydes (Figure 1.5a).[30]

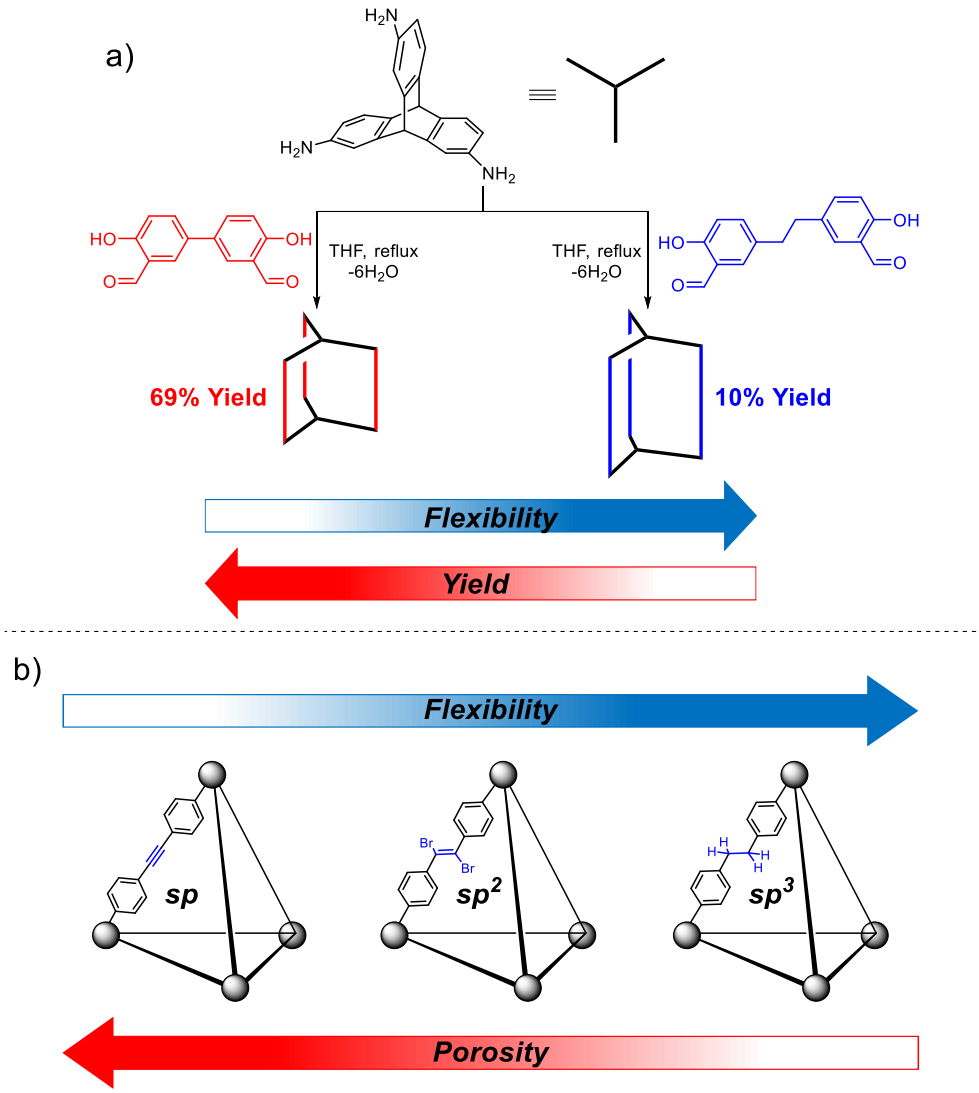

Figure 1.5 – Investigations on the impact of precursor flexibility on cage properties: a) study by Schneider et al. using alternative aldehydes of varied flexibility in the synthesis of isostructural imine cages;[30] b) study by Moneypenny et al. using edge-specific PSM of alkyne cages to form more flexible derivatives.[31]

Whereas the biphenyl-type aldehyde formed cage in a good yield of 69% (Figure 1.5a, red), the more flexible aldehyde tested formed the analogous cage in a lower yield of only 10% (Figure 1.5, blue). The crude reaction mixture of the latter also contained a complex mixture of products as determined by ^{1}H NMR spectroscopy, which required further purification to obtain the target cage. Moore and co-workers also investigated cage shape-persistence *vs* porosity by synthesising three structurally analogous cages using containing either alkynyl, alkenyl, or alkyl edge functionality (Figure 1.5b).[31] This allowed direct comparison between the cages, with combined experimental and computational results showing a direct correlation between shape-persistence and porosity (the more flexible the cage, the lower the porosity).[31]

In general, for cage synthesis, reactive precursors require high dilution and slow addition of precursors (unless solubility is controlled), and low temperatures.[23] Conversely, less reactive precursors may require acid catalysis, higher temperatures, or more concentrated reaction mixtures. [23] The syntheses of **CC1** and **CC3** exemplify this concept. Both cages were originally formed by simple mixing of their relative components,[21] but were later adapted individually with new methodologies. **CC1** was optimised to use high dilution and slow addition of TFB, to "mitigate the increased reactivity and inherent flexibility of the ethylenediamine (EDA) precursor".[23,32] The synthesis of **CC3** evolved to a batch method using layering of a diamine solution onto a suspension of TFB in DCM. This method mimicked slow addition/high dilution conditions due to the poor solubility of TFB. The inclusion of trifluoroacetic acid (TFA) as a catalyst helps to improve the reversibility of the imine formation. This method should be possible with other cage species. Some cages also require the removal of water from the reaction to ensure good conversion to the cage product[23,33] — this can be done with the use of Dean-Stark apparatus, or the addition of a suitable dessicant.[23]

Novel synthetic methods have also been used for the formation of POCs – both flow chemistry and twin-screw extrusion (TSE), named by IUPAC in the top-ten emerging technologies in chemistry 2019,[34] have been used in the synthesis of organic cages. In the flow synthesis of two **Tri^{4}Di^{6}** cages, **CC1** and **CC3**, Briggs *et al.* reported similar, if not improved, yields, at vastly reduced reaction times. The improved reaction time was suspected to be due to the ability to heat reaction solvent above its boiling point, "coupled with highly efficient reagent mixing characteristic of flow systems".[23,35] In another recent report,[36] twin-screw extrusion (TSE) afforded large scale synthesis of **CC3** in a much shorter reaction time (5g in 0.54 h), though with the formation of a new

[3+5] side product, which could only be removed on subsequent purification. The major benefit of this process, however, was the significant reduction in solvent needed for the process (up to 99.5% reduction, accounting for solvent required for both synthesis and purification). This would be beneficial both for industrial scaling-up of the reaction, and also reduce the amount of chlorinated solvent required for synthesis.[36] This is counter-intuitive compared to the more general cage syntheses discussed previously, and may be due to the effects of the highly preconfigured CHDA.[36]

Given the many challenges in synthesising POCs, it would be advantageous to be able to check the synthetic feasibility of producing a novel cage before resorting to "trial and error" laboratory work.[23] Given a set of starting precursors, the topology, geometry, and likelihood to remain shape-persistent, of a target cage can be calculated *in silico*. This can be used to rationalise experimental results by predicting the lowest energy conformers of cages, thus confirming the most favoured structure by comparing relative energies.[23,37,38] More recently, by validating with experimental results, these computational methods have been used for prediction of cage properties, molecular structure, and solid-state packing of cages. In the high-throughput study by Greenaway *et al.*, all cages were modelled computationally prior to experimental screening, with 33 cages forming cleanly, of which 31 cages (94%) were formed with the predicted, targeted topology.[28] For cages where suitable single crystals were obtained for X-ray analysis, the structures obtained had an "excellent geometric match" with the modelled low-energy conformers.[28]

Clearly, there are several considerations to be made when designing novel POCs. However, while the target topology, reaction conditions, and structure of the precursors are key factors, one important consideration is the choice of bond-forming reaction used. The way in which the individual precursors interact can have a drastic impact on how the reaction progresses, particularly as the desired cages become larger and more complex. In relation to the types of bond-forming reactions used for the synthesis of POCs, they can be split into two general areas — reversible and irreversible bond-formation.

1.2.2 Reversible Synthesis

Reversible methods for cage formation often rely on the use of dynamic covalent chemistry (DCvC). First conceptualised by Jehn-Marie Lehn,[39] DCvC utilises the reversible formation of covalent bonds to target the thermodynamic minimum of the system.[40] The dynamic nature of bond formation allows for "error-correction", allowing the transformation of misaligned kinetic products,[40] and can lead to higher yielding systems that require less purification compared to irreversible methods.[4] Elimination of these kinetic traps is beneficial, as they interfere with the identification of thermodynamic minima, noted as the "core value of DCvC".[41] However, in some cases, the desired cage may not be the thermodynamic minimum for the system. Given sufficient space and the correct geometry, interlocked cage catenanes can be formed[28,42] — interactions such as π-π stacking can provide a thermodynamic driving force for catenation, and solvent effects can therefore play a large role in their formation. Whilst these may not be the target product, these catenated structures can still be highly porous.[42] Whilst DCvC covers a large array of potentially reaction types,[41] a range of which have been utilised for the synthesis of cages,[43] the most popular reported methods are imine condensation, boronic acid condensation, and alkyne metathesis.

Imine condensation

Following its initial report over 100 years ago, imine condensation has seen widespread use in materials chemistry in the formation of both extended and molecular species.[44] Imine condensation has also emerged as the most popular route for the formation of porous organic cages, following the initial imine POCs reported by Cooper and coworkers.[21] Much of the **CC** series is based on the reaction of TFB with a vicinal diamine (*e.g.,* CHDA for **CC3**). This has allowed for derivatisation of the basic **Tri^{4}Di^6** structure by expanding the library of potential precursors. Primarily, the use alternative diamines with varying functionalities has led to the development of a large family of imine cages (Figure 1.6).[21,33,45–47] Many of these cages maintain the **Tri^{4}Di^6** topology seen previously, and the presence of new functionalities can often impact the properties of the cages.

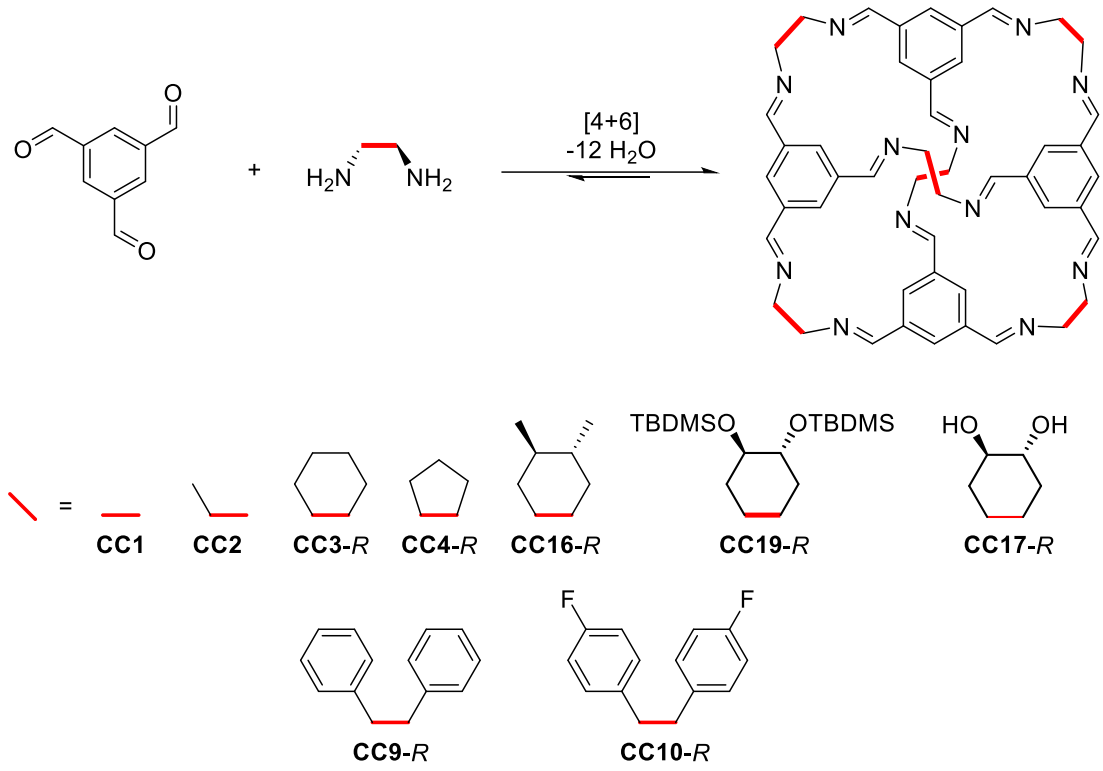

Figure 1.6 – General scheme to show derivatisation of the ***CC*** *series of cages by the combination of TFB with varying vicinal diamines. All combinations shown form cages with a Tri*^{4}*Di*^{6} *topology.* [21,33,45–47]

Cooper and co-workers have also investigated the use of more extended aldehydes and trialdehydes in the synthesis of imine POCs. In 2011, Jones *et al.* reported a study into assembly of POC co-crystals focusing on co-crystallisation of different enantiomers of existing cages *i.e.*, chiral recognition,[48] as well as imine cage **CC5**-*R*, formed by the [4+6] reaction of the larger tris(4-formylphenyl)amine and (*R*,*R*)-1,2-cyclopentanediamine. In the same year, Jelfs *et al.* also reported the use of tris(4-formylphenyl)amine, in combination with either *R,R*-1,2-cyclohexanediamine or *R,R*-1,2-cyclohex-4-enediamine, forming cages **CC7** and **CC8**, respectively.[27] In comparison to **CC5**, **CC7** and **CC8** form as [8+12] cages; it was proposed that this change may be influenced by "differences in steric strain in the respective cage vertices". These larger cages were found to become amorphous on desolvation. Molecular dynamics simulations for **CC7** suggested cage collapse on desolvation, providing an explanation for the lack of porosity exhibited by both **CC7** and **CC8**.

Hydroxy-functionalised derivatives of TFB have also been used in the formation of POCs. In 2016, Petryk *et al.* reported a series of salen-type imine cages formed by

the reaction of 2-hydroxy-1,3,5-triformylbenzene (TFB-OH) with a range of vicinal diamines.[49] Extended reaction time of around two weeks were required which produced cages as mixtures of isomers based on the position of the hydroxy group. It was suggested the inclusion of the OH groups could aid in application into gas selectivity or chromatography, and incorporating TFB-OH into cages has been used for chromatography since this initial report.[50–52] Wang *et al*. investigated separation of chiral alcohols, reporting improved resolution when using **CC3**-*R*-OH compared to **CC3**-*R*, citing the improved hydrogen bonding as a reason for this.[50] Li *et al*. reported investigations into **CC3** and **CC7** hydroxy derivatives across two papers, finding improved resolution in the hydroxy cages compared to commercially available **CC3** and **CC7** columns, across a wide range of substrates.[51,52] TFB-OH has also been used in the formation of POC core-shell crystals.[53]

Mastalerz and co-workers have reported a series of cages formed using imine condensation, with many reports focusing on the use of a triamino-triptycene with 2-hydroxyisophthalaldehyde.[54] Mastalerz originally reported the [4+6] adamantoid cage structure in 2008, though the porosity of the cage was not explored until 2011, finding the cage had a surface area of 1375 m^2g^{-1}.[54,55] Further studies focused on derivatization of this cage structure (Figure 1.7).[30,56–58] Brutschy *et al*. also outlined a series of triptycene-based cages using alternative aldehydes, employed as materials for sensing.[58] These aldehydes included functionalised derivatives of 2-hydroxyisophthalaldehyde, as well as analogous aldehydes to those used in a previous study into cage rigidity.[30] Additional isostructural cages for sensing were also reported the following year.[59] Also in 2013, 2-hydroxyisophthalaldehyde was again employed for cage synthesis, this time using post-synthetic modification to tune the size of the cage cavity by functionalising the aldehyde hydroxy group.[60]

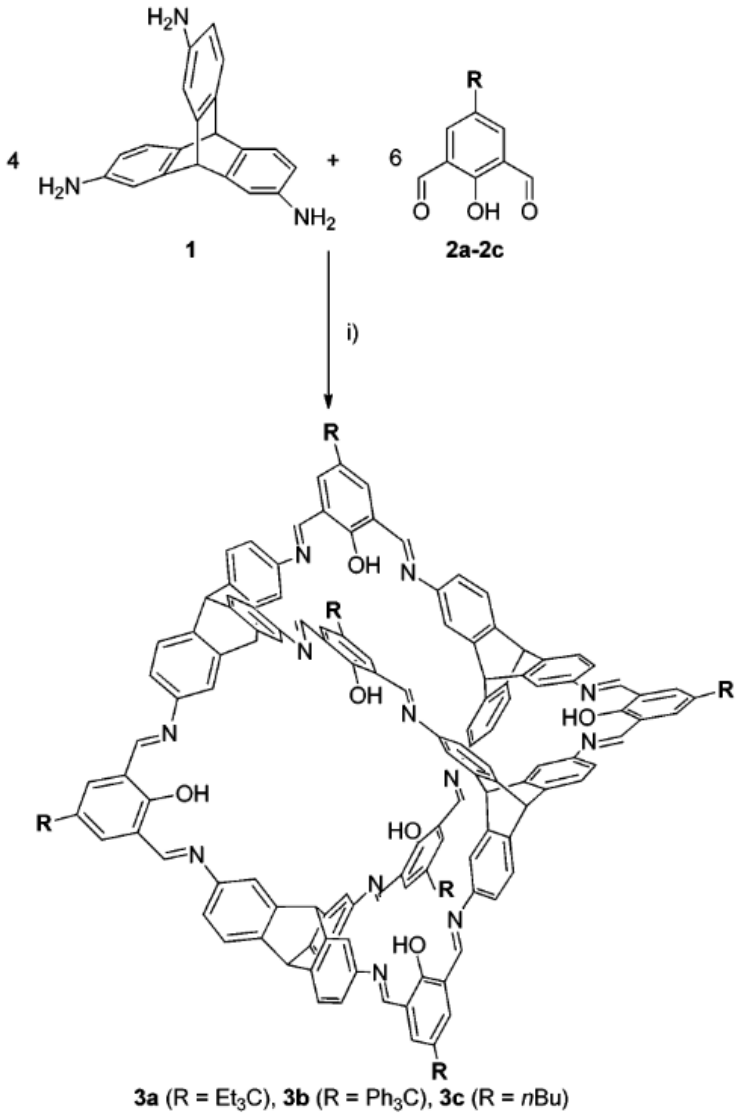

Figure 1.7 – Synthesis of adamantoid cages using a triptycene-based triamine with a range of functionalised salicylaldehydes. Reaction conditions: THF, reflux, three days, the precipitation with n-pentane, or, reaction in THF/acetonitrile, reflux, 2–3 days (reproduced with permissions from Ref. 56).[56]

Boronic acid condensation

Boronic acids have also been used in the synthesis of cages *via* two main condensation routes — reaction with a diol to form boronic esters, and self-condensation of a boronic acid to form a boroxine ring (Scheme 1.1), though there are limited examples of the latter method.[61]

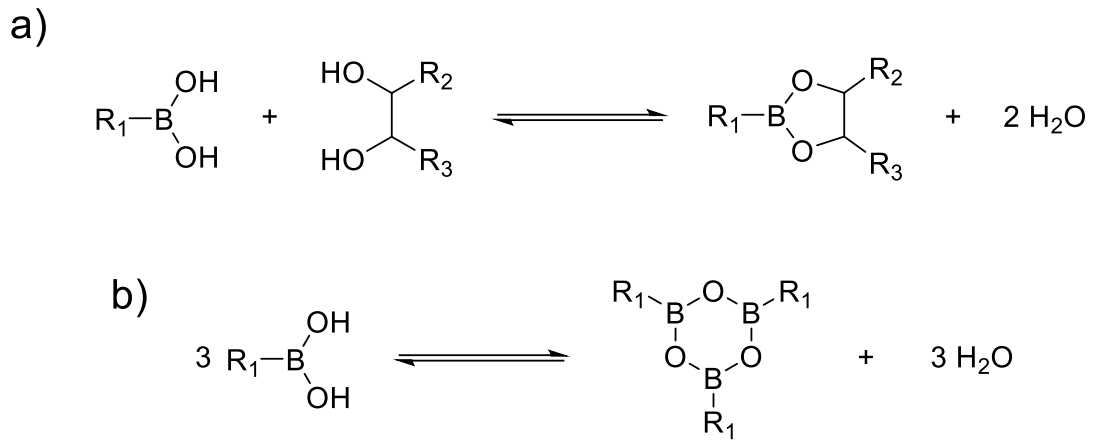

Scheme 1.1 – Methods of boronic acid condensation used in the formation of POCs: a) reaction with a diol to form a boronic ester; b) self-condensation to form a boroxine ring.

Initial studies into cages formed using boronic acids reported small cages, but Nishimura *et al.* also reported larger cages using a functionalised tetraboronic acid cavitand.[62] In combination with a linear, aromatic tetraol, this yielded a **Tet^{2}Di^{4}** boronic ester cage with host-guest functionality.[63] In 2009, Kubo and co-workers reported the synthesis of small molecular capsules using boronate esterification.[64] However, none of these cages were studied for permanent porosity. Mastalerz and co-workers later reported a porous boronic ester by the condensation of a triptycene-based tetraol with 1,3,5-benzene triboronic acid — this led to the formation of a large **Tet^{12}Hex^{8}** cage.[65] Initial studies showed no distinct ^{1}H NMR peaks of the expected cage product — it was assumed that poor solubility of intermediates led to incomplete reaction. To rectify this, solubilizing ethyl chains were added to the starting tetraol — this afforded full conversion to the product cage. The measured N_2 isotherm showed a BET surface area of 3758 m^2g^{-1}, the highest recorded for a porous organic cage to date.[65] This work was further developed by a later report by Mastalerz and co-workers in the same year.[42] An alternative to the original precursor was also designed by functionalising with long alkyl chains on the triptycene bridgehead rather than the central benzene ring, affording a tetraol in 3 steps compared to 8 in the original report. Though the alkyl groups were longer, the new tetraol was found to be less soluble than the original, and high dilution conditions were utilised in the cage synthesis. Cage formation was successful but found to be in the form of a large **Tet^{24}Hex^{16}** cage catenane — it was suggested that alkyl-aromatic interactions may have provided a driving force for catenation.[42]

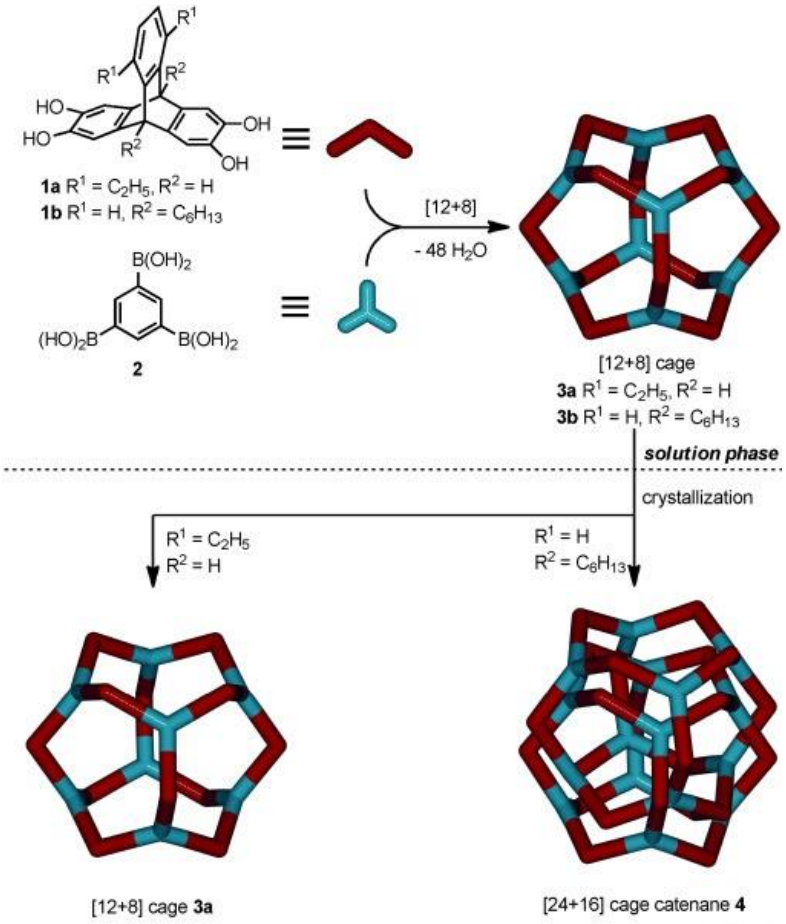

Scheme 1.2 – Synthesis of a ***Tet^{12}Hex^{8}*** *cage and* ***Tet^{24}Hex^{16}*** *cage catenane (using old nomenclature: [12+8] and [24+16], respectively), both by boronic ester condensation as reported by Zhang et al.*[42] *The cage was also studied by itself in an additional report*[65] *(reproduced with permissions from Ref. 42).*[42]

Alkyne metathesis

Following its utilisation in the formation of rigid macrocyles,[66] alkyne metathesis has emerged as a pathway for the formation of POCs. The rigid, linear nature of the ethynylene bonding makes it a good candidate for the formation of discrete organic cages.[67] In this process, the C-C bond formation is only reversible in the presence of a catalyst[43] — this offers the potential to form stable cages in comparison with other reversible methods, which can exhibit poor chemical stability.[4,68] The groups of Zhang and Moore have both been instrumental in the development of alkyne metathesis for the synthesis of cages. In 2011, Zhang and co-workers reported the first template-free synthesis of a shape-persistent cage by alkyne-metathesis. The cage monomer was synthesised in 3 steps in good yield as a rigid, highly pre-configured tetraalkyne. Dimerisation by alkyne metathesis using a molybdenum catalyst gave the target cage

COP-5 in 56% yield (Scheme 1.3). **COP-5** exhibited good thermal and chemical stability, and, whilst no porosity measurements were reported, the cage was shown to exhibit high C_{70}/C_{60} selectivity.[69]

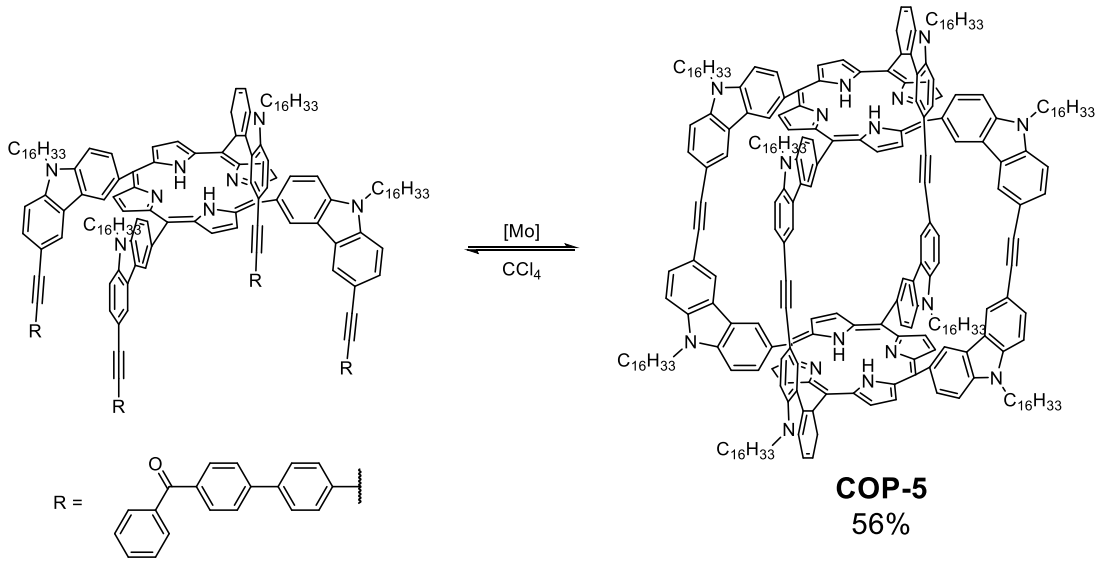

Scheme 1.3 – Report by Zhang et al. of synthesis of POC via template-free alkyne metathesis, utilising a molybdenum catalyst and highly organised cage monomer.[69]

Zhang and co-workers further investigated cages for C_{70} binding in 2014.[70] Utilising a molybdenum-based catalyst as with their previous study, they reported the synthesis of a tetrameric alkyne cage with high C_{70}/C_{60} selectivity. The shape and inherent angle of the monomer indicated that the final cage would be tetrahedral in structure. ^{1}H NMR spectroscopic measurements of the crude product indicated this was incorrect, and further elucidation by single-crystal X-ray diffraction (SCXRD) showed the true structure of the cage as having two macrocyclic panels connected by two side arms.[70] To gain a better understanding, the cage formation was studied over time by ^{1}H NMR spectroscopy and gel permeation chromatography (GPC), which showed fast, initial formation of a dimeric macrocycle formed at reduced reaction time, observed with unreacted monomer. The formation of the unexpected final structure was likely guided by formation of the macrocycle as a key intermediate, rather than the inherent angle of the monomer "arms" (Figure 1.8). Interestingly, attempts to form the cage by coupling of two macrocyclic units were unsuccessful — suggesting the process was dynamic in nature, rather than kinetic trapping of the cage.[70]

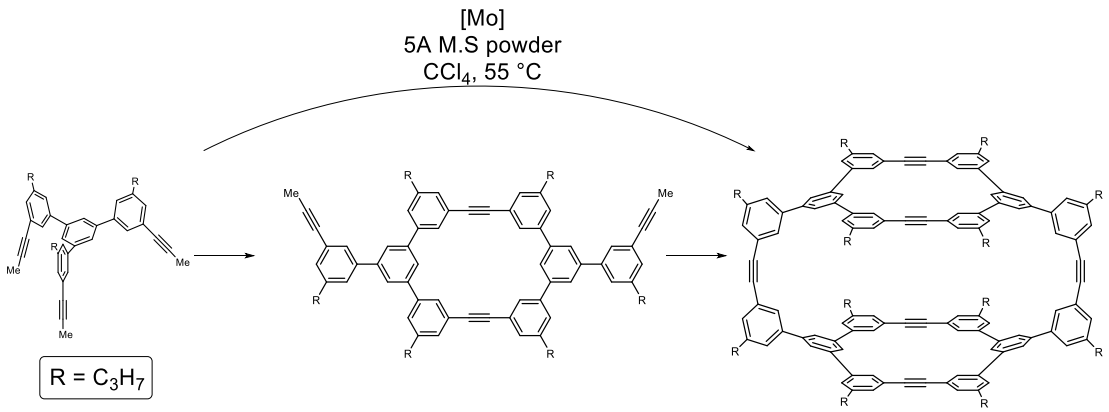

Figure 1.8 – Synthesis of tetrameric cage reported by Zhang et al. Formation of the final cage proceeds first via fast formation of a dimeric macrocyclic intermediate.[70]

Following these studies, Moore and co-workers have studied cage formation with alkyne metathesis. In 2016, they reported two tetrahedral cages formed by alkyne metathesis. Citing Zhang's earlier attempt discussed previously,[70] Moore and co-workers described utilising tritopic precursors based on 1,3,5-tribenzyl-2,4,6-triethylbenzene, to bias the system away from macrocycle formation.[71] The alternating "up-down" conformation preconfigures the monomer into a bowl-shape. In addition, an alternative precursor with less organisation was used for comparison — interestingly, both cages formed in high yield; the degree of pre-configuration had little effect for this system. It was believed that the high yields were in part due to "kinetic-trapping" of the cages,[71] rather than formation as the thermodynamic product as the usual for DCvC. Following the report by Moore and co-workers into the effect on shape persistence on porosity discussed previously,[31] Moneypenny *et al* reported an investigation into the effect of changing the precursor bite angle in cage formation.[72] Targeting analogous tetrahedral cages to previous analogues[71] allowed for incorporation of different heteroatoms and the tuning of the precursor bite angle. Three precursors were formed ranging from a "tight" angle of 31°, a "middle" angle of 51, and an "ideal" tetrahedral angle of 60° (Figure 1.9). Interestingly, it was found that the intermediate angle gave the most efficient formation of the desired cage.[72] Tightening the angle biased the system away from formation of a discrete architecture, whilst the "ideal" angle biased the system such to increase the time needed to locate the desired product.[72]

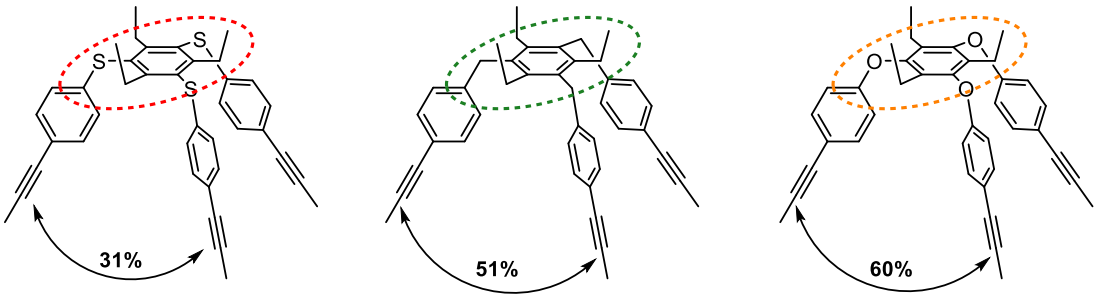

Figure 1.9 – Series of alkyne precursors devised by Moneypenny et al. to investigate effect of precursor bite-angle on product distribution for cages formed by alkyne metathesis.[72]

The increased stability of cages formed by alkyne metathesis makes them interesting synthetic targets. However, whilst the cages may be stable under a range of conditions, the synthesis conditions need to be carefully controlled. A major contribution to this is the use of metal-catalysts for alkyne metathesis procedures *i.e.* substituted molybdenum catalysts utilised by Zhang and Moore. These catalysts can be highly sensitive to air and moisture, and often require manipulation under fully inert conditions (*e.g.* using a glovebox) — compare this with the other reversible methods which can often be uncatalysed or use simple acid catalysis. This issue combined with the high cost of some metal catalysts means that alkyne metathesis could be a less accessible option for those looking to start studies into cage formation by DCvC.

1.2.3 Irreversible syntheses

Cages formed by irreversible routes are much more uncommon. The lack of dynamic bond-formation does not allow for elimination of unwanted side-reactions *i.e.*, once a kinetic product has formed, it remains in the reaction. Not only does this remove available reactants, but the presence of a range of side products makes isolation of the desired product more difficult. The benefit of using irreversible processes is the high stability of the products formed. Two methods that have been successfully utilised in cage formation are carbon-carbon coupling reactions and nucleophilic aromatic substitution (S_NAr).

Carbon-carbon coupling

Whilst there are still few examples of cages produced *via* C-C bond formation, the first examples were not a recent discovery. The first cage with a fully C-C bonded structure was reported in 1977 by Wennerstom *et al*. by a sixfold Wittig reaction — as expected for an irreversible process, the synthesis was very low yielding (1.7%).[73] Further development utilising multistep syntheses was completed by Stoddart and Vogtle, though these pathways still resulted in poor yields.[74,75] A major advancement came from Moore and co-workers, reporting the synthesis of alkyne macrobicycles using a multistep route with successive Sonogoshira-Hagihara couplings (Figure 1.10).[76] This methodology resulted in higher yields for the cage-forming step, but required labour-intensive synthesis of large macrocyclic precursors.

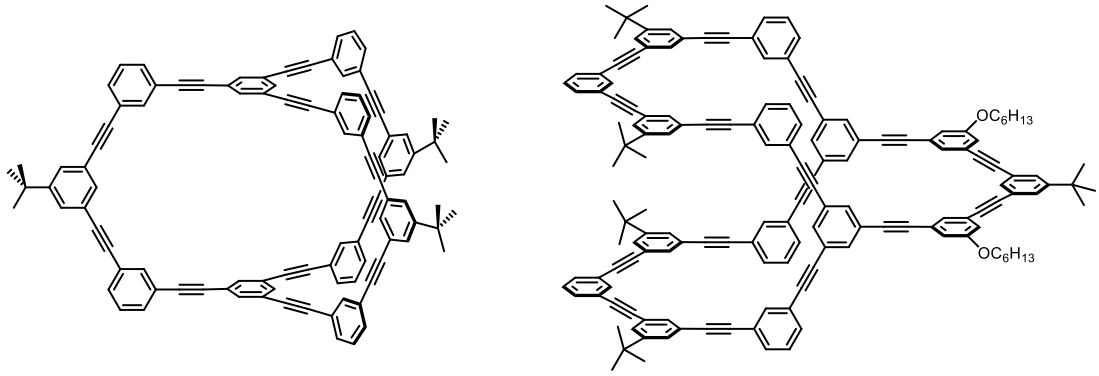

Figure 1.10 – Macrobicycles reported by Moore and co-workers, formed via successive Sonogashira-Hagihara couplings.[76]

More recently, Chen *et al.* reported the synthesis of a C-C bonded triptycene-based cage *via* Eglinton-Glaser coupling.[77] Dimerization of a pre-organised trialkyne by a threefold coupling led to synthesis of the cage in a high yield of 58% (Figure 1.11a). Whilst SCXRD measurements suggested the cage adopted a microporous structure in the solid state, no porosity measurements were reported for this cage. Building on this work, Avellaneda *et al*. reported a cage synthesis *via* an three-fold Eglinton-Glaser coupling (Figure 1.11b).[78] The synthesis was completed under high-dilution conditions with an excess of catalyst in an effort to maximize yield. The cage was formed in a 20% yield — this reduction in comparison to the previous report by Chen is likely due to the increased flexibility of the precursor; this again highlights the effect of preorganisation on cage formation.[79] Kitchin *et al* later showed that this cage could also be synthesised using flow chemistry.[80]

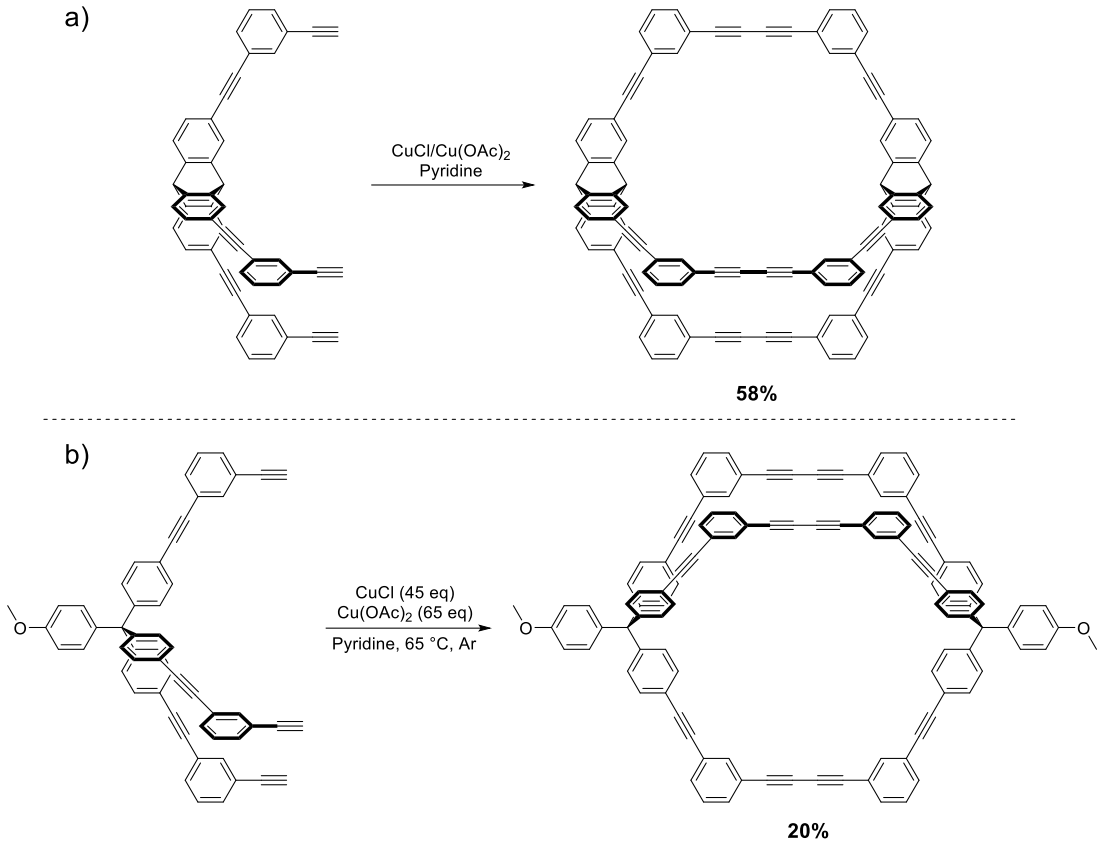

Figure 1.11 – Syntheses of C-C bonded cages via Eglinton-Glaser coupling: a) Report by Chen et al.;[77] *b) Report by Avellaneda et al.*[78]

Further development by Doonan and co-workers allowed access to much higher yields by stepwise Eglinton-Glaser coupling.[79] In a report of endohedrally functionalised cages in 2016, Burgun *et al.* reported the synthesis of two analogous cages incorporating pyridine moieties — initial attempts at formation with their existing conditions resulted in very low yields (4%). To increase this yield, Burgun *et al* reported an alternative methodology using sequential couplings.[79] Selective protection of two of the three alkyne groups allowed first for only one coupling reaction to take place. Following deprotection of the remaining alkyne groups, the final cage formation was intramolecular and gave a much higher-yielding cage synthesis (52-53%), compared to the intramolecular three-fold coupling outlined previously.

Nucleophilic aromatic substitution (S_NAr)

Nucleophilic aromatic substitution (S_NAr) has previously been used in the formation of macrocycles, polymers, and extended frameworks, but only a limited number of examples of cages are reported. In 2005, Katz *et al.* reported the synthesis of a series of small cages formed by the reaction of a triol with a selection of substituted aromatic precursors in an S_NAr process.[81] Initial yields of 58% were achieved using a phenyl-based precursor – later tests using pyridine-based precursors afforded yields up to 95%. The use of Cs_2CO_3 catalyst may have promoted these higher yields by a caesium templating with the pyridine functionalities. Zhang and co-workers have further developed the use of S_NAr in cage formation. In 2015, Zhang *et al.* reported an initial study into a tetraphenylethylene-based cage formed in a one-pot S_NAr process.[82] The cage was formed by the reaction of the large tetraol with the substituted pyridine, giving the desired cage in 21% yield (it may be the case that the Cs^+ cation is too small to effectively template formation of the larger cage). The cage was found to be porous, adopting a "grid-like structure" in the solid state, exhibiting high CO_2/N_2 selectivity. Zhang and co-workers continued to develop this cage architecture with a study into networked cages.[83] The 2018 study by Wang *et al*. focused on an analogue of the earlier **Tet^{2}Di^4** cage – again utilising the extended tetraol, but in combination with a tetra-chloropyridine (Figure 1.12).[83] A one-pot S_NAr reaction of these precursors gave the [2+4] cage **TOC** in a low yield of 15%. SCXRD analysis of **TOC** revealed window-to-arene packing in the solid state – this lack of window connectivity resulted in the formation of a non-porous structure. Periphery functionalisation with chloride groups provided the opportunity for post-synthetic modification to overcome the poor porosity of the molecular cage. Yamamoto-type Ullmann cross-coupling of the cage gave formation of the cage-based polymeric framework **pTOC**, confirmed as amorphous through PXRD.[83] Whilst these examples outline the use of S_NAr in formation of POCs successful reports of cage formation and yields are still limited. Whilst some studies have already investigated conditions to allow dynamic S_NAr reactions, these processes are often very substrate specific and further optimisation would be required before application to dynamic synthesis of POCs.

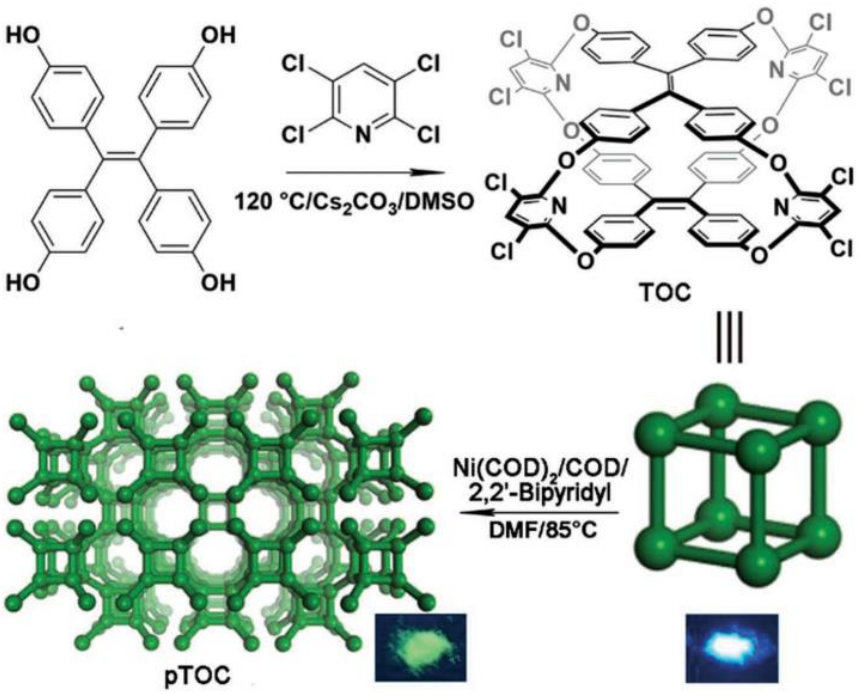

*Figure 1.12 – Synthesis of the cage **TOC** as reported by Wang et al.: following initial synthesis, the cage can be used to form the polymeric framework **pTOC** using by cross-coupling of the cage species (reproduced with permissions from Ref. 83).*[83]

1.3 POCs as functional materials

1.3.1 Properties of POCs

Porosity can be classified as either intrinsic (inherent to the structure), or extrinsic (from how the material packs together to form porous structures).[2] Typically, porosity is limited to one of these options, but for cages both can be accessed due to the intrinsic porosity of the cage cavity, and the extrinsic porosity of the solid-state packing. A key requirement for POCs is therefore shape-persistence, *i.e.* the cage must maintain its shape on removal of solvent or guest from its cavity.[23,84] A lack of shape-persistence leads to cage collapse on guest removal — this causes loss of both the cages intrinsic porosity, but would also disrupt any pore network that might exists between cages.[23]

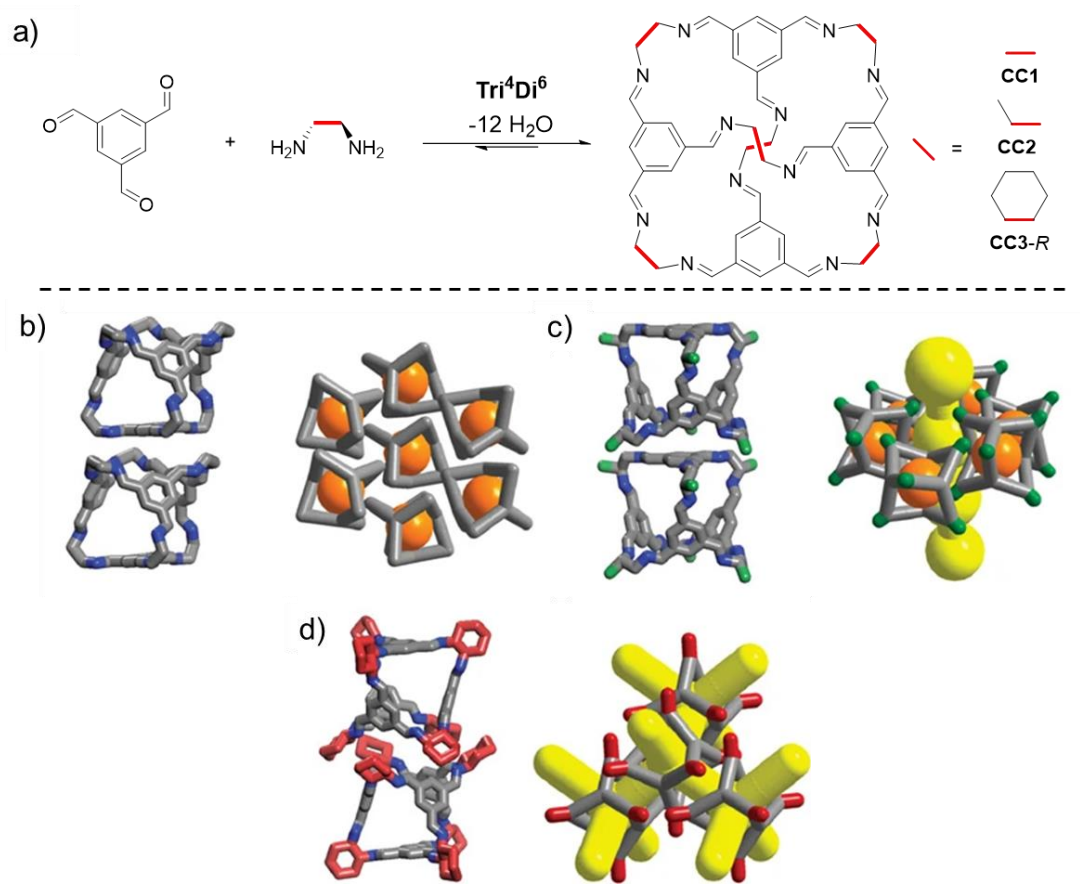

*Figure 1.13 – Synthesis and solid-state packing of cages **CC1**, **CC2** and **CC3** — a) reaction scheme for formation of the three imine cages; b) **CC1** packs in a window-to-arene fashion, exhibiting only intrinsic porosity; c) **CC2** packs window-to-arene, but forms 1D pore channels (shown in yellow) due to the methyl groups frustrating packing; d) CHDA groups direct **CC3** to pack window-to-window, forming a 3D diamondoid-pore network (shown in yellow) (reproduced with permissions from Ref. 21).*[21]

The inherent structure of a cage itself also has a major influence its ability to pack in the solid-state. In their initial report, Cooper *et al.* found that changing the functionality on the cage vertices led to differing interactions between the individual cage molecules. This in turn led to varied packing modes and porosities (Figure 1.13).[21] In the study, the ethylenediamine-based **CC1** was found to pack window-to-arene in the solid state with no interconnectivity between the individual cages — the only porosity for this system is therefore from the inherent cavities within the cages. **CC3** however, with CHDA vertices, packed more efficiently in a “window-to-window” fashion, resulting in of an interconnected diamondoid-pore network. Connecting the voids of the cages led to a substantially higher surface area compared to **CC1** (Figure 1.13).[21]

Additionally, cages have also been found to adopt different polymorphs *i.e.*, the ability to adopt different crystal structures. Although initially found to exhibit only its inherent porosity, Cooper and co-workers also reported that by using an alternative solvent (*o*-xylene over ethyl acetate), **CC1** could be isolated as a porous polymorph with a much improved surface area (Figure 1.14).[21] Further development in a later study demonstrated that **CC1** could be transformed into a range of polymorphs in response to specific chemical triggers.[85] The cage exhibited "on/off switching" between both the porous and non-porous states, as well as selectivity between different gases.[85] By utilising 1,4-dioxane as a directing solvent, this behaviour was also exhibited by other imine cages.[86]

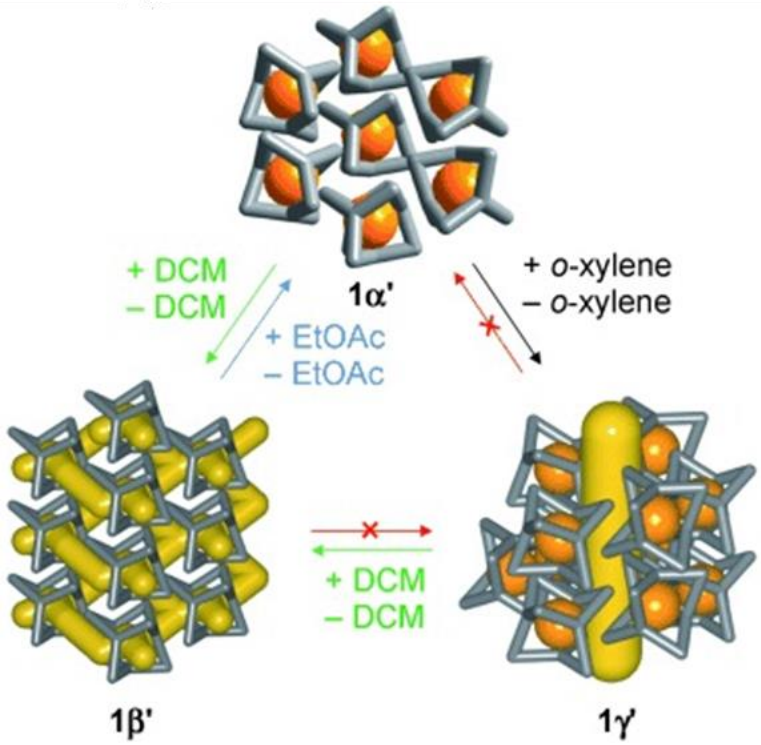

*Figure 1.14 – Solvent induced polymorph switching for imine cage **CC1**, allowing switching between a nonporous form, into two porous forms with interconnected pore channels (reproduced with permissions from Ref. 85).*[85]

The solid-state packing can be further altered by more drastic periphery-functionalisation of the cages. Cooper and co-workers have outlined several methods, initially using bulky diphenyl diamines to frustrate the solid-state packing of the cages engineer extrinsic porosity in addition to the intrinsic cavity of the cage.[33] A later report showed that functionality does not have to be this extreme. Use of a dimethyl-

substituted derivative of CHDA gives the **Tri^{4}Di^6** cage **CC16,** which has 12 methyl groups around the cage periphery. These methyl groups frustrated the cage packing mode, but the small size did not permit penetration of the voids of adjacent cages. The additional extrinsic porosity caused by this packing frustration led to **CC16** having more than double the surface area compared to **CC3**. Additionally, cage scrambling can be used as an alternative, where two different diamines are used in the cage synthesis, resulting in a statistical mixture of cages with varying substituents on the cage peripheries. The system cannot pack efficiently in the solid-state, leading to increased porosity (scrambled cage 704 m^2g^{-1} vs. crystalline **CC3** 624 m^2g^{-1}).

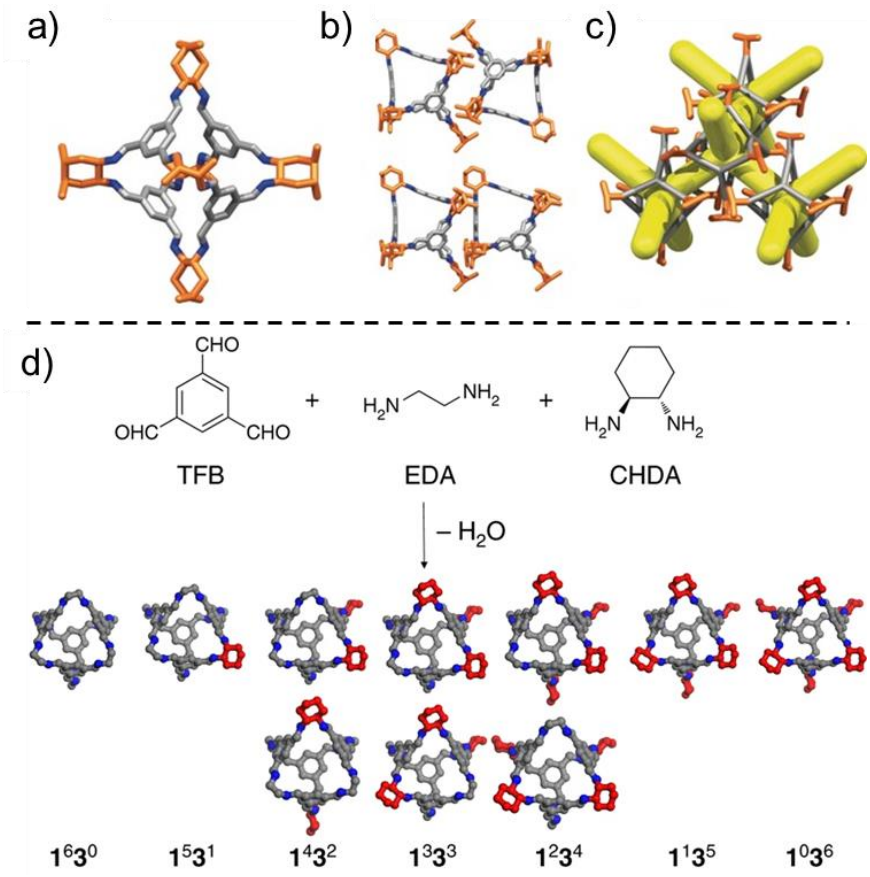

Figure 1.15 – Altering cage structure to affect the solid state packing — a) periphery functionalisation as reported by Reiss et al. by the use of a substituted diamine, giving a cage with 12 methyl groups on the cage periphery[47]*(reproduced with permissions from Ref. 47); b) cage scrambling as outlined by Jiang et al. to create a system that does not pack efficiently;*[87] *(reproduced with permissions from Ref. 87).*

As well as varying the physical diamine used to form the POC, the chirality of the cage can influence the solid-state packing. A large proportion of the **CC** series reported by

the Cooper group are constructed using chiral vicinal diamines These diamines are generally available as either the racemic form, or as the single enantiomers, and both can technically be used for cage formation.[21,88] Use of the *R,R* or *S,S* enantiomers of the diamine results in the formation of the *R* or *S* cage respectively.[45] These cages maintain the chiral character of their precursors, and as such can self-assemble based on the interactions between the two cage enantiomers (Figure 1.16). Whilst this forms the same polymorph as seen for the homochiral cages, the cages of opposite chirality can pack more closely together in the window-to-window arrangement.[89] Chiral recognition can be used to form porous nanoparticles from complementary cage enantiomers.[45,48] Additionally, Slater *et al*. reported that use of the racemic CHDA diamine led to the discovery of dissymmetric cages (that is, lack a centre of symmetry, but have one proper rotation axis).[88,90] These **CC3** cages incorporated both -*R* and -*S* functionalities, and remained in solution while the **CC3**-*R*/*S* co-crystal formed precipitated from the reaction mixture.[88]

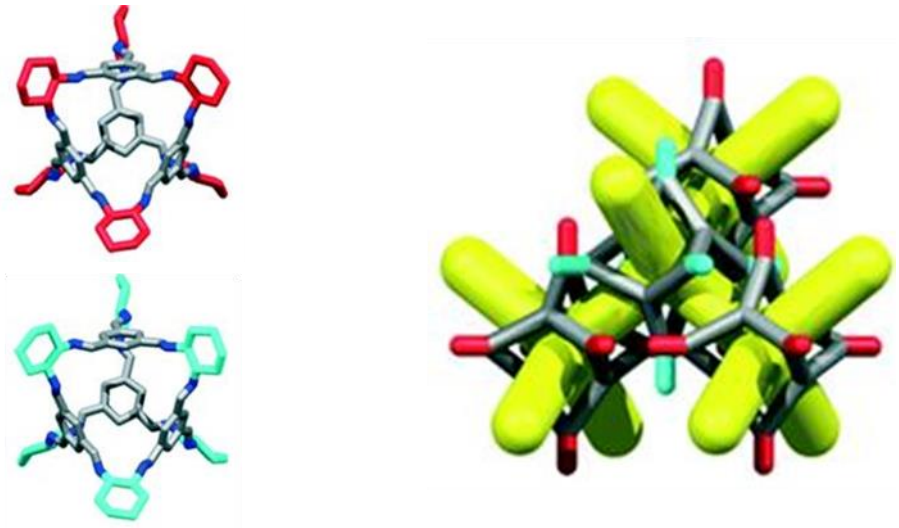

*Figure 1.16 - Window-to-window packing of two enantiomers of **CC3** to form a diamondoid pore network; the chiral recognition between **CC3**-R (red) and **CC3**-S (pale green) allows the cage racemate to more closely pack in the solid-state.*[88]

The topology and geometric shape of the cage can also be tailored to allow assembly of more complex architectures. A series of tubular (**TCC**) cages were formed by the condensation of tetratopic aldehydes with chiral diamines (*R*,*R*- or *S*,*S*-CHDA, the same as used for **CC3**). [22] These cages were found to assemble into 1D nanotubes *via* window-to-window interactions when a heterochiral mixtures of cages was used

— the interactions between just the homochiral cages were not strong enough to lead to the formation of nanotubes. The chiral recognition extended into assembly between **TCC** cages and **CC3** — as the windows of these cages were the same, formation of pillared porous molecular networks between **TCC** cages and **CC3** could be achieved when cages of opposite chirality were used.[22]

1.3.2 Applications of porous organic cages

Arguably, the most useful feature of POCs is the inherent porosity of the structure, allowing for potential capture and storage of guests. The porosity of POCs is usually determined by measuring the N_2 adsorption isotherm; from this, the Brunauer-Emmet-Teller (BET) surface area (SA_{BET}) can be calculated.[4] The SA_{BET} of POCs can vary depending on a number of factors including the structure, size, shape persistence, and solid-state packing or polymorph, of the cage.[30,31] Small changes to the cage structure can lead to large changes in the SA, e.g. a tripling of surface area due to the addition of a second methyl group to a cage vertex.[86] In addition, the crystallinity of a cage can also greatly affect its properties. In some cases, depending on the system, structures that show no crystallinity *i.e.,* amorphous, can sometimes show either a reduced or increased SA compared to crystalline structures.[4] Cooper and co-workers showed that in the formation of **CC3** nanocrystals, the amorphized cage had more than double the SA of its crystalline analogue.[48] It is worth noting, however, that this is not a "general phenomenon"[23] — the porosity in **CC3** is increased in the amorphous sample because the CHDA groups on the cage vertices prevent efficient packing. For comparison, the isostructural **Tri^{4}Di^6** cage **CC1** is formed from EDA — this forms a cage that lacks the bulky CHDA groups on the cage vertices as in **CC3**. Molecular dynamics measurements suggest that **CC1** is rendered non-porous when amorphous.[91] However as discussed previously, additional studies showed various accessible polymorphs for **CC1**, each with different porous properties (Figure 1.14).[85]

Whilst POCs can exhibit high SAs, including limited examples of large cages with SAs approaching that of extended frameworks,[65] uptake of a particular gas (such as N_2) is unlikely to be sufficient for widespread application. A more useful feature is exhibiting selectivity between different guests. This has previously been shown for a variety of gas mixtures including CO_2–N_2,[92,93] CO_2–CH_4,[55] and SF_6–N_2.[94] In the latter case, molecular simulations suggested that the flexibility of the cage crystal allowed for a structural rearrangement that permitted diffusion of larger gases into the void,

followed by relaxation to a form producing near-ideal interactions with the SF_6 molecule. The material showed the highest SF_6–N_2 selectivity for any known material at ambient temperature and pressure,[94] demonstrating how the specific structure of a cage can directly influence its applicability for certain functions. A further example of this is the use of POCs for the isolation of rare gases such as krypton and xenon from air,[95] because of a precise size match between the gases and cage void produced high selectivity at low concentrations.[95] POCs have also been processed into cage membranes, a promising step towards improving applicability in an industrial setting (Figure 1.17a).[96,97]

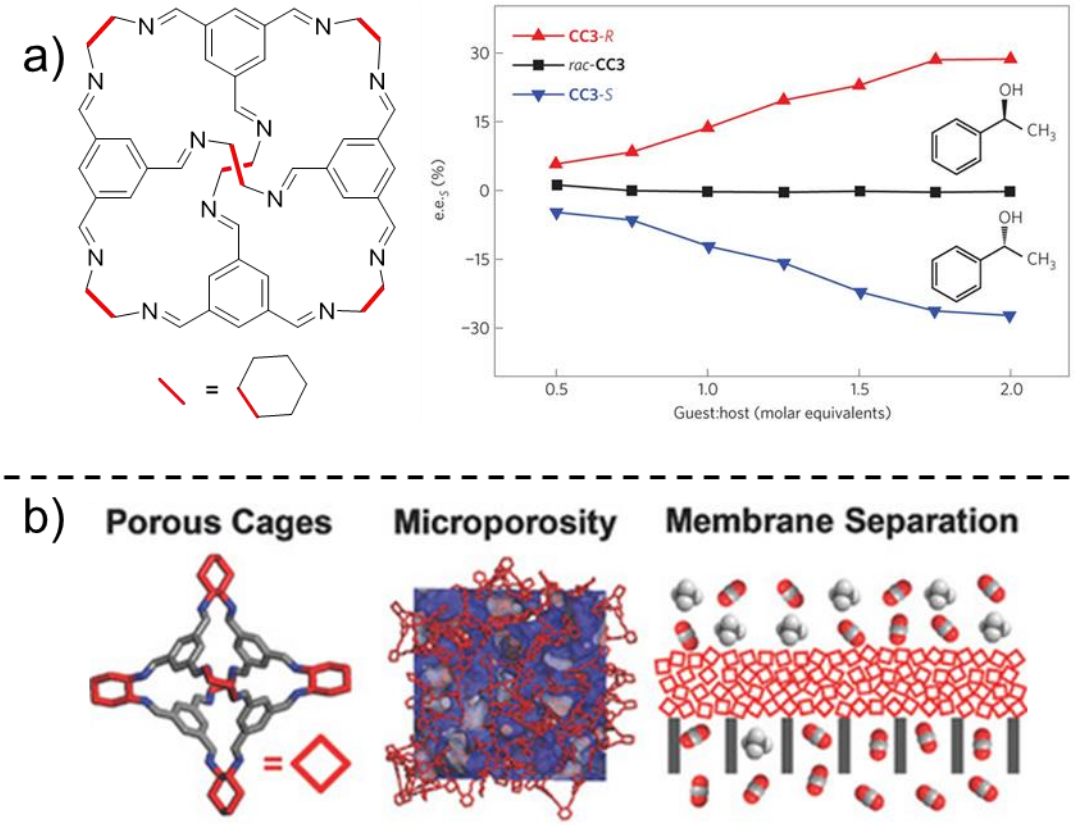

Figure 1.17 – Applications of POCs; a) use of CC3 for the separation of chiral alcohols[95] *(reproduced with permissions from Ref. 95); b) fabrication of an imine cage into a membrane for molecular separations*[96] *(reproduced with permissions from Ref. 96).*

POCs have also been utilised in molecular separations between small organic molecules — the ability to target separations of specific compounds is based on the cavity size of the selected cage. Cooper and co-workers investigated a series of imine POCs for "molecular shape-sorting".[98] **CC1**, **CC3** and **CC5** exhibited solid-state separation of C9 structural isomers (mesitylene and 4-ethyltoluene) — whilst

mesitylene could not diffuse through the **CC3** windows, the more linear 4-ethyltoluene could be adsorbed.[98] In the same report, the methodology was adapted to liquid-chromatography (LC) using a column packed with **CC3** crystals. It was noted that whilst cage solubility is useful for processing and column loading, it would not be viable when carrying out the chromatography.[98] Therefore, choice of solvent is a key factor for further development in using POCs for LC, as well as the greater challenge of designing cages with tailored solubilities – one such example of effectively insoluble racemates is noted.[48]

A more recent development in the applications of POCs are porous liquids (PLs). First conceptualized in 2007,[99] the concept of PLs as "liquids with permanent porosity" presented an opportunity to develop porous materials beyond classic porous solids by introducing the characteristics of fluidity to novel porous materials. POCs present as ideal species for the formation of PLs, due to their discrete nature, ability to functionalise, permanent porosity, and solution processability. PLs can be categorised into 4 types (Figure 1.18):[100]

- **Type 1** – a neat, permanently porous liquid.
- **Type 2** – a molecular porous solid dissolved in a size-excluded solvent.
- **Type 3** – a porous framework dispersed within a size-excluded solvent.
- **Type 4** – a neat, meltable microporous extended frameworks

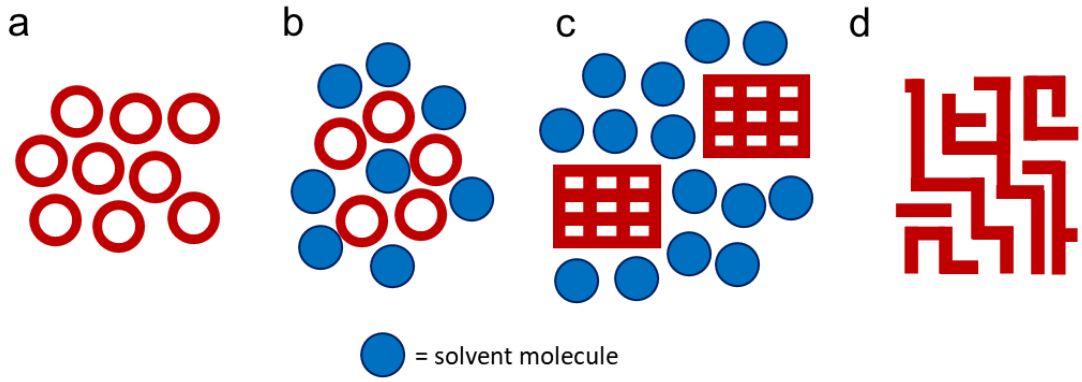

Figure 1.18 – Proposed classes of porous liquids: a) type 1 – a neat, permanently porous liquid; b) type 2 – a molecular porous solid dissolved in a size-excluded solvent; c) type 3 – a porous framework dispersed within a size-excluded solvent; d) a neat, microporous host that forms transient, strongly associated liquids.[100]

In 2014, Melaugh *et al.* reported the first attempt to realise type 1 PLs based on POCs. By decorating the cage periphery with a range of alkyl chains, they aimed to reduce the melting point of the cage such that the alkylated POC was a liquid at low temperatures. A range of cages functionalised with alkyl chains of varying lengths (C_8-C_{14}) were produced, with melting points as low as 40 °C recorded for long chain alkyl cages (*n*-C_5 to *neo*-C_{13}. However, the long alkyl chains can interpenetrate into the cavities of neighbouring cages, thus rendering the materials non-porous. This work was further built on by Giri *et al.* in a 2015 study outlining the first examples of type 2 PLs, again formed with the use of POCs.[101] Two distinct cage-based systems were used, although again, both were still based on the **CC** series. The first of these was a derivative that was periphery functionalised with crown-ether groups. The POC was dissolved in 15-crown-5 which, whilst viscous, was fluid enough for use and was unable to enter the cage cavity, ensuring the porosity was maintained in the liquid state. However, the poor scalability of this POC synthesis led to the development of an alternative PL system. The scrambled system was formed by the reaction of TFB with two vicinal diamines and could be easily scaled to form multigram quantities. A key feature afforded from this POC scrambling was the disorder introduced between the cages, leading to a much higher solubility than discrete cages formed using a single diamine. Subsequent dissolution in the size-excluded solvent hexachloropropene (PCP), again led to the formation of a type 2 PL.[101,102] Kearsey *et al*. further investigated the use of scrambled POCs in the formation of type 2 PLs using high-throughput methods, targeting both new cage systems and also an effective replacement for PCP as the size-excluded solvent.[103] Additionally, Kai et al. has outlined the production of type 3 PLs using a dispersion of POC nanocrystals formed using chiral recognition between the cages.[104] The presence of methyl or hydroxyl groups in structures of the cages used for nanocrystal formation allowed for tuning of the gas selectivity of the corresponding PL.[104]

In summary, POCs have been investigated for use in a range of applications, utilising the intrinsic and extrinsic porosity of the cages for function. The inherent structures of the cages can have a large impact on the properties such as porosity and solubility. Another key factor is the synthesis of the cages. Reversible methodologies are the most preferred for POC synthesis, due to their dynamic allowing for error-correction during bond-formation. However, cages formed using these methods often exhibit poor stability due to the nature of the bonding. Another option is that of irreversible bond-formation — the cages formed using these methods are inherently more stable,

but the syntheses can be more difficult due to the formation of mis aligned kinetic products and other species. An ideal POC would incorporate both the stability of irreversible methods, with the syntheses and higher conversions seen for reversible methods. One approach towards this goal is the use of post synthetic modification to improve the stability of cages formed reversibly.

1.4 Methods for improving cage stability

Save for few examples such as the stability of **CC3** in water,[105] cationic imine cages,[106] and rare examples of hydrazone-based cages,[107,108] DCvC methods yield cage materials that cannot be used in a wide range of conditions due to the inherent instability of the bonding used.[107–112] For example, for removal of SO_x or NO_x contaminants in flue gas streams, any adsorbent material would be expose to acidic, humid environments.[109] Materials formed using DCvC bond-formation such as imines or boronate esters could undergo decomposition under these environments. Additionally, the poor stability of the bonding would limit potential routes for post-synthetic modification which require harsh conditions.[112] Other than irreversible chemistries, another option for the creation of robust materials is the use of combined reversible-irreversible methods. The process typically involves the initial formation of a cage *via* a dynamic pathway, followed by irreversible conversion to a more stable form.

One such method is the reduction of cages. In 2010, Jin *et al*. reported the first instance of reduction of an imine cage to its amine analogue (Figure 1.19).[92] Following this, Mastalerz and co-workers reported the successful reduction of salicylimine-based cages, for use in CO_2/CH_4 adsorption,[55] and molecular sensing.[58] Cooper and co-workers also reported reduction of cage **CC1** to its amine form **RCC1** — this allowed *N*-functionalisation of the cages and use of the reduced cage as an organic linker for MOF formation,[113] and a substrate for the formation of dendritic dodecaamide cages.[114] All these studies reported increased robustness for the amine cages, with the ability to withstand extended periods in aqueous, acidic, and basic media. These studies exhibited imine reduction as a straightforward method for improving cage stability across a range of substrates of different size and structure. In a number of these reports, a major drawback imine of reduction became clear. The increased flexibility of the amine bond caused the reduced cages to be less rigid with

respect to their parent cages — this flexibility led to a loss of shape-persistence, and a loss of porosity as a result.

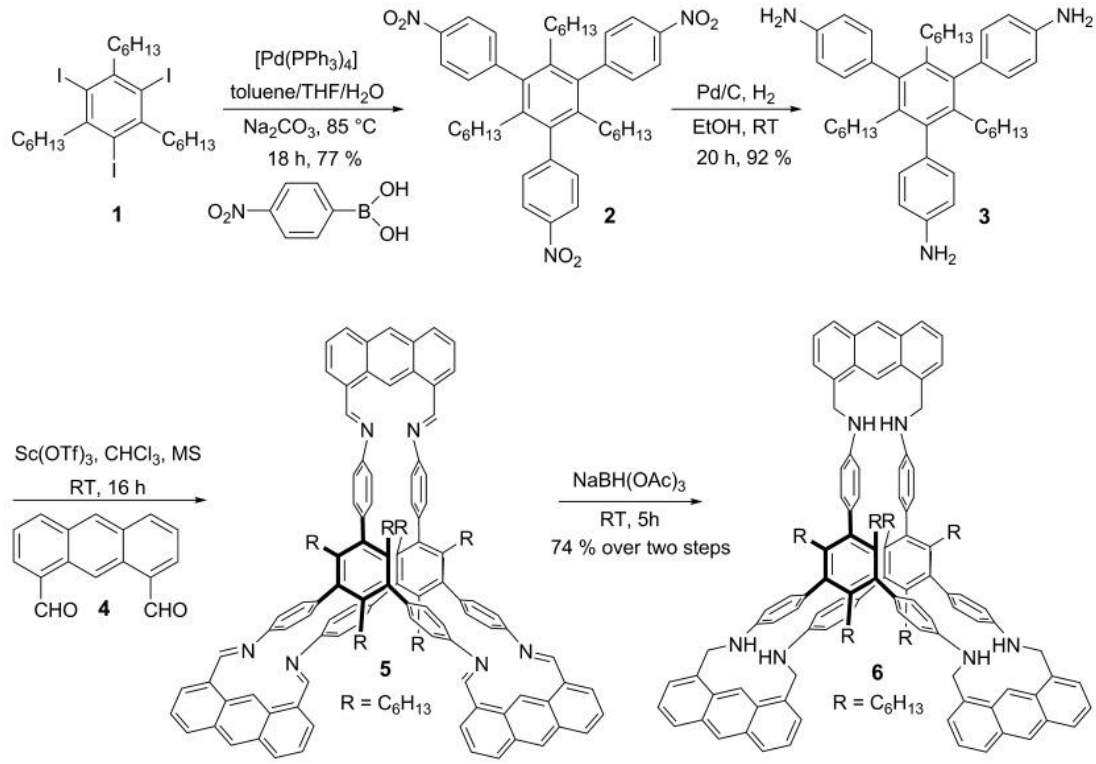

Figure 1.19 – Synthesis of a triamine precursor, imine cage formation and imine cage reduction to the amide derivative as repoted by Jin et al.[92] *MS – molecular sieves, TF – trifluoromethanesulfonyl (reproduced with permissions from Ref. 92).*

In 2014, Liu, *et al*. reported methodology to deal with loss of shape-persistence by the tying of the reduced cage vertices by reaction with small carbonyl molecules, forming aminal bridges.[111] Studying **RCC3**, formed by the reduction of **CC3** (Figure 1.20), Liu *et al.* showed that the tying of the vertices rigidifies the cage, maintaining shape-persistence on desolvation, and preserving some porosity in the reduced form. The number of vertices tied varied based on the molecule used. When acetone was used, forming **AT-RCC3**, one cage vertex was tied by for this rigidified **AT-RCC3** relative to **RCC3**, but the cage did not remain shape-persistent. By using the smaller formaldehyde instead of acetone, all 6 cage vertices could be tied to form **FT-RCC3**. This yielded a porous structure which had improved stability compared to the imine parent cage — no chemical decomposition, loss of crystallinity, or loss of porosity was reported following soaking in acidic or basic media.[111] Subsequiently, Liu *et al.* later outlined a method for tuning the internal cavities by tying of individual vertices with

different molecules, resulting in the formation of hybrid materials for H_2/D_2 quantum sieving.[115]

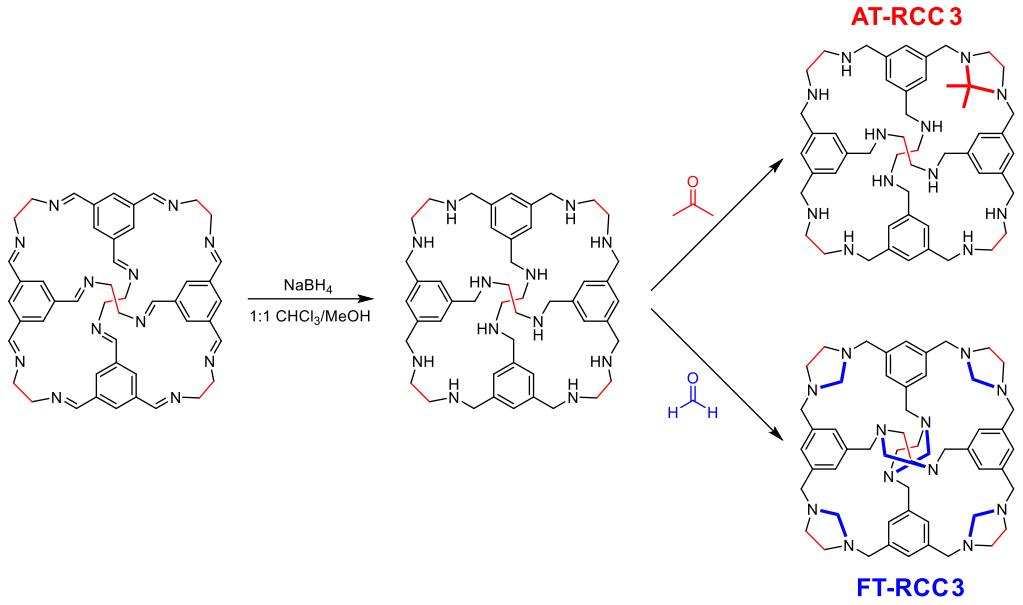

Figure 1.20 – Method for regaining cage porosity of reduced cages by "tying" of cage vertices as reported by Liu et al.[111] *More cage vertices can be tied when using the comparatively smaller formaldehyde.*

Mastalerz and co-workers also utilised cage tying for modification of triptycene-based amine cages.[110] These cages did not contain vicinal diamines as in **CC** series cages, but were functionalised with OH groups adjacent to the amine, and reaction with carbonyldiimidazole (CDI) formed 6 membered carbamate rings. As expected, the carbamate cage was stable over a large pH range, able to maintain crystallinity following treatment in acid. Whilst the cage was permanently porous, its small size limited its potential uses as a porous material, though this methodology could in principle be applied to larger cages, given the necessary functionalisation and structure was present. Mastalerz and co-workers also reported the conversion of imine cages to fully C-C bonded cages.[116] Full nitrosylation of amine cages allowed for reductive elimination by ring contraction — this afforded fully C-C bonded cages, though in some cases, partially reacted cage species were present in comparable amounts.[116] Use of this method with small **Tri^{2}Di^3** cages yielded the corresponding C-C cages in modest yield. Application to larger **Tri^{4}Di^6** cages resulted in much lower yield, though for certain structures these were comparative to existing, much more intensive syntheses.

An alternative method to post-synthetic modification is to build the transformation of linkages into the cage scaffold itself — one method for this is *via* keto-enol tautomerization. Banerjee and co-workers have utilised this methodology using triformylphloroglucinol (TPG).[117,118] After initial reversible imine formation on reaction with a suitable amine, the resultant structure can tautomerize to a more stable keto form with amine linkages (Figure 1.21). The second step is effectively irreversible, and "locks" the structure into the more robust keto-form. In 2017, Banerjee and co-workers reported a series of **Tri^{2}Di^3** cages formed by this tautomerization method.[117] Whilst only moderate surface areas were reported for this series compared to other cages (ranging from 87-202 m^2g^{-1}), the tautomer cages exhibited high stability to water, acids and bases. No decomposition or loss of crystallinity was shown following soaking in acidic or basic solution, as well as no loss of porosity. Whilst some wider peaks were observed for PXRD patterns, it was theorised this may have been due to the incorporation of guests into the structure.[117]

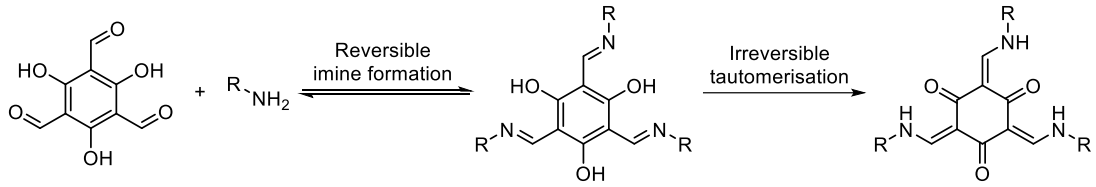

Figure 1.21 – General scheme for tautomerisation route employed by Banerjee and co-workers — reversible imine formation leads to an enol intermediate *which can undergo tautomerisation to a keto-species. This final step is irreversible, "locking" the structure into a stable form.*[117]

As discussed previously, the ideal POC would in incorporate the stability of irreversible systems, with the syntheses of reversible routes. Methods to improve stability with post-synthetic modification have been reported, and while the stability of the final materials can be greatly improved, the processes can inhibit the final properties of the cages. In addition, some methods are substrate specific, requiring additional functional groups or certain precursors. It would be beneficial to develop reversible bond-forming reactions with robust functionalities, to allow use in more straightforward cage synthesis. Introducing a dynamic nature to an existing irreversible bond-formation (e.g., through the applied reaction conditions) could result in for POC formation with a dynamic method as seen in DCvC methods, whilst forming robust, stable cage species without the need for post-synthetic modification. When

examining potential functional groups for a substrate, amides may act as a promising choice for further study.

1.5 Functional materials containing amide bonds

The inherent properties of amides make them ideal candidates for the synthesis of new, robust materials. The resonance structure of an amide leads to a partial-double bond character for the C-N bond imparting robustness and rigidity to the amide group (Figure 1.22),[112] leading to a high stability of the bond of up to ~400 kJmol^{-1}.[119] As a result, amides have seen widespread use in a range of applications including pharmaceuticals (>54% of marketed drugs),[120] and materials — linear polyamides such as nylon or Kevlar see widespread use across a range of applications.[121] Extended polyamide structures have been investigated as functional materials and can be differentiated based on their specific structures. For example, porous amide polymers have been utilised for CO_2 separation and storage.[122–124] In addition to these amorphous structures, crystalline COFs incorporating amides have also been reported both by direct synthesis, and by processing and post-synthetic modification of amorphous polymers.[125,126]

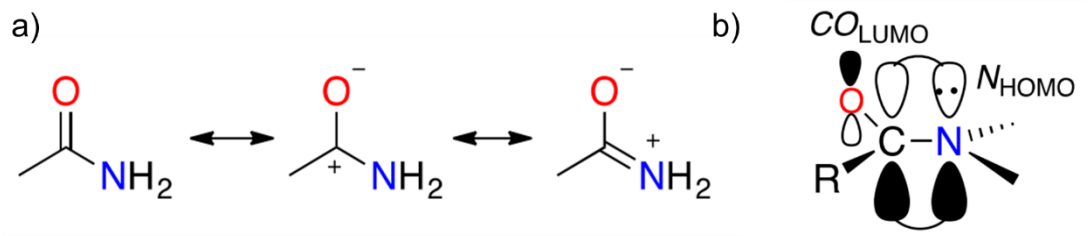

Figure 1.22 – Structure of the amine bond: a) resonance forms of the amide group, showing double bond character for the C-N bond; b) the interaction between the HOMO of the amide nitrogen and the LUMO of the carbonyl group — this interaction gives rise to the resonance structures of the bond (reproduced with permissions from Ref. 127).[127]

Most existing amide materials were formed using classical amide synthesis, *i.e.,* the reaction of a carboxylic acid, or suitable derivative, with a desired amine. However, the irreversible nature of this bond-forming presents a problem when applying this to more complex molecular structures, such as cages. Compared to the reversible DCvC methods described previously, amide formation has no “error-correction” mechanism. Polymer/oligomer formation can be dominating in the reaction, resulting in low yields for the targeted materials. By carefully controlling reaction conditions or using

appropriate precursors, the syntheses can be adapted to attempt to improve these yields. Some of these methods will now be outlined, focusing primarily on amide cages/cage-like structures.

The impact of the irreversibility of the reaction is illustrated in a series of reports by Still and co-workers investigating amide cage structures as peptide receptors.[128–130] The initial report in 1993 used the overall reaction between trimesic acid and *R,R*-CHDA to form the corresponding amide receptor (an amide analogue of the later reported **CC3**).[128] An alternative route using 1,3,5-benzenetricarbonyl trichloride and *R,R*-CHDA led to the cage being formed in a low yield of 13% — additionally, isolation of the cage required separation from a complex mixture of misaligned and oligomeric side-products. Higher yields of 39% were achieved for this process by employing a highly pre-configured precursor – a protected oligomer was first synthesized which, following deprotection, could dimerise to give the amide cage.[130]

Whilst the reports of Still and co-workers clearly detail these formation effects (particularly in **CC** series-type structures), the synthesis of amide cage-like structures predates these studies by a decade. Some earlier studies also outlined how precursor pre-configuration could have major effects on product formation. A 1984 report by Vogtle and co-workers outlines the synthesis of a series of **Tri$_2$Di$_3$** amide cages for metal complexation, produced by the overall coupling of a ditopic acid chloride and tritopic amine under high-dilution conditions (Figure 1.23a).[131] Unsurprisingly, direct reaction of these components results in production of the cage in only 1.5% yield. This was improved by first forming a preconfigured tris(acid chloride), followed by a final cage-closing step to form the target in 13% yield (Figure 1.23b). This variation in the final yield, dependant on direct coupling *vs* the use of preconfigured synthons, was also exhibited in a number of later reports by Vogtle and co-workers on a range of amide cages of different size and structure.[132]

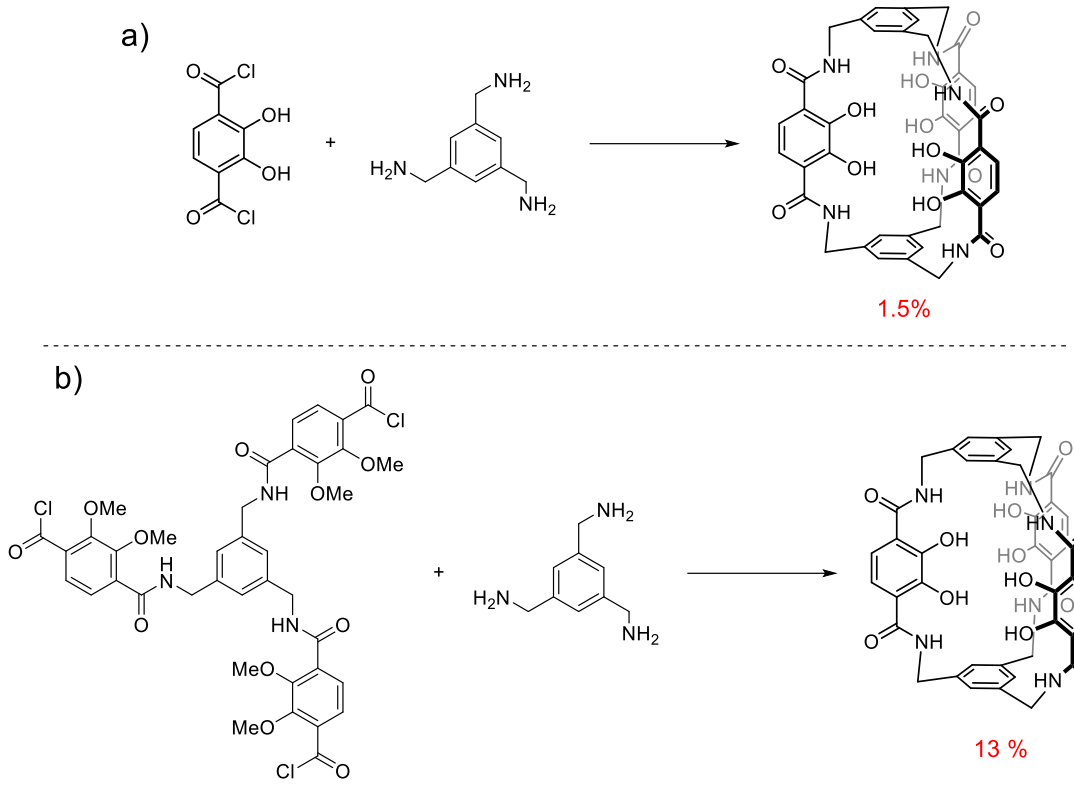

Figure 1.23 - Synthesis of amide cage by Kiggen and Vogtle: a) direct reaction of a ditopic acid chloride and triamine under high-dilution conditions, resulting in very low yields of the target cage; b) use of a highly-preorganised triamide building block in combination with the same triamine resulted in much improved yields in the synthesis of the target cage.[131]

McMurry and co-workers later reported the synthesis of an analogous cage to that of Vogtle, formed by the reaction of a similar ditopic acid chloride with tris(2-aminoethyl)amine (TREN) as the “capping” amine.[133] Again, high dilution methods resulted in poor yields — an alternative procedure described the use of transition metal ions as templating agents within the synthesis.[133] Templating allowed complexation of three functionalised catechol synthons around a metal centre, followed by capping with TREN (Figure 1.24). Pre-configuration resulted in a much higher yield of 70% for the cage forming process. Whilst this methodology is excellent for improving yield, the key drawback with this approach is the potential for metal ions to remain present in the material – this could present issues dependant on the required application.

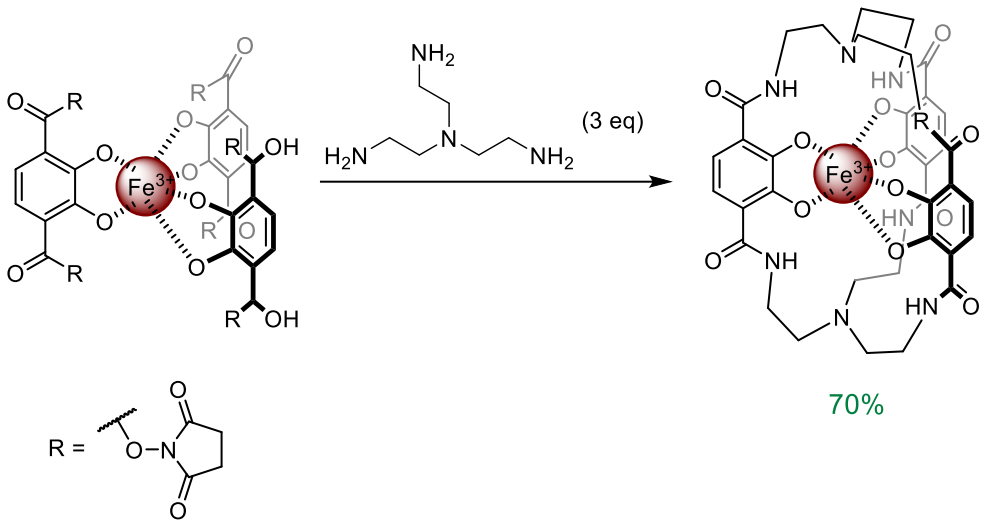

Figure 1.24 – Synthesis of amide cage by McMurry et al, utilising Fe^{3+} templating of catechol precursors to improve reaction yield.[133]

Expanding on a 1998 report,[134], Davis and co-workers subsequently outlined the use of a protected macrocyclic precursor in the synthesis of an amide cage (Figure 1.25).[135] Whilst the final cage forming step proceeded in a promising yield of 62%, the overall synthetic route was 9 individual steps required before the final cage formation, with an overall yield for the process of only 2%.[135] Although the methodology was successful in producing the targeted amide-derived cage, the complexity of the synthesis means it would be difficult to expand its applicability across large families of cage structures, especially compared to current DCvC methods.

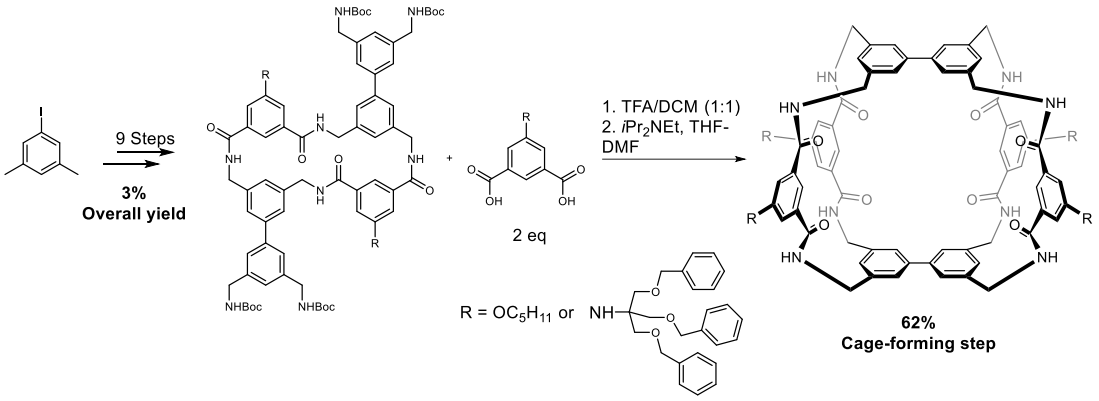

Figure 1.25 – Final step in the synthesis of amide cage by Davis et al.; a protected macrocycle (from a previous 9-step route) undergoes deprotection and reaction to form the target cage in good yield.[134]

Due to the small number of reported amide cages, it can be useful to study other classes of amide-containing materials for further insight into their syntheses — one such example are some amide macrocycles. In a series of studies, Leigh and co-workers reported the synthesis of a family of amide macrocycles, while also investigating how yields and product compositions changed by varying the synthetic approach. A key study focused on a **Di^{2}Di^2** macrocycle, the formation of which had previously been investigated by the direct reaction of isophthaloyl chloride and *p*-xylyenediamine.[136] The major product (and the only product able to be isolated) was the [2]catenane derivative (Figure 1.26). The desired macrocycle, whilst still formed, was only present in small amounts, and trapped within a complex mixture of side products.

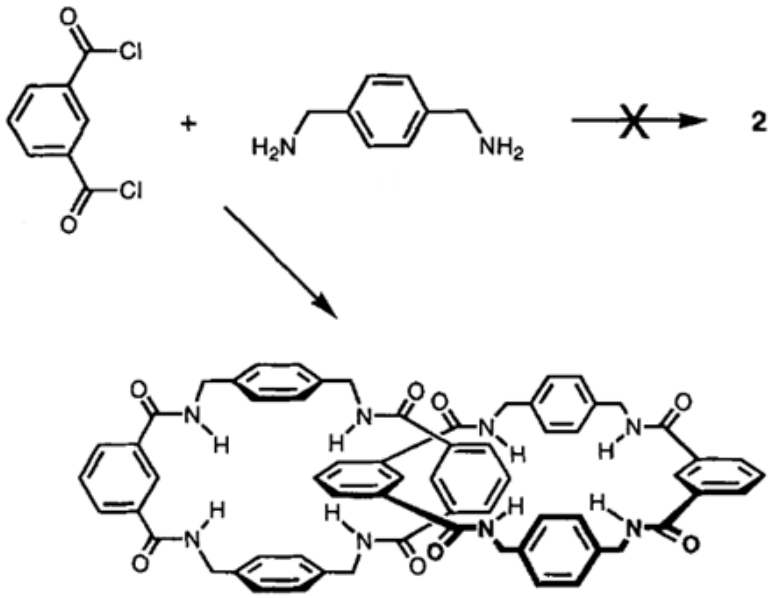

*Figure 1.26 – Attempted **Di^{2}Di^2** macrocycle formation as reported by Johnston et al.*[136] *— only the [2]catenane is found to form, doing so in 20% yield. Reaction conditions: Et_3N (4 eq) , anhydrous $CHCl_3$ (reproduced with permissions from Ref. 136).*[136]

Following this, Leigh and co-workers utilised a rotaxane de-threading route for direct formation of a similar **Di^{2}Di^2** macrocycle using analogous precursors.[137] Use of a suitable thread allowed templating of the macrocycle formation, yielding a [2]rotaxane — this could then be de-threaded *via* transesterification of the rotaxane thread, leading to precipitation of the macrocycle (Figure 1.27). This process is much improved compared to reaction of just the starting components, though the crude

rotaxane was only produced in a 28% yield, and in addition to the unreacted thread, the [2]catenane and other oligomers and side-products were still present. Whilst this method was useful for improving the yield, it is clearly specific to this type of system, and the increased complexity of the overall procedure would perhaps not be highly applicable when attempting to design large families of new cage-like materials.

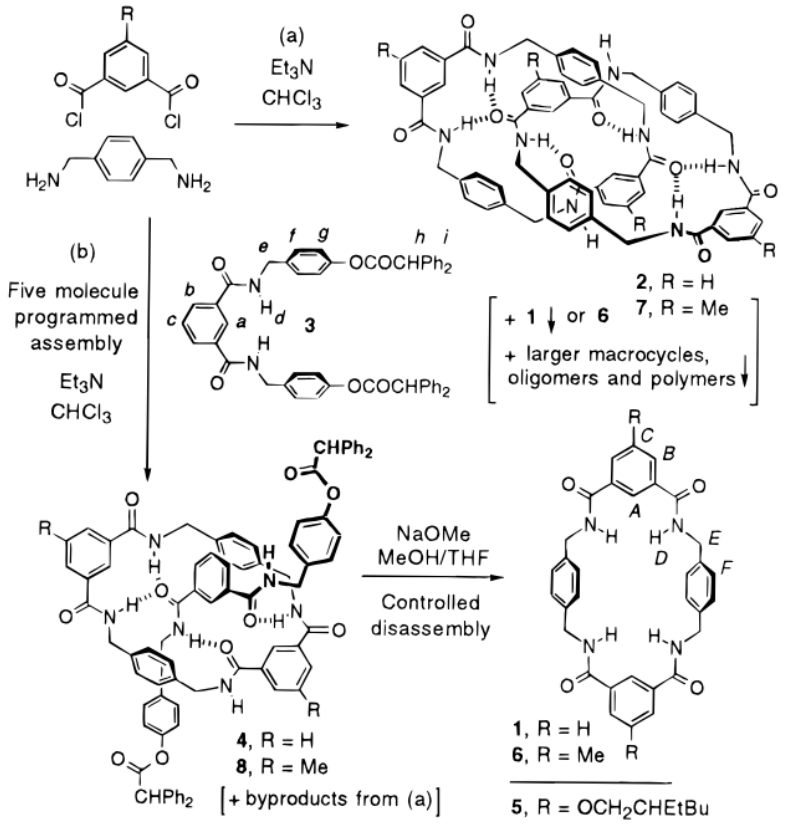

Figure 1.27 – Macrocycle synthesis by rotaxane formation and de-threading, as reported by Johnston et al. (reproduced with permissions from Ref. 137).[137]

In comparison to materials formed using dynamic bond-forming routes, there are still very few examples of amide-based molecular materials, and almost no amide-based POCs – many of the amide cages discussed were not tested for porosity or surface area. In addition, a high proportion of these cages are comparatively small (*i.e.,* **Tri^{2}Di^3** or smaller). In their high-throughput cage study, Greenaway *et al*. noted how computational modelling of similar **Tri^{2}Di^3** imine cages found these species would have cavities too small to accommodate guests.[28] As such, it is likely the **Tri^{2}Di^3** amide cages discussed would exhibit very low, if any, porosity. The underdevelopment of this area presents a lucrative target for further study. The robustness of the amide

group could allow for formation of novel porous cages with increased stability compared to some existing POCs formed using reversible methodologies. This could allow for application under more harsh environments (*e.g.*, large pH range), increasing the potential range of uses.

One potential route to realise novel amide-based POCs is to develop new amide bond-forming reactions – it may be possible to improve the reversibility of amide formation such that the process becomes dynamic, allowing application to materials synthesis akin to existing DCvC methodologies. Important steps have already been made in this area. Recently, Erguven and co-workers reported a novel route to amide formation by the reaction of functionalised imines with acid chlorides to form α-chloroamides (Figure 1.28).[119] Previous studies had shown that the formation of these α-chloroamides "…while rapid, was incomplete…", leading them to believe that the process may have been reversible – a concept hypothesised in other reports, but not studied thoroughly.

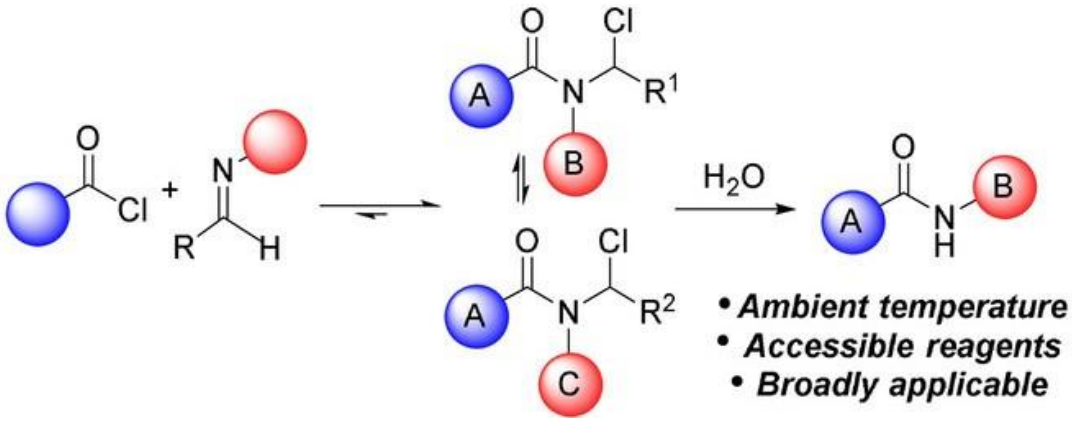

Figure 1.28 – General scheme for dynamic amide formation using imides, as outlined by Erguven et al. (reproduced with permissions from Ref. 119).[119]

To investigate, Erguven *et al*. initially studied a model reaction for amide formation and found that both the forward and reverse reactions could be initiated under ambient conditions, assessing that the system was dynamic, with a bias towards the amide product. Further testing developed the system further, investigating control of equilibrium by varying solvent, temperature, concentration, and structure (both by altering the halide and substituents of the precursors). It was found that manipulating these parameters could shift the equilibrium from quantitative amide formation, to favouring of the reverse reaction in certain cases. In addition to dynamic exchange

and formation of secondary and tertiary products, Erguven *et al*. also showed hydrolysis of the α-chloroamides to effectively "trap target amides" – this led to application in the synthesis of a range of small macrocycles of varying structure. Erguven *et al*. also note the synthesis of small amide **Di^{1}Di^{1}Di^{1}** cages, which would almost certainly be non-porous due to their size.[119]

Whilst this study is an important step in developing dynamic amide formation, it does still have its limitations. Additionally, whilst this methodology was successfully applied to small materials synthesis, the potential need for functionalised precursors may make it difficult to adapt to larger, more complex synthetic targets, or derivatization to larger families of species. Further, whilst the yields for small macrocycles and cages were high in comparison to prior reports, an increase in topicity may present an issue for larger targets, *i.e.,* hydrolysis of twelve chloride groups (such as a [4+6] cage) vs two chloride groups (as reported by Erguven *et al*.[119]). Moving forward, it would be useful to develop methodologies to allow direct synthesis of amide materials (such as cages) from small, simple precursors. This could allow the use of a wide range of pre-existing amides to attempt to form new families of cages, in addition to avoiding the need for large, complex (or highly preorganised) precursors as discussed previously. It may also be possible to develop existing chemistry by altering reaction conditions, such that the system becomes "dynamic enough" to promote cage formation. In their study, Erguven *et al*. cite a limited number of existing studies into reversible amide formation, including a series of investigations by Stahl and co-workers focusing on transamidation reactions. Transamidation is a well-documented and understood process for amide formation. Considering this, and the work of reversible transamidation by Gellman and Stahl, transamidation present as a potential methodology for further study, *i.e.*, development of transamidation to function as a route for more straightforward formation of robust materials.

This chapter has outlined existing work into porous organic cages including the inherent properties of these porous molecular solids, and some of the applications in which they have been utilised. Of great importance is the synthesis of these cages — the most popular routes for cage formation involve the use of reversible bond-formation with its inherent error-correction, allowing for high yielding processes. Unfortunately, cages formed this way can often have stability issues due to the reversible nature of the bonding. Whilst irreversible routes provide more robust cages, the syntheses of these structures are often more difficult due to the nature of the bond-formation. Additionally, post-synthetic modification has already been utilised to

transform cages to a more stable form. Whilst there are limitations in existing methods, alternative routes could provide more useful methods for providing increased stability. Finally, the synthesis and properties of a cage can be heavily influenced by the precursors used in its formation. It may therefore be possible to impart useful traits, such as stability, using functionalised precursors, while still allowing for dynamic formation of the cages. Accessing more robust cages using a dynamic synthesis would be an ideal methodology for stable cage formation.

1.6 Aims and Objectives

Reviewing the literature shows that while POCs have seen much development in recent years (particularly those formed using reversible bond-formation), there is a need for investigation into the formation of more stable structures. This thesis describes studies into a range of methods for the formation of more robust, amide-based organic materials, primarily focusing on the synthesis of porous amide cages. Initially studies focused on developing a synthetic methodology for the direct synthesis of amide-based cages. This focus later shifted to applying post-synthetic modification of existing imine structures, and finally the targeted synthesis of cages using functionalised precursors.

Chapter 2, *Promoting dynamic transamidation towards the synthesis of amide POCs,* presents the development of a methodology for dynamic transamidation using acid catalysis. A model system was first developed to optimise the transamidation reaction, followed by further investigation to better understand the catalytic process and product formation. These conditions were then applied in the attempted synthesis of amide cages based on known imine structures.

Chapter 3, *Targeting amide cages by the oxidation of imine precursors*, presents attempts to form amide cages based on the **CC** series by the post-synthetic modification of existing imine cages, using a reported methodology for imine cage oxidation.

Chapter 4, *Synthesis of part-amide Janus cages by social self-sorting*, presents the development of mixed amide-imine (part-amide) cages. These were targeted by combining known cage building blocks with new, amide-functionalised precursors using social self-sorting reactions. The precursor combinations were informed by molecular modelling of potential structures based on the prototypical cage **CC3**.

1.7 References

1 J. Rouquerol, D. Avnir, C. W. Fairbridge, D. H. Everett, J. M. Haynes, N. Pernicone, J. D. F. Ramsay, K. S. W. Sing and K. K. Unger, *Pure Appl. Chem.*, 1994, **66**, 1739–1758.

2 J. R. Holst, A. Trewin and A. I. Cooper, *Nat. Chem.*, 2010, **2**, 915–920.

3 R. Millini and G. Bellussi, 2017, pp. 1–36.

4 T. Hasell and A. I. Cooper, *Nat. Rev. Mater.*, 2016, **1**, 16053.

5 H. Furukawa, K. E. Cordova, M. O'Keeffe and O. M. Yaghi, *Science (80-.).*, , DOI:10.1126/science.1230444.

6 N. Stock and S. Biswas, *Chem. Rev.*, 2012, **112**, 933–969.

7 A. P. Côté, A. I. Benin, N. W. Ockwig, M. O'Keeffe, A. J. Matzger and O. M. Yaghi, *Science (80-.).*, 2005, **310**, 1166–1170.

8 K. Geng, T. He, R. Liu, K. T. Tan, Z. Li, S. Tao, Y. Gong, Q. Jiang and D. Jiang, *Chem. Rev.*, , DOI:10.1021/acs.chemrev.9b00550.

9 A. G. Slater and A. I. Cooper, *Science (80-.).*, 2015, **348**, aaa8075.

10 A. Thomas, *Angew. Chemie - Int. Ed.*, 2010, **49**, 8328–8344.

11 T. Zhang, G. Xing, W. Chen and L. Chen, *Mater. Chem. Front.*, 2020, **4**, 332–353.

12 J. Jiang, Y. Zhao and O. M. Yaghi, *J. Am. Chem. Soc.*, 2016, **138**, 3255–3265.

13 M. A. Little and A. I. Cooper, *Adv. Funct. Mater.*, , DOI:10.1002/adfm.201909842.

14 J. L. Atwood, L. J. Barbour, A. Jerga and B. L. Schottel, *Science (80-.).*, 2002, **298**, 1000–1002.

15 J. L. Atwood, L. J. Barbour and A. Jerga, *Science (80-.).*, 2002, **296**, 2367–2369.

16 S. Lim, H. Kim, N. Selvapalam, K. J. Kim, S. J. Cho, G. Seo and K. Kim, *Angew. Chemie - Int. Ed.*, 2008, **47**, 3352–3355.

17 K. Jie, M. Liu, Y. Zhou, M. A. Little, A. Pulido, S. Y. Chong, A. Stephenson, A. R. Hughes, F. Sakakibara, T. Ogoshi, F. Blanc, G. M. Day, F. Huang and A. I. Cooper, *J. Am. Chem. Soc.*, 2018, **140**, 6921–6930.

18 A. I. Joseph, S. H. Lapidus, C. M. Kane and K. T. Holman, *Angew. Chemie - Int. Ed.*, 2015, **54**, 1471–1475.

19 A. V. Leontiev and D. M. Rudkevich, *Chem. Commun.*, 2004, **4**, 1468–1469.

20 J. Tian, P. K. Thallapally, S. J. Dalgarno, P. B. McGrail and J. L. Atwood, *Angew. Chemie - Int. Ed.*, 2009, **48**, 5492–5495.

21 T. Tozawa, J. T. A. Jones, S. I. Swamy, S. Jiang, D. J. Adams, S. Shakespeare, R. Clowes, D. Bradshaw, T. Hasell, S. Y. Chong, C. Tang, S. Thompson, J. Parker, A. Trewin, J. Bacsa, A. M. Z. Slawin, A. Steiner and A. I. Cooper, *Nat. Mater.*, 2009, **8**, 973–978.

22 A. G. Slater, M. A. Little, A. Pulido, S. Y. Chong, D. Holden, L. Chen, C. Morgan, X. Wu, G. Cheng, R. Clowes, M. E. Briggs, T. Hasell, K. E. Jelfs, G. M. Day and A. I. Cooper, *Nat. Chem.*, 2016, **9**, 17.

23 M. E. Briggs and A. I. Cooper, *Chem. Mater.*, 2017, **29**, 149–157.

24 V. Santolini, M. Miklitz, E. Berardo and K. E. Jelfs, *Nanoscale*, 2017, **9**, 5280–5298.

25 P. Skowronek and J. Gawronski, *Org. Lett.*, 2008, **10**, 4755–4758.

26 Y. Jin, A. Jin, R. McCaffrey, H. Long and W. Zhang, *J. Org. Chem.*, 2012, **77**, 7392–7400.

27 K. E. Jelfs, X. Wu, M. Schmidtmann, J. T. A. Jones, J. E. Warren, D. J. Adams and A. I. Cooper, *Angew. Chemie Int. Ed.*, 2011, **50**, 10653–10656.

28 R. L. Greenaway, V. Santolini, M. J. Bennison, B. M. Alston, C. J. Pugh, M. A. Little, M. Miklitz, E. G. B. Eden-Rump, R. Clowes, A. Shakil, H. J. Cuthbertson, H. Armstrong, M. E. Briggs, K. E. Jelfs and A. I. Cooper, *Nat. Commun.*, 2018, **9**, 1–27.

29 J. C. Lauer, W. S. Zhang, F. Rominger, R. R. Schröder and M. Mastalerz, *Chem. - A Eur. J.*, 2018, **24**, 1816–1820.

30 M. W. Schneider, I. M. Oppel and M. Mastalerz, *Chem. - A Eur. J.*, 2012, **18**, 4156–4160.

31 T. P. Moneypenny, N. P. Walter, Z. Cai, Y. R. Miao, D. L. Gray, J. J. Hinman, S. Lee, Y. Zhang and J. S. Moore, *J. Am. Chem. Soc.*, 2017, **139**, 3259–3264.

32 D. P. Lydon, N. L. Campbell, D. J. Adams and A. I. Cooper, *Synth. Commun.*, 2011, **41**, 2146–2151.

33 M. J. Bojdys, M. E. Briggs, J. T. A. Jones, D. J. Adams, S. Y. Chong, M. Schmidtmann and A. I. Cooper, *J. Am. Chem. Soc.*, 2011, **133**, 16566–16571.

34 F. Gomollón-bel, *Chem. Int.*, 2019, **41**, 12–17.

35 M. E. Briggs, A. G. Slater, N. Lunt, S. Jiang, M. A. Little, R. L. Greenaway, T. Hasell, C. Battilocchio, S. V. Ley and A. I. Cooper, *Chem. Commun.*, 2015, **51**, 17390–17393.

36 B. D. Egleston, M. C. Brand, F. Greenwell, M. E. Briggs, S. James, A. Cooper, D. E. Crawford and R. Greenaway, *Chem. Sci.*, , DOI:10.1039/d0sc01858a.

37 K. E. Jelfs, E. G. B. Eden, J. L. Culshaw, S. Shakespeare, E. O. Pyzer-Knapp, H. P. G. Thompson, J. Bacsa, G. M. Day, D. J. Adams and A. I. Cooper, *J. Am. Chem. Soc.*, 2013, **135**, 9307–9310.

38 K. E. Jelfs and A. I. Cooper, *Curr. Opin. Solid State Mater. Sci.*, 2013, **17**, 19–30.

39 J. M. Lehn, *Essays Contemp. Chem. From Mol. Struct. Towar. Biol.*, 2007, 307–326.

40 S. J. Rowan, S. J. Cantrill, G. R. L. Cousins, J. K. M. Sanders and J. F. Stoddart, *Angew. Chemie Int. Ed.*, 2002, **41**, 898–952.

41 Y. Jin, C. Yu, R. J. Denman and W. Zhang, *Chem. Soc. Rev.*, 2013, **42**, 6634.

42 G. Zhang, O. Presly, F. White, I. M. Oppel and M. Mastalerz, *Angew. Chemie - Int. Ed.*, 2014, **53**, 5126–5130.

43 F. Beuerle and B. Gole, *Angew. Chemie - Int. Ed.*, 2018, 57, 4850–4878.

44 M. E. Belowich and J. F. Stoddart, *Chem. Soc. Rev.*, 2012, 41, 2003–2024.

45 J. T. A. Jones, T. Hasell, X. Wu, J. Bacsa, K. E. Jelfs, M. Schmidtmann, S. Y. Chong, D. J. Adams, A. Trewin, F. Schiffman, F. Cora, B. Slater, A. Steiner, G. M. Day and A. I. Cooper, *Nature*, 2011, **474**, 367–371.

46 T. Mitra, X. Wu, R. Clowes, J. T. A. Jones, K. E. Jelfs, D. J. Adams, A. Trewin, J. Bacsa, A. Steiner and A. I. Cooper, *Chem. - A Eur. J.*, 2011,

17, 10235–10240.

47 P. S. Reiss, M. A. Little, V. Santolini, S. Y. Chong, T. Hasell, K. E. Jelfs, M. E. Briggs and A. I. Cooper, *Chem. - A Eur. J.*, 2016, **22**, 16547–16553.

48 T. Hasell, S. Y. Chong, K. E. Jelfs, D. J. Adams and A. I. Cooper, *J. Am. Chem. Soc.*, 2012, **134**, 588–598.

49 M. Petryk, J. Szymkowiak, B. Gierczyk, G. Spólnik, Popenda, A. Janiak and M. Kwit, *Org. Biomol. Chem.*, 2016, **14**, 7495–7499.

50 Z. M. Wang, Y. Y. Cui, C. X. Yang and X. P. Yan, *ACS Appl. Nano Mater.*, 2020, **3**, 479–485.

51 H. X. Li, T. P. Xie, K. Q. Yan, S. M. Xie, B. J. Wang, J. H. Zhang and L. M. Yuan, *Microchim. Acta*, , DOI:10.1007/s00604-020-04252-4.

52 H. X. Li, T. P. Xie, S. M. Xie, B. J. Wang, J. H. Zhang and L. M. Yuan, *Chromatographia*, 2020, **83**, 703–713.

53 S. Jiang, Y. Du, M. Marcello, E. W. Corcoran, D. C. Calabro, S. Y. Chong, L. Chen, R. Clowes, T. Hasell and A. I. Cooper, *Angew. Chemie - Int. Ed.*, 2018, **57**, 11228–11232.

54 M. Mastalerz, *Chem. Commun.*, 2008, **0**, 4756.

55 M. Mastalerz, M. W. Schneider, I. M. Oppel and O. Presly, *Angew. Chemie - Int. Ed.*, 2011, **50**, 1046–1051.

56 M. W. Schneider, L. G. Lechner and M. Mastalerz, *J. Mater. Chem.*, 2012, **22**, 7113–7116.

57 M. W. Schneider, H. J. S. Hauswald, R. Stoll and M. Mastalerz, *Chem. Commun.*, 2012, **48**, 9861–9863.

58 M. Brutschy, M. W. Schneider, M. Mastalerz and S. R. Waldvogel, *Adv. Mater.*, 2012, **24**, 6049–6052.

59 M. Brutschy, M. W. Schneider, M. Mastalerz and S. R. Waldvogel, *Chem. Commun.*, 2013, **49**, 8398.

60 M. W. Schneider, I. M. Oppel, A. Griffin and M. Mastalerz, *Angew. Chemie - Int. Ed.*, 2013, **52**, 3611–3615.

61 R. Nishiyabu, Y. Kubo, T. D. James and J. S. Fossey, *Chem. Commun.*, 2011, **47**, 1124–1150.

62 N. Nishimura and K. Kobayashi, *Angew. Chemie - Int. Ed.*, 2008, **47**,

6255–6258.

63 N. Nishimura, K. Yoza and K. Kobayashi, *J. Am. Chem. Soc.*, 2010, **132**, 777–790.

64 K. Kataoka, S. Okuyama, T. Minami, T. D. James and Y. Kubo, *Chem. Commun.*, 2009, **1**, 1682–1684.

65 G. Zhang, O. Presly, F. White, I. M. Oppel and M. Mastalerz, *Angew. Chemie - Int. Ed.*, 2014, **53**, 1516–1520.

66 W. Zhang and J. S. Moore, *Angew. Chemie Int. Ed.*, 2006, **45**, 4416–4439.

67 Y. Jin, Q. Wang, P. Taynton and W. Zhang, *Acc. Chem. Res.*, 2014, **47**, 1575–1586.

68 M. Mastalerz, *Acc. Chem. Res.*, 2018, **51**, 2411–2422.

69 C. Zhang, Q. Wang, H. Long and W. Zhang, *J. Am. Chem. Soc.*, 2011, **133**, 20995–21001.

70 Q. Wang, C. Zhang, B. C. Noll, H. Long, Y. Jin and W. Zhang, *Angew. Chemie - Int. Ed.*, 2014, **53**, 10663–10667.

71 S. Lee, A. Yang, T. P. Moneypenny and J. S. Moore, *J. Am. Chem. Soc.*, 2016, **138**, 2182–2185.

72 T. P. Moneypenny, A. Yang, N. P. Walter, T. J. Woods, D. L. Gray, Y. Zhang and J. S. Moore, *J. Am. Chem. Soc.*, 2018, **140**, 5825–5833.

73 H. E. Högberg, B. Thulin and O. Wennerström, *Tetrahedron Lett.*, 1977, **18**, 931–934.

74 F. Vögtle, J. Gross, C. Seel and M. Nieger, *Angew. Chemie Int. Ed. English*, 1992, **31**, 1069–1071.

75 P. R. Ashton, N. S. Isaacs, F. H. Kohnke, G. S. D'Alcontres and J. F. Stoddart, *Angew. Chemie Int. Ed. English*, 1989, **28**, 1261–1263.

76 Z. Wu, S. Lee and J. S. Moore, *J. Am. Chem. Soc.*, 1992, **114**, 8730–8732.

77 C. Zhang and C. F. Chen, *J. Org. Chem.*, 2007, **72**, 9339–9341.

78 A. Avellaneda, P. Valente, A. Burgun, J. D. Evans, A. W. Markwell-Heys, D. Rankine, D. J. Nielsen, M. R. Hill, C. J. Sumby and C. J. Doonan, *Angew. Chemie - Int. Ed.*, 2013, **52**, 3746–3749.

79 A. Burgun, P. Valente, J. D. Evans, D. M. Huang, C. J. Sumby and C. J.

Doonan, *Chem. Commun.*, 2016, **52**, 8850--8853.

80 M. Kitchin, K. Konstas, M. L. Czyz, P. Valente, C. J. Sumby, M. R. Hill, A. Polyzos and C. J. Doonan, *Chem. Commun.*, 2015, **51**, 14231–14234.

81 J. L. Katz, K. J. Selby and R. R. Conry, *Org. Lett.*, 2005, **7**, 3505–3507.

82 C. Zhang, Z. Wang, L. Tan, T. L. Zhai, S. Wang, B. Tan, Y. S. Zheng, X. L. Yang and H. B. Xu, *Angew. Chemie - Int. Ed.*, 2015, **54**, 9244–9248.

83 Z. Wang, H. Ma, T. L. Zhai, G. Cheng, Q. Xu, J. M. Liu, J. Yang, Q. M. Zhang, Q. P. Zhang, Y. S. Zheng, B. Tan and C. Zhang, *Adv. Sci.*, 2018, **5**, 1800141.

84 G. Zhang and M. Mastalerz, *Chem. Soc. Rev.*, 2014, **43**, 1934–1947.

85 J. T. A. Jones, D. Holden, T. Mitra, T. Hasell, D. J. Adams, K. E. Jelfs, A. Trewin, D. J. Willock, G. M. Day, J. Bacsa, A. Steiner and A. I. Cooper, *Angew. Chemie Int. Ed.*, 2011, **50**, 749–753.

86 T. Hasell, J. L. Culshaw, S. Y. Chong, M. Schmidtmann, M. A. Little, K. E. Jelfs, E. O. Pyzer-Knapp, H. Shepherd, D. J. Adams, G. M. Day and A. I. Cooper, *J. Am. Chem. Soc.*, 2014, **136**, 1438–1448.

87 S. Jiang, J. T. A. Jones, T. Hasell, C. E. Blythe, D. J. Adams, A. Trewin and A. I. Cooper, *Nat. Commun.*, 2011, **2**, 207.

88 A. G. Slater, M. A. Little, M. E. Briggs, K. E. Jelfs and A. I. Cooper, *Mol. Syst. Des. Eng.*, 2018, **3**, 223–227.

89 T. Hasell, M. A. Little, S. Y. Chong, M. Schmidtmann, M. E. Briggs, V. Santolini, K. E. Jelfs and A. I. Cooper, *Nanoscale*, 2017, **9**, 6783–6790.

90 P. Li, S. Xu, C. Yu, Z. Y. Li, J. Xu, Z. M. Li, L. Zou, X. Leng, S. Gao, Z. Liu, X. Liu and S. Zhang, *Angew. Chemie - Int. Ed.*, 2020, **59**, 7113–7121.

91 S. Jiang, K. E. Jelfs, D. Holden, T. Hasell, S. Y. Chong, M. Haranczyk, A. Trewin and A. I. Cooper, *J. Am. Chem. Soc.*, 2013, **135**, 17818–17830.

92 Y. Jin, B. A. Voss, R. D. Noble and W. Zhang, *Angew. Chemie - Int. Ed.*, 2010, **49**, 6348–6351.

93 Y. Jin, B. A. Voss, A. Jin, H. Long, R. D. Noble and W. Zhang, *J. Am. Chem. Soc.*, 2011, **133**, 6650–6658.

94 T. Hasell, M. Miklitz, A. Stephenson, M. A. Little, S. Y. Chong, R. Clowes, L. Chen, D. Holden, G. A. Tribello, K. E. Jelfs and A. I. Cooper, *J. Am. Chem. Soc.*, 2016, **138**, 1653–1659.

95 L. Chen, P. S. Reiss, S. Y. Chong, D. Holden, K. E. Jelfs, T. Hasell, M. A. Little, A. Kewley, M. E. Briggs, A. Stephenson, K. M. Thomas, J. A. Armstrong, J. Bell, J. Busto, R. Noel, J. Liu, D. M. Strachan, P. K. Thallapally and A. I. Cooper, *Nat. Mater.*, 2014, **13**, 954–960.

96 Q. Song, S. Jiang, T. Hasell, M. Liu, S. Sun, A. K. Cheetham, E. Sivaniah and A. I. Cooper, *Adv. Mater.*, 2016, **28**, 2629–2637.

97 Z. Zhai, C. Jiang, N. Zhao, W. Dong, P. Li, H. Sun and Q. J. Niu, *J. Memb. Sci.*, 2020, **595**, 117505.

98 T. Mitra, K. E. Jelfs, M. Schmidtmann, A. Ahmed, S. Y. Chong, D. J. Adams and A. I. Cooper, *Nat. Chem.*, 2013, **5**, 276–281.

99 N. O'Reilly, N. Giri and S. L. James, *Chem. - A Eur. J.*, 2007, **13**, 3020–3025.

100 B. D. Egleston, A. Mroz, K. E. Jelfs and R. L. Greenaway, *Chem. Sci.*, 2022, **13**, 5042–5054.

101 N. Giri, M. G. Del Pópolo, G. Melaugh, R. L. Greenaway, K. Rätzke, T. Koschine, L. Pison, M. F. C. Gomes, A. I. Cooper and S. L. James, *Nature*, 2015, **527**, 216–220.

102 R. L. Greenaway, D. Holden, E. G. B. Eden, A. Stephenson, C. W. Yong, M. J. Bennison, T. Hasell, M. E. Briggs, S. L. James and A. I. Cooper, *Chem. Sci.*, 2017, **8**, 2640–2651.

103 R. J. Kearsey, B. M. Alston, M. E. Briggs, R. L. Greenaway and A. I. Cooper, *Chem. Sci.*, 2019, **10**, 9454–9465.

104 A. Kai, B. D. Egleston, A. Tarzia, R. Clowes, M. E. Briggs, K. E. Jelfs, A. I. Cooper and R. L. Greenaway, *Adv. Funct. Mater.*, , DOI:10.1002/adfm.202106116.

105 T. Hasell, M. Schmidtmann, C. A. Stone, M. W. Smith and A. I. Cooper, *Chem. Commun.*, 2012, **48**, 4689.

106 Y. Lei, Q. Chen, P. Liu, L. Wang, H. Wang, B. Li, X. Lu, Z. Chen, Y. Pan, F. Huang and H. Li, *Angew. Chemie - Int. Ed.*, 2021, **60**, 4705–4711.

107 X. Zheng, Y. Zhang, G. Wu, J.-R. Liu, N. Cao, L. Wang, Y. Wang, X. Li,

X. Hong, C. Yang and H. Li, *Chem. Commun.*, 2018, **54**, 3138–3141.

108 M. Yang, F. Qiu, E. S. M. El-Sayed, W. Wang, S. Du, K. Su and D. Yuan, *Chem. Sci.*, 2021, **12**, 13307–13315.

109 F. Rezaei, A. A. Rownaghi, S. Monjezi, R. P. Lively and C. W. Jones, *Energy and Fuels*, 2015, **29**, 5467–5486.

110 X.-Y. Hu, W.-S. Zhang, F. Rominger, I. Wacker, R. R. Schröder and M. Mastalerz, *Chem. Commun.*, 2017, **53**, 8616–8619.

111 M. Liu, M. A. Little, K. E. Jelfs, J. T. A. Jones, M. Schmidtmann, S. Y. Chong, T. Hasell and A. I. Cooper, *J. Am. Chem. Soc.*, 2014, **136**, 7583–7586.

112 A. S. Bhat, S. M. Elbert, W.-S. Zhang, F. Rominger, M. Dieckmann, R. R. Schröder and M. Mastalerz, *Angew. Chemie Int. Ed.*, 2019, 1–6.

113 S. I. Swamy, J. Bacsa, J. T. A. Jones, K. C. Stylianou, A. Steiner, L. K. Ritchie, T. Hasell, J. A. Gould, A. Laybourn, Y. Z. Khimyak, D. J. Adams, M. J. Rosseinsky and A. I. Cooper, *J. Am. Chem. Soc.*, 2010, **132**, 12773–12775.

114 J. L. Culshaw, G. Cheng, M. Schmidtmann, T. Hasell, M. Liu, D. J. Adams and A. I. Cooper, *J. Am. Chem. Soc.*, 2013, **135**, 10007–10010.

115 M. Liu, L. Zhang, M. A. Little, V. Kapil, M. Ceriotti, S. Yang, L. Ding, D. L. Holden, R. Balderas-Xicohténcatl, D. He, R. Clowes, S. Y. Chong, G. Schütz, L. Chen, M. Hirscher and A. I. Cooper, *Science (80-.).*, 2019, **366**, 613–620.

116 T. H. G. Schick, J. C. Lauer, F. Rominger and M. Mastalerz, *Angew. Chemie - Int. Ed.*, 2019, **58**, 1768–1773.

117 S. Bera, A. Basu, S. Tothadi, B. Garai, S. Banerjee, K. Vanka and R. Banerjee, *Angew. Chemie - Int. Ed.*, 2017, **56**, 2123–2126.

118 S. Kandambeth, A. Mallick, B. Lukose, M. V Mane, T. Heine and R. Banerjee, *J. Am. Chem. Soc.*, 2012, **134**, 19524–19527.

119 H. Erguven, E. N. Keyzer and B. A. Arndtsen, *Chem. – A Eur. J.*, 2020, 1–9.

120 S. D. Roughley and A. M. Jordan, *J. Med. Chem.*, 2011, **54**, 3451–3479.

121 J. A. Reglero Ruiz, M. Trigo-López, F. C. García and J. M. García, *Polymers (Basel).*, , DOI:10.3390/polym9090414.

122 S. Zulfiqar, M. I. Sarwar and C. T. Yavuz, *RSC Adv.*, 2014, **4**, 52263–52269.

123 V. M. Suresh, S. Bonakala, H. S. Atreya, S. Balasubramanian and T. K. Maji, *ACS Appl. Mater. Interfaces*, 2014, **6**, 4630–4637.

124 N. Manoranjan, D. H. Won, J. Kim and S. I. Woo, *J. CO2 Util.*, 2016, **16**, 486–491.

125 D. Stewart, D. Antypov, M. S. Dyer, M. J. Pitcher, A. P. Katsoulidis, P. A. Chater, F. Blanc and M. J. Rosseinsky, *Nat. Commun.*, 2017, **8**, 1102.

126 M. M. Unterlass, *Angew. Chemie - Int. Ed.*, 2018, **57**, 2292–2294.

127 S. A. Glover and A. A. Rosser, *Molecules*, , DOI:10.3390/molecules23112834.

128 S. S. Yoon and W. C. Still, *J. Am. Chem. Soc.*, 1993, **115**, 823–824.

129 S. Soo Yoon and W. Clark Still, *Tetrahedron Lett.*, 1994, **35**, 2117–2120.

130 S. S. Yoon and W. C. Still, *Tetrahedron Lett.*, 1994, **35**, 8557–8560.

131 W. Kiggen and F. Vögtle, *Angew. Chemie Int. Ed. English*, 1984, **23**, 714–715.

132 F. Ebmeyer and F. Vögtle, *Angew. Chemie Int. Ed. English*, 1989, **28**, 79–81.

133 T. J. McMurry, S. J. Rodgers and K. N. Raymond, *J. Am. Chem. Soc.*, 1987, **109**, 3451–3453.

134 A. P. Davis and R. S. Wareham, *Angew. Chemie Int. Ed.*, 1998, **37**, 2270–2273.

135 T. J. Ryan, G. Lecollinet, T. Velasco and A. P. Davis, *Proc. Natl. Acad. Sci. U. S. A.*, 2002, **99**, 4863–4866.

136 A. G. Johnston, D. A. Leigh, R. J. Pritchard and M. D. Deegan, *Angew. Chemie Int. Ed. English*, 1995, **34**, 1209–1212.

137 A. G. Johnston, D. A. Leigh, A. Murphy, J. P. Smart and M. D. Deegan, *J. Am. Chem. Soc.*, 1996, **118**, 10662–10663.

Chapter 2

Promoting dynamic transamidation towards the synthesis of amide porous organic cages

2.1 Introduction

Classic amide synthesis generally consists of the direct reaction of an amine with a carbonyl derivative, *i.e.*, carboxylic acids or acid chlorides (Figure 2.1a).[1] For carboxylic acids, the process is not spontaneous and requires high temperatures to promote amide formation — alternatively, carboxylic acid derivatives with better leaving groups can be utilised under less forcing conditions. With the widespread use of amides through organic chemistry, materials, and in pharmaceuticals and drug discovery, developing alternative methods for amide synthesis is a key target moving forward. In particular, the dynamic formation of amides is an attractive target. In comparison to existing DCvC methods, where the final materials can exhibit poor stability due to the reversible nature of the formed bonds, dynamic formation of amides could allow for a more straightforward formation of analogous materials with increased robustness due to the increased strength of the amide bonding.

Recently, a report by Erguven *et al*. outlined a procedure for dynamic amide formation using imides.[1] This method focused on the reaction of acid chlorides with appropriate imine nucleophiles to form α-chloroamides (Figure 2.1b). It was noted from previous studies that while these condensations were rapid, they often did not react to completion, potentially indicating a degree of reversibility in the system. Development of this procedure confirmed dynamic amide formation, with the potential for equilibrium tuning by choice of reaction conditions. The procedure was generally used to form small organic structures; but Erguven *et al*. also used this method in the formation of amide macrocycles, although these structures were small and unlikely to exhibit any porosity.[1] More importantly, the requirement of imine nucleophiles could introduce difficulties if applied to more complex materials, *i.e.,* whilst commercially available imides were used in the report, other materials may require the independent formation of complex nucleophiles to allow use of this methodology. A potentially more useful development would be dynamic synthesis of amides directly from designed precursors – one potential synthetic route for this is transamidation.

a) *Classic amide synthesis*

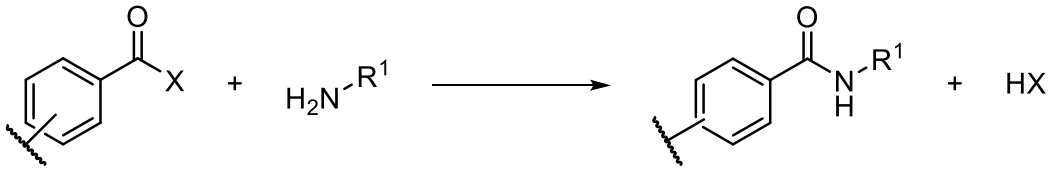

X = CO_2H, Cl

b) *Dynamic amide formation with imides (Erguven et al)*

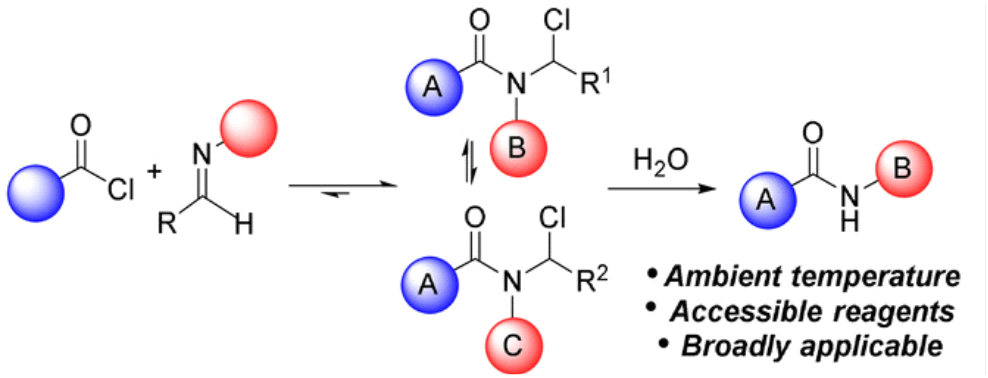

Figure 2.1 – Methods of amide synthesis: a) classical amide synthesis by the coupling of a carboxylic acid or acid chloride derivative with a suitable amine; b) general procedure for dynamic amide synthesis as reported by Erguven et al.[1] (reproduced with permissions from Ref. 1).

Transamidation describes the process of the reaction between an amide and an amine to form a new amide derivative. Following its initial report nearly 150 years ago,[2] this process was largely unexplored until a 1994 report by Bon *et al*. describing the first complete study of a direct transamidation process, using aluminium (III) chloride as a promoter.[3] Since then, transamidation has seen much development with numerous studies, many focusing on the use of catalysis to further develop the transamidation process. A wide variety of catalysts of varying structures have been employed, including acids,[4,5] small organic molecules,[6,7] inorganic salts,[8–10] metal complexes,[11–13] and zeolites.[14]

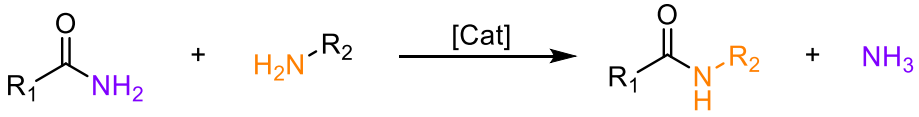

Figure 2.2 – General procedure for the catalysed transamidation of a primary amide with a new primary amine — this forms a new secondary amide, liberating ammonia in the process.

In general, previous studies have applied transamidation in the formation of small organic structures. As such, there are two common themes that appear through many of the studies:

1. The use of monofunctional amides as a substrate

2. The use of primary or basic secondary amides as the substrate, *i.e*., minimal or no *N*-substitution

The latter of these is a key feature of many of the processes. The use of a primary amide results in the loss of ammonia or a similar small amine during the transamidation process, providing a driving force for the reaction through the loss of a gaseous or volatile liquid amine. Whilst this is suitable when targeting small molecules or intermediates for further reaction, this method would not be desirable in the formation of materials. For materials synthesis, multitopic amides would be necessary as precursors, in addition to the need for transamidation of more complex, substituted amides and amines.

However, whilst this is the norm for the majority of transamidation reports, there are notable exceptions. Stahl and Gellman have reported several advances in transamidation using more complex, substituted amides. An initial 2003 study by Eldred *et al*. reported the catalytic transamidation of monofunctional, phenyl-substituted amides.[11] A range of catalysts were initially screened, focusing on Lewis acidic metal complexes and a range of metal-amides. Eldred *et al*. initially focused on a thermodynamically favoured direct transamidation reaction.[11] Targeting long-term use in dynamic covalent chemistry, focus then shifted to investigating exchange in a system with no thermodynamic driving force. Equilibrium transamidation was investigated using an analogous model system used for catalyst screening – amide substituents were varied, along with a small selection of catalysts, whilst gas chromatography (GC) was utilised to track the elimination and formation of the present amide species. Both the forward and reverse reactions were tested, targeting the same product distribution to show that equilibrium was achieved (Figure 2.3). Utilising $Al_2(NMe)_6$ as a catalyst provided the correct product ratios – this could also be adapted to use *N*-aryl amides as nucleophiles by employing $Ti(NMe)_6$ as the catalyst.[11] $Ti(NMe)_6$ was also utilised in mechanistic studies to investigate transamidation versus amidine formation.[15]

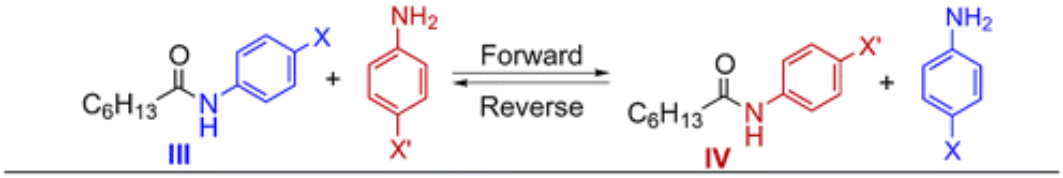

	X	X'	Catalyst	Amide Ratio (III/IV)[b] Forward	Reverse
1	H	CH_3	$Sc(OTf)_3$	98/2	1/99
			$Ti(NMe_2)_4$	**42/58**	**42/58**
			$Al_2(NMe_2)_6$	65/35	43/57

Figure 2.3 – Catalyst study for the transamidation of N-aryl amides as outlined by Eldred et al. — representative example included, additional substrates were tested where X = CH_3, X' = CH_3O; reaction conditions: amine (0.33 mmol), amide (0.33 mmol), catalyst (0.033 mmol), 2 mL of p-xylene, 120 °C, 20 hours. [b] Determined by GC (internal standard - triphenylmethane); (reproduced with permissions from Ref. 11).[11]

Following this initial success, Gellman and Stahl continued to develop this methodology to enable transamidation of increasingly complex systems[12,13,16] — most of these later studies returned to the use of $Al_2(NMe)_6$ ([Al]) as the catalytic species, with the common theme of investigating the mechanism of the transamidation with different amide systems. Hoerter *et al*. reported the use of this [Al] catalyst for transamidation with unactivated secondary amides,[17] determining through mechanistic studies that the bifunctional character of the Al^{III} atom allowed activation of both the amine nucleophile and amide electophile.[17] Clearly, the ability to use more substituted amides is necessary in regards to the long term goal of materials formation — Hoerter *et al*. showed further development with the transamidation of tertiary amides (Figure 2.4).[12] Returning to the original procedure of GC (gas chromatography)-monitored reactions, Hoerter *et al.* screened the forward and reverse reactions for two model amide systems with varying *N*-substitution.[12] Transamidation of tertiary amides was successful, with mechanistic studies confirming a hypothesis of the inability for formation of stable tertiary amide-Al^{III} species. Hoerter *et al*. also suggested adapting this methodology for the metathesis of secondary amides, though attempts to induce metathesis with the Al-based catalyst were unsuccessful.[12]

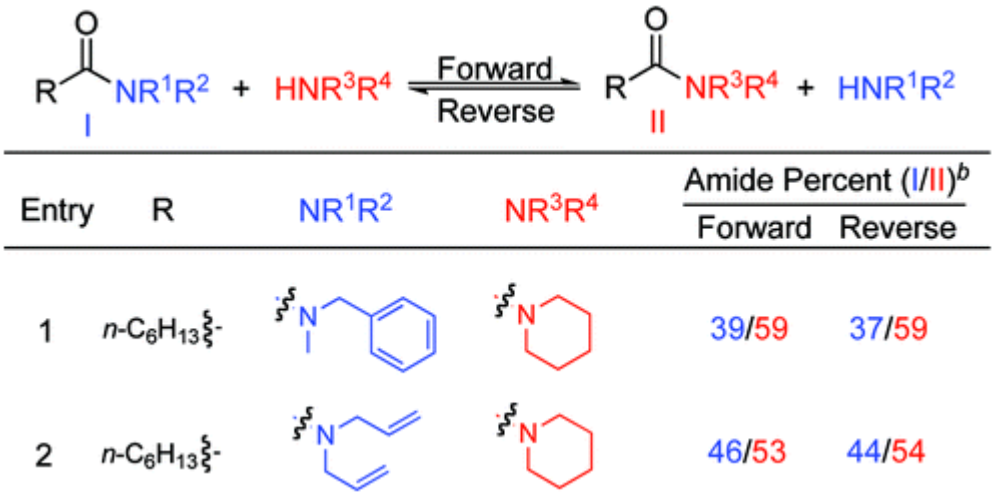

Entry	R	NR^1R^2	NR^3R^4	Amide Percent (I/II)[b] Forward	Reverse
1	*n*-C_6H_{13}-			39/59	37/59
2	*n*-C_6H_{13}-			46/53	44/54

Figure 2.4 – General scheme for transamidation of tertiary amides using [$Al_2(NMe_2)_6$], with two representative combinations of amide and amine as reported by Hoerter et al. — both reactions exhibit the same amide product ratio for the forward and reverse reaction; Reaction conditions: [Al2(NMe_2)$_6$], 4.3 mM, [carboxamide], 0.17 M, [amine], 0.17 M, 2 mL of toluene, 90 °C, 16 hours; [b] Determined by GC (internal standard - triphenylmethane); data represent the average of two reactions; (reproduced with permissions from Ref. 12).[12]

Tertiary amide metathesis was later realised in a 2009 report by Stephenson *et al*.[13] which focused on screening a range of alternative catalysts for metathesis. Initial screens with a monofunctional model system presented several alternative metal-amido catalysts with effective reactivity at lower temperatures than tested previously. From these catalysts, $Zr(NMe_2)_4$ and $Hf(NMe_2)_4$ were shown to be the most effective, displaying “indistinguishable reactivity”, with $Zr(NMe_2)_4$ selected for further testing (Figure 2.5). Further screening again utilised amide ratio studies for forward and reverse reactions, identifying a range of viable solvents for the reaction, as well as investigating the limitations for both the amide substrate and amine nucleophile. Amide metathesis was shown for a range of monofunctional amides with varying substituents, again with temperatures as low as 25 °C.

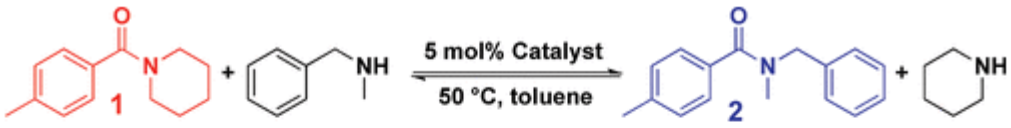

Entry	Catalyst	Time (min)	Amide Ratio (1) / (2)	
			Forward	Reverse
1	$Hf(NMe_2)_4$	60	0.63/0.37	0.62/0.38
2	$Zr(NMe_2)_4$	60	0.63/0.37	0.63/0.37

Figure 2.5 – General scheme for tertirary amide metathesis as outlined by Stephenson et al. — $Hf(NMe_2)_4$ and $Zr(NMe_2)_4$ were found to be the best candidates from a catalyst screen (reproduced with permissions from Ref. 13).[13]

Overall, these reports outline major strides towards fully reversible amide formation, although there are still limitations for application to materials synthesis. Principally, the majority of reports of Gellman and Stahl focused on monofunctional amides[11–13,15–17] — whilst there is no suggestion that this methodology would not be applicable to multifunctional amides, further work would be necessary to investigate this given the use of multitopic precursors is essential for materials formation. In addition, it would be useful if metal catalysts could be avoided — not only to avoid high cost, or potential safety concerns, but also to eliminate the possibility of trace metal compounds interfering with potential function of the formed products. Organic catalysts would be preferred — this is not an unexplored area, with existing reports successfully using small organic molecules as transamidation catalysts,[6] for example, a 2014 report by Wu *et al.* outlined the use of benzoic acid as the catalytic species.[5] As expected, the study focused on the transamidation of small primary amides, but also included examples of amides with further functionalisation. Considering the substrates explored by Wu et al., and the desire to use a small organic catalyst for this work, this presented benzoic acid as an ideal candidate for further testing. Despite the more complex amide shown in the report by Wu et al., a new model system was required that better represented potential materials formation.

2.2 Developing suitable reaction conditions for dynamic transamidation

2.2.1 Developing a model system

To effectively study benzoic acid as a transamidation catalyst for materials formation, a suitable model system was first devised. This system was designed to more accurately mimic the types of structures seen within reported functional materials – both existing amide species, as well as non-amide targets of desirable structures. Clearly, for this purpose, primary amides would not be suitable as a substrate. Additionally, topicity is also key for materials precursors, and as such was a requirement in the model system — a monofunctional substrate is not suitable for materials formation. In addition, the identification of the transamidation product composition was key to determining the effectiveness of the applied conditions. Whilst the earlier work by Stahl and Gellman utilised GC,[12,13,16] ^{1}H NMR spectroscopy would also be a useful tool for quick, straightforward characterisation — importantly, the model system would have to be designed carefully to allow this characterisation technique to be applicable.

Based on these criteria, a model transamidation system was devised, combining *N,N'*-dibenzylterephthalamide (herein referred to as benzyl amide) as a starting substrate with 4-methylbenzylamine as the nucleophilic amine (Scheme 2.1). The target product was the doubly methyl-substituted derivative *N,N'*-bis(4-methylbenzyl)-terephthalamide (herein referred to as tolyl amide). When considering the work of Stahl and Gellman, it was thought that the reaction would not progress to completion, *i.e.*, full exchange to *N,N'*-bis(4-methylbenzyl)terephthalamide, the tolyl amide, would not occur — however, two equivalents of amine were used for this process to ensure complete exchange was feasible for the bifunctional substrate. Based on the precursors present, the model reaction was theorised to form a mixture of three products (Figure 2.6):

1) *N,N'*-dibenzylterephthalamide, **benzyl amide**

2) *N,N'*-bis(4-methylbenzyl)terephthalamide, **tolyl amide**, formed by complete exchange of the amide groups

3) *N,N*-dibenzylterephthalamide, **mixed amide**, formed when only one amide group undergoes exchange

The distribution of these products could then be determined to assess the degree of transamidation taking place in the reaction. With a starting point of 100:0 benzyl amide:tolyl amide, it was deemed that a target ratio of 50:50 benzyl:tolyl amide within the product mixture was an appropriate goal, showing that the system exhibited enough reactivity to be used for further study.

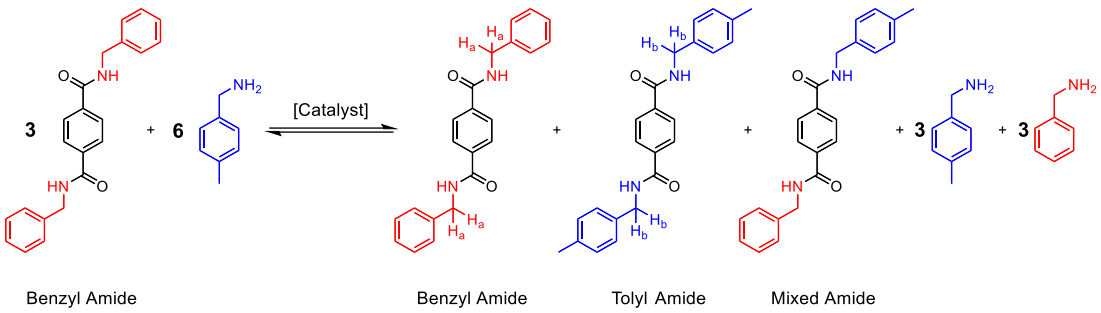

Figure 2.6 – Proposed model system utilising the reaction of N,N'dibenzylterephthalamide (benzyl amide), in the presence of a suitable catalyst, to form a mixed amide product. The target product mixture would constitute 3 amide species: the starting benzyl amide, the disubstituted N,N'-bis(4-methylbenzyl)terephthalamide (tolyl amide), and N-benzyl-N'-(4-methylbenzyl)terephthalamide (mixed amide); as well as the two free diamines benzylamine and 4-methylbenzylamine.

Additionally, it was necessary to develop a method for analysis that allowed quick and straightforward determination of the species present in the product mixture. It was hoped that use of ^{1}H NMR spectroscopy would allow for this by monitoring the relative change in the shift for the methylene CH_2 peak in each of the amides. To ensure this was feasible before extended testing, the parent substrate and product diamides were first synthesised directly by the irreversible condensation of terephthaloyl chloride with either benzylamine or 4-methylbenzylamine, to give *N,N'*-dibenzylterephthalamide (benzyl amide, Figure 2.7a) and *N,N'*-bis(4-methylbenzyl)terephthalamide (tolyl amide, Figure 2.7b), respectively. ^{1}H NMR spectroscopic analysis showed that the methylene CH_2 groups of the amides both appear as doublets — overlaying of the individual spectra shows a difference in shift for the CH_2 groups of ~0.05 ppm between the two amides. This difference would allow for differentiation between the two species within the crude reaction mixture (Figure 2.7c).

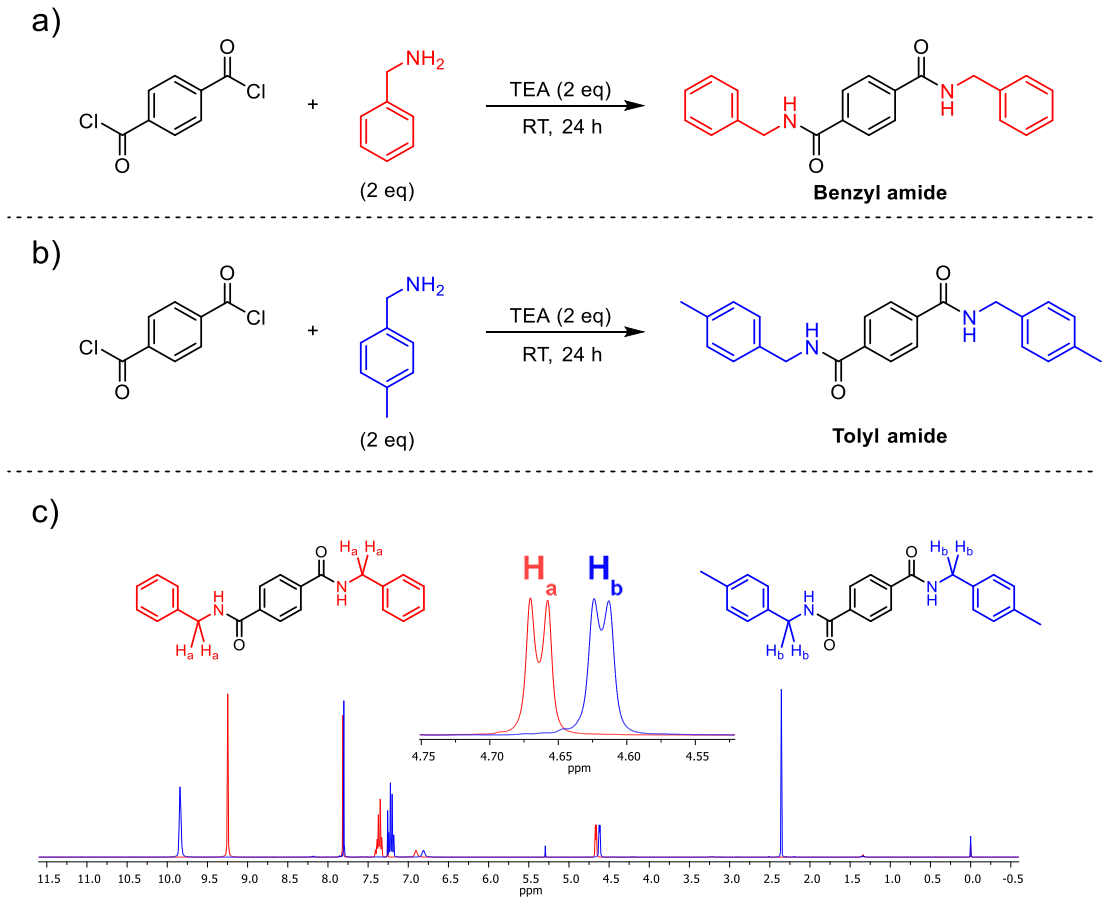

Figure 2.7 – Development of suitable compounds for the model transamidation reaction: a) synthesis of N,N'-dibenzylterephthalamide (benzyl amide); b) synthesis of N,N'-bis(4-methylbenzyl)terephthalamide (tolyl amide); c) overlaid ^{1}H NMR spectra of the benzyl amide and tolyl amide to show relative shifts of the methylene α-CH_2 peaks of the two amides — the slight difference in peak shift allows for identification of the amides by ^{1}H NMR spectroscopy.

Initial reaction parameters for the model system were selected based on several previous transamidation studies. The study using benzoic acid by Wu *et al.* reported a small solvent screen during their initial studies, and the best option from their screen, *p*-xylene, was selected as the starting solvent for this work.[5] For the catalyst loading, reports of organocatalysts for transamidation varied between 5-15 mol% (15 mol% for benzoic acid)[5,6] – as the model system used in this work was unlike those used previously, 10 mol% was selected as a compromise, and this was increased to 20 mol% to reflect the bifunctional nature of the amides used (10 mol% per amide functionality). Wu *et al.* reported the need to complete transamidation under an inert (Ar) atmosphere, but in the work described in this chapter, the reaction was carried

out under ambient conditions with no extra measures taken to eliminate air or moisture. In addition, reactions were completed using a Biotage Initiator+ microwave reactor (MWR). Use of the MWR facilitated easier running of reactions, by allowing for queuing, faster cooling, and the ability to access higher temperatures and pressures than other conventional heating sources available. Heating conditions could also be controlled more carefully, using stepwise increases to allow for gradual pressure increase. Additionally, the MWR was equipped with an internal pressure sensor, and could prematurely halt reactions if potentially unsafe pressures were detected.

A key distinction to make for the initial studies is the focus on transamidation *vs* the dynamic nature of the reaction. Whilst a 50:50 ratio of products was desired as an ideal result, the reaction can only be determined as dynamic if the same product distribution is achieved for both the forward and reverse reactions. This model system does not use a traditional forward/reverse process, as there is mixture of potential amides accessible by alternative routes — this is discussed further later in this chapter. The focus of the model reaction screen was to identify promising conditions for transamidation that could be further optimised; this was done using the proposed model reaction of the designed benzyl amide with 4-methylbenzylamine (Figure 2.6). The next section discusses the initial optimisation of the model system, using a series of bar charts to outline the progress of each reaction. The progress of the reactions can be observed by assessing the relative bars for benzyl amide (red) and tolyl amide (blue) — *i.e.*, consumption of benzyl amide and formation of tolyl amide leads to a reduction for the red bar and increase for the blue. The target is to achieve 50% of both the benzyl and tolyl amides, marked by dotted lines across each of the plots.

2.2.2 Reaction condition screen for model system

First, a range of reaction temperatures was investigated for the model process, starting at 100 °C (Figure 2.8). Wu *et al.* reported successful transamidation at 130 °C,[5] though this was mainly using primary, monofunctional amides. It was therefore expected that higher temperatures may be necessary to achieve reaction with the substituted, bifunctional amides used in this study. The long reaction time of 8 hours reported by Wu *et al*.[5] was also not employed, instead using 3 hours for this study – lower reaction times for the screen were preferential, with the ability to extend for further optimisation and later study into materials formation.

An initial temperature of 100 °C was tested as a benchmark for the reaction — unsurprisingly, no reaction was seen at 100 °C, and there was also no reaction exhibited when the temperature was increased to 150 °C. The reaction was then screened from 200-250 °C — on increasing to 200 °C, a small degree of transamidation was observed, and as might be expected, increasing the temperature even further increased the amount of tolyl amide formed. Unfortunately, at the maximum tested temperature of 250 °C, a ratio of only 76:24 benzyl:tolyl species was achieved, much lower than the desired 50:50 ratio.

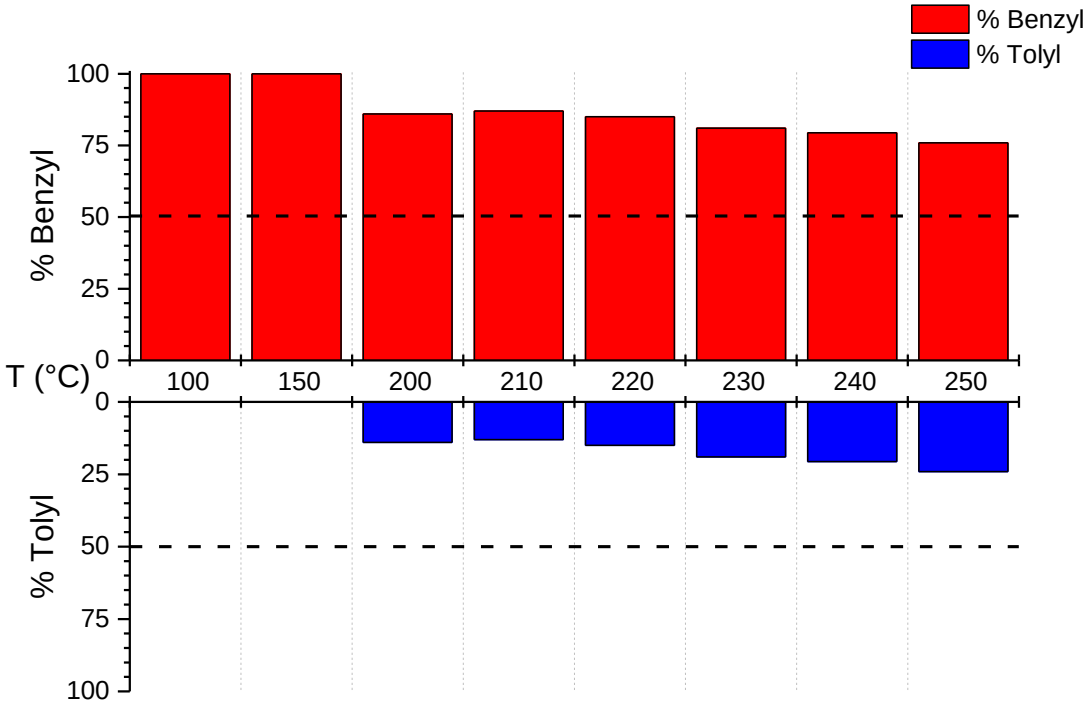

Figure 2.8 - Reaction temperature screening of model transamidation reaction — N,N' dibenzylterephthalamide (0.29 mmol, 1.0 eq.), 4 methylbenzylamine (0.58 mmol, 2.0 eq.), and benzoic acid (20 mol%), in p-xylene (4 mL) for 3 hours, at a range of reaction temperatures. Increasing the reaction temperature leads to an increase in conversion, with a shift away from 100:0 benzyl:tolyl species as more tolyl amide is formed.

Concurrently to screening the optimal reaction temperature, the reaction time and solvent were also investigated. As a result, the temperature for these tests was set to 200 °C, rather than the 250 °C determined in the temperature study. First, the reaction time was varied from 1 hour up to 12 hours (Figure 2.9). As expected, an increase in reaction time led to further conversion, though the desired amide ratio was not

achieved in moderate time, with a 12-hour reaction still only yielding a 75:25 benzyl:tolyl ratio for the product distribution (Figure 2.9).

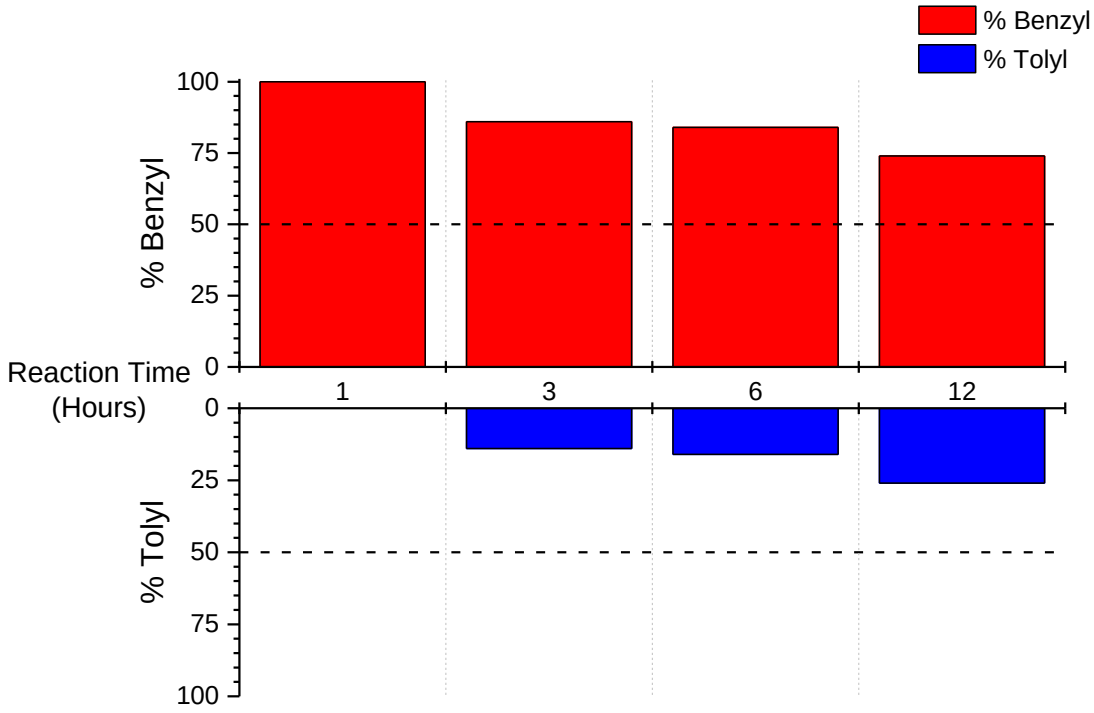

Figure 2.9 – Reaction time screen for model transamidation reaction: N,N'-dibenzylterephthalamide (0.29 mmol, 1.0 eq.), 4-methylbenzylamine (0.58 mmol, 2.0 eq.), and benzoic acid (20 mol%), in p-xylene (4 mL), at 200 °C for a range of reaction times. Increasing the reaction time leads to an increase in reaction, with a shift away from 100:0 benzyl:tolyl species as more tolyl amide is formed.

The choice of reaction solvent was also investigated for the model system — in addition to *p*-xylene, a range of solvents of varying structures and polarities were also examined (Figure 2.10). In their initial report, Wu *et al.* suggested possible mechanisms for the benzoic acid catalysis, with one of the proposed routes involving hydrogen bonding of the carboxylic acid to the amide structure.[5] As such, it would be expected that using solvents with the potential to form hydrogen-bonds could lead to competitive interactions, thus reducing the reactivity. To investigate this, *n*-butanol, ethylene glycol, and THF were examined as examples of monotopic alcohol, multitopic alcohol, and an aprotic H-bond acceptor, respectively. In addition, toluene and mesitylene were included to test the effect of methyl group placement compared to *p*-xylene.

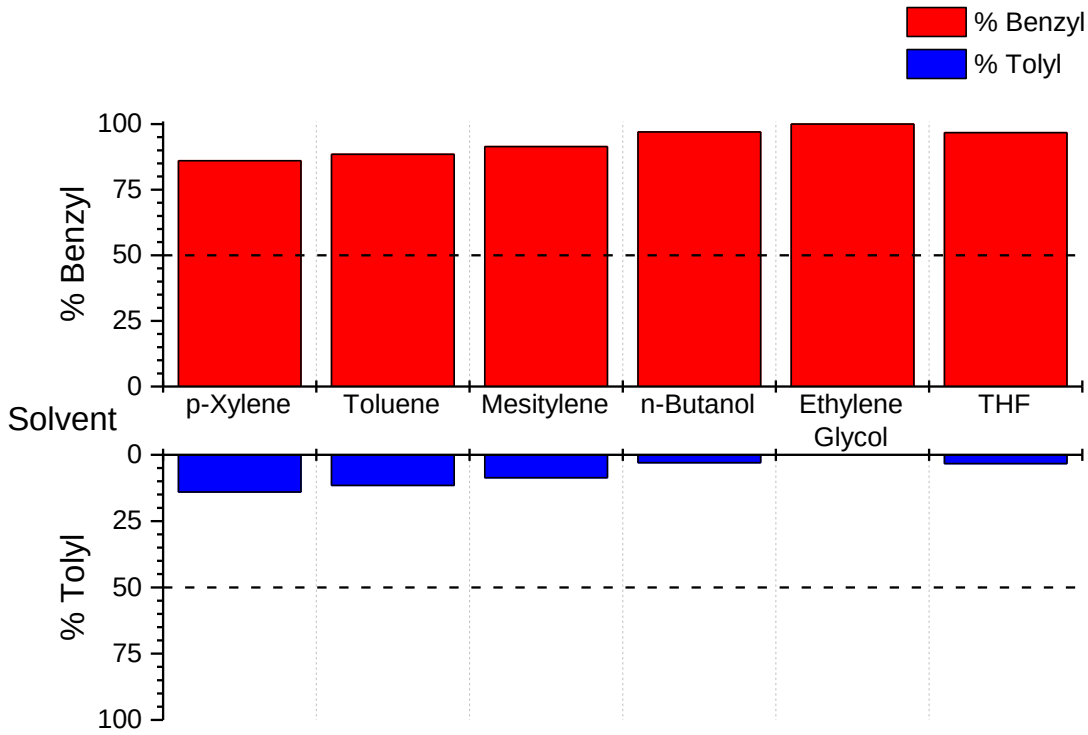

Figure 2.10 – Reaction solvent screen for model transamidation reaction: N,N'-dibenzylterephthalamide (0.29 mmol, 1.0 eq.), 4 methylbenzylamine (0.58 mmol, 2.0 eq.), and benzoic acid (20 mol%), in a selected solvent (4 mL). Aromatic solvents such as p-xylene and toluene showed the best activity, with non-aromatic solvents showing little to no reaction. p-Xylene remained the best solvent and was used for all further testing.

Overall, the observed ratios in the product mixtures from the screen appeared to prove the hypothesis correct – solvents with the potential to hydrogen-bond showed reduced conversion compared to the methylated aromatic solvents studied. The reactions carried out in *n*-butanol and THF (each with one functionality able to H-bond) showed similarly low degrees of transamidation, whereas the use of trifunctional ethylene glycol resulted in no reaction. The aromatic solvents however, in general, showed improved conversion, with the reaction carried out in *p*-xylene showing the best product ratio of 86:14 benzyl:tolyl species. As such, *p*-xylene was used in all following studies.

Whilst these initial optimisation screens had improved the transamidation in part, the desired product distribution ratio of 50:50 had not yet been achieved. Increasing the reaction temperature to 250 °C was a clear choice for future testing, and *p*-xylene remained the best available solvent. Whilst a 12-hour reaction time was shown to

promote the reaction further, a compromise of a 3 hours was used going forward to make this system a viable choice when compared with the timescales of other catalytic procedures. At this stage, it was therefore decided to shift focus onto investigating the catalyst itself.

2.2.3 Catalyst screening for model transamidation system

In their original report, Wu *et al*. outlined a small catalyst screen, with benzoic acid selected as the optimal catalyst.[5] However, due to the structural differences between Wu's system and the model system presented in this work, it was theorised that an alternative catalyst may enable improved conversion for this bifunctional model system. With the desired amide ratio not reached *via* the previous reaction optimisation steps using the same catalyst, we shifted our efforts to identifying a new catalyst for further study.

Strong acid catalyst screen

The report of Wu *et al*. theorised catalytic transamidation mechanisms based on the catalyst taking part in either hydrogen-bonding or salt formation .[5] On this basis, strong acids (*i.e.*, those with low pK_a values) would be expected to promote transamidation, based on their increased propensity to form hydrogen-bonds or undergo deprotonation. To test this, the transamidation screen with the model system was repeated using a range of simple strong acids as catalysts for comparison with benzoic acid as a control (Figure 2.11a). Several strong acids with pK_a values lower than 0 were utilised, and acetic acid was also included as an aliphatic acid with a pK_a similar to that of the control catalyst (4.76 vs 4.2 for benzoic acid). This initial catalyst study was completed concurrently with the previous reaction condition screens, and as such, the reactions were only heated at 200 °C for 3 hours, again allowing direct comparison with the conversion observed when using benzoic acid as the catalyst. Interestingly, the additional strong acids tested exhibited no transamidation for the model system. This suggests that while acidity may play a key role in promoting catalysis, the inherent structure of the catalyst plays an equal, or arguably more important, role — clearly, the type of acidic functionality may also play strongly into this. Comparing benzoic acid and *p*-toluenesulfonic acid monohydrate, these two species generally have a similar structure, though the specific acid group differs

greatly — only benzoic acid exhibited any activity for transamidation in this system (Figure 2.11b).

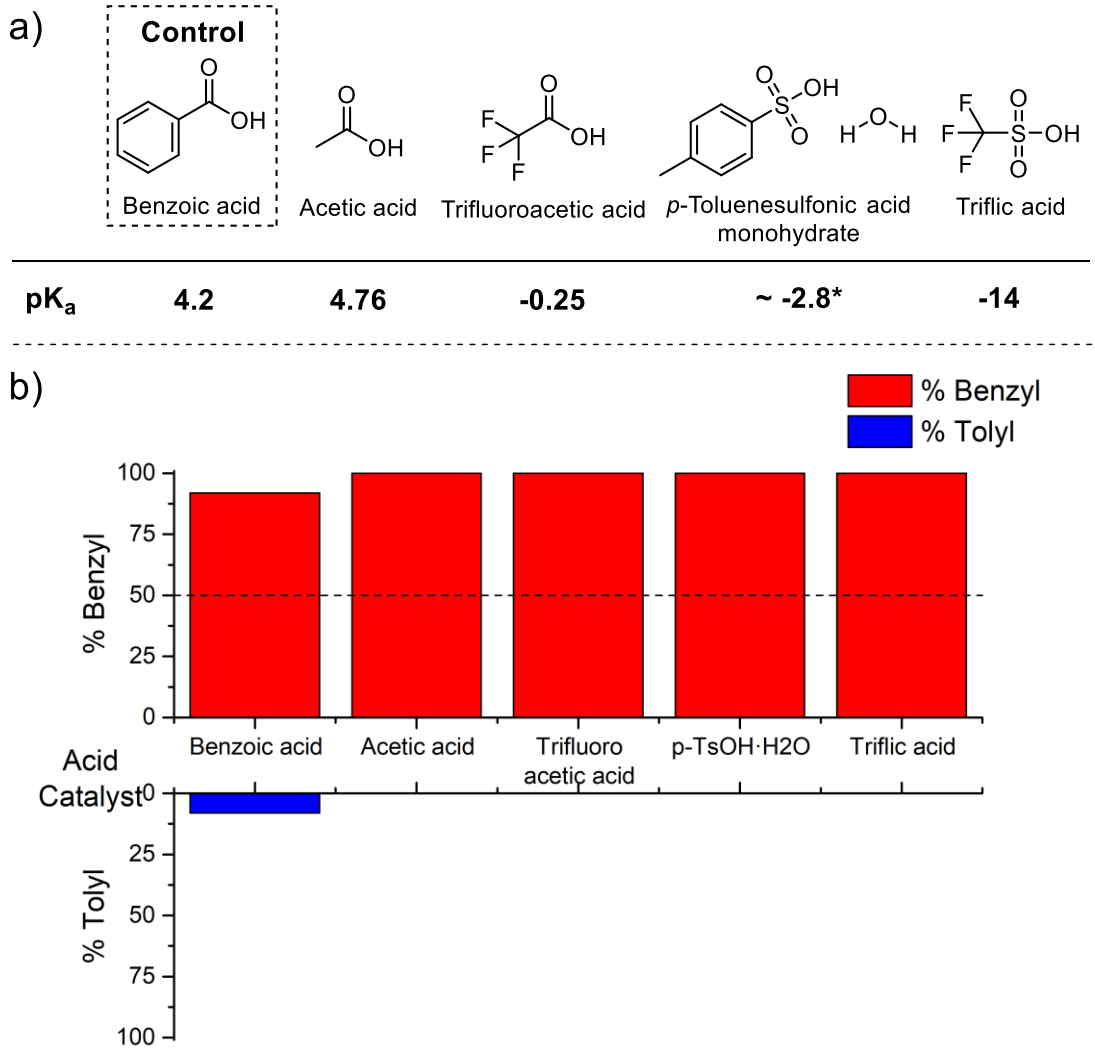

*Figure 2.11 – Strong acid catalyst screen for the model transamidation reaction: a) selected acids with their accompanying pK_a values, collated from various sources; b) benzyl:tolyl amide ratios as determined by ^1H NMR spectroscopic analysis.*value stated is for benzenesulfonic acid.*

Expanded catalyst screening

To further investigate the catalyst choice on the degree of reaction exhibited, a large catalyst screen was undertaken to try to find a catalyst that promoted further transamidation. Considering the proposed mechanism by Wu et al.,[5] catalyst choice was largely focused on small, organic acids that could undergo hydrogen-bonding with the amide substrate. Within this, a range of structures were investigated, including carboxylic acids, boronic acids, sulfonic acids, and phosphonic acids. In all, 55 catalysts were selected and tested during this screen, with benzoic acid included as the control catalyst (Figure 2.12). Due to the large number of catalysts being tested, reactions were completed under non-optimised conditions (200 °C for 1 hour) to facilitate more rapid screening. Whilst this resulted in much lower degrees of transamidation than desired, it was hoped that any catalysts with increased activity would show large jumps in conversion relative to the benzoic acid control catalyst.

Performance of the different acids as transamidation catalysts varied between the different classes of structure (Figure 2.12). The marked point within the plot represents 37 of the catalysts tested which promoted no reaction for the model system — these included all the sulfonic and phosphonic acids, as well as the majority of boronic acids screened. Of the 18 catalysts that did successfully promote transamidation, nearly all were carboxylic acid derivatives. The amount of conversion exhibited was low across all reactions relative to the previous studies, though this was expected due to the use of non-optimised conditions to allow rapid screening as discussed previously.

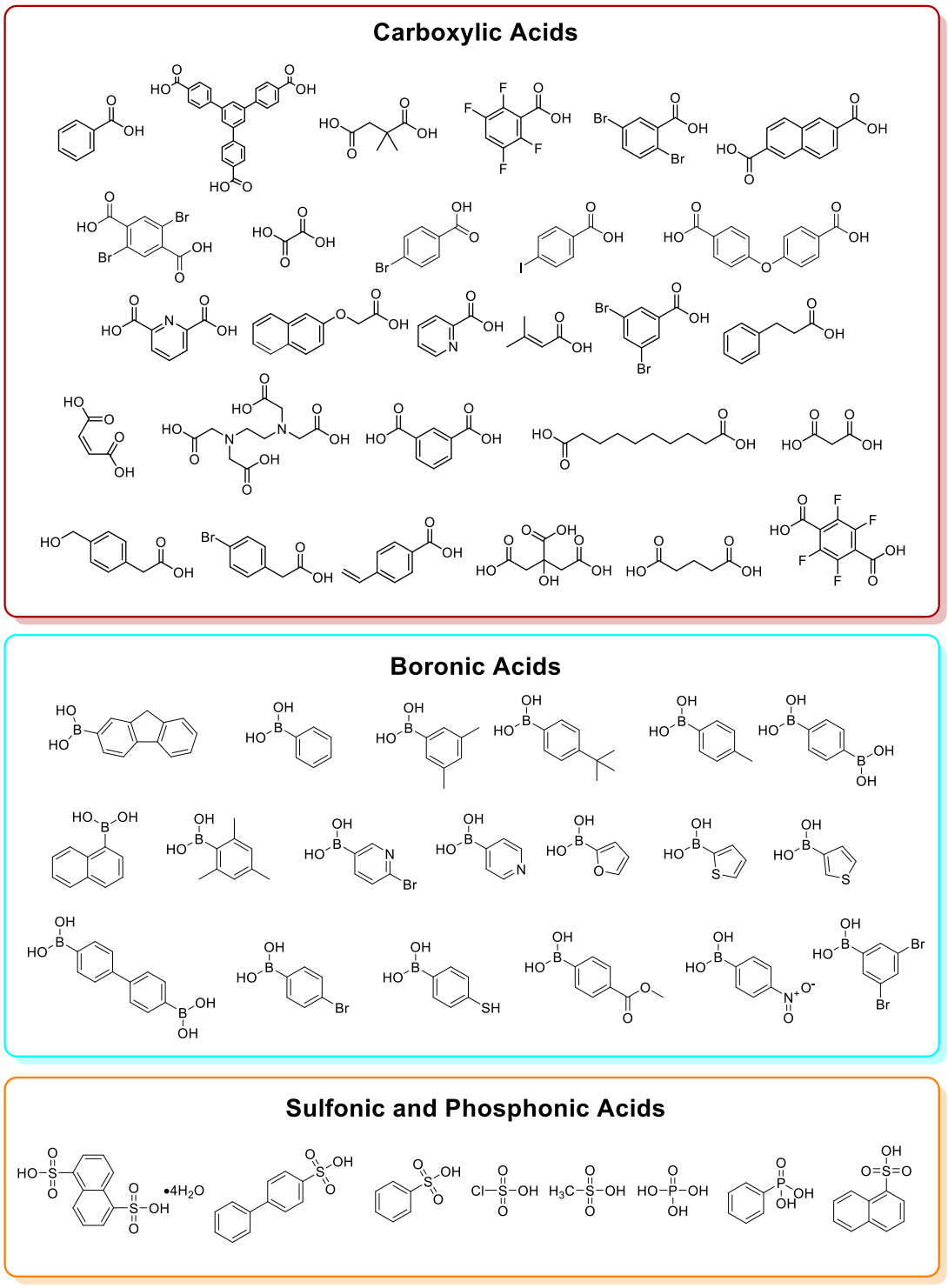

Figure 2.12 – Small organic acids tested as part of larger catalyst screen: a range of structures were used, encompassing three main groups based on a number of examples: carboxylic acids (red, top), boronic acids (blue, middle), and sulfonic and phosphonic acids (orange, bottom).

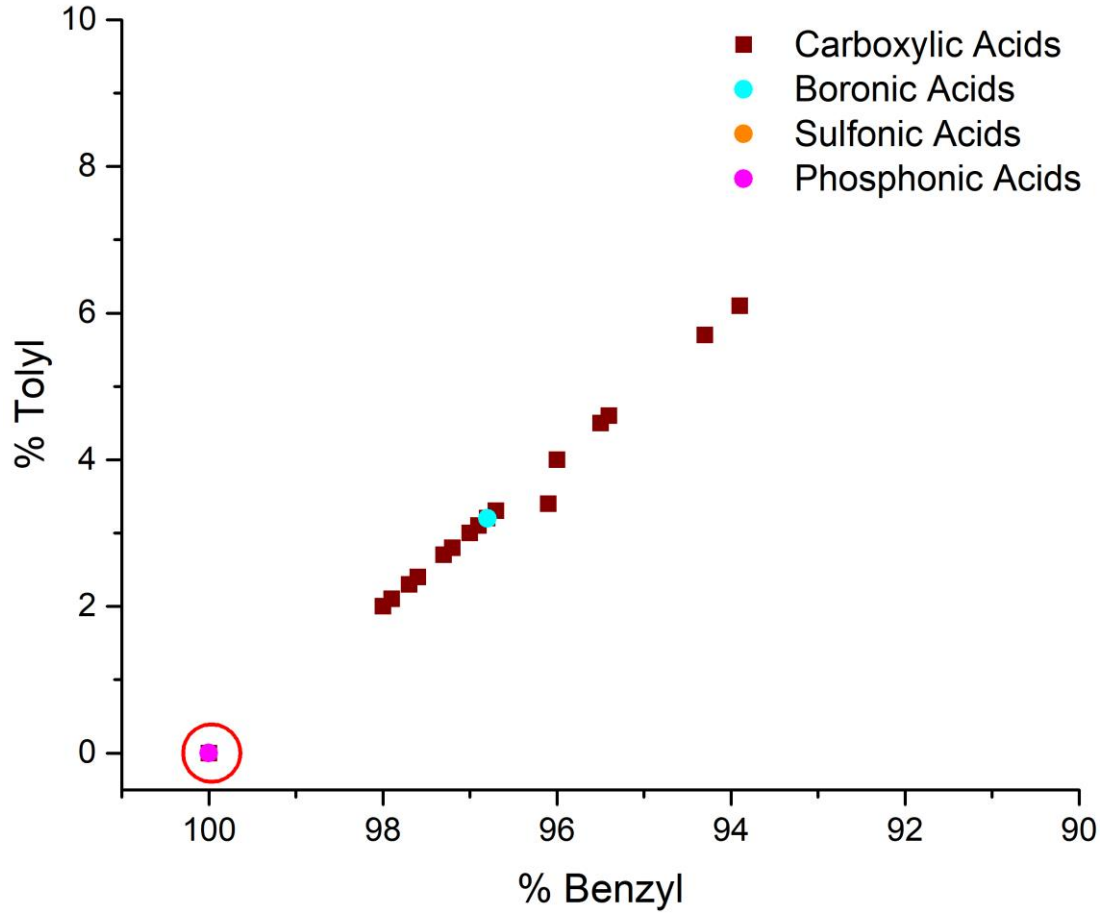

Figure 2.13 – Relative amide amounts from the transamidation reactions for extended catalyst screening, determined by ^{1}H NMR spectroscopy; the point circled in red represents 37 catalysts which promoted no transamidation for the model reaction.

Unfortunately, none of the tested catalysts promoted a dramatic increase in conversion as desired. The general findings of this screen correlates well with the short catalyst study reported by Wu *et al*.,[5] with poor catalytic activity for simple carboxylic acids such as acetic acid and its derivatives, and much improved activity for benzoic acid and its derivatives and analogues, *i.e.*, acids with the presence of aryl-based functionalities.[5] Considering the types of structures that showed success as catalysts, there could potentially be other interactions between catalyst and substrate to promote further reaction, for example, π-π interactions between phenyl/benzyl rings. Also of interest was the lack of boronic acids exhibiting catalytic activity considering their ability to form hydrogen-bonds, and with a previous report of boric acid-catalysed transamidation.[4] Nevertheless, carboxylic acids remained the top-performing class of catalysts, and the best options from this broad screen were

selected for further study. Many of the best-performing catalysts shared similar structural motifs, including the presence of aromatic rings and more than one carboxylic acid group. To ensure a complete understanding of the effect of catalyst structure, eight catalysts were selected, incorporating a range of structures including multitopicity, aromatic and aliphatic structures, and the presence of additional functional groups that may impact on the catalytic activity (*i.e.,* electronic effects). Benzoic acid was also included as the control catalyst (Figure 2.14).

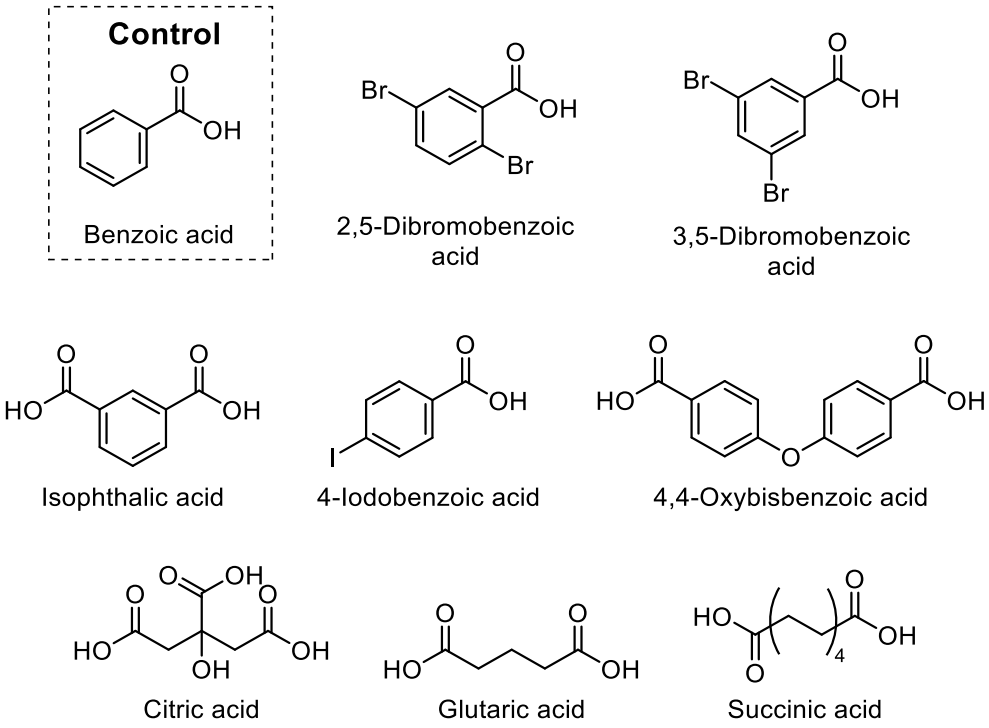

Figure 2.14 – Outcome from extended catalyst screening: organic acids selected for further investigation that promoted as-good or better degrees of transamidation compared to the benzoic acid control molecule.

Initially, the catalysts were re-tested using an increased temperature of 250 °C – this had a marked positive effect on the degree of transamidation, but unfortunately did not achieve the desired 50:50 tolyl:benzyl amide ratio. At this stage, the maximum achievable temperature in the MWR was already being used, along with a suitable reaction time — as such, it was decided to increase the catalyst loading from 20 mol% to 60 mol% to try and improve the degree of transamidation (Figure 2.15).

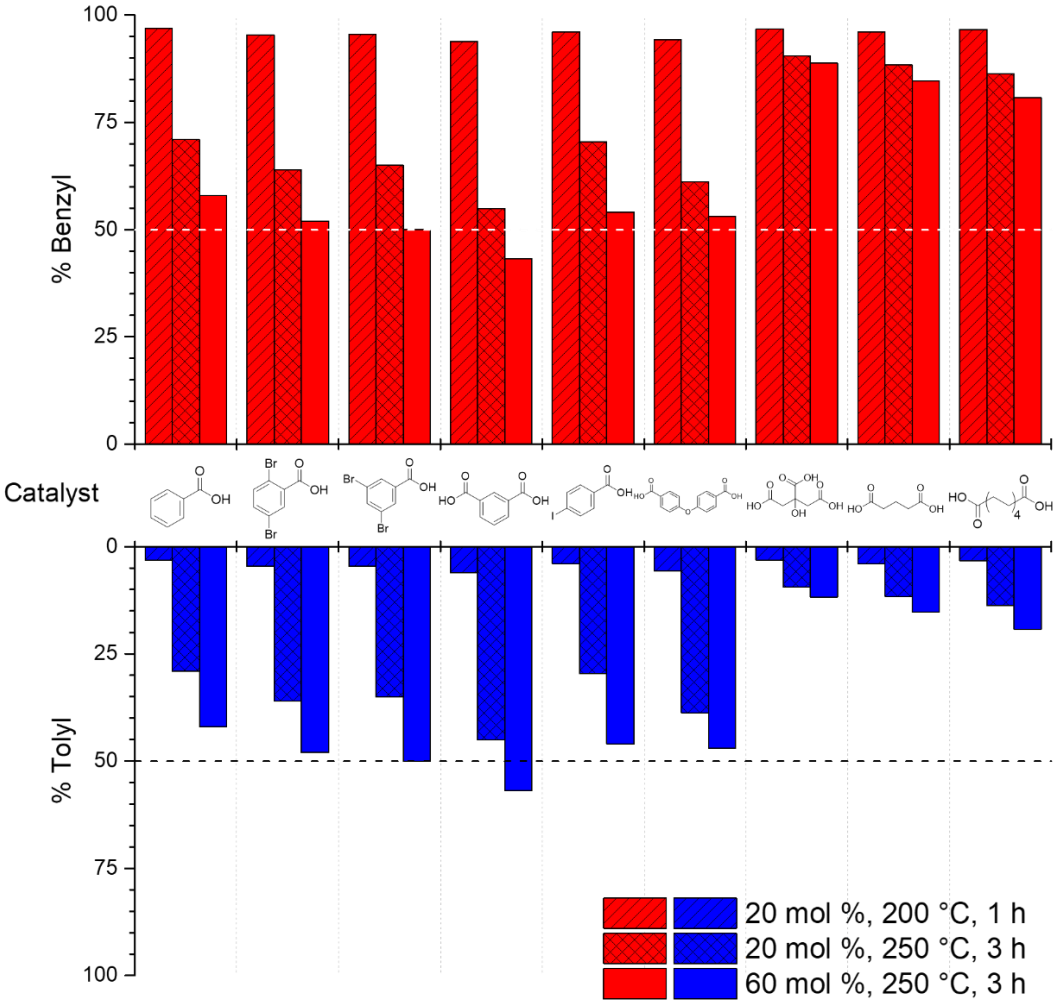

Figure 2.15 – Additional testing with the best candidates from the previous expanded catalyst screen, varying temperature, reaction time, and the catalyst loading.

Pleasingly, increasing the catalyst loading promoted transamidation to the desired ratio for several catalysts. The product distribution was found to contain more tolyl amide as determined by analysis of the ^{1}H NMR spectra, though it is uncertain whether this result was due to the reaction progressing to favour the tolyl structure, though this was investigated further in a later study. It was also noted that as the catalysts were all carboxylic acids, and the procedure was carried out at high temperatures, a side reaction between the catalyst and free amine could potentially occur. Whilst several acids showed desirable catalytic activity, the presence of multiple acid groups meant that if there were side reactions, these could lead to the production of undesired oligomeric or polymeric species, removing reagents from the reaction. 3,5-dibromobenzoic acid (DBA) was therefore selected as the primary

catalyst moving forward, as it gave the desired 50:50 benzyl:tolyl ratio in 3 hours at 250 °C, and only contained a single carboxylic acid group

2.3 Further investigation of the optimised transamidation model system

Following the optimisation of the reaction conditions to promote transamidation in the model system, more specific studies were undertaken to: (i) better understand the catalytic system; (ii) gain a better understanding of how the reaction was progressing; (iii) determine what the =potential limitations were, if any; and (iv) enable further comparison with the earlier report of Wu *et al*. into benzoic acid-catalysed transamidation.[5]

2.3.1 Clarification of observations for the optimised model reaction

Effect of temperature vs catalysis on the degree of transamidation

First, to confirm the efficacy of the catalyst, the uncatalysed reaction was carried out at the optimised temperature of 250 °C for 3 hours, to ensure the increased temperature was not the major influence on the observed increase in transamidation. Fortunately, this was the case, with a final product ratio of 92:8 benzyl:tolyl amide obtained in the absence of the catalyst. Whilst a small degree of conversion was observed, it was far below the 50:50 target ratio, confirming that the catalyst was indeed causing the transamidation in the model system.

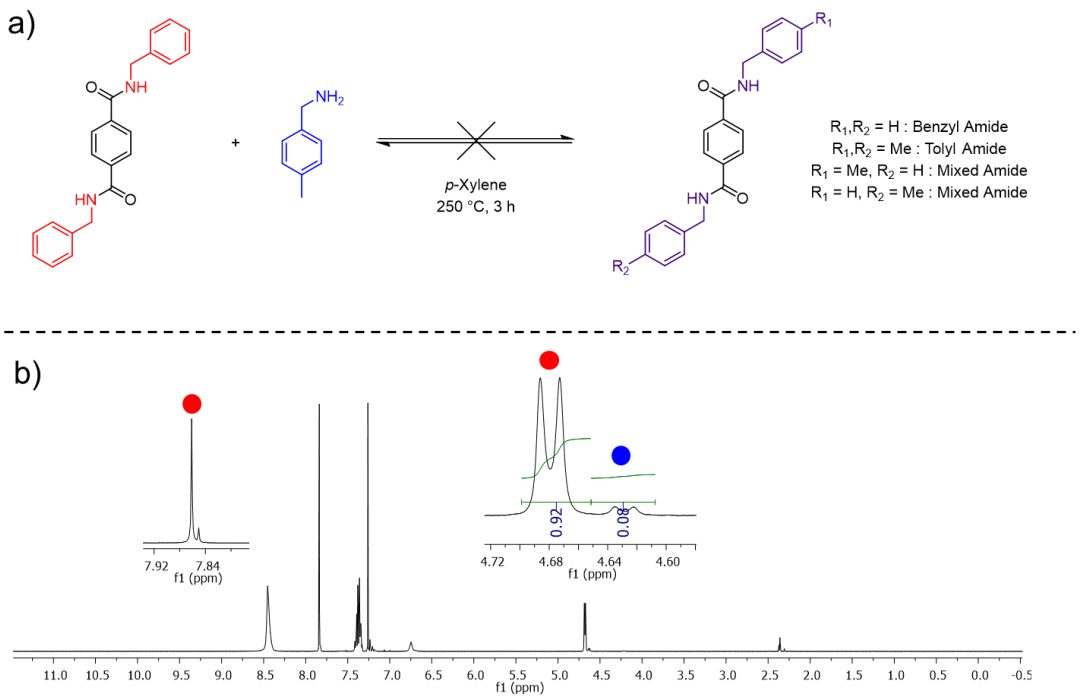

Figure 2.16 - Investigation of the uncatalysed model reaction with optimised reaction conditions; a) scheme for the uncatalysed reaction; b) ^{1}H NMR spectrum of the mixed amide product. Peaks for the benzyl amide are labelled red, while peaks for the tolyl amide are labelled blue.

Clarification of the product distribution for the model system

Throughout the previous optimisation studies, the reactions were assessed by the relative integrations of the methylene α-CH_2 groups of the benzyl and tolyl amides. Whilst the third mixed amide species was also formed in the reaction, it could only partially be identified in the aromatic region of the ^{1}H NMR spectra (Figure 2.13). A series of three peaks representing the three species appear between 7.8 and 7.84 ppm, and while the overall peak heights implied a triplet, it was suspected to be three singlets in a 1:2:1 ratio, representing the benzyl, mixed, and tolyl species, respectively. This ratio can be rationalised due to the bifunctional nature of the benzyl amide — either of the two amide groups can undergo transamidation to form the mixed species; as such, this gives twice the opportunity for mixed amide formation compared to either of the benzyl or tolyl amides, where there must be no exchange, or exchange of both groups respectively. The identities of these peaks were confirmed by selectively doping samples of the mixed amide product with each of the pure reference amides, and the^{1}H NMR spectroscopic measurements were then repeated to determine how the addition of the pure amides affected the aromatic region of the

amide mixture, using the mixed amide as a reference. As visible from the ^{1}H NMR spectra, addition of the benzyl amide led to an increase in peak intensity for the downfield shift of the group of aromatic singlets, whilst addition of the tolyl amide altered the upfield shift peak in the same way (Figure 2.17). In both cases, the central peak remained unchanged, indicating that this was the mixed amide species. This change in the aromatic region of the doped samples confirmed that the proposed identities for the set of aromatic peaks were correct, and. this was further supported by the respective methylene α-CH_2 doublets increasing on addition of each of the reference amides (Figure 2.17).

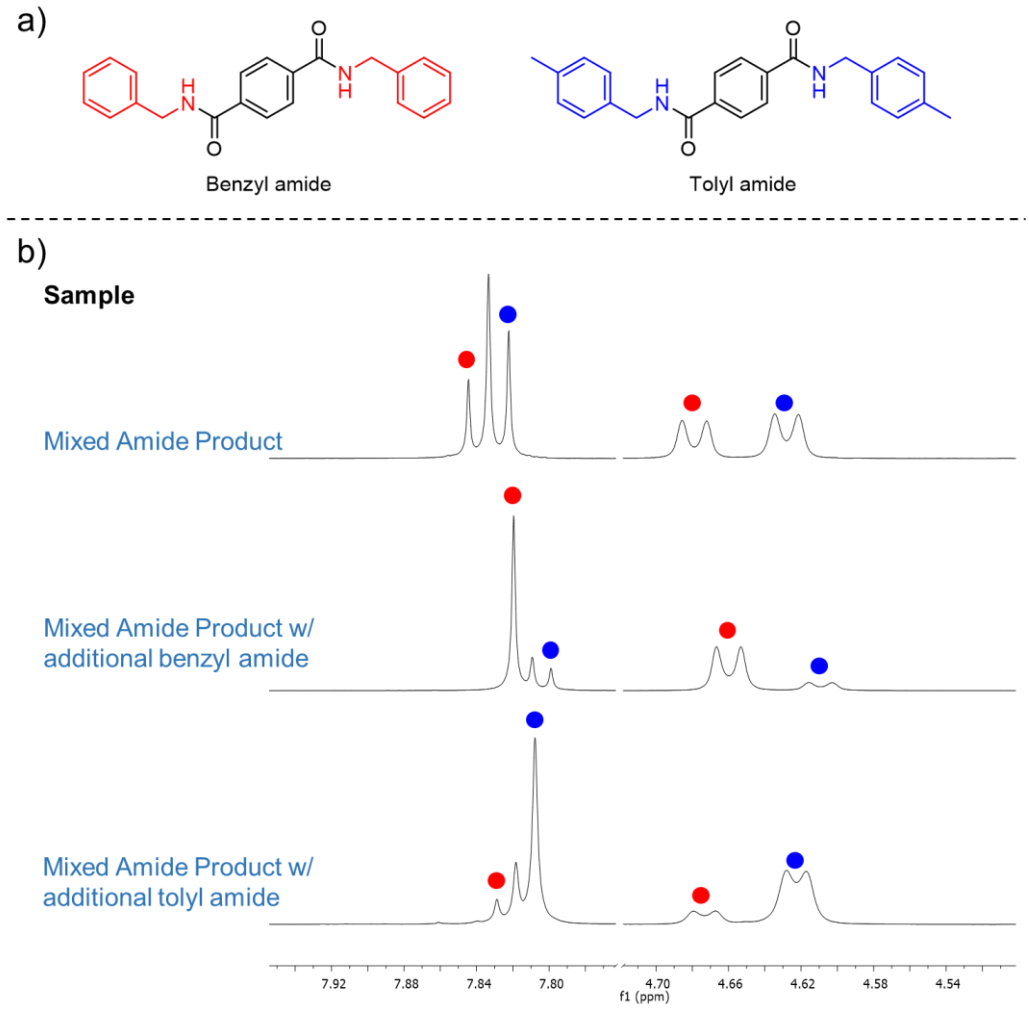

Figure 2.17 – ^{1}H NMR spectroscopic doping study to confirm the identity of the aromatic singlets and methylene α-CH_2 doublets with respect to the two reference amides: top - the mixed amide product as synthesised under the optimised conditions; middle - the mixed amide with additional benzyl amide added; bottom - the mixed amide with additional tolyl amide added. Peaks for the benzyl amide are labelled red, while peaks for the tolyl amide are labelled blue.

The presence of all three species, that is the benzyl amide, the mixed amide, and the tolyl amide, was also confirmed by mass spectrometry of the product mixture (Figure 2.14) formed during transamidation:

- Benzyl amide – calculated 344.1525, measured $[M+H]^+$ 345.1600
- Tolyl amide – calculated 372.1838, measured $[M+H]^+$ 373.1912
- Mixed amide – calculated 358.1681, measured $[M+H]^+$ 359.1754

Following confirmation of the presence of all three amide species, the model system was further investigated to assess the role of the catalyst in the reaction, in addition to any potential limitations of the system.

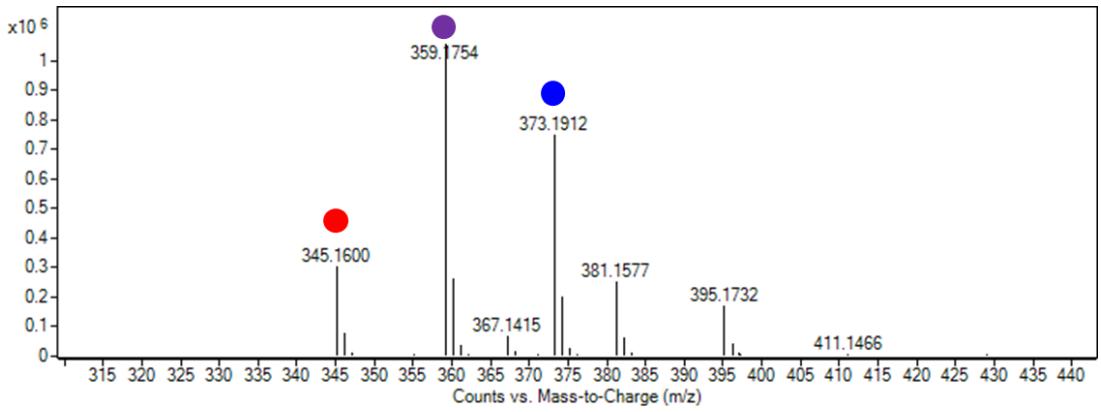

Figure 2.18 – HRMS spectrum of mixed amide product: a) full spectrum, b) expanded section showing the desired amide species; benzyl amide $[M+H]^+$ = 345.1600 (red), tolyl amide $[M+H]^+$ = 373.1912 (blue), mixed amide $[M+H]^+$ = 359.1754 (purple).

2.3.2 Specific interactions of the catalyst within the model system

Following the optimisation studies, it was desired to further investigate how 3,5-dibromobenzoic acid (DBA) functioned as a transamidation catalyst. In their earlier report, Wu *et al*. did not address any potential issues of side reaction between the catalyst and free amine.[5] It is possible that the relatively lower temperature of 130 °C used did not permit side reactions of this type — the use of elevated temperatures, as in this report, as well as the increased catalyst loading, may have promoted these side reactions more. As such, a series of studies were conducted to check the propensity of these side reactions, as well as the effect they had on the system more generally.

Reactivity of the catalyst with free amine

As discussed previously, multitopic catalysts were omitted from further study due to the potential for side reactions to occur, potentially forming oligomeric or polymeric species. To investigate this for the optimised reaction conditions and model system, the direct reaction between DBA and 4-methylbenzylamine (tolyl amine) was investigated in the absence of the starting benzyl amide (Figure 2.19a). The same quantities from the model system were used, and the reaction was heated under the optimised conditions outlined previously (*p*-xylene, 250 °C, 3 hours).

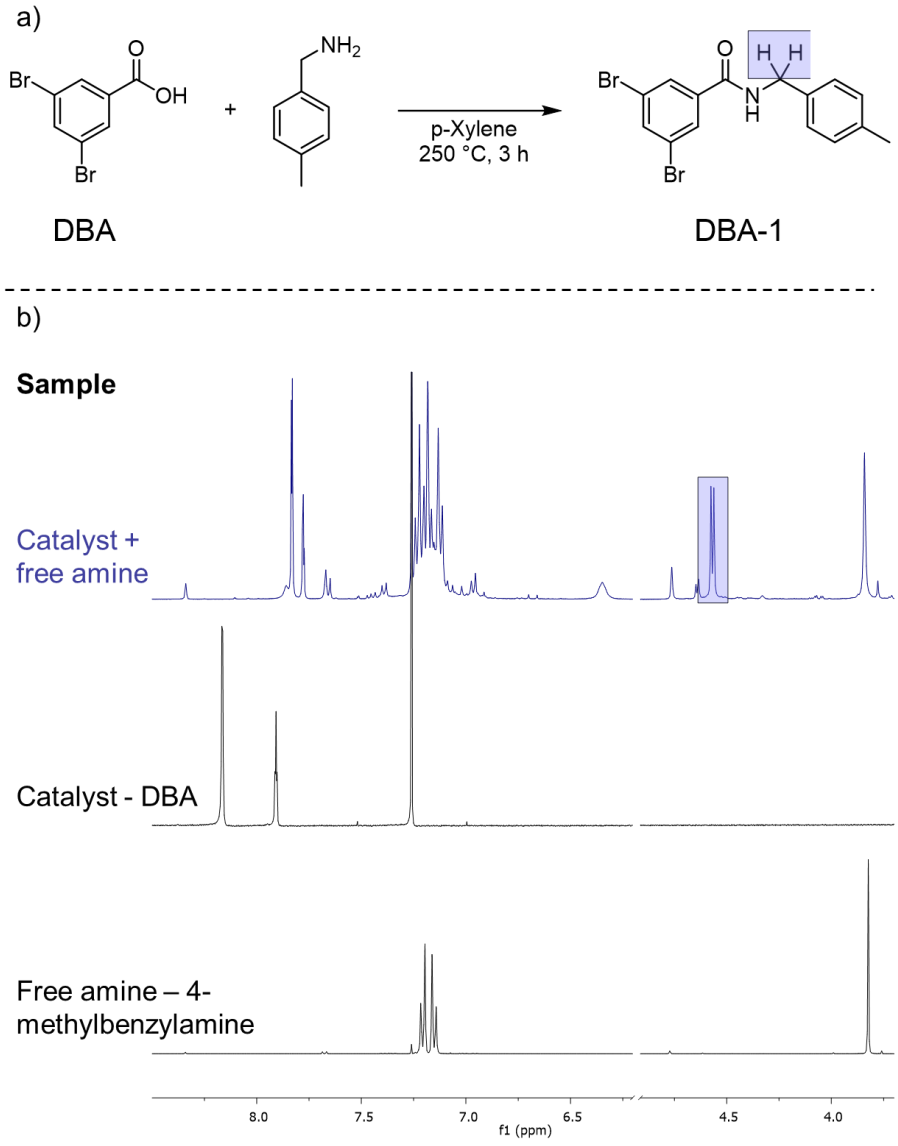

Figure 2.19 - a) Scheme to show the proposed reaction of DBA with 4-methylbenzylamine to form the intermediate structure DBA-1; b) stacked ^{1}H NMR spectra for the crude product obtained from reaction of the catalyst DBA and 4-methylbenzylamine to the optimised conditions, compared with neat DBA, and the neat free amine 4-methylbenzylamine.

The reaction mixture was concentrated to assess all species present, and ^{1}H NMR spectroscopic analysis of the residue showed the presence of a new doublet in the ~4.5 ppm region (Figure 2.19b). Methylene α-CH_2 doublets for both the benzyl and tolyl amides also appear in this region and considering the structural similarities between the benzyl/tolyl amides and the proposed side-product DBA-1 (Figure 2.19), this peak suggested its formation. For further confirmation of the formation of DBA-1, the crude sample was submitted for MS analysis to check for the corresponding mass ion, however an ion representative of DBA-1 could not be identified. The formation of DBA-1 suggests that, at least at higher loading, the catalyst may take part in the process by the formation of these amide intermediates, rather than by simply hydrogen-bonding or undergoing salt formation as proposed with benzoic acid. To investigate this, the catalyst/amine reaction to form DBA-1 was repeated, and after heating, a sample of benzyl amide was added (Figure 2.20). No additional free amine was added to the reaction. Analysis of the product mixture showed a ratio of 72:28 benzyl:tolyl amide. While this is lower than the optimised 50:50 ratio, this is unsurprising considering the free amine lost due to reaction with the catalyst. What this did show however, was that even with formation of the intermediate DBA-1, transamidation could still occur, utilising the remaining free amine to allow some formation of the mixed and tolyl amide. This 72:28 crude mixture of amides was also compared to an existing 50:50 mixture, as well as the crude DBA-1 product outlined previously. Comparison of the peak shifts showed that the peaks assessed in Figure 2.20 were those of the benzyl and tolyl amides.

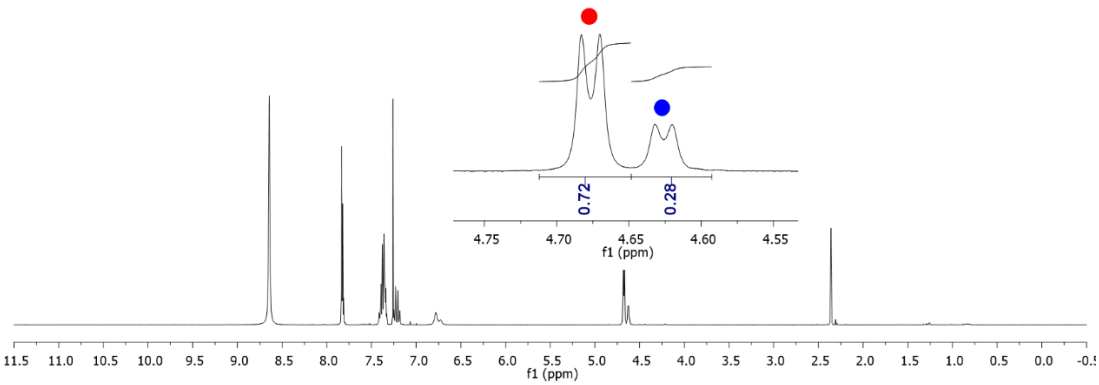

Figure 2.20 – ^{1}H NMR spectrum of the mixed tolyl:benzyl amide product mixture following the pre-formation of DBA-1 from the catalyst (DBA) and free amine (4-methylbenzylamie), and subsequent addition of benzyl amide. Peaks for the benzyl amide are labelled red, while peaks for the tolyl amide are labelled blue.

Use of a lower catalyst loading

Whilst lower catalyst amounts had been utilised during this work (*i.e.*, 20 mol% in earlier screens), a lower loading had not been tested extensively at elevated temperatures for prolonged reaction times. Initial temperature screens found that while some transamidation did occur when using 20 mol% catalyst at 250 °C for 3 hours, the product ratio was far below the desired 50:50 ratio of benzyl:tolyl species (Figure 2.8). To investigate this further, transamidation of the model system was carried out using 10 mol% catalyst at 250 °C – a lower loading than any of the previous reactions (Figure 2.21a). Whilst the desired product ratio was obtained (Figure 2.21b), a much longer reaction time of ten hours was required. This highlights the necessity for compromise within the model system, with much increased catalyst loadings required to avoid long reaction times. This is particularly relevant for application to materials synthesis — a large increase in reaction time for a ditopic molecule could indicate a poor system for application to the synthesis of cages or other materials where a number of multitopic precursors would be required for formation of the target structure.

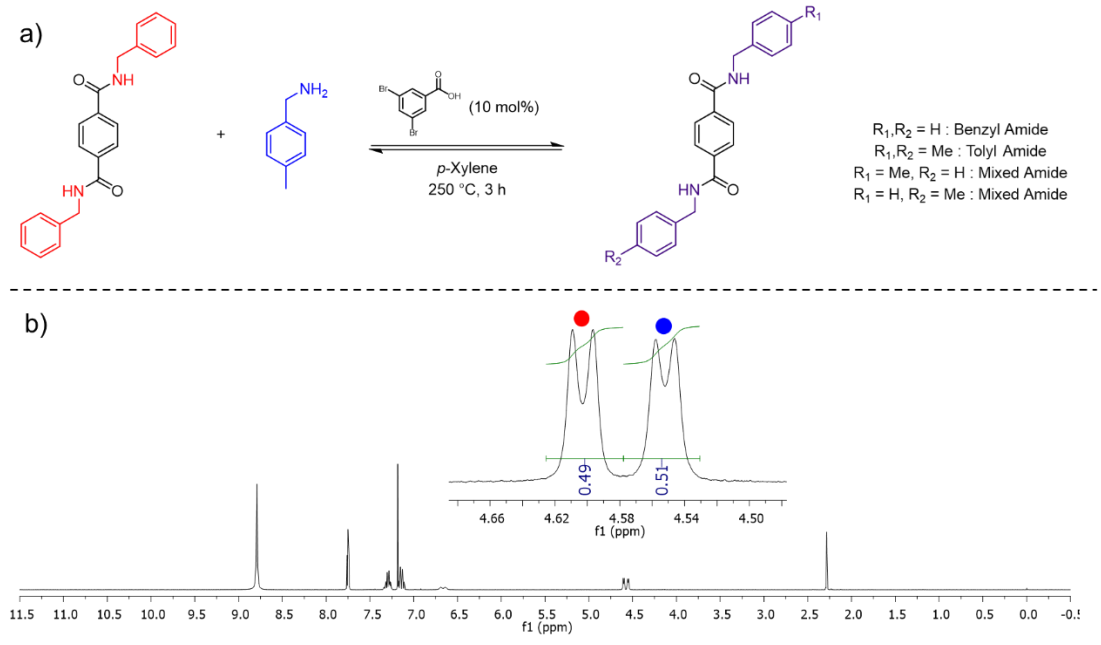

Figure 2.21 – Investigation of use of lower catalyst loading: a) reaction scheme showing transamidation of the model benzyl amide with 4-methylbenzylamine to give a mixed amide product distribution; b) ^{1}H NMR spectrum of mixed amide product, showing the desired ratio of two product amides (49:51 benzyl:tolyl species). Peaks for the benzyl amide are labelled red, while peaks for the tolyl amide are labelled blue.

2.3.3 Investigating the dynamic nature of the transamidation process

Following studies into the function of the catalyst, it was important to further investigate the dynamic nature of the transamidation for the model system. The work of Stahl and co-workers offered key insights into how to tackle this issue.[12,13,17] The main requirement for checking whether a procedure of this nature is dynamic is to ensure that the forward and reverse procedures give the same result. Contrasting to the reports by Stahl, Gellman and co-workers,[12,13,17] the system presented here does not cycle between two sets of species for the "forward" and "reverse" procedures. Instead, the processes are separate reactions that converge to a distribution of the same mixture of amide species, but differ in the starting precursors used (Figure 2.17). Considering this, it was deemed that the transamidation could be dynamic in nature if the two reactions achieve the same final product distribution. To assist with studying this process, an alternative naming convention was adopted – the previously studied model reaction, combining benzyl amide with the tolyl amine was named **Pathway A**, and the converse reaction, combining the tolyl amide with benzylamine, was named **Pathway B**.

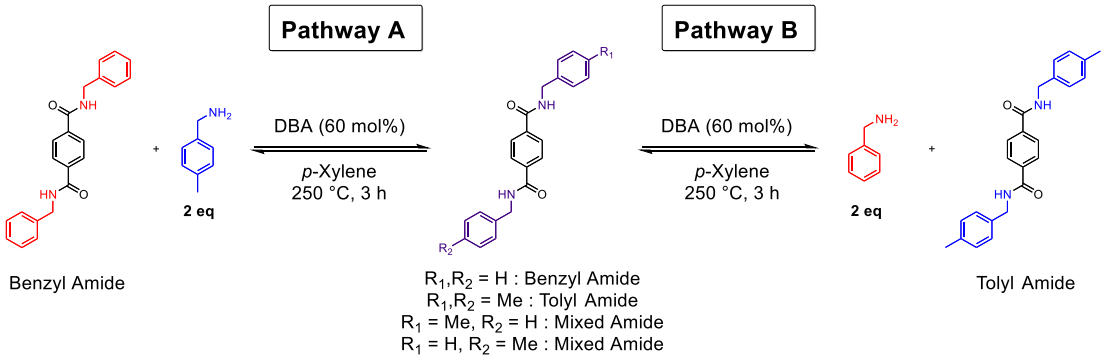

Figure 2.22 – Adopted naming convention for the studied model reaction, pathway A, and the converse reaction using tolyl amide as a starting material, pathway B.

First, it was important to check that the tolyl amide was not a much more thermodynamically desired product. This was done in two ways – first, pathway B was carried out using the previously optimised conditions, combining the tolyl amide with 2 equivalents of benzylamine and 60 mol% DBA in *p*-xylene, and heating at 250 °C for 3 hours (Figure 2.23a). Pleasingly, this gave a similar distribution of amide products as seen for the forward reaction (pathway A), with a ratio of 48:52 benzyl:tolyl amide observed in the ^{1}H NMR spectra.

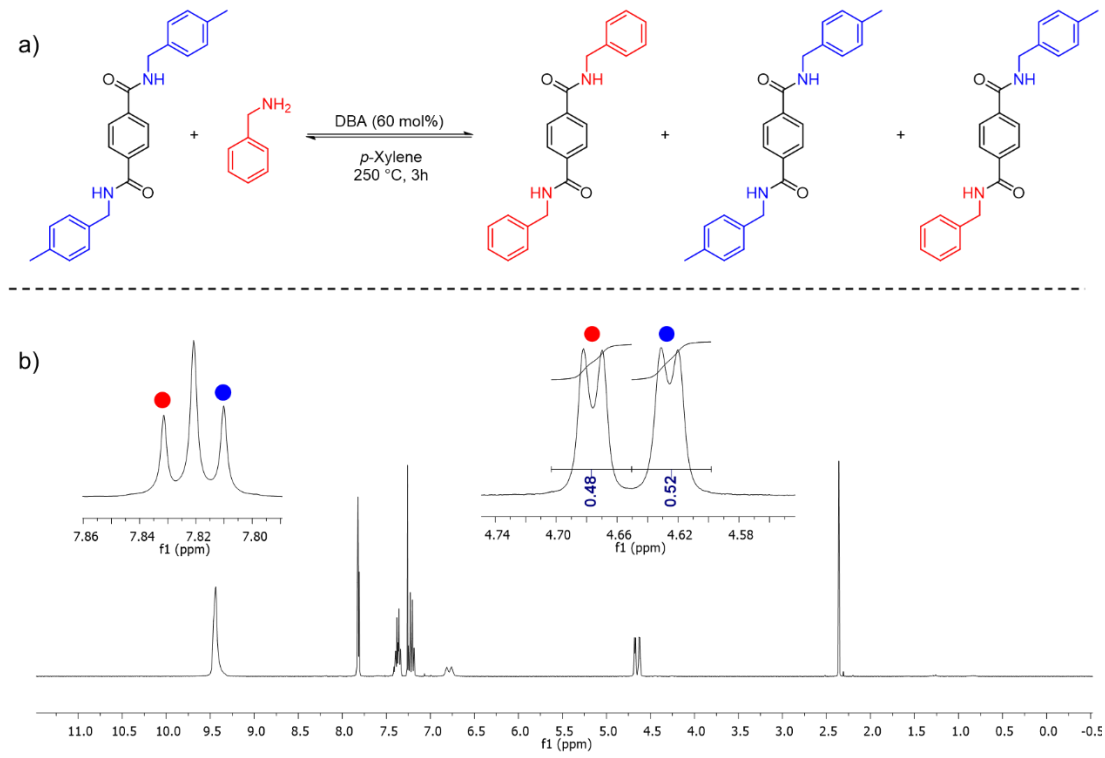

Figure 2.23 - Alternative reaction pathway starting from tolyl amide — combination of the tolyl amide with benzylamine under the optimised reaction conditions (250 °C, 3 h, 60 mol% catalyst) to form the mixed amide products. Peaks for the benzyl amide are labelled red, while peaks for the tolyl amide are labelled blue.

Second, attention was focused on attempting to shift the equilibrium of the transamidation process by the addition of further reagents (Figure 2.24a). Pathway A was used for this study, combining benzyl amide, DBA and 4-methylbenzylamine, and heating at 250 °C for 3 hours. Following this reaction, the mixture of amide species was first isolated and analysed by ^{1}H NMR spectroscopy to ensure the target ratio had been reached (Figure 2.24b). Following confirmation of the ratio (48:52 benzyl:tolyl species), the amide product was combined with fresh catalyst, *p*-xylene, and an excess of benzylamine. Whilst the previous test had shown that the tolyl amide could undergo transamidation to the benzyl amide, it was hoped that the presence of excess benzylamine would bias the reaction back to just the starting amide, *i.e.*, benzyl:tolyl ratio of 100:0. Following heating under the optimised reaction conditions, the product ratio was again checked by ^{1}H NMR spectroscopic analysis, and found to be 83:17 benzyl:tolyl species (Figure 2.24c). Whilst this was not 100:0, it did show

that the formation of tolyl amide was not a thermodynamic sink for the reaction, and that the process could be tuned based on the amount of each free amine added.

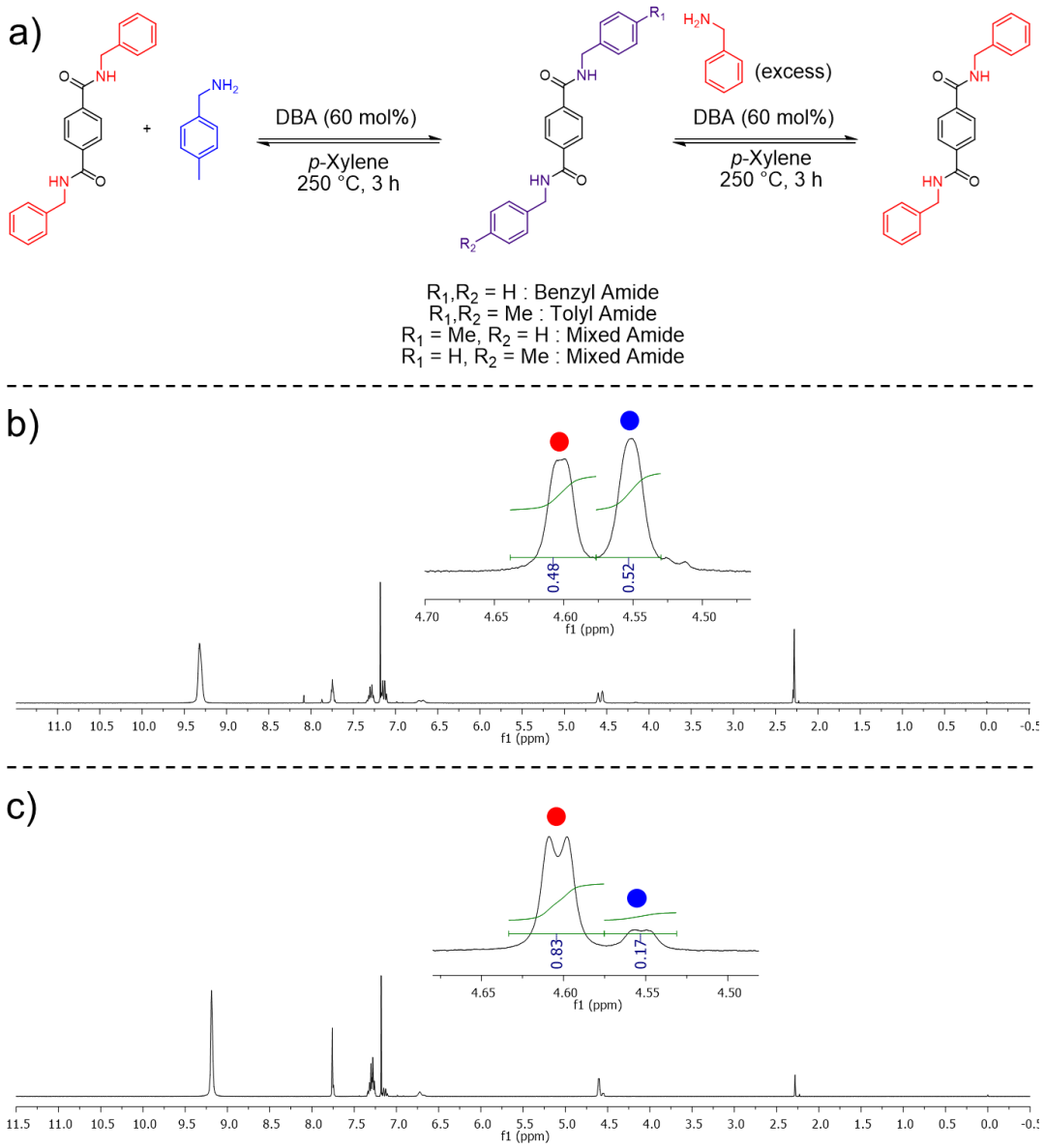

Figure 2.24 – Attempt to shift the equilibrium of the model transamidation reaction: a) proposed reaction by first forming a mixture of amide products, followed by reaction of this mixture with an excess of benzylamine; b) ^{1}H NMR spectra of the initial amide product distribution; c) ^{1}H NMR spectra of the final product distribution following reaction with benzylamine. Peaks for the benzyl amide are labelled red, while peaks for the tolyl amide are labelled blue.

To investigate dynamic exchange more thoroughly, the same principle of monitoring the product amide ratios for both pathways A and B was expanded by completing kinetic screens for these reactions (Figure 2.25). To study the process, the reactions were heated using the optimised conditions, but for extended periods of time (1-9

hours with analysis at 1 hour intervals) to allow the product distributions to reach their final, thermodynamic ratios, that may not have been achieved after the previous 3 hours of heating. In addition, when applied in the formation of materials extended heating may also be required compared to the model system, Therefore, an understanding of how the transamidation changes over longer reaction times could assist future studies. Due to the nature of the programming needed for effective microwave heating, and the precipitation of the amide products, a single reaction sample was not used. Instead, a series of identical reactions were set up for each pathway, varying only the reaction time. Using this method also eliminated the chance of affecting the reaction equilibrium through removal of reagents or products. Following heating, the mixture of amide products were isolated and analysed by ^{1}H NMR spectroscopy, and the ratios compared over time. As before, the target for this study was for both pathways to achieve the same product distribution.

As shown in the plots in Figure 2.25c, the results from these extended kinetic screens initially matched what was expected – both reaction pathways reached an ~50:50 ratio of benzyl:tolyl species after 3 hours (pathway A – 54:46, pathway B – 50:50). These ratios continued to change slightly over the following hours before both reaching a plateau, maintaining the ratios over the more extended heating time. The final benzyl:tolyl amide ratios for pathway A and B were found to be 36:64 and 60:40, respectively. Whilst the ratios are not identical, they are comparable and within error, especially when taking into account the ^{1}H NMR interpretation, or slight differences between reagent amounts between individual reactions. Of interest was the final product bias between the benzyl and tolyl amides. Both pathways need to reach the same end-point, *i.e.,* the thermodynamic product/products of the process (as seen in the previous work of Stahl *et al*.). However, for each reaction, the final ratios were biased towards different products — pathway A in favour of the tolyl amide, and pathway B in favour of the benzyl amide. It was desired to attempt to understand this difference and determine why this was occurring.

One potential reason for the deviance of the final amide ratios from 50:50 towards either benzyl or tolyl species comes from the relative amounts of free amine in the reactions. Using pathway A as an example, successful transamidation with 4-methylbenzylamine for one functionality liberates one equivalent of benzylamine. In a dynamic system, this benzylamine would then be able to react again, potentially liberating 4-methylbenzylamine to shift the product back towards the benzyl amide. However, when the benzylamine is liberated, its relative amount as a free amine

means that the 2 equivalents of 4-methylbenzylamine present is in effect in a huge excess. Therefore, the more likely reaction to take place is further exchange of the benzyl amide with 4-methylbenzylamine to form the tolyl amide — this in turn leads to a bias towards tolyl amide in the final product distribution. For pathway B the opposite would be the case, with a bias towards the benzyl amide.

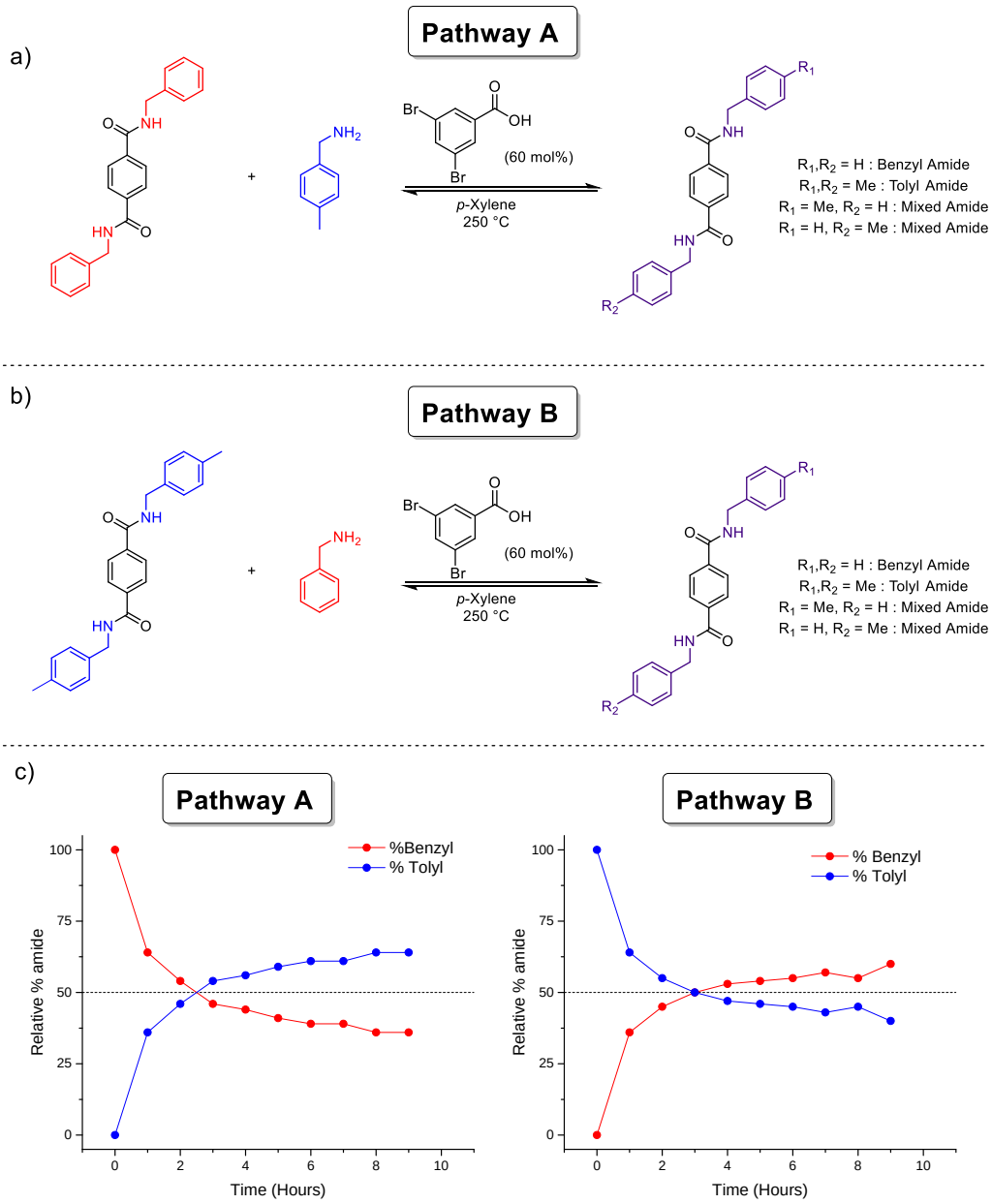

Figure 2.25 – Investigating dynamic exchange for transamidation: a) pathway A, the previously studied model reaction; b) pathway B, the converse reaction combining the tolyl amide and benzylamine; c) plots of relative % of amide vs time for both pathway A and pathway B as determined by ^{1}H NMR spectroscopic analysis, benzyl amide values are shown in red, and tolyl amide values in blue.

To investigate the differing amount of free amine as a potential cause of varied product ratios, an alternative system was devised for further study. Each of the two diamides was individually heated under the optimised conditions, but with 2 equivalents of each of the free amines, benzylamine and 4-methylbenzylamine (Figure 2.26). These processes were named pathway C (starting from the benzyl amide, a) and pathway D (starting from the tolyl amine, Figure 2.26). Use of both benzylamine and 4-methylbenzylamine provided equal amounts of each free amine starting material within each of the reactions, *i.e.*, each amine had equal opportunity to undergo reaction with the respective diamide. Less individual reactions were set up for this study, but the reaction time was extended to 24 hours to allow for full equilibration with the additional amine present.

Both reactions proceeded with successful transamidation; however, the product distributions were opposite to what was seen previously for pathways A and B. The earlier kinetic studies using only one free amine found a bias in the product towards the “product amide”. When using both amines however, it was found that the product now favoured the starting amide, *i.e.*, the product mixture from pathway C contained more benzyl amide, and pathway D contained more tolyl amide. Whilst the starting amounts of free amine were the same, as the reaction progressed and more amine is liberated from the starting amide as part of the transamidation process, the relative ratio of free amine would shift. In each case, it shifts towards the starting moiety, *i.e.*, pathway A favours benzyl, pathway B favours tolyl. This leads to a bias towards the starting amide. As with the previous model reaction, whilst the favoured amide differed in the product distributions, the benzyl:tolyl ratios for pathways C and D were similar, with a final value of ~60:40 in favour of the starting amide for each pathway. As stated previously, the ideal outcome for these studies would have been achieving the same final value for each amide ratio regardless of the pathway used. Whilst this was not the case, the ability to shift the final product distribution by altering the amines used showed that there was a dynamic nature to this process, as neither of the amides were found to be drastically favoured over the other.

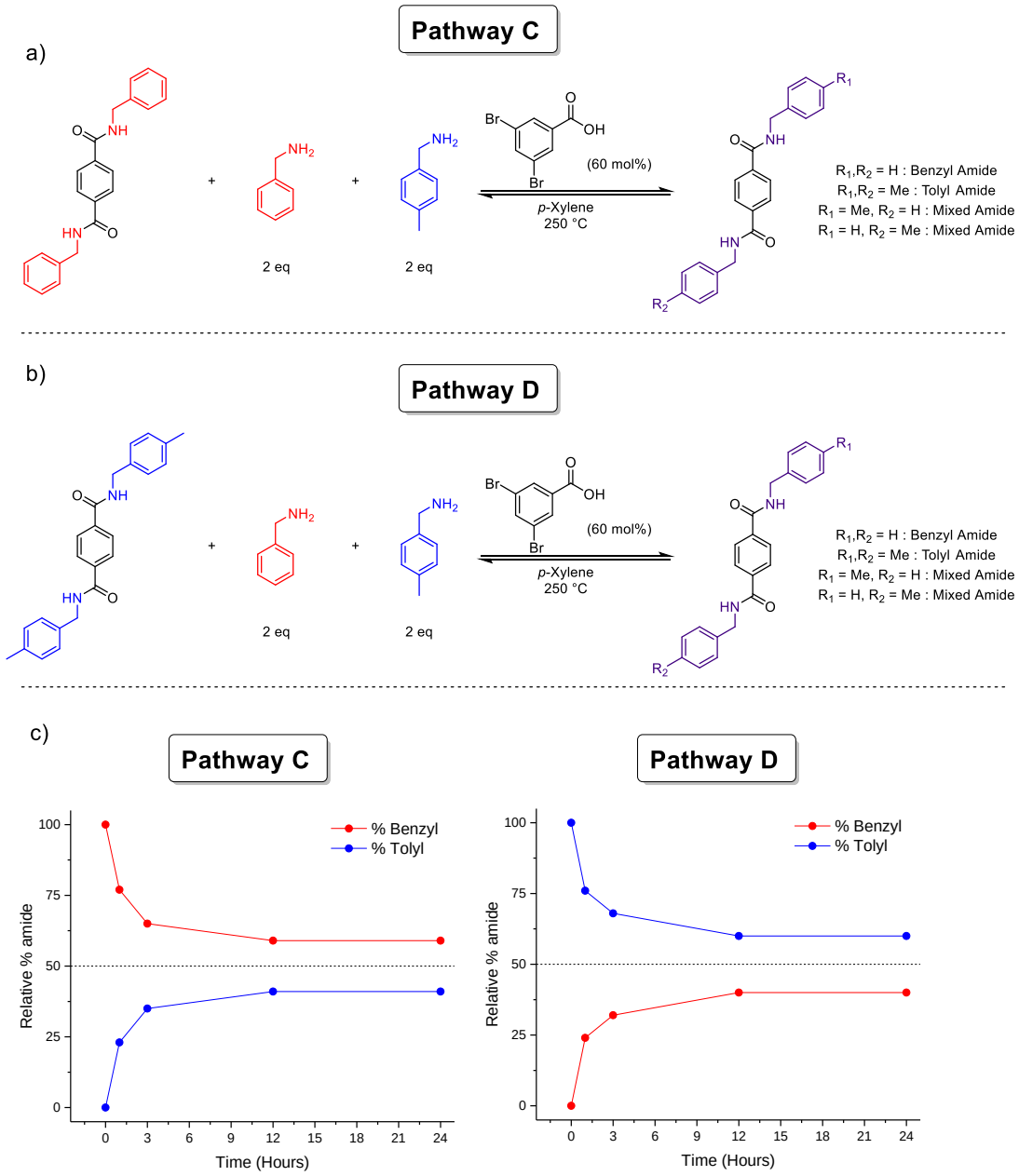

Figure 2.26 - Investigating dynamic exchange for transamidation using a mixture of both free amines: a) pathway C, reaction of the benzyl amide with both free amines; b) pathway B, the converse reaction combining the tolyl amide with both free amines; c) plots of relative % of amide vs time for both pathway C and pathway D as determined by ^{1}H NMR spectroscopic analysis, benzyl amide values are shown in red, and tolyl amide values in blue.

2.4 Dynamic transamidation for amide cage synthesis

Following the development of catalysed dynamic transamidation conditions for a representative model system, and the extended study of the transamidation process, the optimised conditions were used in the attempted synthesis of amide-derived materials. When selecting potential targets, it was important that the precursors matched well with the previous model system – specifically, it was ensured that the structures were based on the *N*-benzylbenzamide moiety. Two cages were theorised, targeting analogues of existing imine cages reported by Greenaway *et al*. and Lauer *et al*.[18,19] The syntheses were based on the reaction of (2,4,6-trimethylbenzene-1,3,5-triyl)trimethanamine (TMT) with either *N,N'*-dibenzylterephthalamide (benzyl amide) or *N,N',N''*-tribenzylbenzene-1,3,5-tricarboxamide (triamide-1). TMT was synthesised according to a known method,[18] and triamide-1 was formed by the reaction of benzylamine with 1,3,5-benzenetricarbonyl trichloride.

Whilst the preferred outcome for the reaction was the successful formation of the target cages, clearly there was the potential for side products, polymeric or otherwise, to form. However, these polymeric or framework materials may well have still shown promise as functional materials. As the crystallinity of these species can have a major impact on their function, efforts have been made to develop methods to improve the crystallinity of amide structures by the application of simple conditions. This includes the efforts of Unterlass and co-workers,[20] as well as a recent report by Stewart *et al.,*[21] investigating conversion of amide polymers into COFs by de-vitrification. Similarly, if the desired materials were not formed, it was hoped that the conditions discussed here could be used for improving the crystallinity of amide-derived materials. The attempted synthesis of these cages was carried out in the same manner as the previous studies, using a MWR and the optimised reaction conditions developed (250 °C, *p*-xylene), for both 3 hour and 24-hour reaction times. The amounts of precursor used were directly based on the model system, maintaining the overall concentration of amide at 0.29 mmol, with the catalyst at 60 mol%. The amide precursor used was then varied based on the number of equivalents required for each target topology.

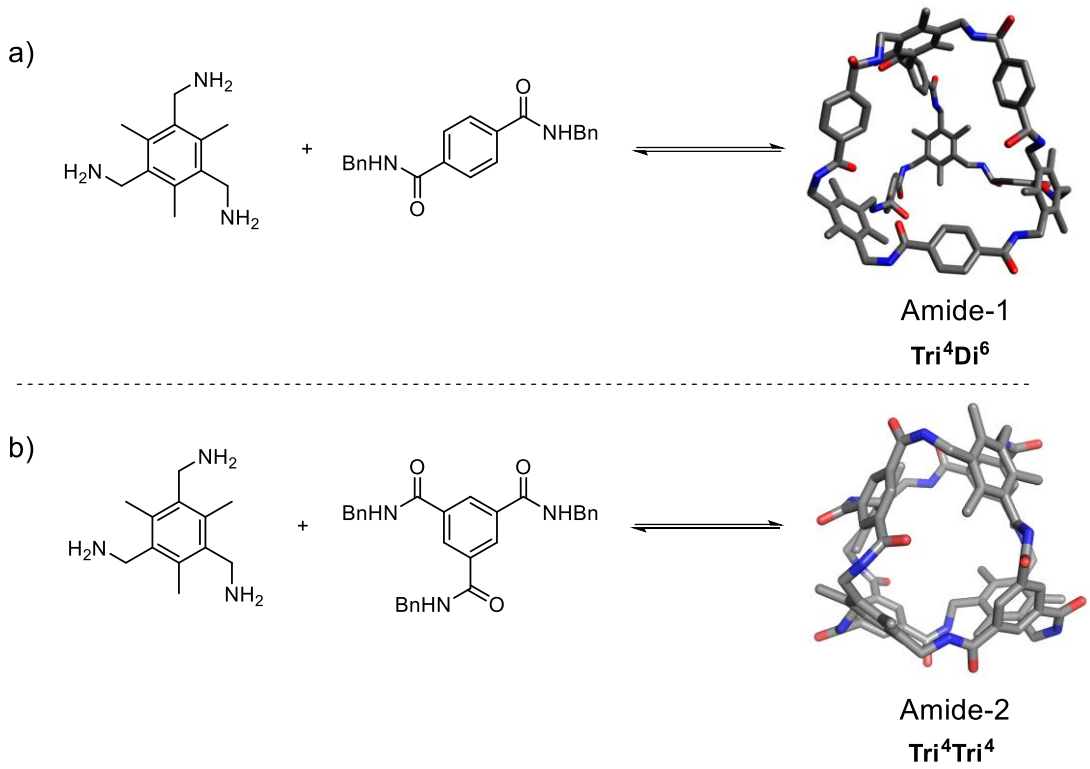

Figure 2.27 - Synthetic targets for attempted transamidations for cage synthesis: a) Amide-1: ***Tri^{4}Di^6*** *cage analogous to imine structure by Greenaway et al.;*[18] *b) Amide-2:* ***Tri^{4}Tri^4*** *cage structure analogous to imine structure reported by Lauer et al.*[19]

All reactions resulted in the formation of dark-brown or black precipitates – it was initially thought these solids may have been misaligned oligomers or polymers formed due to both precursors containing multiple reactive groups. Considering the generally soluble nature of POCs, the reaction filtrates were first examined. ^{1}H NMR spectroscopic analysis of the filtrates showed the presence of peaks within the aromatic region, with an increasing degree of complexity observed in the spectra for the reactions run for a 24-hour reaction time (Figure 2.28). Additionally, the presence of multiple peaks in the ~4.6 ppm region suggested the presence of multiple amide structures. However, without direct literature comparison possible, it was difficult to differentiate characteristic amide-cage peaks in the ^{1}H NMR spectra.

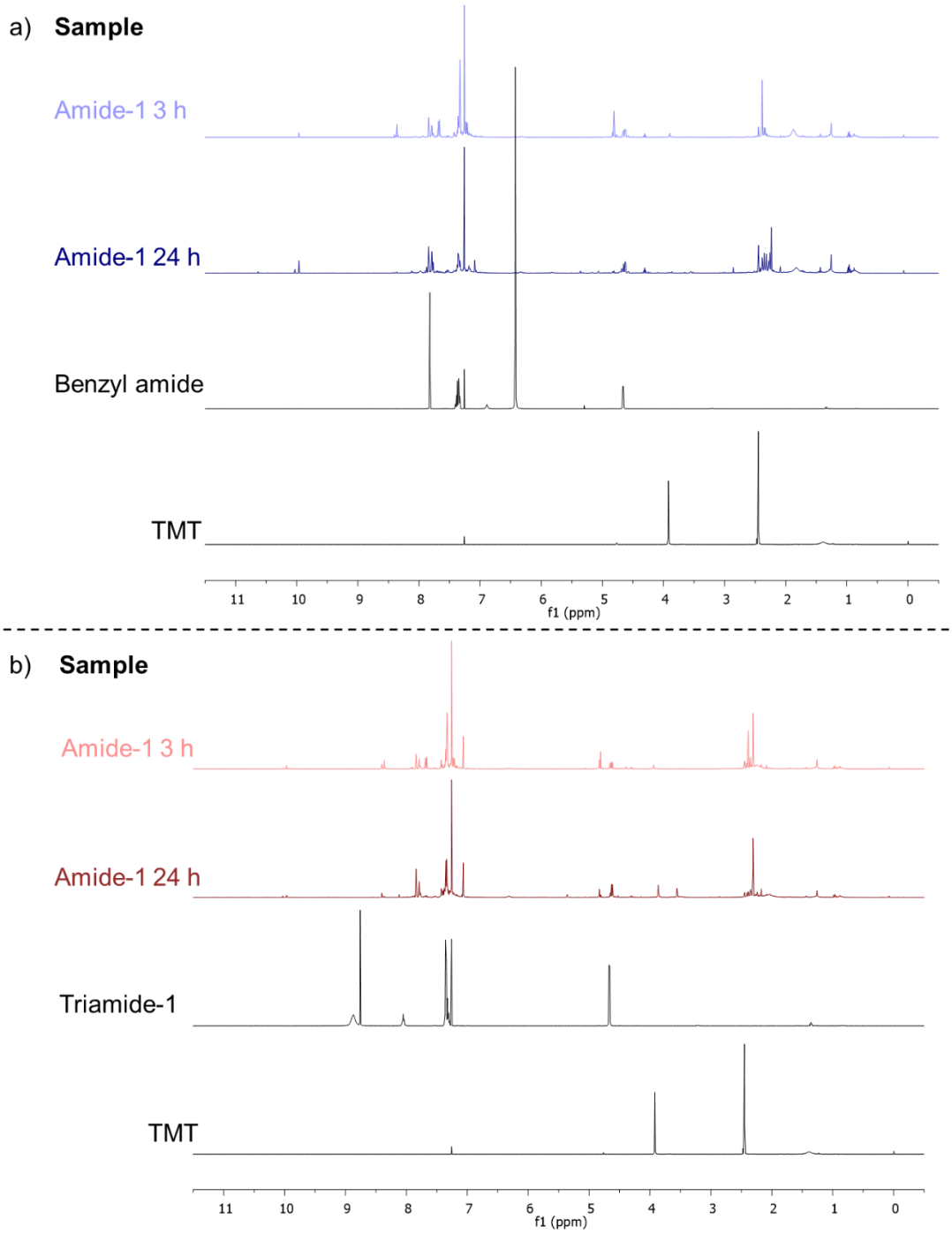

Figure 2.28 – Stacked ^{1}H NMR spectra ($CDCl_3$) for the targeted synthesis of the amide cages; a) ^{1}H NMR spectra of the reaction filtrate for the attempted synthesis of Amide-1 for 3 hours and 24 hours, with precursors benzyl amide and TMT for reference (The large peak visible at ~6.5 ppm for benzyl amide is TFA, used to solubilise the sample for analysis); b) ^{1}H NMR spectra of the reaction filtrate for the attempted synthesis of Amide-2 for 3 hours and 24 hours, with precursors triamide-1 and TMT for reference.

To enable determination of whether there had been any success in cage formation, the product mixtures were therefore investigated using mass spectrometry, with the hope of being able to identify key intermediates or different cage topologies. Expected mass ions for cage structures and key intermediates were first calculated, and then the mass spectra were assessed for the presence of any of these mass ions as their respective charged adducts. Unfortunately, no pre-determined cage or intermediate mass ions could be identified for these filtrate samples

Following this, the insoluble reaction precipitates were also studied. All four products were collected as brown-black solids which were not readily soluble in a range of solvents. The mass recovery of the solids varied slightly between amide-1 and amide-2 — in both cases, less solid was recovered from the 24-hour reactions, though this effect was less pronounced for amide-2 (amide-1 3 h, 78%; 24 h, 65%; amide-2: 3 h, 85%; 24 h, 82%). Clarification of the identity of the solids was difficult, as their poor solubility meant it was not possible to obtain homogenous samples for analysis by ^{1}H NMR spectroscopy or mass spectrometry. IR spectroscopy was therefore attempted for each of the solid products to assess any changes compared to the starting precursors. The IR spectra for both the amide-1 and amide-2 samples presently as extremely similar to those of their respective starting materials (Figure 2.29). In general, definition in the peaks is lost across the spectra — this effect is more pronounced for the samples tested at extended reaction time. Considering the transamidation procedure used, it was expected that any target materials formed would contain the same structural motifs as the starting amides — this includes potential polymeric or oligomeric species formed during the transamidation process.

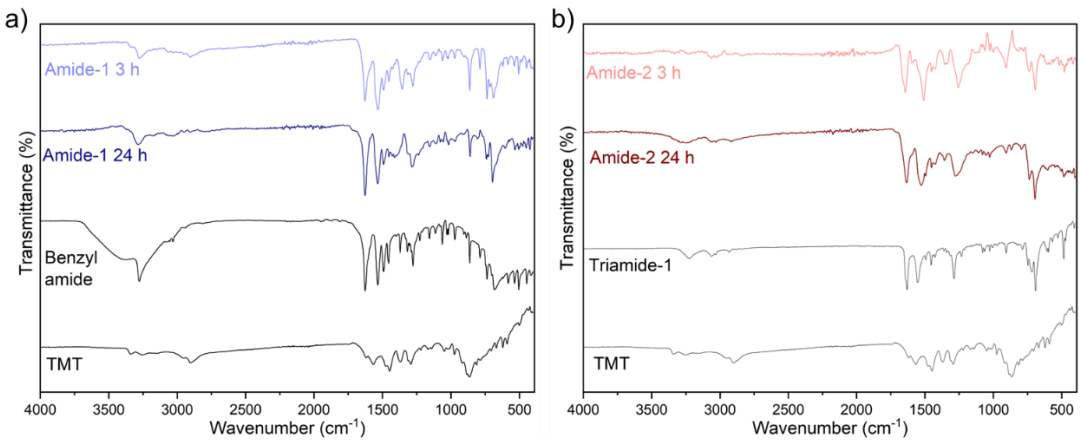

Figure 2.29 – Stacked IR spectra for the solid products formed during attempted amide cage synthesis, with the relative precursors for each cage target; a) amide-1 solid product after 3 h and 24 hour reaction time, with benzyl amide and TMT; b) amide-1 solid product after 3 h and 24 hour reaction time, with triamide-1 and TMT.

Considering the results from IR spectroscopic testing, and the insoluble nature of the solids, the theory remained that these were polymeric species. To assess whether this was the case, the isolated solids were also investigated in terms of their crystalline character. As discussed previously, methods of improving polymer crystallinity have been reported, and it was possible the conditions applied here may exhibit similar effects. For the solid samples, powder X-ray diffraction (PXRD) was used to investigate this concept, but unfortunately, all the samples exhibited generally amorphous PXRD patterns (Figure 2.30). The 3-hour reaction targeting amide-1 resulted in a PXRD pattern that contained some Bragg peaks, indicating some crystallinity, though comparison with the PXRD patterns for the starting materials shows that these Bragg peaks are likely due to unreacted precursor (Figure 2.30a). Increasing the reaction time to 24 hours renders the sample amorphous; some very small Bragg peaks remain, though again these are likely due to remaining precursor. A similar effect is seen for the attempts at amide-2 with very few Bragg peaks present, though it is unknown what caused the peak present at 47°, as this was not present within the precursor patterns. However, the diffraction pattern did not improve on heating for 24 hours, with loss of the present peaks to leave an amorphous spectrum.

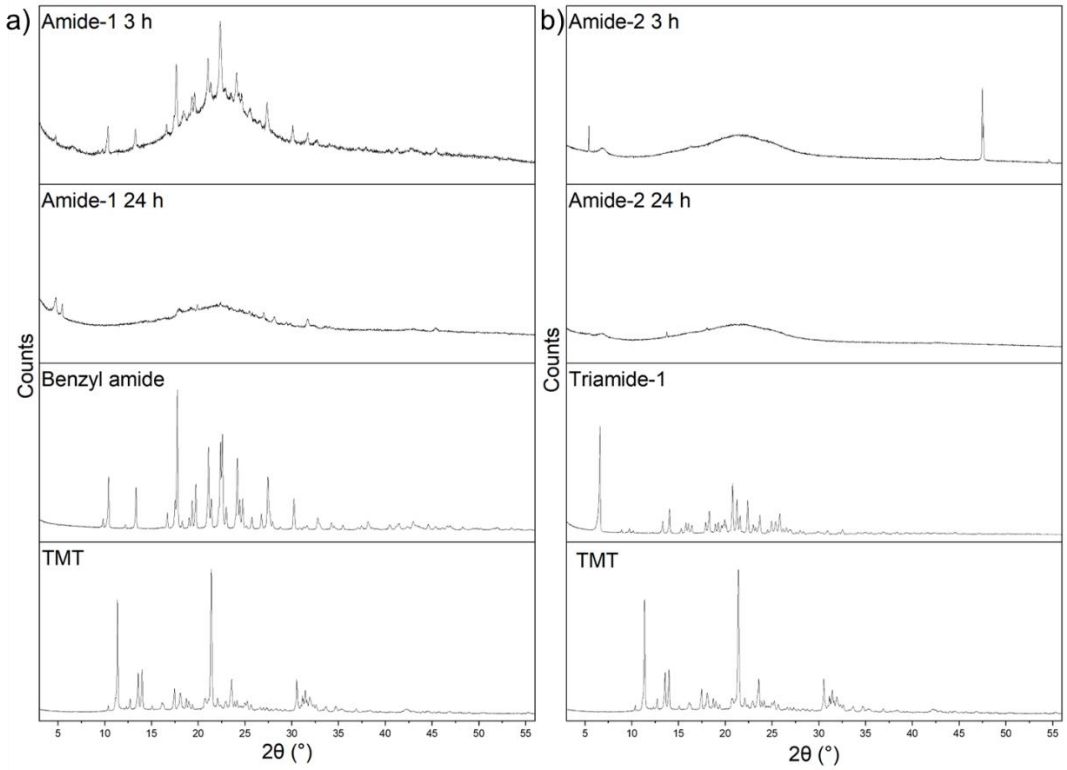

Figure 2.30 – Stacked PXRD patterns for the attempted syntheses of the cages amide-1 (a), and the cage amide-2; (b) also included are the specific starting materials for each cage attempt for reference.

In summary, two potential amide cage targets based were designed, based on both the benzylic amide model system outlined previously, as well as known imine analogues. The precursor combinations were heated using the optimised conditions developed for the previous model system, testing for both 3 hour and 24 hour reaction times. All reactions resulted in the formation of black/brown insoluble precipitates — the reaction filtrates were analysed using 1H NMR spectroscopy and mass spectrometry, but no species indicative of cage formation could be identified. IR spectroscopic analysis of the insoluble solids showed high similarity to the amide starting materials, potential due to polymer/oligomer formation. This was further supported by PXRD patterns for the solids presenting as mostly amorphous, with some crystalline character likely due to the presence of remaining starting material.

2.5 Conclusions and future work

Chapter 2 has outlined attempts to use transamidation as a method for the direct formation of amide cages. A suitable model system was first devised, focused on the reaction of *N*,*N*'-dibenzylterephthalamide with a substituted amine to target a desired 50:50 ratio of amides within the crude reaction product mixture. The model system was chosen such that it could be monitored using ^{1}H NMR spectroscopy, to aid with quick, facile determination of the reaction progress. Following optimisation of the model system, and an investigation into the scope of the catalysis, the conditions were applied in the attempted synthesis of two amide cages, analogous to existing imine structures. The reactions primarily formed insoluble polymeric material, which was difficult to characterise, with analysis by PXRD showing no improvement in crystallinity with extended heating. Analysis of the reaction filtrate showed the presence of peaks in the aromatic region of the ^{1}H NMR spectra, although mass spectrometry of the samples did not show the presence of any mass ions or adducts representative of the target cages or key intermediates.

Despite these target amide cages not being formed, the methodology explored in chapter 2 has outlined an alternative route for dynamic transamidation. In contrast to many existing literature reports, this work has outlined the use of more functionalised benzyl and *p*-tolyl secondary amides. While these functionalities were used to design a model system for analysis by ^{1}H NMR spectroscopy, there is no reason why this could not be expanded to other functional groups. Additionally, the reactions used in this study have all been multitopic, in contrast to most literature transamidation studies which focus on monofunctional amides. During investigation of the model system, it was found that the amount of free amine included was a key factor in what final product ratio was achieved. This shows that the reaction could be suitably tuned to target desired ratios by tailoring the amount of precursor added. In addition, the method of transamidation provides a starting point for further studies into materials formation. A dynamic and tuneable nature was exhibited for the model system — this could be used in conjunction with alternative precursors to target different cages. For example, it may be more effective to target a smaller cage such as **Tri^{2}Di^{3}** topology, or even simpler structures, such as macrocycles, as a starting point. Reaction conditions could also be altered further for materials specific reactions, for example, they may benefit from being carried out at a higher dilution, though clearly this may require additional changes to the reaction method to account for a change in concentration, *i.e.,* longer reaction times.

2.6 Experimental procedures

2.6.1 General synthetic methods

Materials: 1,3,5-Triformylbenzene was purchased from Manchester Organics (UK). Other chemicals were purchased from Fluorochem UK, TCI UK or Sigma-Aldrich. Solvents were reagent grade and purchased from Fischer Scientific, Sigma-Aldrich or Fluorochem. All materials were used as received unless stated otherwise.

Synthesis: Synthesis of reference compounds and materials precursors were stirred magnetically using Teflon-coated stirrer bars. Where heating was required, the reactions were warmed using a stirrer hotplate with heating blocks, with the stated temperature being measured externally to the reaction flask with an attached probe. The syntheses of 2,2',2''-((2,4,6-trimethylbenzene-1,3,5-triyl)tris(methylene))tris(isoindoline-1,3-dione) and (2,4,6-trimethylbenzene-1,3,5-triyl)trimethanamine were completed using a 5 L jacketed reactor. Removal of solvents was done using a rotary evaporator.

Microwave reactions were completed using a Biotage Initiator+ microwave reactor, using a stepwise program for heating to 250 °C. Samples were prepared in 2-5 mL reaction vials, power settings varied but achieved a maximum of 400 W. Pre-stirring was set to 10 seconds, and the stirring rate for the reactions was between 600-900 rpm.

IR Spectra: Infra-red (IR) spectra were recorded on a Bruker Tensor 27 FT-IR using ATR measurements for solids as neat samples.

NMR Spectra: ^{1}H Nuclear magnetic resonance (NMR) spectra were recorded using an internal deuterium lock for the residual protons in $CDCl_3$ (δ = 7.26 ppm), or D_2O (δ = 4.79 ppm) at ambient probe temperature on a Bruker Avance 400 (400 MHz).

Data are presented as follows: chemical shift, peak multiplicity (s = singlet, d =doublet, t = triplet, q = quartet, quint = quintet, m = multiplet, br = broad), coupling constants (J / Hz) and integration. Chemical shifts are expressed in ppm on a δ scale relative to δ_{TMS} (0 ppm) or δ_{CDCl3} (7.26 ppm).

^{13}C NMR Spectra were recorded using an internal deuterium lock using $CDCl_3$ (δ = 77.16 ppm) at ambient probe temperatures on a Bruker Avance 400 (101 MHz).

HRMS spectra: High resolution mass spectrometry (HRMS) was carried out using a 6200 series TOF/6500 series Q-TOF B.09.00 mass spectrometer (fragmentor 120 V) in positive-ion detection mode. The mobile phase was MeOH.

Additional HRMS was carried out using an Agilent Technologies 6530B accurate-mass QTOF Dual ESI mass spectrometer (capillary voltage4000 V, fragmentor 225 V) in positive-ion detection mode. The mobile phase was MeOH +0.1% formic acid at a flow rate of 0.25 mL/min.

PXRD: Laboratory powder X-ray diffraction (PXRD) data were collected in transmission mode on samples held on a held on thin Mylar film in aluminium well plates on a Panalytical X'Pert PRO MPD equipped with a high-throughput screening (HTS) XYZ stage, X-ray focusing mirror and PIXcel detector, using Ni-filtered Cu Kα radiation. Data were measured over the range 0–56° in ~0.013° steps over 30 minutes.

2.6.2 Synthesis of reference compounds

***N,N'*-Dibenzylterephthalamide:**,

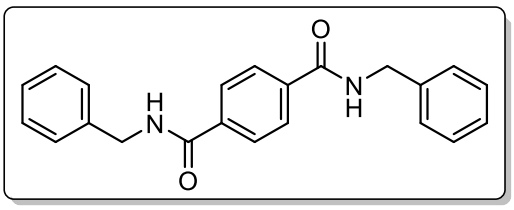

To a round-bottomed flask was added a stirrer bar, terephthaloyl chloride (5.89 g, 29.0 mmol, 1.0 eq), DCM (300 mL), and triethylamine (8.9 mL, 63.8 mmol, 2.2 eq), and the solution left to stir for 5 minutes. Benzylamine (6.97 mL, 63.8 mmol, 2.0 eq) was added and the suspension formed was left to stir overnight at room temperature. After stirring, water (100 mL) was added, and the suspension was filtered under vacuum through a fritted funnel. The collected solid was washed with DCM and left to dry in air. *N*,*N*'-Dibenzylterephthalamide was collected as a colourless powder (Yield = 8.37 g, 24.3 mmol, 84%).

^{1}H NMR (400 MHz, $CDCl_3$) δ_H 7.82 (s, 4H), 7.43 – 7.30 (m, 10H), 6.89 (s, 2H), 4.66 (d, *J* = 5.4 Hz, 4H); **^{13}C NMR** (101 MHz, $CDCl_3$) δ_C 168.87, 136.67, 136.37, 129.24, 128.45, 128.19, 127.88, 45.17. Data in accordance with literature values.[22]

***N,N'*-bis(4-Methylbenzyl)terephthalamide:**

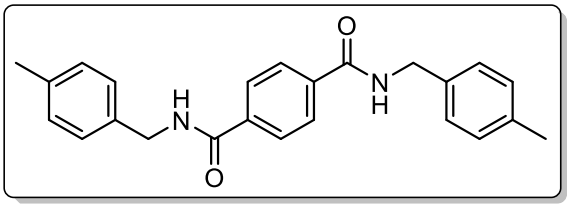

To a round-bottomed flask was added a stirrer bar, terephthaloyl chloride (5.89 g, 29.0 mmol, 1.0 eq), DCM (300 mL), and triethylamine (8.9 mL, 63.8 mmol, 2.2 eq). 4-Methylbenzylamine (6.97 mL, 63.8 mmol, 2.0 eq) was added, with stirring, and the suspension formed was left to stir overnight at room temperature. After stirring, water (100 mL) was added, and the suspension collected by vacuum filtration, washed with DCM, and left to dry under vacuum. *N*,*N*'-bis(4-Methylbenzyl)terephthalamide was collected as a colourless solid (9.67 g, 25.0 mmol, 87%).

IR (ν_{max}/cm^{-1}) 3275, 1634, 1540, 1515, 1498, 1453, 1365, 1302, 1275; **^{1}H NMR** (400 MHz, $CDCl_3$) δ_H 7.81 (s, 4H), 7.26 – 7.16 (m, 8H), 6.79 (br, 2H), 4.62 (d, *J* = 4.6 Hz, 4H), 2.36 (s, 6H); **^{13}C NMR** (101 MHz, $CDCl_3$) δ_C 169.12, 138.45, 136.54, 133.05, 129.91, 128.24, 127.91, 45.10, 21.22; **HRMS** (ES+) calculated for $C_{24}H_{24}N_2O_2$ 372.1838, found $[M+H]^+$ 373.1988; **CHN Analysis**: calculated for $C_{24}H_{24}N_2O_2$: C, 77.39; H, 6.50; N, 7.52; found: C, 75.14; H, 6.36; N, 7.31.

2.6.3 Initial development of transamidation model system

General procedure for the model transamidation reaction:

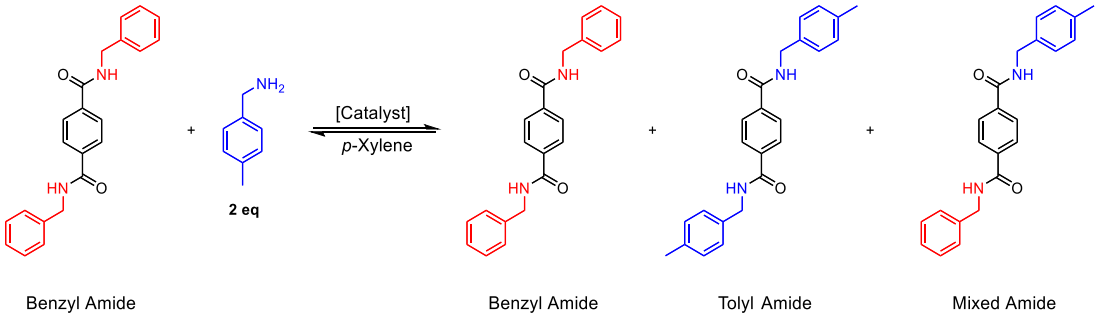

To a MWR vial (2-5 mL) was added a stirrer bar, *N,N*'-dibenzylterephthalamide (100 mg, 0.29 mmol, 1.0 eq) and a selected catalyst (0.058 mmol, 20 mol%), *p*-xylene (4 mL), and 4-methylbenzylamine (0.074 mL, 0.58 mmol, 2.0 eq). The vial was capped and heated in a microwave reactor for a range of reaction times and temperatures. The crude mixture of amide precipitates formed was collected as a colourless solid by vacuum filtration, and washed with acetone, prior to analysis by ^{1}H NMR spectroscopy.

Screening of reaction time for model system:

The general procedure as shown above was used, with testing completed at 1 hour, 3 hour, 6 hour and 12 hour reaction times.

Screening of reaction temperature for model system:

The general procedure as shown above was used, with testing at 100 °C, 150 °C, 200 °C, 210 °C, 220 °C, 230 °C, 240 °C, and 250 °C.

Screening of reaction solvent for model system: The general procedure as shown above was used, with a range of solvents: *p*-xylene, toluene, mesitylene, *n*-butanol, ethylene glycol and tetrahydrofuran.

General procedure for strong acid catalyst screening for model reaction:

To a MWR vial (2-5 mL) was added a stirrer bar, *N,N'*-dibenzylterephthalamide (100 mg, 0.29 mmol, 1.0 eq) and a selected catalyst (0.058 mmol, 20 mol%), *p*-xylene (4 mL), and 4-methylbenzylamine (0.074 mL, 0.58 mmol, 2.0 eq). The vial was capped and heated in a microwave reactor at 200 °C for 3 hours. The crude mixture of amide precipitates formed was collected by vacuum filtration, washed with acetone, and dried under vacuum.

2.6.4 Extended catalyst screening for model reaction

General procedure for extended catalyst screening:

To a MWR vial (2-5 mL) was added a stirrer bar, *N,N'*-dibenzylterephthalamide (100 mg, 0.29 mmol, 1.0 eq) and a selected catalyst (Figure 2.31)(0.058 mmol, 20 mol%), *p*-xylene (4 mL), and 4-methylbenzylamine (0.074 mL, 0.58 mmol, 2.0 eq). The vial was capped and heated in a microwave reactor for 1 hour at 200 °C. The crude mixture of amide precipitates formed was collected by vacuum filtration, washed with acetone, and dried under vacuum to give the amide products, prior to analysis by ^{1}H NMR spectroscopy (Figure 2.32).

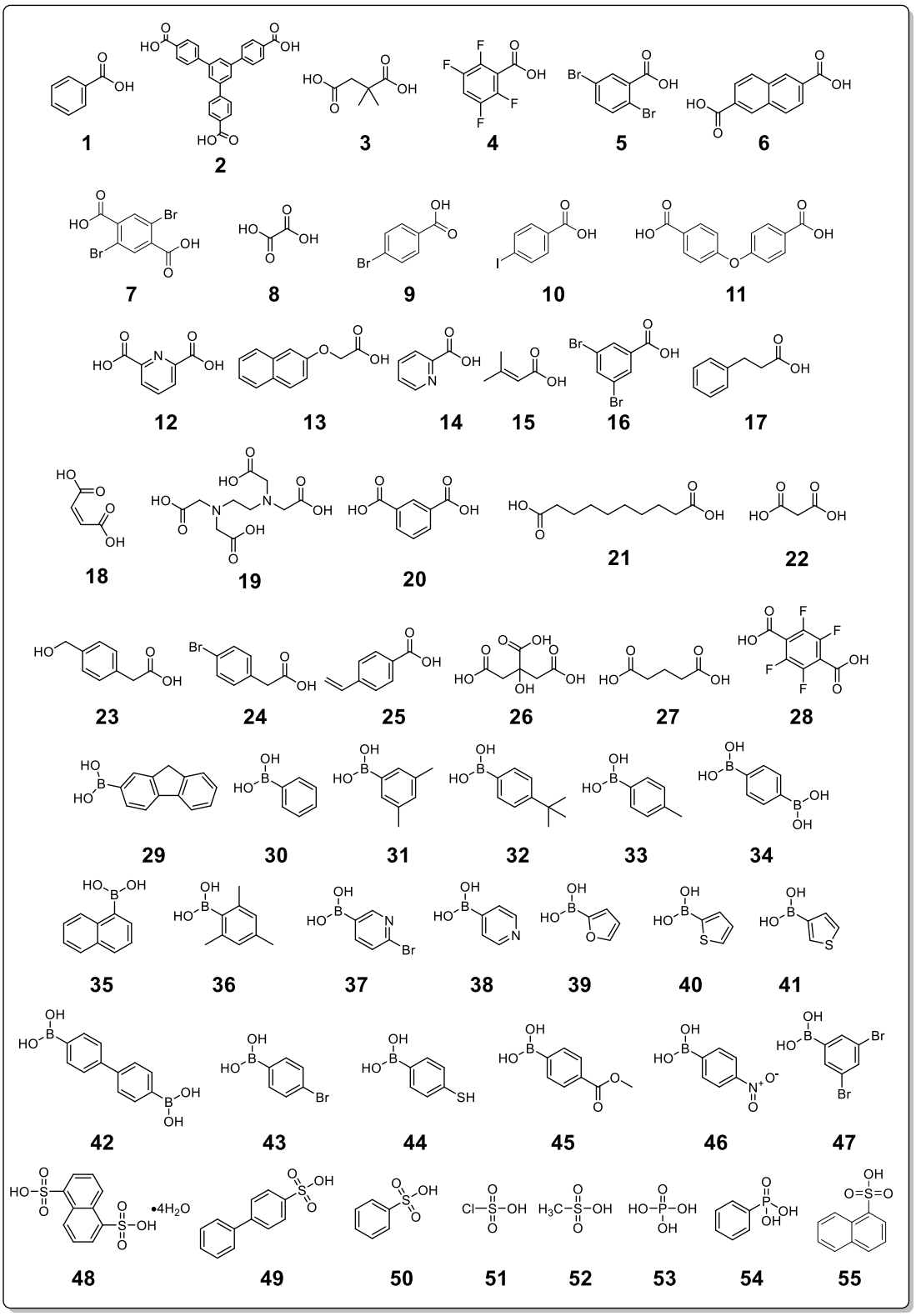

Figure 2.31 – Structures of the 55 catalysts tested as part of the extended catalyst screen, using a variety of carboxylic, boronic, sulfonic and phosphonic acids.

Figure 2.32 – Amide product distributions values for reactions from extended catalyst screen.

Product distributions for large scale catalyst testing:

Reference Number	Catalyst Name	% Benzyl Amide	% Tolyl Amide
1	Benzoic acid	97	3
2	1,3,5-Tris(4-carboxyphenyl)benzene	100	0
3	2,2-Dimethylsuccinic acid	98	2
4	2,3,5,6-Tetrafluorobenzoic acid	100	0
5	2,5-Dibromobenzoic acid	95.4	4.6
6	2,6-Naphthalenedicarboxylic acid	100	0
7	2,5-Dibromoterephthalic acid	100	0
8	Oxalic acid	100	0
9	4-Bromobenzoic acid	96.1	3.9
10	4-Iodobenzoic acid	96	4
11	4,4'-Oxybis(benzoic acid)	94.3	5.7
12	2,6-Pyridinedicarboxylic acid	100	0
13	2-Naphthoxyacetic acid	100	0
14	2-Picolinic acid	100	0
15	3,3-Dimethylacrylic acid	97.6	2.4
16	3,5-Dibromobenzoic acid	95.5	4.5
17	3-Phenylpropionic acid	97	3
18	Maleic acid	97.7	2.3
19	Ethylenediaminetetraacetic acid	97.9	2.1
20	Isophthalic acid	93.9	6.1
21	Sebacic acid	96.7	3.3
22	Malonic acid	100	0
23	4-(Hydroxymethyl)phenylacetic acid	100	0
24	4-Bromophenylacetic acid	97.3	2.7
25	4-Vinylbenzoic acid	97.2	2.8
26	Citric acid	96.8	3.2
27	Glutaric acid	96	4
28	Tetrafluoroterephthalic acid	100	0
29	Fluorene-2-boronic acid	100	0

30	Phenylboronic acid	100	0
31	3,5-Dimethylbenzeneboronic acid	100	0
32	4-tert-Butylphenylboronic acid	100	0
33	4-Tolylboronic acid	100	0
34	Benzene-1,4-diboronic acid	100	0
35	1-Naphthaleneboronic acid	100	0
36	2,4,6-Trimethylphenylboronic acid	100	0
37	2-Bromo-5-pyridineboronic acid	100	0
38	4-Pyridinylboronic acid	100	0
39	2-Furanylboronic acid	100	0
40	2-Thienylboronic acid	100	0
41	3-Thienylboronic acid	100	0
42	4,4'-Biphenyldiboronic acid	100	0
43	4-Bromophenylboronic acid	96.8	3.2
44	4-Mercaptophenylboronic acid	100	0
45	4 Methoxycarbonylphenylboronic acid	100	0
46	4-Nitrophenylboronic acid	100	0
47	3,5-Dibromophenylboronic acid	100	0
48	1,5-Naphthalenedisulfonic acid tetrahydrate	100	0
49	4-Biphenylsulfonic acid	100	0
50	Benzenesulfonic acid	100	0
51	Chlorosulfonic acid	100	0
52	Methanesulfonic acid	100	0
53	Phosphoric acid	100	0
54	Phenylphosphonic acid	100	0
55	1-Naphthalenesulfonic acid	100	0

2.6.5 Synthetic procedures for investigation of the catalyst role

Synthetic procedure for optimised transamidation model reaction

To a MWR vial (2-5 mL) was added a stirrer bar a stirrer bar, *N,N'*-dibenzylterephthalamide (100 mg, 0.29 mmol, 1.0 eq), 3,5-dibromobenzoic acid (48.7 mg, 0.174 mmol, 60 mol%), *p*-xylene (4 mL), and 4-methylbenzylamine (0.074 mL, 0.58 mmol, 2.0 eq). The vial was capped and heated in a microwave reactor at 250 °C for 3 hours, then left to cool to room temperature. The crude mixture of amide precipitates formed was collected as a colourless solid by vacuum filtration, washed with *p*-xylene, and dried under vacuum.

Synthetic procedure for investigation of temperature *vs* catalysis on the degree of transamidation

To a MWR vial (2-5 mL) was added with a stirrer bar, *N,N'*-dibenzylterephthalamide (100 mg, 0.29 mmol, 1.0 eq), *p*-xylene (4 mL), and 4-methylbenzylamine (0.074 mL, 0.58 mmol, 2.0 eq). The vial was capped and heated in a microwave reactor at 250 °C for 3 hours, then left to cool to room temperature. The crude mixture of amide precipitates formed was collected as a colourless solid by vacuum filtration, washed with *p*-xylene, and dried under vacuum.

Synthetic procedure for the direct reaction of DBA catalyst with free amine

To a MWR vial (2-5 mL) was added a stirrer bar, 3,5-dibromobenzoic acid (48.7 mg, 0.174 mmol, 60 mol%), *p*-xylene (4 mL), and 4-methylbenzylamine (0.074 mL, 0.58 mmol, 2.0 eq). The vial was capped and heated in a microwave reactor at 250 °C for 3 hours, then left to cool to room temperature. The crude mixture of amide precipitates formed was collected as a colourless solid by vacuum filtration, washed with *p*-xylene, and dried under vacuum.

Synthetic procedure for model reaction using lower catalyst loading

To a MWR vial (2-5 mL) was added a stirrer bar, 3,5-dibromobenzoic acid (0.029 mmol, 10 mol%), *p*-xylene (4 mL), and 4-methylbenzylamine (0.074 mL, 0.58 mmol, 2.0 eq). The vial was capped and heated in a microwave reactor at 250 °C for 3 hours, then left to cool to room temperature. The crude mixture of amide precipitates was

collected as a colourless solid by vacuum filtration, washed with *p*-xylene, and dried under vacuum.

2.6.6 Synthetic procedures for investigation of dynamic transamidation.

Synthetic procedure for transamidation model reaction starting from tolyl amide (pathway B)

To a MWR vial (2-5 mL) was added a stirrer bar, *N,N'*-bis(4-methylbenzyl)terephthalamide (108 mg, 0.29 mmol, 1.0 eq), 3,5-dibromobenzoic acid (48.7 mg, 0.174 mmol 60 mol %), *p*-xylene (4 mL), and benzylamine (0.06 mL, 0.58 mmol, 2.0 eq). The vial was capped and heated in a microwave reactor at 250 °C for 3 hours, then left to cool to room temperature. The crude mixture of amide precipitates formed was collected as a colourless solid by vacuum filtration, washed with *p*-xylene, and dried under vacuum.

Synthetic procedure for reaction of benzyl amide with both free amines (pathway C)

To a MWR vial (2-5 mL) was added a stirrer bar, *N,N'*-dibenzylterephthalamide (100 mg, 0.29 mmol, 1.0 eq), 3,5-dibromobenzoic acid (48.7 mg, 0.174 mmol 60 mol %), *p*-xylene (4 mL), benzylamine (0.06 mL, 0.58 mmol, 2.0 eq), and 4-methylbenzylamine (0.074 mL, 0.58 mmol, 2.0 eq). The vial was capped and heated in a microwave reactor at 250 °C for 3 hours, then left to cool to room temperature. The crude mixture of amide precipitates formed was collected as a colourless solid by vacuum filtration, washed with *p*-xylene, and dried under vacuum.

Synthetic procedure for reaction of benzyl amide with both free amines (pathway D)

To a MWR vial (2-5 mL) was added a stirrer bar, *N,N'*-bis(4-methylbenzyl)terephthalamide (108 mg, 0.29 mmol, 1.0 eq), 3,5-dibromobenzoic acid (48.7 mg, 0.174 mmol, 60 mol %) , *p*-xylene (4 mL), benzylamine (0.06 mL, 0.58 mmol, 2.0 eq) and 4-methylbenzylamine (0.074 mL, 0.58 mmol, 2.0 eq). The vial was capped and heated in a microwave reactor at 250 °C for 3 hours, then left to cool to room temperature. The crude mixture of amide precipitates formed was collected as a colourless solid by vacuum filtration, washed with *p*-xylene, and dried under vacuum.

2.6.7 Synthesis of precursors for materials screen

Synthesis of *N,N',N''*-tribenzylbenzene-1,3,5-tricarboxamide:

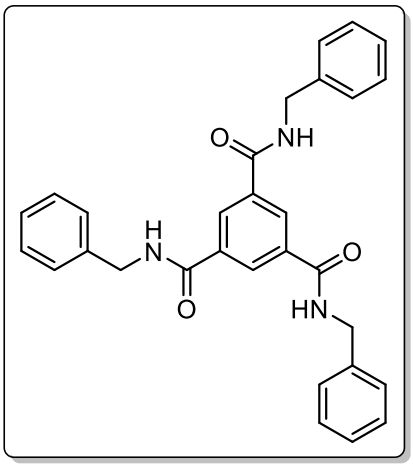

To a solution of 1,3,5-benzenetricarbonyl trichloride (1.00 g, 3.77 mmol, 1.0 eq) in DCM (100 mL) was added triethylamine (1.57 mL, 11.3 mmol, 3.0 eq), and the mixture was left to stir for 5 minutes. Benzylamine (1.23 mL, 11.3 mmol, 3.0 eq) was added, and the reaction was left to stir overnight. The solvent was then removed *in vacuo*, and THF (100 mL) was added to precipitate triethylamine-hydrochloride (TEA·HCl) salts which were removed under vacuum filtration. The THF was removed from the filtrate to give *N,N',N''*-tribenzylbenzene-1,3,5-tricarboxamide as a colourless solid, which was used without further purification (1.14 g, 2.34 mmol 63%).

^{1}H NMR (400 MHz, DMSO) δ_H 9.27 (t, *J* = 6.0 Hz, 3H), 8.51 (s, 3H), 7.37 – 7.30 (m, 12H), 7.28 – 7.22 (m, 3H), 4.51 (d, *J* = 5.9 Hz, 6H); **^{13}C NMR** (101 MHz, DMSO) δ_C 165.46, 139.39, 134.91, 128.76, 128.31, 127.38, 126.84, 42.84. Data in accordance with literatures values.[23]

Synthesis of 2,2',2''-((2,4,6-trimethylbenzene-1,3,5-triyl)tris(methylene))tris(isoindoline-1,3-dione)

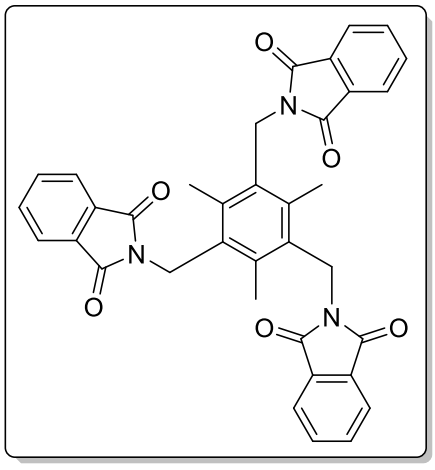

A modification of the procedure by Greenaway *et al*. was used for this reaction.[18] To a solution of 1,3,5-tris(bromomethyl)-2,4,6-trimethylbenzene (75.00 g, 188 mmol, 1.0 eq.) and 18-crown-6 (14.89 g, 56.36 mmol, 0.3 eq.) in toluene (2.4 L) was added potassium phthalimide (125.3 g, 676.76 mmol, 3.6 eq.). The mixture was heated at 100 °C under N_2 for 72 hours before being allowed to cool to room temperature. The mixture was filtered and the resulting solid suspended in water (1200 mL) and collected by filtration. The resulting solid was further washed with water (2 × 800 mL) and MeOH (1200 mL) before being dried *in vacuo* to afford

the desired product as a colourless solid which was used without further purification (111 g, 186 mmol 99%).

^{1}H NMR (400 MHz, $CDCl_3$) δ_H 7.78 (dd, *J* = 5.5, 3.0 Hz, 6H), 7.67 (dd, *J* = 5.5, 3.1 Hz, 6H), 4.95 (s, 6H, 2.50 (s, 9H); **^{13}C NMR** (101 MHz, $CDCl_3$) δ_C 168.19, 138.54, 133.89, 131.94, 130.18, 123.24, 38.58, 17.32. Data in accordance with literature values.[24]

Synthesis of (2,4,6- trimethylbenzene-1,3,5-triyl)trimethanamine:

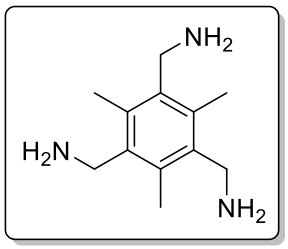

A modification of the procedure by Greenaway *et al*. was used for this reaction.[18] To a suspension of 2,2',2''-((2,4,6-trimethylbenzene-1,3,5-triyl)tris(methylene))tris(isoindoline-1,3-dione) (74.86 g, 125.26 mmol, 1.0 eq.) in a mixture of toluene (1100 mL) and EtOH (2200 mL) was added hydrazine hydrate in a single portion (46.8 mL, 50 wt% solution in water, 751.58 mmol, 6.0 eq.). The resulting mixture was heated at 90 °C for 5 days, at which point a large amount of solid had precipitated, before being allowed to cool to room temperature. The reaction mixture was concentrated *in vacuo* (not to dryness) and partitioned between an aqueous KOH solution (400 mL, 40 wt%) and $CHCl_3$ (1000 mL). The aqueous layer was further extracted with $CHCl_3$ (2 × 600 mL) before the combined organic layers were dried (Na_2SO_4) and concentrated *in vacuo* to afford the desired triamine as a pale-yellow solid which was used without further purification (23.5 g, 113 mmol, 90%).

^{1}H NMR (400 MHz, $CDCl_3$) δ_H 3.92 (s, 6H), 2.45 (s, 9H), 1.36 (s, 6H); **^{13}C NMR** (101 MHz, $CDCl_3$) δ_C 138.12, 133.50, 40.82, 15.41. Data in accordance with literature values.[24]

2.6.8 Synthesis of amide materials using transamidation

Attempted synthesis of Greenaway *et al.* cage analogue (Tri^4Di^6 cage, Amide-1)

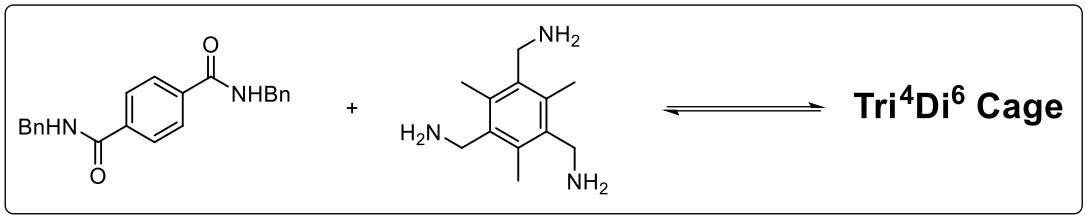

To a MWR vial (2-5 mL) was added a stirrer bar, *N,N'*-dibenzylterephthalamide (100 mg, 0.29 mmol, 1. eq.), 3,5-dibromobenzoic acid (48.7 mg, 0.174 mmol, 60 mol %), (2,4,6-trimethylbenzene-1,3,5-triyl)trimethanamine (40 mg, 0.19 mmol, 0.67 eq) and *p*-xylene (4 mL). The vial was sealed and heated in an MWR reactor to 250 °C for either 3 or 24 hours. The vial was left to cool, and any precipitate formed was collected using vacuum filtration, washed with *p*-xylene and dried under vacuum, then analysed using PXRD and IR spectroscopy. The reaction filtrates were reduced to dryness, dissolved in $CDCl_3$, and analysed with ^{1}H NMR spectroscopy and HRMS.

Amide-1, 3 hours solid sample: 109 mg; mass recovery = 78%

Amide-1, 24 hours solid sample: 91 mg; mass recovery = 65%

Attempted synthesis of Lauer *et al.* cage analogue (Tri^4Tri^4 cage, Amide-2)

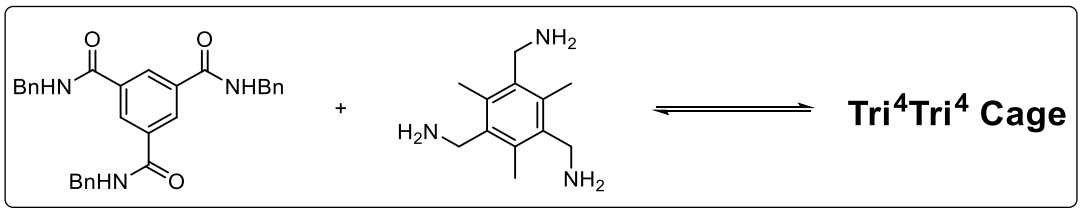

To a MWR vial (2-5 mL) was added a stirrer bar, *N,N',N''*-tribenzylbenzene-1,3,5-tricarboxamide (138 mg, 0.29 mmol, 1.0 eq.), 3,5-dibromobenzoic acid (48.7 mg, 0.174 mmol, 60 mol %), (2,4,6-trimethylbenzene-1,3,5-triyl)trimethanamine (60 mg, 0.29 mmol, 1 eq.) and *p*-xylene (4 mL). The vial was sealed and heated in an MWR reactor to 250 °C for either 3 or 24 hours. The vial was left to cool, and any precipitate formed was collected using vacuum filtration, washed with *p*-xylene and dried under vacuum. The reaction filtrates were reduced to dryness, dissolved in $CDCl_3$, and analysed with ^{1}H NMR spectroscopy and HRMS.

Amide-2, 3 hours solid sample: 168 mg; mass recovery = 85%

Amide-2, 24 hours solid sample: 163 mg; mass recovery = 82%

2.6.9 Supplementary spectra

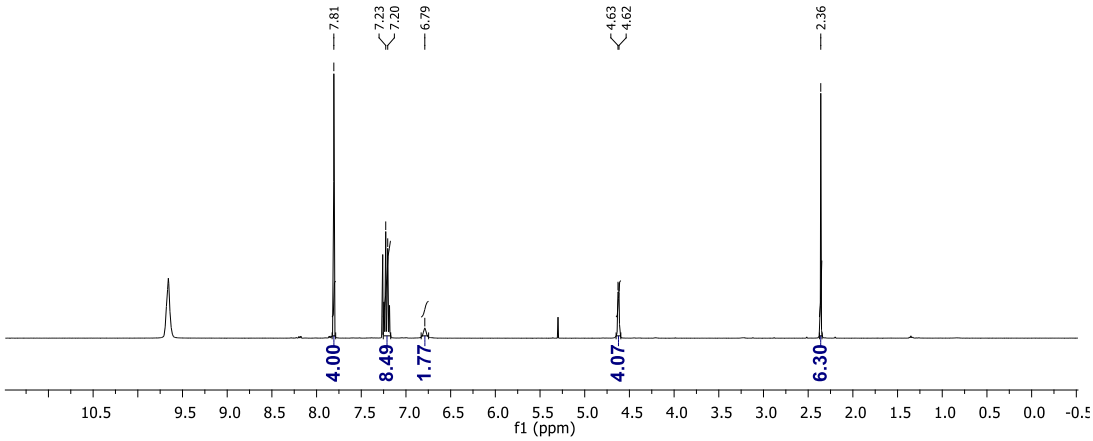

Figure 2.33 - ^{1}H NMR spectrum ($CDCl_3$) of N,N'-bis(4-methylbenzyl)terephthalamide "tolyl amide"; the peak at ~9.6 ppm is trifluroacetic acid used to assist dissolution of the sample.

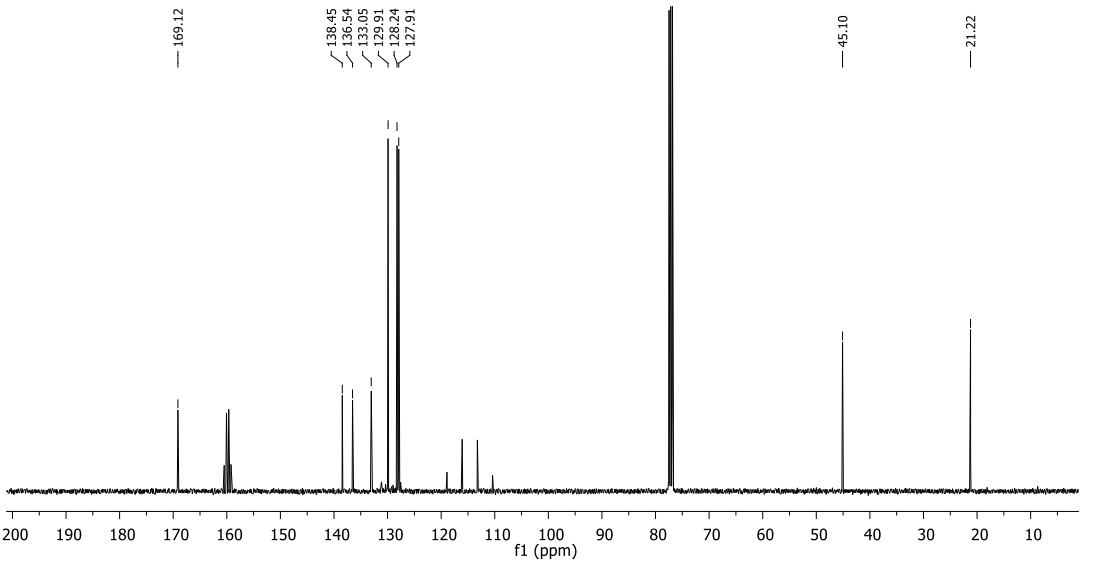

Figure 2.34 - ^{13}C NMR spectrum ($CDCl_3$) of N,N'-bis(4-methylbenzyl)terephthalamide "tolyl amide".

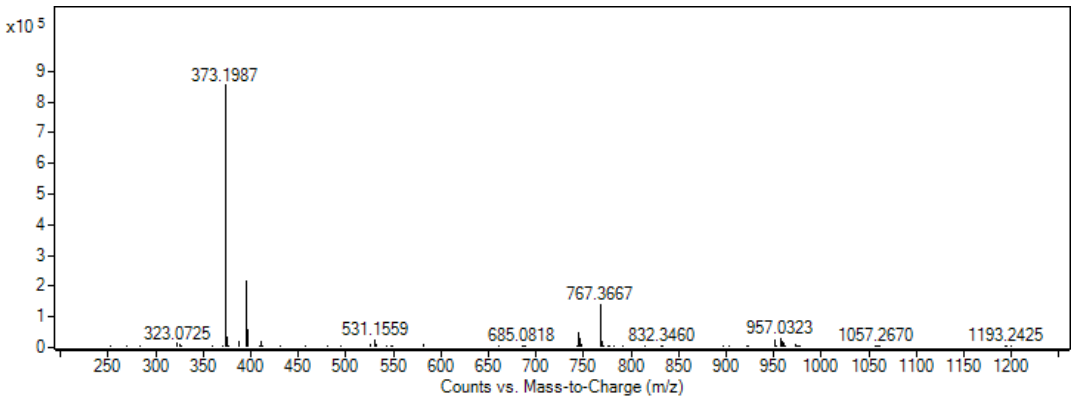

Figure 2.35 – Mass spectrum of N,N'-bis(4-methylbenzyl)terephthalamide "tolyl amide".

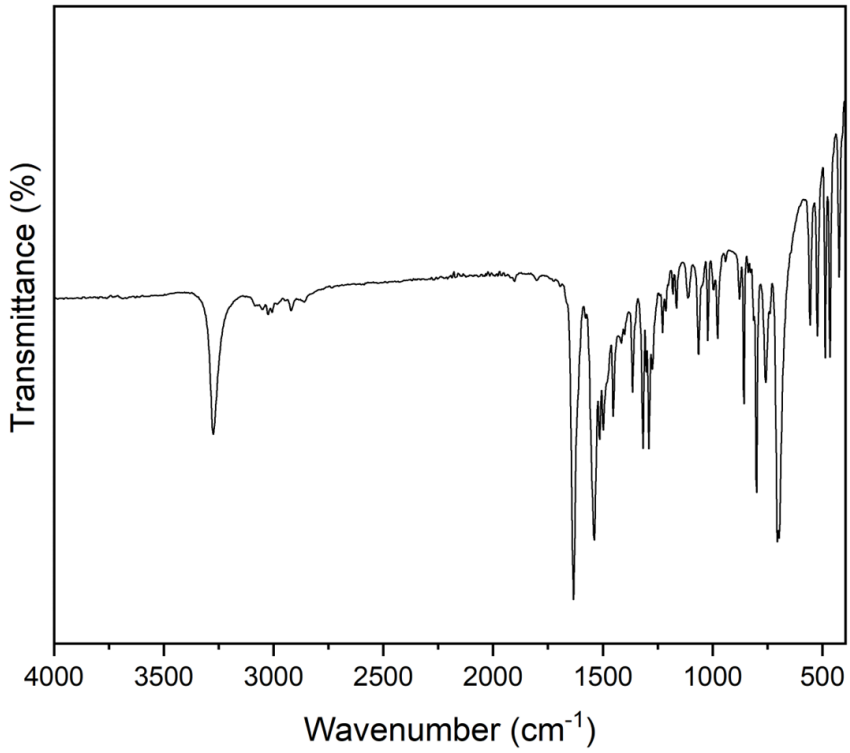

Figure 2.36 – IR spectrum of N,N'-bis(4-methylbenzyl)terephthalamide "tolyl amide".

2.7 References

1 H. Erguven, E. N. Keyzer and B. A. Arndtsen, *Chem. – A Eur. J.*, 2020, 1–9.

2 A. Fleischer, *Berichte der Dtsch. Chem. Gesellschaft*, 1876, **9**, 992–995.

3 E. Bon, D. C. H. Bigg and G. Bertrand, *J. Org. Chem.*, 1994, **59**, 4035–4036.

4 T. B. Nguyen, J. Sorres, M. Q. Tran, L. Ermolenko and A. Al-Mourabit, *Org. Lett.*, 2012, **14**, 3202–5.

5 J. W. Wu, Y. D. Wu, J. J. Dai and H. J. Xu, *Adv. Synth. Catal.*, 2014, **356**, 2429–2436.

6 S. N. Rao, D. C. Mohan and S. Adimurthy, *Org. Lett.*, 2013, **15**, 1496–1499.

7 R. Vanjari, B. Kumar Allam and K. Nand Singh, *RSC Adv.*, 2013, **3**, 1691–1694.

8 M. Srinivas, A. D. Hudwekar, V. Venkateswarlu, G. L. Reddy, K. A. A. Kumar, R. A. Vishwakarma and S. D. Sawant, *Tetrahedron Lett.*, 2015, **56**, 4775–4779.

9 S. L. Yedage, D. S. D'silva and B. M. Bhanage, *RSC Adv.*, 2015, **5**, 80441–80449.

10 L. Becerra-Figueroa, A. Ojeda-Porras and D. Gamba-Sánchez, *J. Org. Chem.*, 2014, **79**, 4544–4552.

11 S. E. Eldred, D. A. Stone, S. H. Gellman and S. S. Stahl, *J. Am. Chem. Soc.*, 2003, **125**, 3422–3423.

12 J. M. Hoerter, K. M. Otte, S. H. Gellman, Q. Cui and S. S. Stahl, *J. Am. Chem. Soc.*, 2008, **130**, 647–654.

13 N. A. Stephenson, J. Zhu, S. H. Gellman and S. S. Stahl, *J. Am. Chem. Soc.*, 2009, **131**, 10003–10008.

14 S. N. Rao, D. Chandra Mohan and S. Adimurthy, *RSC Adv.*, 2015, **5**, 95313–95317.

15 D. A. Kissounko, J. M. Hoerter, I. A. Guzei, Q. Cui, S. H. Gellman and S. S. Stahl, *J. Am. Chem. Soc.*, 2007, **129**, 1776–1783.

16 C. M. Bell, D. A. Kissounko, S. H. Gellman and S. S. Stahl, *Angew. Chemie - Int. Ed.*, 2007, **46**, 761–763.

17 J. M. Hoerter, K. M. Otte, S. H. Gellman and S. S. Stahl, *J. Am. Chem. Soc.*, 2006, **128**, 5177–5183.

18 R. L. Greenaway, V. Santolini, M. J. Bennison, B. M. Alston, C. J. Pugh, M. A. Little, M. Miklitz, E. G. B. Eden-Rump, R. Clowes, A. Shakil, H. J. Cuthbertson, H. Armstrong, M. E. Briggs, K. E. Jelfs and A. I. Cooper, *Nat. Commun.*, 2018, **9**, 1–27.

19 J. C. Lauer, W. S. Zhang, F. Rominger, R. R. Schröder and M. Mastalerz, *Chem. - A Eur. J.*, 2018, **24**, 1816–1820.

20 M. M. Unterlass, *Angew. Chemie - Int. Ed.*, 2018, **57**, 2292–2294.

21 D. Stewart, D. Antypov, M. S. Dyer, M. J. Pitcher, A. P. Katsoulidis, P. A. Chater, F. Blanc and M. J. Rosseinsky, *Nat. Commun.*, 2017, **8**, 1102.

22 R. Katoono, H. Kawai, K. Fujiwara and T. Suzuki, *Tetrahedron Lett.*, 2004, **45**, 8455–8459.

23 K. P. Patel, E. M. Gayakwad and G. S. Shankarling, *New J. Chem.*, 2020, **44**, 2661–2668.

24 T. Grawe, T. Schrader, M. Gurrath, A. Kraft and F. Osterod, *Org. Lett.*, 2000, **2**, 29–32.

Chapter 3

Targeting amide cages by the oxidation of imine structures

3.1 Introduction

As outlined previously, the typically irreversible nature of the amide bond means straightforward, direct synthesis of complex amide materials can be difficult. Factors such as side-product formation and a lack of error-correction lead to reduced yields and difficult separations. Higher yielding processes are possible, but often require employing pre-organisation, either by templating effects,[1] or using highly pre-configured precursors,[2] the syntheses of which can be difficult and time-consuming. As outlined in Chapter 2, dynamic amide formation could provide an alternative route. However, this area is still relatively unexplored, and application to materials formation could prove difficult due to the inherent synthetic complexities of forming molecular materials such as cages. A potential way of avoiding these pitfalls could be post-synthetic modification by directly converting existing imine structures into their amide analogues. This could allow synthesis of both novel materials, as well as existing materials, using a more facile route. Additionally, this methodology could be applied to suitable existing families of materials, potentially enabling the rapid development of large quantities of new amide-derived materials. When surveying potential routes for the conversion of imines to amides, oxidation presents itself as an ideal choice of reaction.

Recent studies into the oxidation of imine materials have focused on the use of the Pinnick oxidation. First reported in 1973 by Lindgren and Nilsson,[3] the Pinnick oxidation is named as such due to the later work by Pinnick and co-workers outlining the generality of the procedure.[4] The process was developed as a modification to earlier oxidation procedures, focusing on application to the synthesis of α,β-unsaturated aldehydes. The Pinnick oxidation utilises sodium chlorite as an oxidant under mildly acidic conditions, with *t*-butanol as the solvent, and 2-methyl-butene also added as a scavenger of hypochlorous acid (HOCl), which is formed as a by-product during the reaction. Though traditionally used for the conversion of aldehydes to carboxylic acids, the Pinnick oxidation has also been used for the direct amidation of small aldehydes, and direct conversion of imines to amides.[5,6] This methodology for imine oxidation was recently adapted for the oxidation of both imine covalent organic frameworks (COFs) and cages.[7–9]

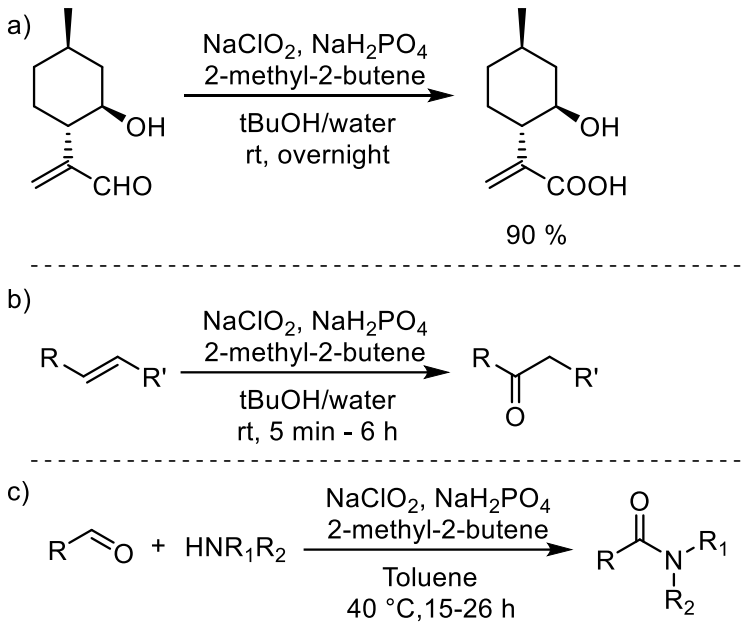

Figure 3.1 – Previous reports of the Pinnick oxidation: a) oxidation of an α,β-unsaturated ketones outlined by Pinnick et al.[4]; b) general procedure for oxidation of imines as reported by Mohamed et al.[5]; c) general procedure for one-pot imine formation and oxidation as outlined by Goh et al.[6]

The first of these applications was outlined in a 2016 report by Yaghi and co-workers, where two known imine COFs were converted to their amide analogues using the Pinnick oxidation (Figure 3.1).[7] In this study, it was reported that use of these conditions resulted in the formation of COFs with poor crystallinity, but through optimisation, the crystallinity was improved by using acetic acid in place of a phosphate buffer, as well as by adding more olefin scavenger. The sodium chlorite oxidant was used in excess, with 12 equivalents used per imine functionality.

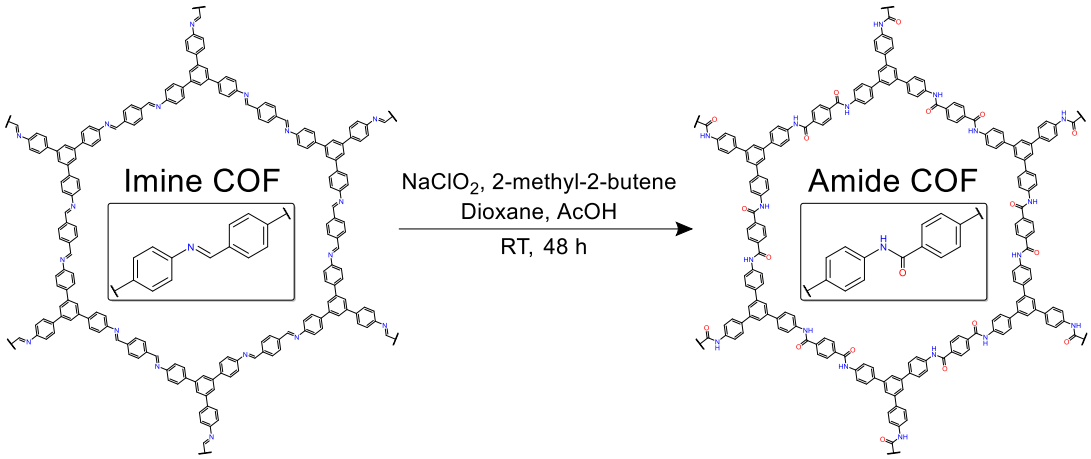

Figure 3.2 – Example scheme to show the oxidation of an imine COF to its amide analogue using Pinnick oxidation conditions as reported by Yaghi and co-workers (a second COF was also found to undergo oxidation on exposure to the same conditions).[7]

Both of the resulting amide-derived COFs were found to have reduced surface areas compared to their respective precursors — this loss of surface area was attributed to an increase in the mass of the framework, along with a decrease in pore volume. In addition, ^{13}C magic-angle spinning (MAS) NMR spectroscopic analysis of one of the amide COFs indicated the presence of oxidised oligomers within the pores, thus leading to reduced porosity. The chemical stability was also investigated by comparing the imine and amide structures following treatment of each of the COFs in 12 M HCl and 1 M NaOH for 24 hours. PXRD measurements showed that whilst the imine structures were "…nearly or completely dissolved and the remaining material rendered amorphous", the amide COFs maintained their crystallinity, although there were indications of some structural damage to the COFs.[7] One potential issue presented was the yield for the oxidation process – whilst no yields were reported for the COF oxidation, the model system used for initial testing was shown to progress in 82% yield. Whilst this is promising, this is for an individual, small molecule containing just two functionalities — when applied to a cage molecule, or COF, with multiple functionalities that require oxidation, it may result in an overall low yield for amide formation. Nevertheless, this report outlines the first use of this oxidation method for the synthesis of robust amide-derived materials by chemical conversion of linkages.

Building on this work, the 2019 report of Bhat *et al.* outlined the Pinnick oxidation of an imine cage to its amide analogue (Figure 3.2).[8] The parent imine cage **IC1** was previously reported by Mastalerz and co-workers, formed by the condensation of a

triptycene triamine derivative[10] and a substituted dialdehyde to form a **Tri^{4}Di^6** cage species in high yield.[11] Attempts to make the amide-derivative of this cage directly by reaction of the triamine with the bis(acid chloride) resulted in a large number of products, with none of the desired amide cage observed. Oxidation of the imine cage was therefore employed to target the desired amide structure instead. The oxidation conditions generally followed the optimised method of Waller *et al*. described previously,[7] continuing the use a phosphate buffer, though the reaction was conducted in THF rather than 1,4-dioxane, and with a longer reaction time. Additionally, whilst the oxidant was again used in excess, the quantity was not as high as for the COF oxidation, with 5 equivalents per imine functionality used for the cage oxidation. The hydroxy groups of the cage were also protected as methyl ethers prior to oxidation to avoid unwanted side reactions.

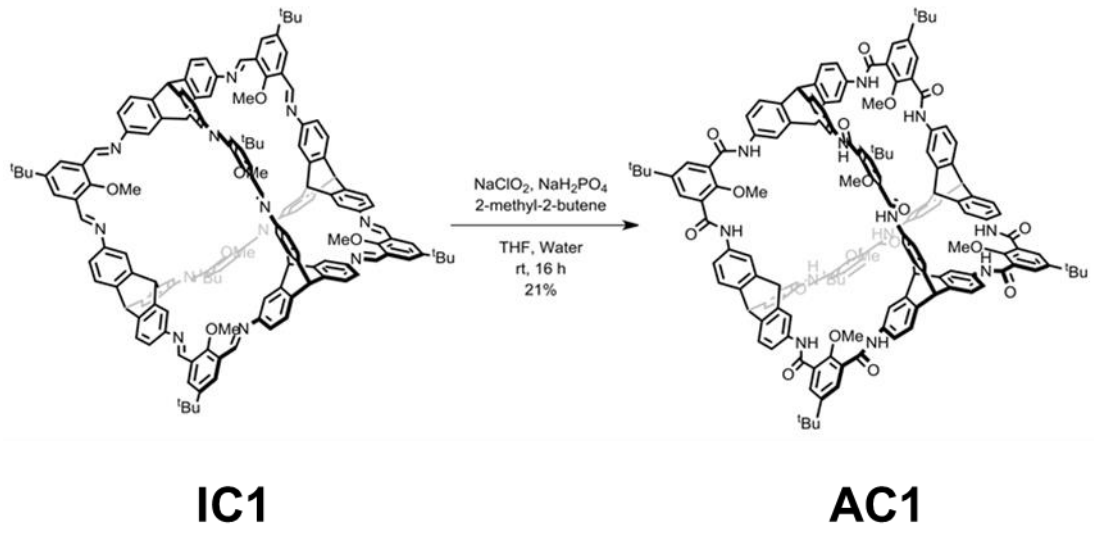

*Figure 3.3 – Conversion of imine cage **IC1** to amide cage **AC1** by Pinnick oxidation, as reported by Bhat et al. (reproduced with permissions from Ref. 8).*[8]

Whilst HPLC analysis showed only a single peak, ^{1}H NMR spectroscopic analysis suggested the presence of several side-products. Subsequent washing and crystallisation steps gave the target amide cage **AC1** in a yield of 21%. The amide cage showed greatly improved stability compared to the parent imine cage in both highly acidic and alkali media, only showing decomposition when treated with 36 M H_2SO_4. In addition, the stability of the amide cage also allowed for post-functionalisation under harsh conditions: cleavage of the methyl ethers, nitration in strong acid, and bromination by *N*-bromosuccinimide were all successfully applied to

form a small family of functionalised amide-derived cages. The latter of these also allowed for cross-coupling reactions, thus increasing the potential for derivatisation into new families of cages. Bhat *et al*. also cited the previous report of the amine derivative of the cage, **RC1**, formed by reduction of the parent imine cage.[12] The increased flexibility of the amine bond leads **RC1** to collapse on desolvation, resulting in a loss of porosity. The increased rigidity of the bonds in the amide cage rectifies this, restoring porosity with a measured SA_{BET} of 275 m^2g^{-1}. Cleavage of the methyl ethers to yield the hydroxyl groups increased groups increased the SA_{BET} to 398 m^2g^{-1} — this correlates with the loss of the bulky methyl groups from within the cage cavity. However, this was still much lower than the previously reported imine cage analogue (SA_{BET} of 2071 m^2g^{-1})[12] — unfortunately there was no clear explanation for the dramatic decrease in surface area. Nonetheless, this initial report of successful cage oxidation offers an ideal starting point for application to other families of imine cages.

In this chapter, it was hoped that the Pinnick oxidation outlined previously could be applied to other families of imine cages to develop new series of amide cage structures. The oxidation of imines and the resulting incorporation of amide groups could have large effects on the cage properties, including stability, porosity, crystallinity, and guest binding.

3.2 Determining a suitable oxidation methodology

3.2.1 Selecting a suitable imine cage

While selecting potential imine cages for investigation, the **CC**-series outlined previously presented itself as an ideal family of cages, as successful oxidation on a model cage species could allow facile application to a wide range of derivatised imine structures with different applications. The subject of numerous studies since its initial report,[13,14] the synthesis and properties of the prototypical imine cage **CC3** are very well understood, and was therefore selected as an ideal candidate for initial study. Additionally, crystals of **CC3** possess excellent hydrolytic stability, with no degradation when submerged in boiling water for 4 hours,[15] which could mitigate the potential for cage hydrolysis should aqueous solutions be required during the oxidation.

The amide derivative of **CC3** has also previously been reported by Still and colleagues, while investigating the formation of cyclooligomeric receptors for protein binding (Figure 3.3), and would allow for straightforward comparison to any amide derivatives formed by oxidation.[16–18] The receptors were formed by coupling benzene-

1,3,5-tricarbonyl derivatives with a range of vicinal diamines, including *R*,*R*-CHDA. These reacted in a **Tri^{4}Di^6** fashion to give a series of cage species, although the yields of these cages were very low due to the need for separation from several unwanted side-products. Whilst crystal structures were reported, the potential porosities of these cages were not investigated. In addition to altering the cage stability, it would be interesting to see the effect of amidation on the properties of the cage — principally the stability, but also the solid-state packing, porosity, or host-guest interactions.

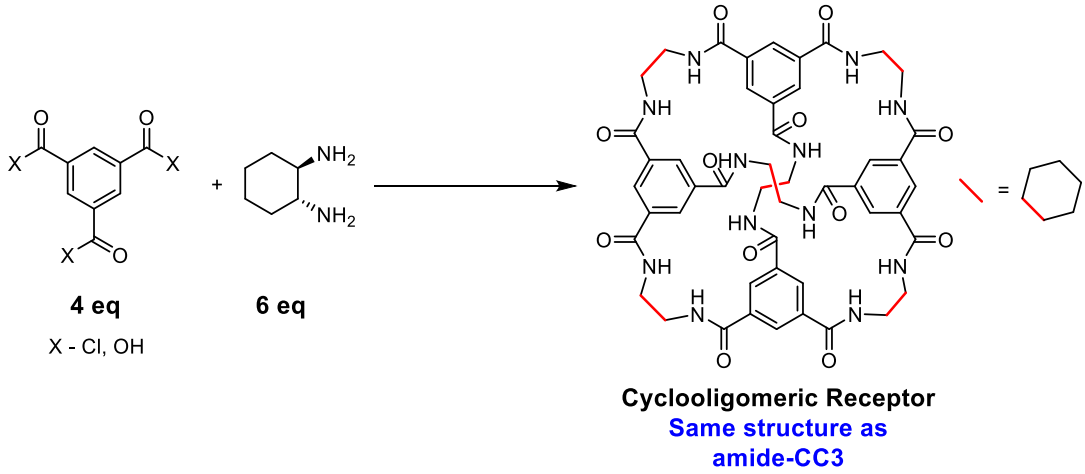

*Figure 3.4 – Synthesis of cyclooligomeric receptor as outlined by Still and co-workers — this is the same structure as the target amide-derived cage **ACC3**.*[16–18]

3.3 Attempted oxidation of imine-derived CC3

To investigate potential oxidation for the **CC**-series of cages, the previously described conditions were applied to **CC3**-*R*, targeting the amide derivative **ACC3**-*R* (Figure 3.5). Though the structures of **IC1** and **CC3** differ significantly, they both contain 12 imine functional groups. As such, the synthesis conditions were directly carried over from Bhat *et al*.,[8] maintaining the use of 5 equivalents of oxidant per imine functionality, however, changes were made to the initial work-up and purification.

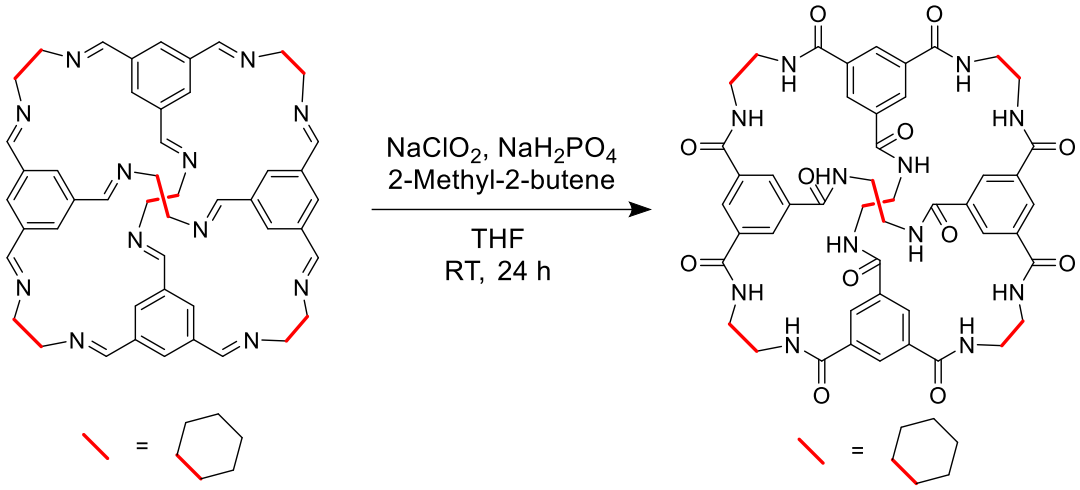

*Figure 3.5 – Attempted synthetic route for the oxidation of **CC3** to the target amide derivative **ACC3**.*

When determining a suitable method for purification, the aqueous work-up included in the original method was omitted as the solubility of **ACC3** was unknown. As such, the crude reaction mixture was simply reduced in volume, suspended in DCM, and filtered to remove any insoluble impurities. Precipitation using an anti-solvent was then carried out, as in the synthesis of parent **CC3**. This resulted in the formation and isolation of a crude solid, and while ^{1}H NMR spectroscopic analysis suggested that some reaction had occurred due to a change in the peak integrations for **CC3**. The normal ratio of 1:1 aromatic:imine was reduced to 1:0.84, with significant broadening of the peaks — it is possible that this change represents the presence of a partially-oxidised cage species. However, there also appeared to be significant degradation of **CC3**-*R*, with the predominant presence of the cage precursor TFB within the crude reaction mixture (Figure 3.6).

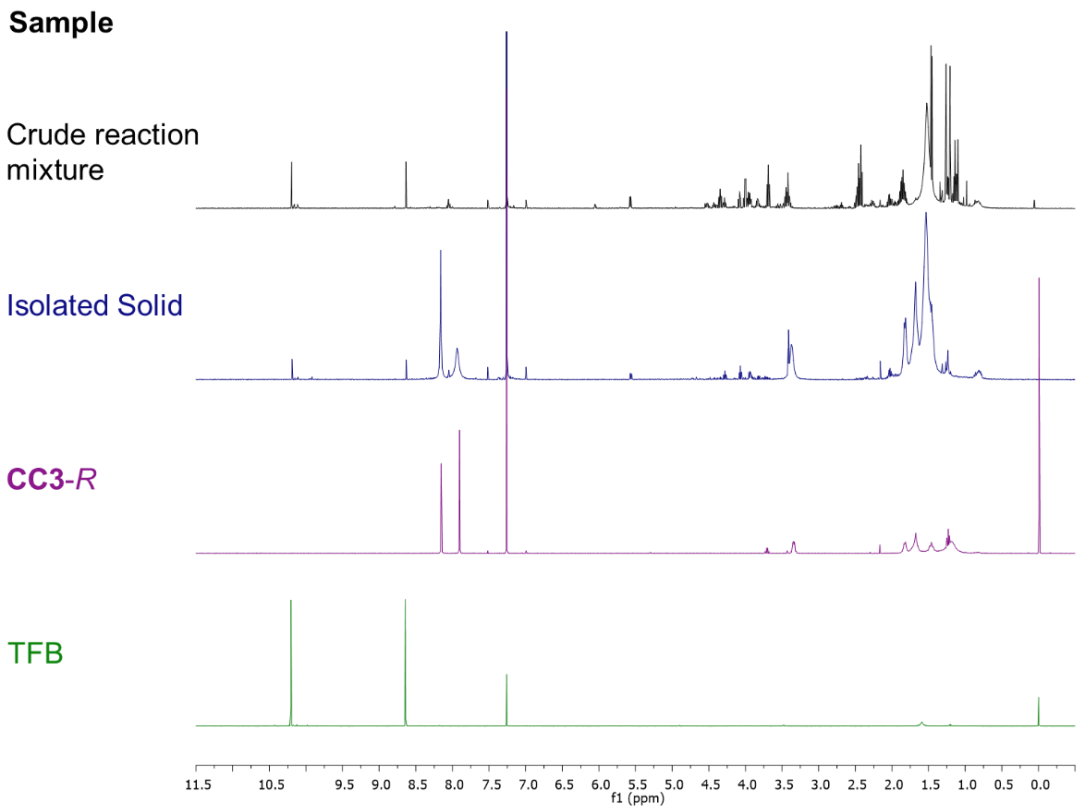

*Figure 3.6 – Stacked ^{1}H NMR ($CDCl_3$) spectra for the attempted oxidation of **CC3**-R to its amide derivative **ACC3**-R; showing the crude reaction mixture, the solid isolated following the reaction work-up, with **CC3**-R and TFB reference spectra.*

In their original report, Bhat *et al.* discuss the difficulty in assessing the ^{1}H NMR spectra and cite the use of HPLC as an alternative.[8] They noted that for the successful oxidation reaction, whilst the ^{1}H NMR spectra indicated the presence of several species, the HPLC trace presented with only a single peak, confirming the presence of only one cage-like species. As such, HPLC measurements were conducted on the isolated solid for comparison with **CC3** (Figure 3.7a) – the method used had previously been optimised for assessing the formation of **CC3** and other related cage analogues. As expected, the main component was **CC3**-*R*, though there was the emergence of an additional species at an elution time of ~7.5 minutes - it was thought that this was either a partially oxidised species or fully-oxidised derivative **ACC3**-*R*, though the ratio of the two peaks showed that this was representative of less than 5% of the mixture. Therefore, even if the oxidation had proceeded, it had not done so efficiently. HRMS was also carried out on the isolated solid to check for the presence of **ACC3**-*R* (expected mass ion 1308.6326), and any partially oxidised species (an

increase of ~15.995 for each imine oxidised to an amide). As expected, **CC3** was present, appearing as the singly, doubly, and triply charged species ($[M+H]^+$ calculated 1117.7015, found 1117.7053; $[M+H]^{2+}$ calculated 559.3544, found 559.3561, $[M+H]^{3+}$ calculated 373.2387, found 373.2400), but there was no indicative mass ion for the fully oxidised cage species. However, there was evidence of a very small quantity of partially-oxidised **CC3** with a single imine to amide species ([M+H+ calculated 1133.6964, found 1133.6974).

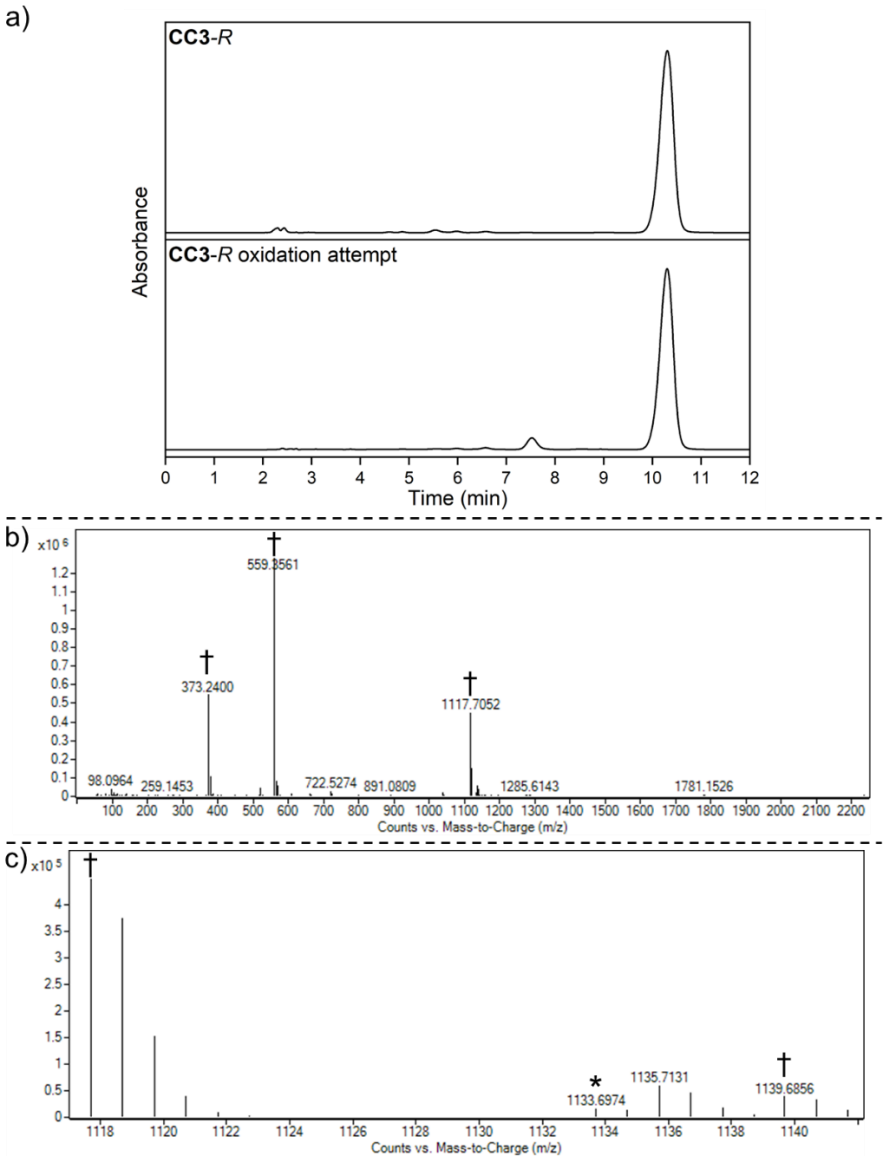

*Figure 3.7 – a) Stacked HPLC traces of **CC3**-R, and the isolated solid from the attempted oxidation of **CC3**-R — an additional peak is present in the oxidation solid at ~7.5 minutes elution time; b) high-resolution mass spectrum of the isolated solid from the attempted oxidation of **CC3**; c) expanded reegion to show the peak potentially representing singly-oxidised **CC3**; peaks representing **CC3** are denoted by †.*

At this stage, it was unclear why the oxidation was not progressing as desired, though it was clear that one option may be in the reaction methodology itself. To test this, the conditions were applied to a known oxidation substrate – it was hoped this would give an unambiguous result as to whether oxidation had taken place.

3.4 Ensuring correct function of the oxidation procedure

Following the lack of success seen for the attempted oxidation of **CC3**, it was important to ensure that the method of oxidation was functioning correctly. As such, the diimine model compound, (1*E*,1'*E*)-1,1'-(1,4-phenylene)bis(*N*-phenylmethanimine) (PBNP), earlier utilised by Waller *et al*.,[7] was used in conjunction with the conditions of Bhat *et al*.[8] to target *N,N'*-diphenylterephthalamide (DPT) (Figure 3.8). This test reaction progressed as in the previous report, with the amounts of reagents adapted to reflect the reduced number of imine groups in PBNP compared to **IC1**.

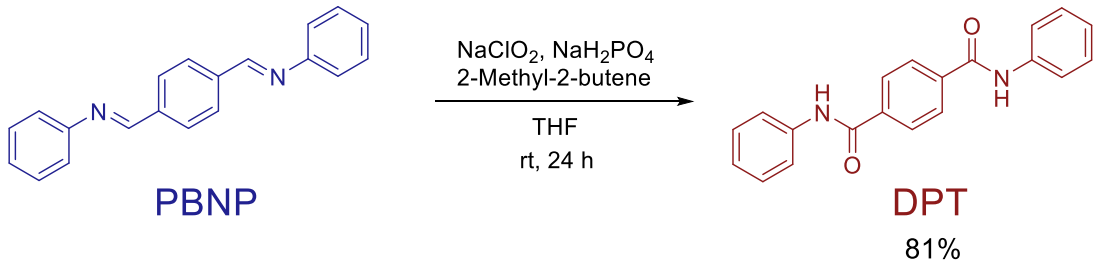

Figure 3.8 – Oxidation conditions for the conversion of 1,1'-(1,4-phenylene)bis(N-phenylmethanimine) (PBNP) to N,N'-diphenylterephthalamide (DPT).

The method of purification used was also adapted, due to the precipitation of a colourless solid during the reaction. ^{1}H NMR spectroscopic analysis showed a marked difference between the imine precursor and the isolated product (Figure 3.9a), and both spectra corresponded extremely well with the data reported by Waller *et al*. in their initial report of COF oxidation,[7] confirming that the oxidation procedure had been a success.

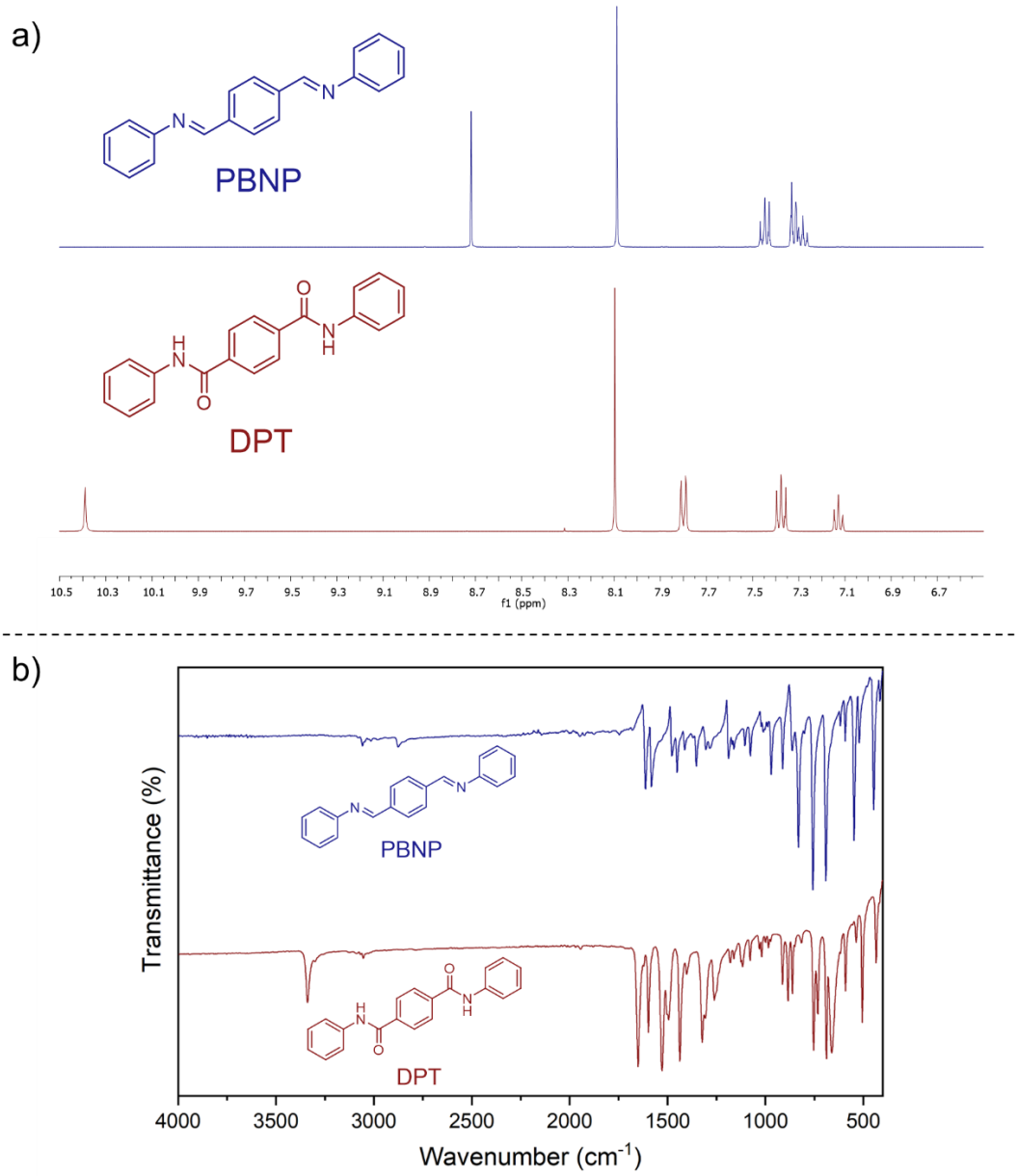

Figure 3.9 - Analysis of oxidation of imine precursor PBNP to form target amide DPT; a) stacked ^{1}H NMR spectra showing the aromatic region for PBNP (blue) and DPT (red); b) stacked IR spectra for PBNP (blue) and DBT (red).

Comparison of the ^{1}H NMR spectra suggests that the loss of the peak at ~8.7 ppm corresponds to the transformation of the imine group to an amide. IR spectroscopy was used as an additional confirmation of oxidation (Figure 3.9b), with clear changes apparent in the spectrum between the precursor and product – additional peaks are visible in the *c.a.* 1600 cm^{-1} region, corresponding to the formation of the C=O group

in the amide species. Additionally, the emergence of a sharp N-H peak at c.a. 3300 cm^{-1} was another indication of amide formation.

Oxidation of this model reaction confirmed the conditions were functioning as required and were being applied correctly. It was decided that more fundamental testing was therefore required, examining any other potential limitations for oxidation of **CC3**. Therefore, **CC3** was first compared to other successful oxidation substrates reported previously.

3.5 Fundamental testing of imine substrates

3.5.1 Identifying suitable substrates

When examining both previous COF and cage oxidation substrates, both materials contain the same structural motif, whereby the imine is bonded directly to two aromatic rings — this is in comparison to the structure of **CC3**, where one portion of the imine is directly bonded to a cyclohexyl ring (Figure 3.10). It was thought that this structural difference may be limiting the ability to apply the oxidation conditions to **CC3**. Assessing reported studies into the Pinnick oxidation of small imine molecules shows that the process has a good functional group tolerance, with a variety of substrates undergoing successful oxidation. The report by Mohamed *et al*. included successful oxidation of small imines with structures similar to those seen in the materials of Yaghi and Mastalerz.[5] However, no substrates were included with high similarity to the imine structure found in **CC3**. The report of Goh and Tan included a small number of aliphatic-substituted imines, which all proceeded to oxidise in good yields, though these again did not match well with the imine structure found in **CC3**.[6]

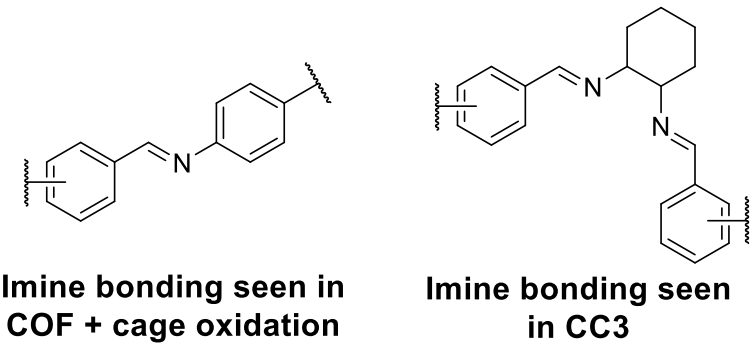

Figure 3.10 – Comparison of the general imine bonding as seen in the COF and cage reported by Waller et al. and Bhat et al.,[7,8] *and prototypical cage **CC3**.*

It was proposed that this difference in structure was the main factor leading to the lack of conversion exhibited in the previous attempt at oxidising **CC3**. To investigate this further, more fundamental testing was carried out to clarify the relationship between structure and the resulting outcome of the Pinnick oxidation. Considering the structural differences (Figure 3.11), it was also desired to investigate a potential "mid-point" between the bonding of the imine cages **IC1** and **CC3**. This was envisioned as a structure similar to that of **IC1,** with aromatic moieties for each portion of the bonding, but with a break in conjugation due to the presence of additional bonds. A number of cages with such bonding have been reported — for this study, the cages reported by Greenaway *et al*. were selected.[19] These utilised triamines with benzylic $–CH_2NH_2$ functionality, resulting in overall loss of conjugation due to the presence of α-CH_2 groups. Whilst several cages were reported in this study, the imine cage **B11** was selected as a potential target for study — **B11** is a **Tri^{4}Di^6** cage formed from the reaction of a benzylic triamine with terephthalaldehyde.[19] Following their original oxidation report, Bhat outlined extended study into the application of the Pinnick oxidation to imine cages.[9] However, much of this work continued to explore the triptycene-based cages seen previously, though an additional study looked into a series of **Tri^{2}Di^3** cages. Whilst these were smaller than the **Tri^{4}Di^6 B11** cage, the style of bonding was maintained, and it was found that oxidation of these cages was successful in most cases, as well as for a larger **Tri^{4}Tri^4** cage.

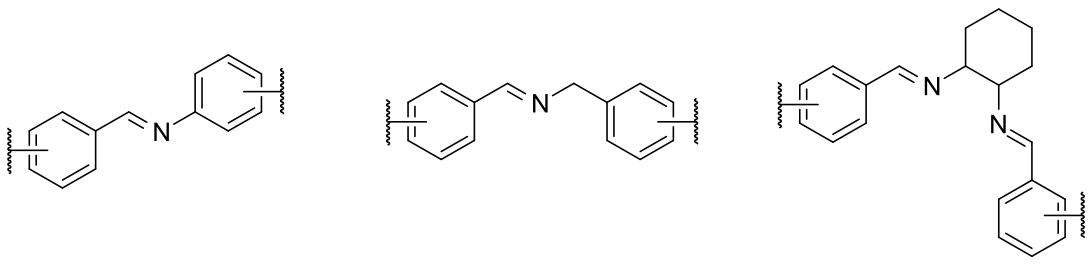

IC1
Aromatic-Aromatic
Conjugated

B11
Aromatic-Aromatic
Non-conjugated

CC3
Aromatic-Aliphatic
Non-conjugated

Figure 3.11 – Modes of bonding within the three imine cages selected for investigation, ***IC1,*** ***B11,*** *and* ***CC3****.*

Selecting structures based on the types of imine bonds led to a set of three representative cages being chosen for study: **IC1**, **B11**, and **CC3** (Figure 3.12).

Assessment of the extended study by Bhat detailed additional limitations with application of the Pinnick oxidation when applied to cage species, for example, solubility of the cage in solvents that are miscible with water was found to be critical to the success of the oxidation. **CC3** exhibits poor solubility in THF, though it was hoped the suspension would still be applicable as in the previous COF synthesis. Additionally, dichloromethane (DCM) (in which **CC3** is relatively soluble) was also examined by Bhat as a reaction solvent, but its use led to many more side-products present in the ultra-performance liquid chromatography traces.[9] It was also found that sterically bulky substituents adjacent to the imine bond could significantly hinder the Pinnick oxidation, theorising the groups may interrupt the required trajectory by the oxidant $^{-}ClO_2$ – this effect had not been seen previously for small imine structures.[9] These factors, in combination with the lack of oxidation seen previously for **CC3**, meant that it was not desirable to carry out comparative testing directly on cage samples. Instead, small representative molecules were better suited to a more fundamental study, allowing for assessment of the bond type on oxidation, while avoiding pitfalls discussed surrounding steric bulk or solubility.

To enable this, a series of representative test substrates were designed to allow a stepwise approach to study. Using the three cages as a starting point, a series of three “mono” compounds were designed (Figure 3.12) – these would allow direct study of whether the type of imine bond seen in the different cage species could undergo oxidation. On successful oxidation, efforts could then shift to the designed multi-functional compounds, for example, di- and tri-topic derivatives, to test oxidation on multiple functionalities in a single reaction. Conversely, a lack of reaction on the simplest of substrates may suggest that the lack of oxidation is inherent to the structure. The three mono-compounds were therefore studied first. These were *N*-benzylideneaniline, *N*-benzylidenebenzylamine, and *N*-benzylidenecyclohexamine, denoted **IC1-mono**, **B11-mono**, and **CC3-mono**, respectively (Figure 3.12).

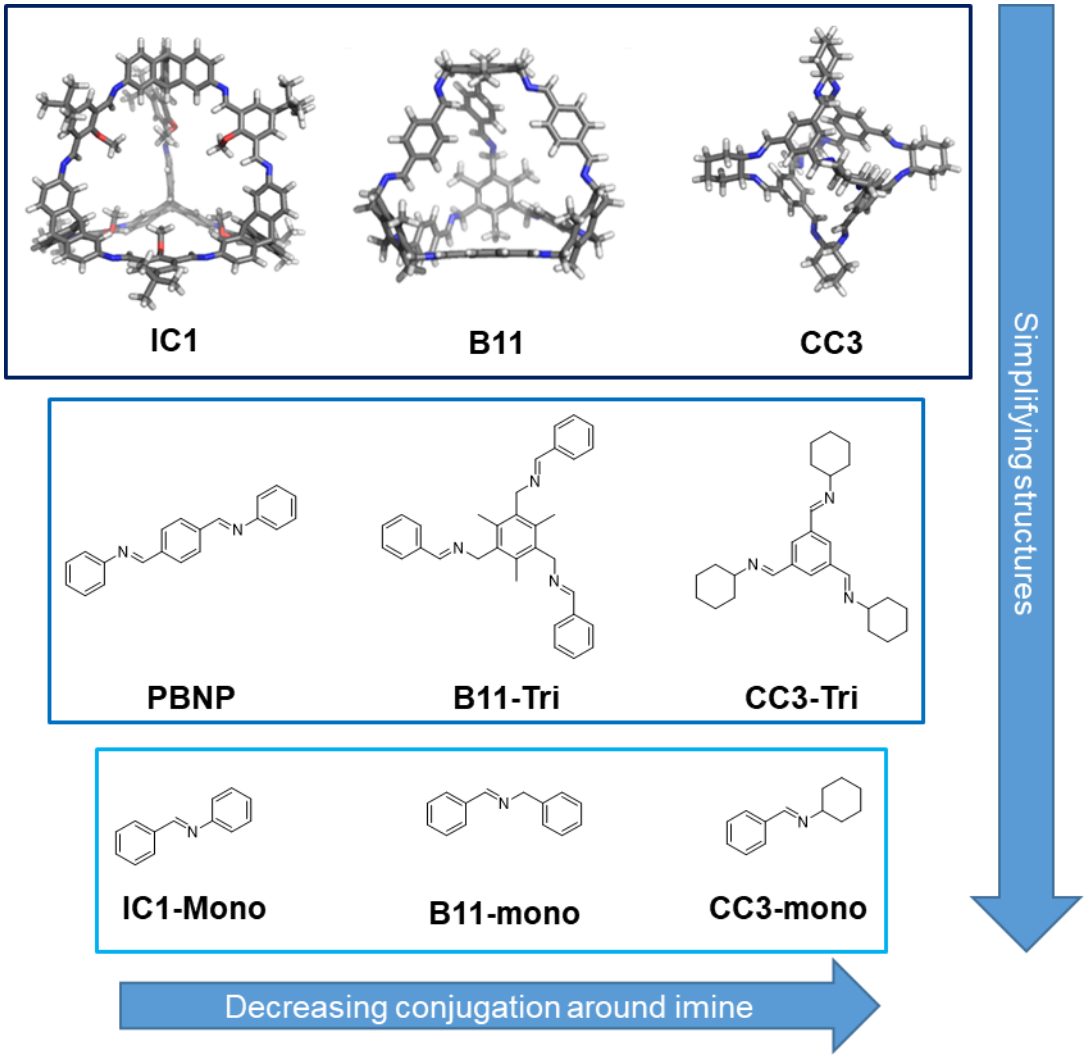

*Figure 3.12 – Design of substrates for oxidation based on the target cages **IC1**, **B11** and **CC3**: mono-substituted representative compounds can be used to assess general reactivity, moving onto multiple functionalities with di- and tri-substituted derivatives prior to extension to the cage species themselves.*

3.5.2 Attempted oxidation of representative mono-substrates

Oxidation was first attempted on each of the representative mono-compounds, with reaction conditions adapted from the methodology outlined by Bhat *et al*.[8] (Figure 3.13). The equivalents of reagent used were altered to account for only a single imine in each of the compounds. All three of the substrates were fully soluble in THF, and the reactions were carried out as for the previous model reaction with TBTP. As with the attempted oxidation of **CC3** outlined previously, the work-up was adapted slightly for these compounds – to ensure no desired species were lost in an aqueous wash, the reaction mixtures were reduced to dryness, and the residue suspended in $CDCl_3$

for subsequent analysis by ^{1}H NMR spectroscopy. The presence of insoluble precipitates in $CDCl_3$, potentially salts from the oxidation process, meant that the samples had to first be filtered. As the oxidation process resulted in the formation of several by-products, the success of the reaction was determined by comparison of the imine C-H peak between the starting imines and the crude oxidation products (Figure 3.14).

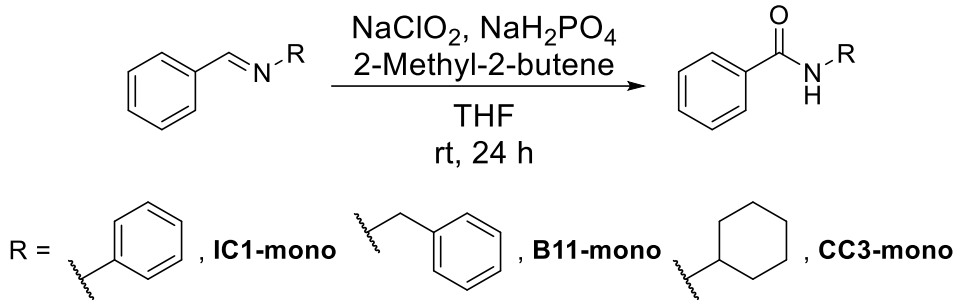

Figure 3.13 – Pinnick oxidation of representative mono-functionalised substrates using conditions adapted from the report of Bhat et al.[8]

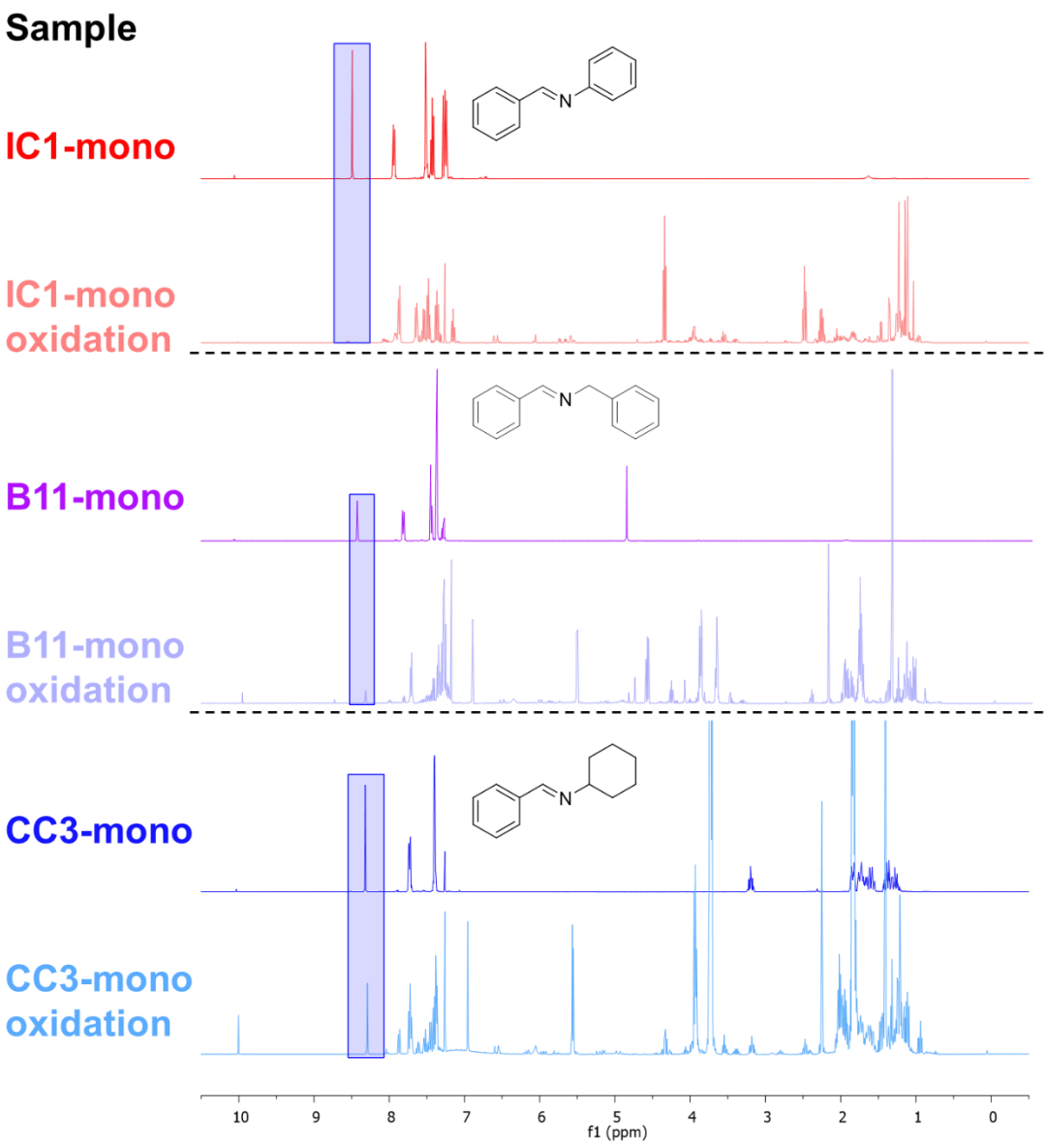

Figure 3.14 – Stacked ^{1}H NMR spectra ($CDCl_3$) for the representative oxidations on the mono-functionalised substrates: red/pale red – ***IC1-mono*** *oxidation process; purple/pale purple –* ***B11-mono*** *oxidation process; blue/pale-blue -* ***CC3-mono*** *oxidation process. Change in the presence of the imine C-H peaks are highlighted in blue boxes.*

Overall, the ^{1}H NMR spectra of the soluble material showed varied levels of success for the three oxidation reactions. Comparison of the **IC1-mono** reaction showed complete loss of the imine peak in the crude product, suggesting the oxidation process had been a success. This was expected due to the previous success of the oxidation of PBNP (Figure 3.9). The oxidation of **B11-mono** appeared to have some success, with a reduction in the imine peak relative to the other signals present.

However, the presence of the imine peak in the crude oxidation product mixture suggests that while the process occurred to a significant degree, it did not progress to completion. The process for **CC3-mono** was less successful than the other substrates, with a large amount of starting imine apparent in the crude reaction mixture. This suggested that very little oxidation had taken place for the cyclohexyl-substituted imine. In addition, for all three substrates, a peak at ~10 ppm appeared in the spectra of the samples, which correlates with known values for the aldehyde peak in benzaldehyde, suggesting decomposition during the oxidation process. For **IC1-mono** and **B11-mono**, this peak at ~10 ppm did not change much (a slight increase for **B11-mono**), whereas for **CC3-mono**, the peak changed dramatically, suggesting there had been greater decomposition of the imine into its starting materials under the applied conditions.

Considering the lack of oxidation exhibited for **CC3-mono**, it was decided not to continue application of the conditions to **CC3-Tri** or **B11-Tri** (PBNP had already undergone successful oxidation). At this stage, a number of issues had arisen during these studies. It was known that the conditions applied were functioning as expected due to the oxidation of PBNP, and the apparent oxidation of **IC1-mono**. The lack of oxidation of both **CC3** and **CC3-mono** suggested that the Pinnick oxidation methodology may not be wholly applicable to the **CC**-series of cages. The large quantity of aldehyde within the crude product of **CC3-mono** suggests that the imine group is undergoing decomposition. Clearly this is only for a small imine structure, and while **CC3** has been shown to have good hydrolytic stability,[15] TFB is also present in the solid product obtained for the attempted oxidation of **CC3**. This suggests the inherent structure of the imine group may not allow for the oxidation process to occur as desired. Considering these points, and the progress obtained in other related projects, it was decided to discontinue further investigations into the possible oxidation of the **CC**-series of cages at this stage of the study.

3.6 Conclusions and future work

This chapter has outlined efforts to oxidise the prototypical imine cage **CC3** to its amide derivative. Pinnick oxidation conditions were adapted from existing reports into imine cage oxidation as reported by Bhat *et al*.,[8,9] and applied to **CC3**. ^{1}H NMR spectroscopic analysis suggested very little oxidation had taken place, along with possible decomposition of the cage. Whilst an additional peak was present by HPLC, along with the correct mass ion present by mass spectrometry, these were both present in small amounts. The oxidation conditions were subsequently applied to a model imine compound to ensure the conditions were functioning as desired. With successful oxidation of the model system, more fundamental testing was completed to investigate the reason for this low amount of oxidation for **CC3**, focusing a range of analogues small imine molecules. This study showed that the functionalities around the imine bond likely play a significant role in the success of the oxidation, with comparable reactivity and decomposition seen for **CC3** and **CC3-mono**, both of which have a cyclohexyl functionality. Due to the lack of reactivity seen in the initial testing, it was decided to shift efforts towards other methods of amide-cage synthesis.

The goal of this work was to test conditions on **CC3** to allow for application to the **CC** series of cages, potentially forming a new family of amide cages. Other **CC** cages contain similar alkyl-functionalities, likely making the Pinnick oxidation not applicable. However, other cages contain alternative diamine functionalities which may be more suitable for this oxidation methodology, though these may introduce more issues with steric bulk around the imine bond. In their extended report, Bhat discussed reaction conditions for different imine molecules — for example the use of H_2O_2 as an oxidant, and of use of a lower pH for aliphatic amines. These points could be further investigated for **CC3**, though it should be noted that the aliphatic amines investigated by Bhat were the hexasubstituted-aromatic based triamines discussed previously.[9,19,20] Additionally, other methods of imine oxidation have also been reported — these could be investigated as an alternative route that is better suited to the imine bonds found in the **CC** series of cages.

3.7 Experimental procedures

3.7.1 General synthetic and analytical methods

Materials: 1,3,5-Triformylbenzene was purchased from Manchester Organics (UK). Other chemicals were purchased from Fluorochem UK, TCI UK or Sigma-Aldrich. Solvents were reagent grade purchased from Fischer Scientific, Sigma-Aldrich or Fluorochem. All materials were used as received unless stated otherwise.

Synthesis: All reactions were stirred magnetically using Teflon-coated stirrer bars. Where heating was required, the reactions were warmed using a stirrer hotplate with heating blocks, with the stated temperature being measured externally to the reaction flask with an attached probe. Removal of solvents was done using a rotary evaporator.

IR Spectra: Infra-red (IR) spectra were recorded on a Bruker Tensor 27 FT-IR using ATR measurements for solids as neat samples.

NMR Spectra: ^{1}H Nuclear magnetic resonance (NMR) were recorded using an internal deuterium lock for the residual protons in $CDCl_3$ (δ = 7.26 ppm), or DMSO-*d*6 (δ = 2.50 ppm) at ambient probe temperature on a Bruker Avance 400 (400 MHz).

Data are presented as follows: chemical shift, peak multiplicity (s = singlet, d =doublet, t = triplet, q = quartet, quint = quintet, m = multiplet, br = broad), coupling constants (*J* / Hz), and integration. Chemical shifts are expressed in ppm on a δ scale relative to δ_{TMS} (0 ppm), $\delta_{DMSO\text{-}d6}$ (2.50 ppm), or δ_{CDCl3} (7.26 ppm).

^{13}C NMR Spectra were recorded using an internal deuterium lock using $CDCl_3$ (δ = 77.16ppm) at ambient probe temperatures on the following instrument: Bruker Avance 400 (101 MHz).

HPLC Spectra: HPLC analysis was carried out using an Agilent 1260 Mass Directed Preparative HPLC with a diode array UV detector using a Zorbax SB-C8 column, 250 x 4.6 mm, 5 µm (S.N. USSE038506, L.N B19524). The mobile phase was isocratic MeOH at a flow rate of 1 mL/min for a 10-30 min run time, and the column temperature was set to 30 °C. The injection volume was 10 µL and the sample concentration was approximately 1 mg/mL. Detection for UV analysis was conducted at 254 nm.

HRMS spectra: High resolution mass spectrometry (HRMS) was carried out using a 6200 series TOF/6500 series Q-TOF B.09.00 mass spectrometer (fragmentor 120 V) in positive-ion detection mode. The mobile phase was MeOH.

3.7.2 Synthesis of substrates and reference materials for Pinnick oxidation reactions

CC3-*R*

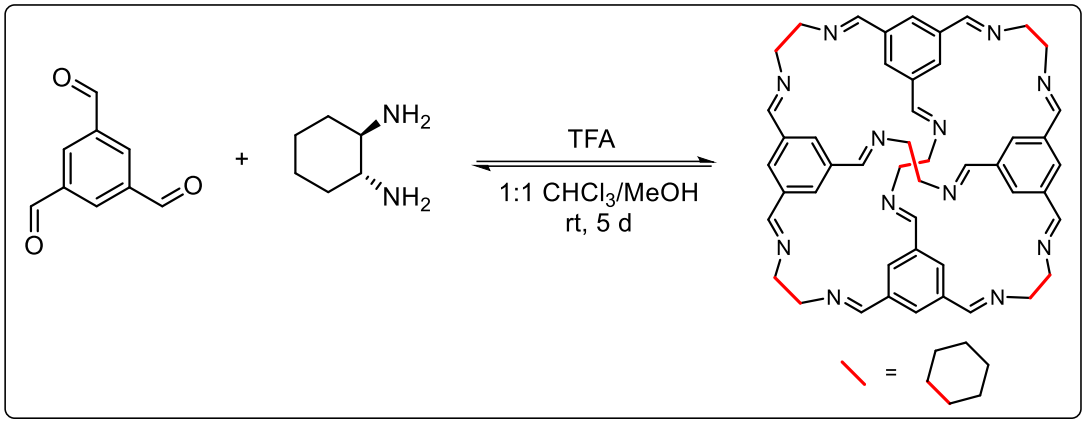

DCM (20 mL) was added slowly onto solid 1,3,5-triformylbenzene (1.0 g, 6.2 mmol, 1 eq.) without stirring at room temperature. Trifluoroacetic acid (100 µL) was added directly to this solution as a catalyst for imine bond formation. Finally, a solution of (*R*,*R*)-1,2-cyclohexyldiamine (1.0 g, 8.7 mmol, 1.4 eq.) in DCM (20 mL) was added. The unmixed reaction was covered and left to stand. Over 5 days, the solid 1,3,5-triformylbenzene was consumed, and **CC3**-*R* precipitated out of the reaction solution. The solid product was removed by filtration and washed with a mixture of 95% ethanol/5% DCM, before being dried under vacuum to give **CC3**-*R* as an off-white solid (750 mg, 0.67 mmol, 44%).

^{1}H NMR (400 MHz, $CDCl_3$) δ_H 8.15 (s, 12H), 7.90 (s, 12H), 3.39 – 3.29 (m, 12H), 1.89 – 1.40 (m, 48H); **^{13}C NMR** (101 MHz, $CDCl_3$) δ_C 159.80, 136.54, 130.01, 74.58, 32.94, 24.35. Data in accordance with literature values.[21]

(1*E*,1'*E*)-1,1'-(1,4-Phenylene)bis(*N*-phenylmethanimine) (PBNP)

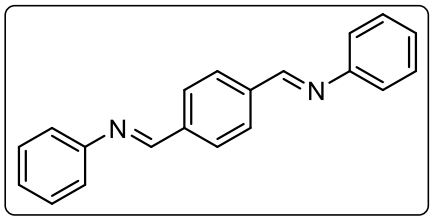

To a solution of terephthalaldehyde (2.0g, 14.9 mmol, 1.0 eq.) in DCM (30 mL) was added aniline (2.91 g, 2.86 mL, 31.3 mmol, 2.1 eq.) and anhydrous magnesium sulfate (9 g, 74.6 mmol, 5.0 eq.), and the resulting mixture was stirred at 25 °C for 16 h before being filtered. The filtrate was concentrated using rotary

evaporation, and the resulting solid was dissolved in DCM. On the addition of hexane, a large amount of solid precipitated into the solution. The volume was reduced *in vacuo*, and the remaining solid isolated under vacuum to afford PBNP as a yellow-green solid (2.88 g, 10.1 mmol, 68 %)

^{1}H NMR (400 MHz, DMSO-d6) δ_H 8.72 (s, 2H), 8.09 (s, 4H), 7.48 – 7.41 (m, 4H), 7.35 – 7.25 (m, 6H); **^{13}C NMR** (101 MHz, DMSO-d6) δ_C 160.06, 151.19, 138.42, 129.26, 129.03, 126.33, 121.10. Data in accordance with literature values.[7]

N-benzylidenecyclohexylamine (CC3-mono)

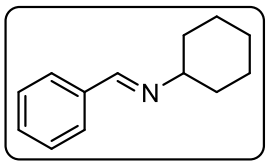

Benzaldehyde (2.9 mL, 28.5 mmol, 1.0 eq.) was stirred in DCM (200 mL) until complete dissolution had occurred. Cyclohexylamine (3.2 mL, 28.5 mmol, 1.0 eq.) was added, and the mixture was stirred overnight at room temperature. Solvents were removed in vacuo affording **CC3-mono** as a viscous, dark orange liquid which was used without further purification. (4.2 g, 22.4 mmol, 79%)

^{1}H NMR (400 MHz, $CDCl_3$) δ_H 8.32 (s, 1H), 7.76 – 7.69 (m, 2H), 7.43 – 7.36 (m, 3H), 3.25 – 3.15 (m, 1H), 1.89 – 1.79 (m, 2H), 1.79 – 1.53 (m, 5H), 1.44 – 1.20 (m, 3H); **^{13}C NMR** (101 MHz, $CDCl_3$) δ_C 158.7, 136.8, 130.4, 128.6, 128.2, 70.2, 34.5, 25.8, 24.9. Data in accordance with literature values.[22]

3.7.3 Synthetic procedures for the Pinnick oxidation process

Oxidation of PBNP to *N,N'*-diphenylterephthalamide

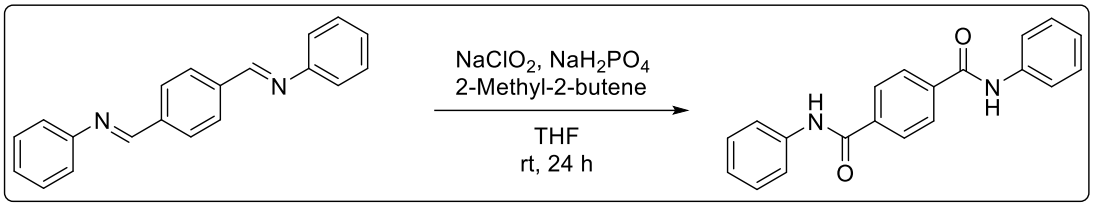

To a solution of PBNP (157 mg, 0.55 mmol, 1.0 eq.) in THF (255 mL) was added 2-methyl-2-butene (0.98 mL, 9.2 mmol, 16.6 eq.) and sodium chlorite (500 mg, 5.52 mmol, 10.0 eq.) with stirring. An aqueous solution of monobasic sodium phosphate (1 M, 1.66 mmol, 3.0 eq.) was added dropwise over 1 minute, and the mixture was left to stir overnight at room temperature, affording a large amount of precipitate. Water (100 mL) was added, and the mixture stirred for 5 minutes. The remaining solid was collected by vacuum filtration, washed with water and acetone, and left to dry under vacuum, affording *N,N'*-diphenylterephthalamide as a colourless solid (141 mg, 0.44 mmol, 81%).

^{1}H NMR (400 MHz, DMSO-d6) δ_H 10.39 (s, 2H), 8.10 (s, 4H), 7.80 (d, J = 7.5 Hz, 2H), 7.41 – 7.34 (m, 2H), 7.17 – 7.09 (m, 1H); **^{13}C NMR** (101 MHz, DMSO-d6) δ_C 164.83, 138.97, 137.46, 128.68, 127.73, 123.92, 120.48. Data in accordance with literature values.[7]

Attempted oxidation of CC3-*R* to ACC3-*R*

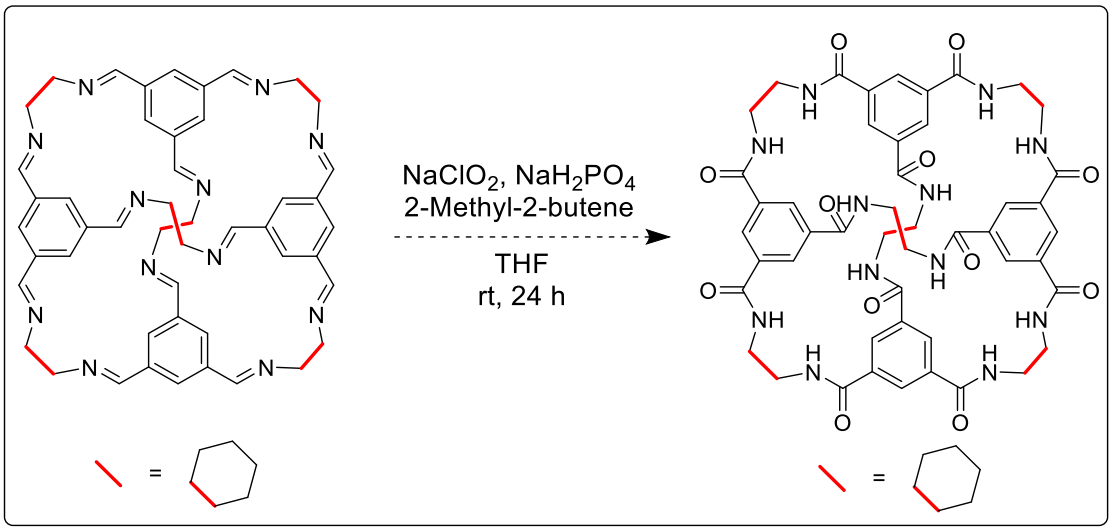

To a suspension of **CC3** (121 mg, 0.108 mmol, 1.0 eq.) in THF (50 mL) was added 2-methyl-2-butene (1.1mL, 10.8 mmol, 100 eq.) and sodium chlorite (586mg, 6.48 mmol, 60 eq.). An aqueous solution of monobasic sodium phosphate (1 M, 233mg, 1.94 mmol, 18.0 eq.) was added dropwise over 1 minute, and the reaction mixture was stirred for 24 hours at room temperature. The solvent was removed in vacuo, and the residue suspended in DCM (50 mL). The mixture was filtered, hexane (50 mL) was added, and the volume reduced *in vacuo*, resulting in the formation of a precipitate. The mixture was filtered to yield a crude oxidation product which was dried under vacuum before further analysis was carried out.

Isolated solid: 34 mg; mass recovery = 28%

Attempted oxidation of imine mono substrates

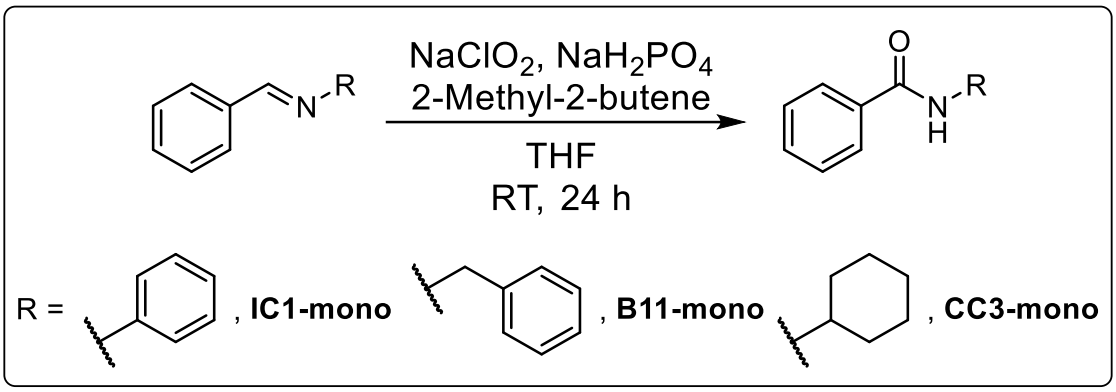

To a solution of mono-substrate (0.552 mmol, 1.0 eq) in THF (255 mL) was added 2-methyl-2-butene (0.49 mL, 4.6 mmol, 8.3 eq.) and sodium chlorite (250 mg, 2.76 mmol, 5.0 eq). An aqueous solution of monobasic sodium phosphate (1 M, 0.828 mmol, 1.5 eq.) was added dropwise over 1 minute, and the mixture stirred overnight at room temperature. Solvents were then removed *in vacuo*, and the resultant residue suspended in $CDCl_3$. An aliquot of this mixture was filtered and analysed by ^1H NMR spectroscopy.

Prepared using the general procedure for oxidation of imine mono substrates with:

IC1-mono: *N*-benzylideneaniline, 100 mg

B11-mono: *N*-benzylidenebenzylamine, 108 mg

CC3-mono: *N*-benzylidenecyclohexylamine, 103 mg

3.8 References

1 W. Kiggen and F. Vögtle, *Angew. Chemie Int. Ed. English*, 1984, **23**, 714–715.

2 A. P. Davis and R. S. Wareham, *Angew. Chemie Int. Ed.*, 1998, **37**, 2270–2273.

3 B. O. Lindgren and T. Nilsson, *Acta Chem. Scand.*, 1973, 27, 888–890.

4 B. S. Bal, W. E. Childers and H. W. Pinnick, *Tetrahedron*, 1981, **37**, 2091–2096.

5 M. A. Mohamed, K. ichi Yamada and K. Tomioka, *Tetrahedron Lett.*, 2009, **50**, 3436–3438.

6 K. S. Goh and C. H. Tan, *RSC Adv.*, 2012, **2**, 5536–5538.

7 P. J. Waller, S. J. Lyle, T. M. Osborn Popp, C. S. Diercks, J. A. Reimer and O. M. Yaghi, *J. Am. Chem. Soc.*, 2016, **138**, 15519–15522.

8 A. S. Bhat, S. M. Elbert, W.-S. Zhang, F. Rominger, M. Dieckmann, R. R. Schröder and M. Mastalerz, *Angew. Chemie Int. Ed.*, 2019, 1–6.

9 A. S. Bhat, 2021.

10 C. Zhang and C.-F. Chen, *J. Org. Chem.*, 2006, **71**, 6626–6629.

11 M. Mastalerz, *Chem. Commun.*, 2008, **0**, 4756.

12 M. Mastalerz, M. W. Schneider, I. M. Oppel and O. Presly, *Angew. Chemie - Int. Ed.*, 2011, **50**, 1046–1051.

13 P. Skowronek and J. Gawronski, *Org. Lett.*, 2008, **10**, 4755–4758.

14 T. Tozawa, J. T. A. Jones, S. I. Swamy, S. Jiang, D. J. Adams, S. Shakespeare, R. Clowes, D. Bradshaw, T. Hasell, S. Y. Chong, C. Tang, S. Thompson, J. Parker, A. Trewin, J. Bacsa, A. M. Z. Slawin, A. Steiner and A. I. Cooper, *Nat. Mater.*, 2009, **8**, 973–978.

15 T. Hasell, M. Schmidtmann, C. A. Stone, M. W. Smith and A. I. Cooper, *Chem. Commun.*, 2012, **48**, 4689.

16 S. S. Yoon and W. C. Still, *J. Am. Chem. Soc.*, 1993, **115**, 823–824.

17 S. Soo Yoon and W. Clark Still, *Tetrahedron Lett.*, 1994, **35**, 2117–2120.

18 S. S. Yoon and W. C. Still, *Tetrahedron Lett.*, 1994, **35**, 8557–8560.

19 R. L. Greenaway, V. Santolini, M. J. Bennison, B. M. Alston, C. J. Pugh, M. A. Little, M. Miklitz, E. G. B. Eden-Rump, R. Clowes, A. Shakil, H. J. Cuthbertson, H. Armstrong, M. E. Briggs, K. E. Jelfs and A. I. Cooper, *Nat. Commun.*, 2018, **9**, 1–27.

20 J. C. Lauer, W. S. Zhang, F. Rominger, R. R. Schröder and M. Mastalerz, *Chem. - A Eur. J.*, 2018, **24**, 1816–1820.

21 T. Hasell, S. Y. Chong, K. E. Jelfs, D. J. Adams and A. I. Cooper, *J. Am. Chem. Soc.*, 2012, **134**, 588–598.

22 G. Zhang and S. K. Hanson, *Org. Lett.*, 2013, **15**, 650–653.

Chapter 4

Synthesis of part-amide Janus porous organic cages by social self-sorting

4.1 Introduction to part-amide cages and self-sorting

As outlined previously, the direct synthesis of amide cages is difficult due to the irreversible nature of the bond-formation. Additionally, alternative methods, such as those outlined in chapters 2 and 3, were unfortunately unsuccessful in yielding amide-based POCs. An alternative strategy was therefore devised focussing on combining reversible and irreversible bond-formation. The aim was to first form pre-configured amide-containing precursors (using irreversible amide formation), then attempt the cage-forming step using traditional DCvC methods, *i.e.*, imine condensation. It was hoped that this method would allow partial introduction of the desired amide properties to be incorporated into the material, whilst avoiding the often-problematic syntheses of amide materials by using dynamic bond-formation (Figure 4.1).

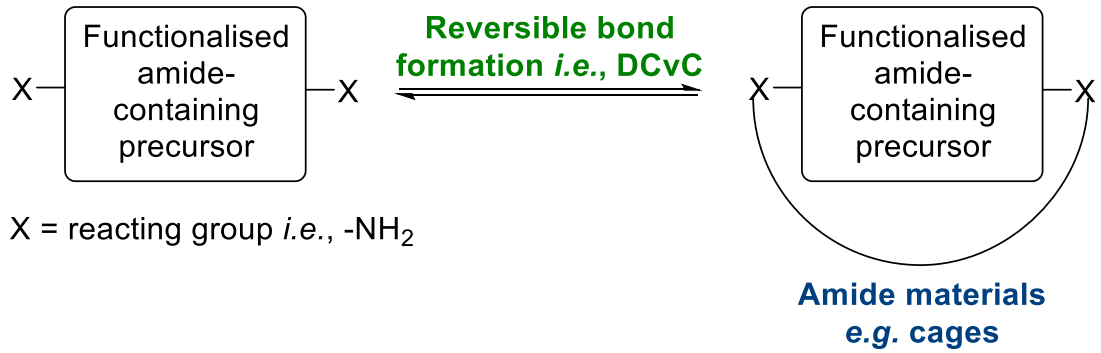

Figure 4.1 – Proposed method for forming part-amide structures: an amide-containing precursor is first produced, which can then be used in the synthesis of materials, i.e., porous organic cages, using DCvC reactions.

Organic cages that incorporate amide bonds have been reported within the literature,[1–3] although none of these reports have focused on the targeted synthesis of "part-amide cages" as a route to more stable POCs. Reported materials can be split into two classes; the first of these are cages that include simple amide bonds as part of the cage backbone. As outlined previously, these structures are often small capsules that have not been tested for porosity and would likely exhibit poor porosity due to their size. Additionally, examples of pseudopeptidic and hydrazone-based cages have also been reported, where the structures are built by the reversible formation of imine bonds (Figure 4.2).[4–7] Rivera and Wessjohann have also outlined the synthesis of amide containing cages by multiple Ugi macrocyclisations (Figure 4.2b).[8,9]

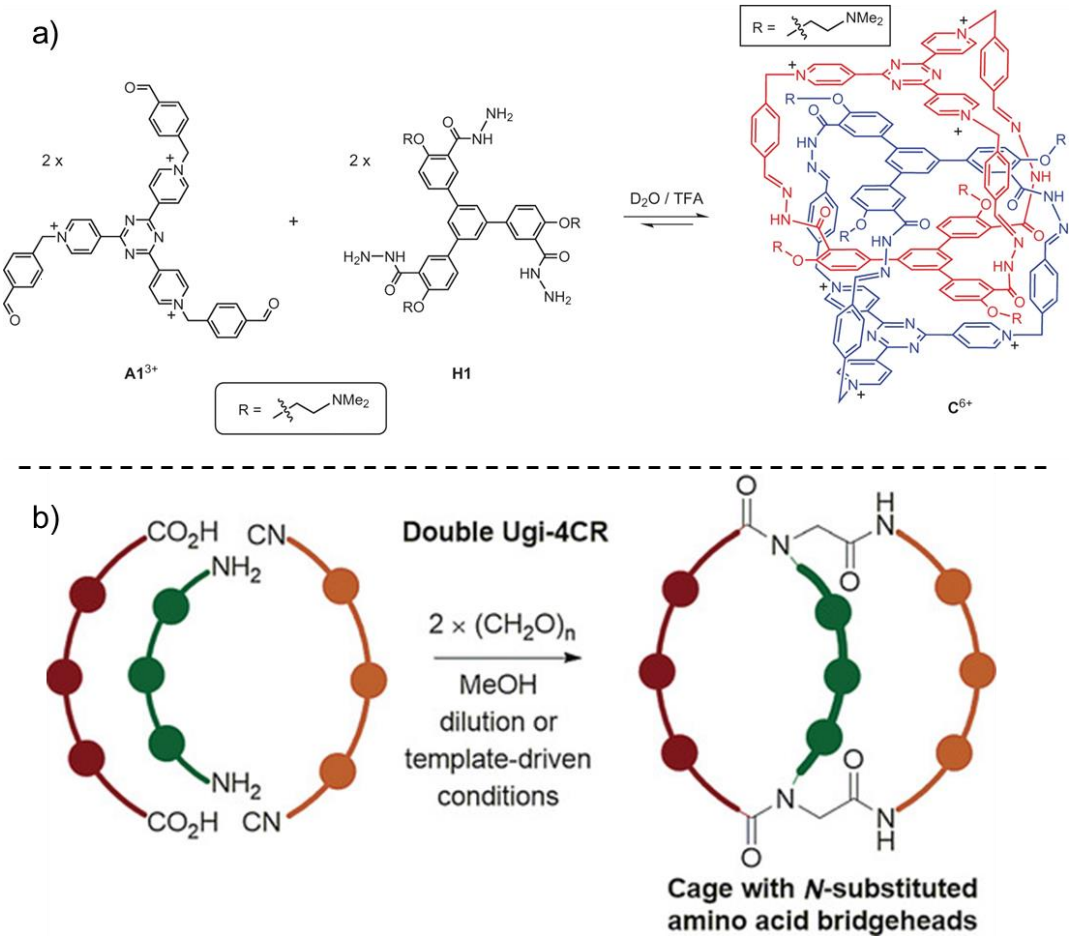

Figure 4.2 – a) Synthesis of hydrazone-based cage catenane as reported by Li et al.[6]*(reproduced with permissions from Ref. 6); b) General method for cage synthesis using Ugi macrocyclisation as reported by Wessjohann et al*[9] *(reproduced with permissions from Ref. 9).*

Alternatively, supramolecular cages have also been formed using incorporated imide groups rather than traditional amides. These reported cages often utilise naphthalene diimide (NDI) or perylene diimide (PDI)-based precursors, in part due to their large, planar structure.[10] A number of these reports focus on the formation of metal-organic structure using these precursors,[10–13] though recently, fully organic structures have also been realised. In 2019, Feng *et al.* reported a PDI-based cage formed by the reaction of a PDI-based diamine with a large planar tetraaldehyde to form a **Tet^{2}Di^4** structure (Figure 4.3a).[14] Though the cage was not tested for porosity, it did exhibit the ability to accommodate guest molecules, as well as showing promise for catalysis.

The pre-configured nature of the two precursors may aid in the synthesis of this cage, though this could hinder derivatisation to large families of novel structures if specific sizes or topologies of precursors are required when screening reagents. Following this work, a 2021 report by Huang *et al.* outlined the synthesis of cages incorporating PDI and NDI groups, but also the smaller pyromellitic dianhydride (PMDI) group (Figure 4.3b).[15] Triamines incorporating these groups were combined with 1,3,5-triformylbenzene (TFB) to form a series of three cages. Unlike the previous cage of Feng *et al.*, these cages were tested for porosity, with a BET surface area of 522 m^2g^{-1} measured for the NDI-based cage — though values were not reported for the PDI- or PMDI-based cages.

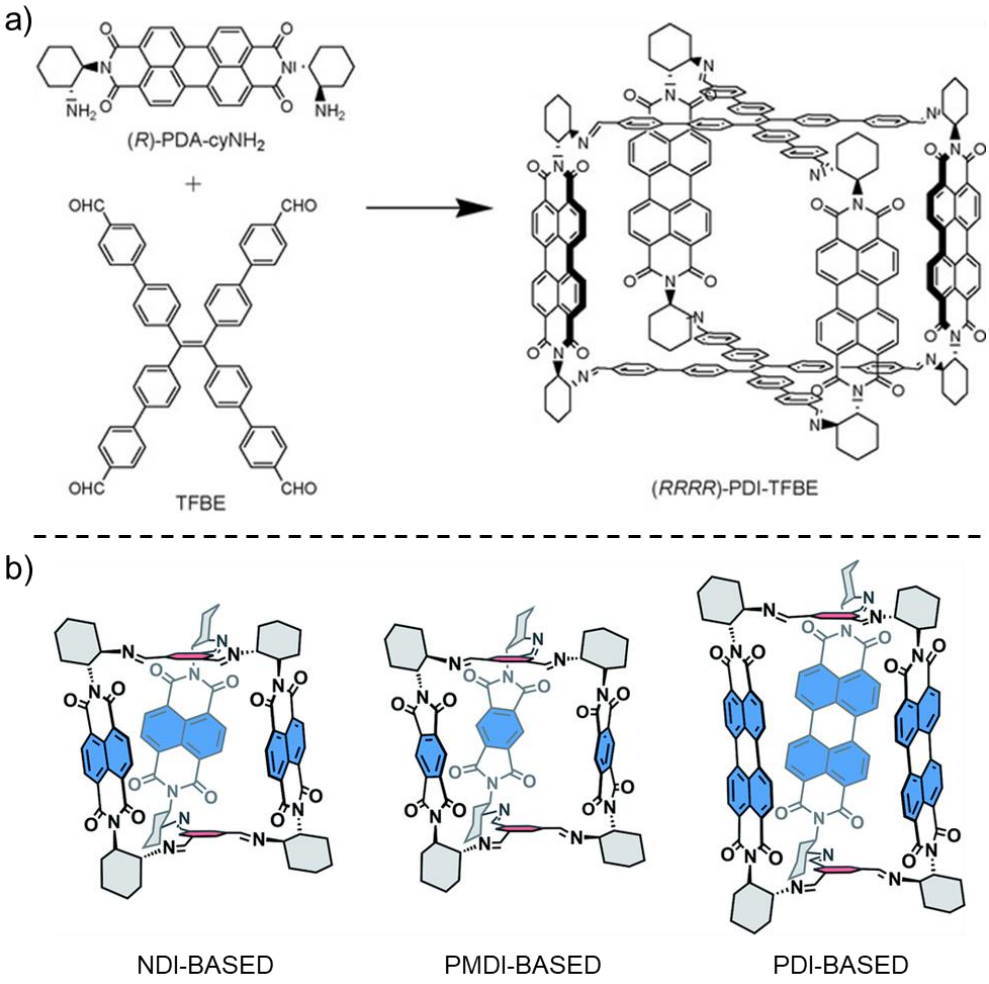

Figure 4.3 – a) Synthesis of part-imide cage as reported by Feng et al., utilising a PDI-based triamine (reproduced with permissions from Ref. 11);[11] b) Synthesis of a series of part-imide cages as reported by Huang et al., utilising triamines based on PDI[15] (reproduced with permissions from Ref. 15).

Despite the handful of examples outlined above, the targeted synthesis of porous part-amide derived cages remains largely unexplored. However, outlined attempts of imide-based cages provides an interesting approach, *i.e.*, use of a methodology whereby more robust, irreversible functional groups are incorporated into the cage structure, but reversible bond-formation is used for the cage-forming step. The design of the precursors would clearly have a huge influence on how the amide groups are distributed within the cage scaffold, *i.e.*, are the amides spread throughout the cage structure, or localised to one region of the cage. Both options have potential benefits — the former could potentially introduce stabilising effects throughout the whole cage, though the synthesis may prove more difficult due to the potential need for highly pre-configured precursors. The latter could introduce stability by allowing for an "anchoring" effect, where one portion of the cage remains stable and resistant to attack — even if the more labile groups were to dissociate, the anchor point may keep the labile groups in close enough proximity to allow reformation of bonds, and thus the cage. The presence of amide functionalities could also influence additional properties including solubility, and potential binding effects with suitable guests. In this work, focus was placed on the design and synthesis of part-amide derived porous organic cages, where the amide groups are localised to one region of the cage.

Self-sorting reactions can be used for the formation of complex structures from a mixture of at least 3 precursors. The products formed from such reactions depend on the nature of the self-sorting taking place, *i.e.*, the recognition between the individual precursors. In general, self-sorting can be categorised in three ways (Figure 4.4)[16]:

1. Self-sorting – where the precursor components form their discrete parent structures with no new combinations of precursors.

2. Social self-sorting – where the components react together to form a new species incorporating all moieties.

3. Scrambling – where no self-sorting has taken place; every potential product is formed in a statistical distribution.

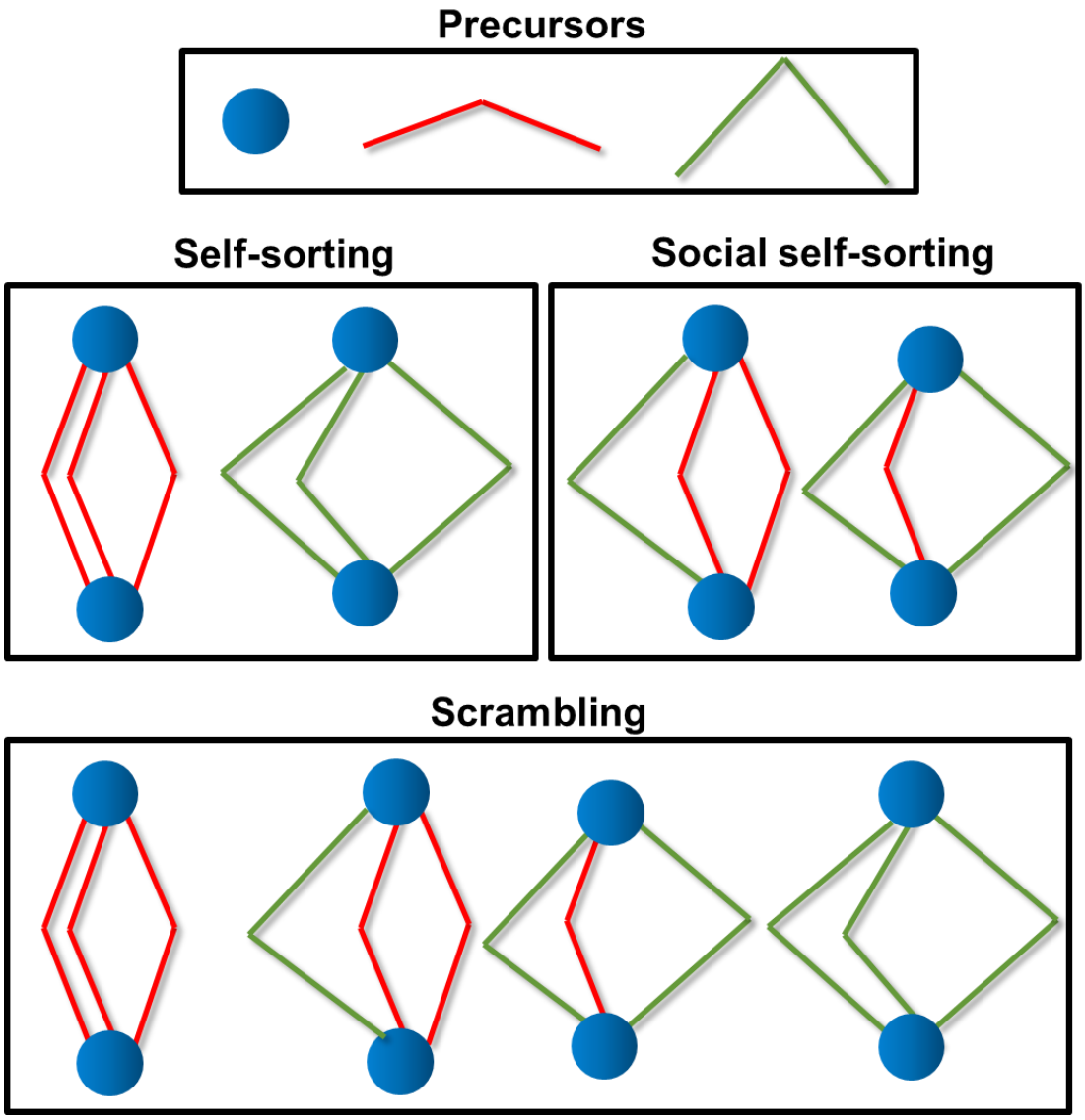

Figure 4.4 – Representative scheme for the three different categories of self-sorting in relation to cage formation incorporating 3 potential precursors: self-sorting – where the discrete, parent cages are formed; social self-sorting – where new mixed species are formed, incorporating all three precursors; scrambling – where no self-sorting takes place, and all potential species are formed in a statistical distribution. The formation of each of these can be influenced by the relative ratios of each precursor used.

Self-sorting reactions have been investigated for a range of supramolecular architectures, such as metal organic cages,[13,17,18] metal complexes,[19] and rotaxanes.[20] However, examples of cage formation by self-sorting are still relatively uncommon. This can be attributed to the difficulty in designing these kinds of multi-component syntheses, contrasting with traditional approaches which often only utilise

the direct condensation of two precursors. An early report of social self-sorting for cages was outlined by Mukherjee and co-workers in 2013,[21] where a combination of two different aldehydes and two different triamines were employed, and self-sorting to form only two discrete cage structures was observed. It was also shown this could be adapted for cage-to-cage transformations by the exchange of more preferred molecular partners. Self-sorting was further explored by Mukherjee and co-workers in 2014, demonstrating the role of hydrogen-bonding in directing synthesis towards specific targets.[22] In 2015 and 2016, Beuerle and co-workers reported a series of self-sorted cages based on a hexahydroxy tribenzotriquinacene (TBTQ) precursor, including what is stated to be the first example of covalent organic cage formation using social self-sorting (Figure 4.5).[23,24] In 2017, Mastalerz and co-workers also utilised a chiral triamino-TBTQ analogue for study, forming a series of three cages, including a socially self-sorted species incorporating both chiral forms of the triamine.[25] This work was continued in a 2021 study by Wagner *et al*. utilising a TBTQ-aldehyde derivative with diaminobenzene, leading to the formation of large **Tri^{8}Di^{12}** cubic cages.[26]

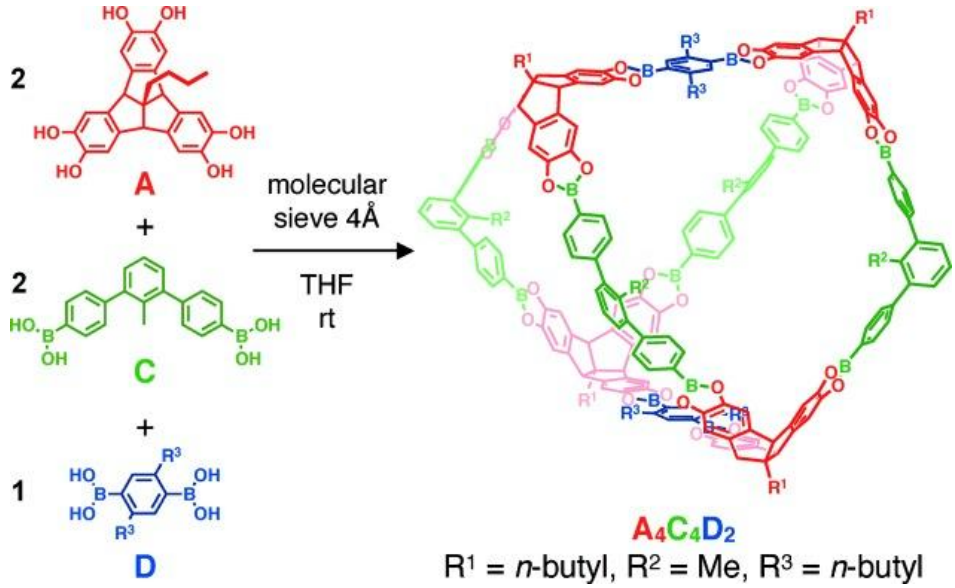

Figure 4.5 – Synthesis of organic cage $A_4C_4D_2$ using social self-sorting, as reported by Beuerle et al. (reproduced with permissions from Ref. 23).[23]

Greenaway *et al*. later reported two studies of POC formation using social self-sorting to form more complex structures.[16,27] The most recent report combined known cage-forming precursors with a series of three extended tetratopic aldehydes (Figure 4.6).[16]

The selected precursors were designed to contain two structurally analogous dialdehydes to a previously used aldehyde employed in the synthesis of **Tri²Di³** capsular cages, such as **B1**.[28] Social self-sorting of the three components resulted in the formation of organic cage dumbbells, with the cage capping units connected by an aromatic linker to form dumbbell-like structures. Due to the presence of the original cage-forming precursors, the parent cage **B1** was also formed as a side product, but the dumbbell species could be separated and isolated using preparative-HPLC.

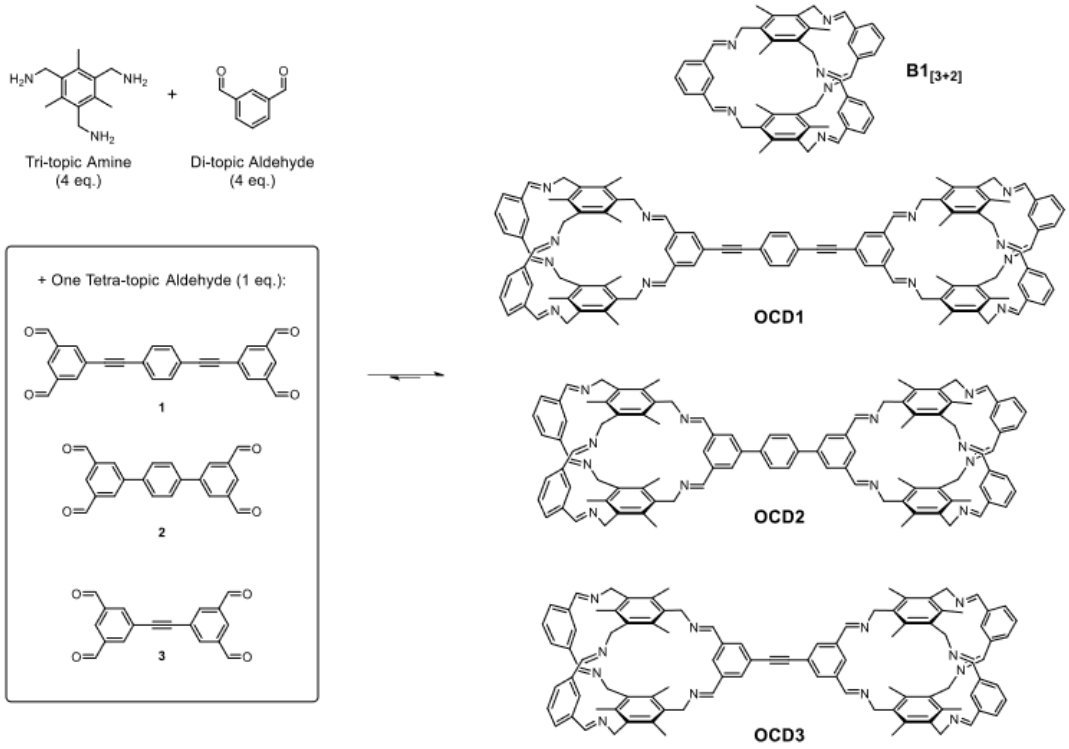

*Figure 4.6 – Method for organic cage dumbbell (OCD) synthesis as reported by Greenaway et al. — reaction of the tritopic amine and ditopic aldehyde, in combination with a tetratopic aldehyde, formed a selected OCD as well as the parent **Tri²Di³** cage **B1** (reproduced with permissions from Ref. 16).*[16]

The second report by Greenaway *et al.* focused on the formation of organic cage pots (OCPs).[27] The OCPs were primarily based on the **CC** series of cages reported by Cooper and co-workers — traditional **CC** cage components (*i.e.*, TFB and a vicinal ditopic amine) were combined with the tritopic amine tris(2-aminoethyl)amine (TREN), and formed the OCPs by social self-sorting of all three precursors (Figure 4.7). Like the earlier dumbbell species, the parent cages were also formed and required separation by chromatography. The OCPs were designed such that while the tritopic

species were incorporated, part of the new structure maintained the window-shape of the existing **CC** cages, presenting the possibility for window-to-window interactions with existing cage species.[27]

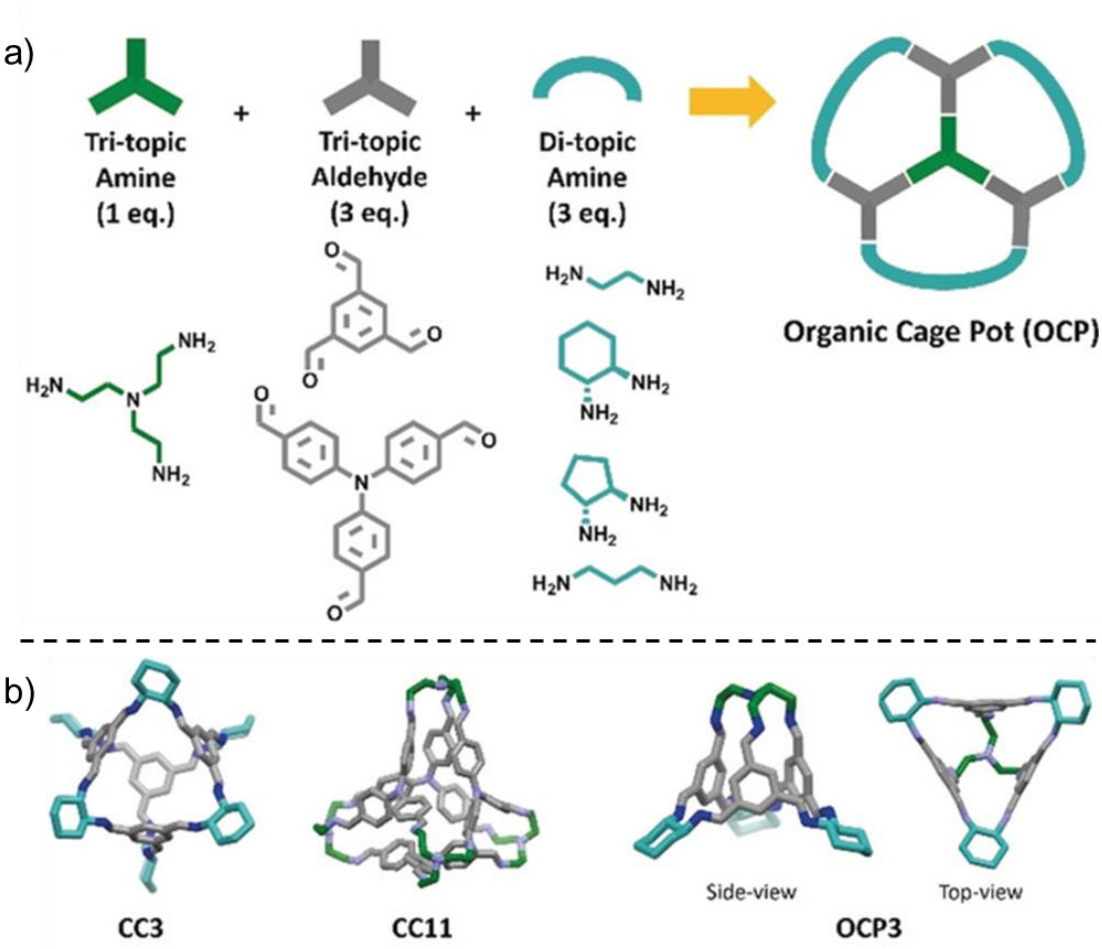

*Figure 4.7 – Synthesis of organic cage pots (OCPs) as outlined by Greenaway et al.: a) general scheme for OCP synthesis by combination of the tritopic amine, TREN, with a tritopic aldehyde and a ditopic amine; b) structural comparison between **CC** series cage, **CC3**, and the other potential parent cage, **CC11**, with **OCP3**, showing the similarity in window structure, formed as a result of the similar precursors used in the synthesis of all the structures (reproduced with permissions from Ref. 27).*[27]

The methodology used to form the organic cage pots presented a route for the potential formation of part-amide derived cages that are structurally analogous to the **CC**-series, using an amide-functionalised triamine in the place of TREN (Figure 4.8). This would clearly result in a less stable structure than if amides were exclusively used, though of interest would be how the presence of even a few amide groups could

influence the overall stability of the cage structure. Using this method would also result in a cage where the amide groups are localised in one region of the cage, and as outlined previously, this could have a beneficial anchoring effect in terms of cage stability. Additionally, this methodology could allow for tackling of a key challenge in POC formation, the control of amine placement – the ability to directly control how different amines are distributed around the cage structure would be hugely beneficial, allowing for specific tuning of the groups around the cage periphery. This could have a profound impact on the solid-state packing and crystal structure of the cage, potentially leading to drastically altered porosity and properties.

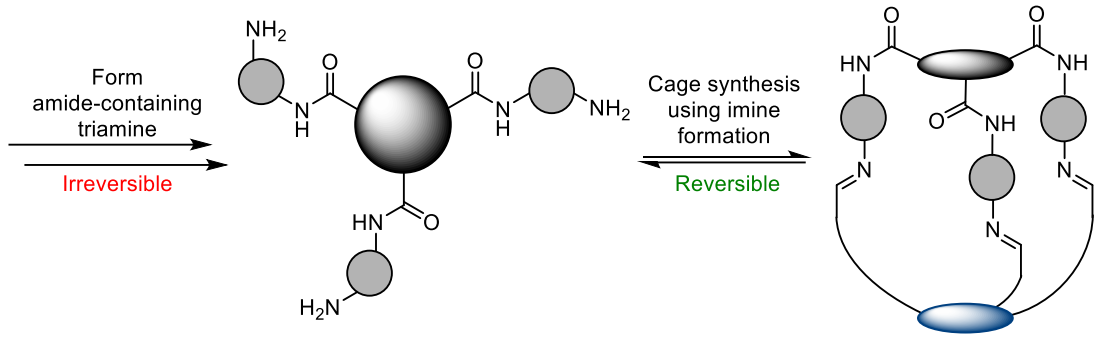

Figure 4.8 – Scheme theorising a method for the synthesis of part-amide derived organic cages using amide-functionalised triamines. After first synthesising the precursor using irreversible methods, the cage forming step can be completed using reversible imine bond-formation, allowing for more straightforward cage formation in comparison to irreversible methods.

During traditional imine cage synthesis using DCvC, very little control can be exhibited over the placement of specific amine groups within the cage structure. This can be exemplified by cage 'scrambling', where the use of a mixture of diamines leads to a statistical distribution of cages which is heavily dependent on their relative ratios.[29,30] The first report of **CC** series cage scrambling in 2011 utilised TFB in combination with ethylenediamine (EDA) and *R,R*-cyclohexyldiamine (*R,R*-CHDA).[29] These precursors react to form the parent cages **CC1** and **CC3**, along with each possible **Tri^{4}Di^6** combination of TFB with the two diamines, in a statistical distribution. In all, this leads to the formation of 10 individual cage species, each of which has a unique distribution of amines throughout the cage structure. The individual cages are described in terms of the number of equivalents of each diamine present, where EDA is **1**, and CHDA is **3**. The structures range from **CC1** itself, *i.e.*, **1**^{6}**3**^{0}, where all amine functionalities are EDA, to **CC3** itself, *i.e.*, **1**^{0}**3**^{6}, where all functionalities are CHDA (Figure 4.9). Of these structures, the **1**^{3}**3**^{3} isomers are of particular interest. In one of these, **1**^{3}**3**^{3}-A (Figure

4.9, highlighted), the placement of amine functionalities creates a POC with two hemispheres, one cyclohexyl and one ethyl — this can be described as a Janus-type structure. Janus, in reference to the god of Roman mythology,[31] refers to materials that "show different properties on two opposing sides or faces".[32] Normally used to refer to Janus nanoparticles — particles in which there are two distinct regions of functionality such as chemical nature and/or polarity,[33] this type of structure has since been translated to other classes of materials, such as 2D materials,[32] silsesquioxanes,[34] and MOF composites.[35] Janus-type structures have been exhibited within cages, though examples are limited – a structure reported by Pattillo and Moore includes regions of imine and alkyne bonding within a single cage structure;[36] and Lei *et al*. outlined the synthesis of small, water-soluble cages that contain regions of different functionality[37]— in both cases, no cages were tested for porosity. Additionally, cages that incorporate different chiral forms of the same precursor in a single structure have also been reported — whilst the functionalities present are the same, these cages could also be classed as Janus-type due to the difference in chirality around the cage scaffold.[25,38]

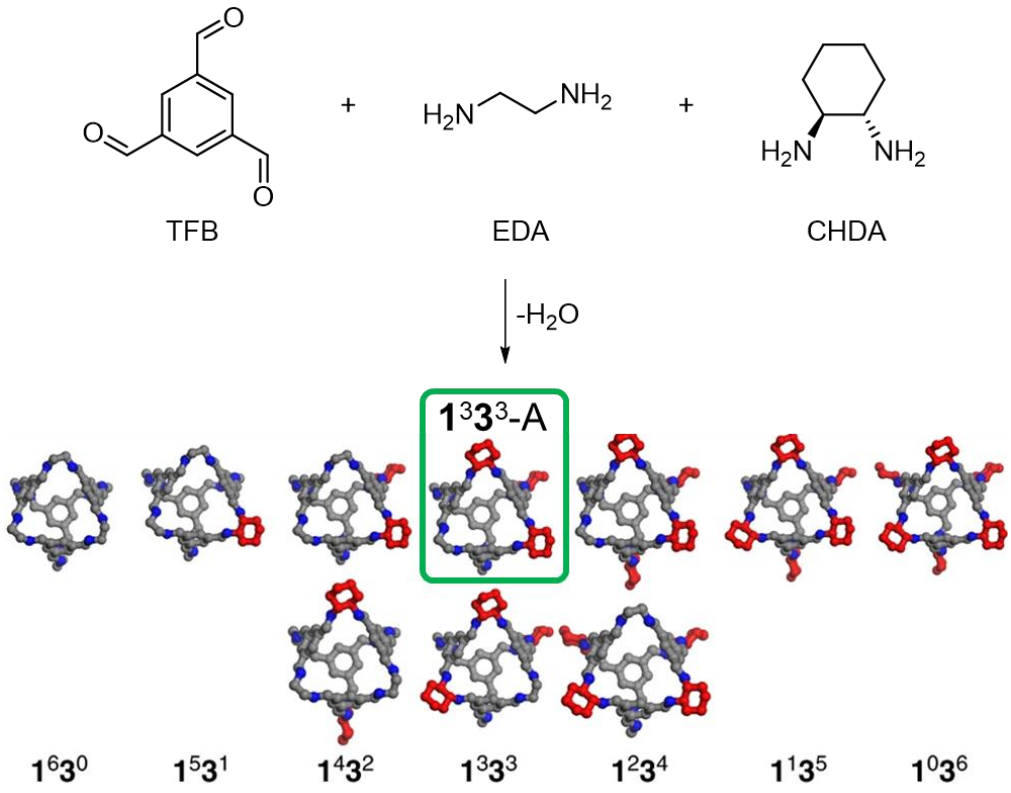

*Figure 4.9 – **CC1**/**CC3** cage scrambling reaction as outlined by Jiang et al. —10 structures formed in a statistical mixture ranging from **CC1** (**$1^6 3^0$**) to **CC3** (**$1^0 3^6$**) (reproduced with permissions from Ref. 29).*[29]

In general, controlling the distribution of functionalities around a cage would be extremely beneficial for studying the properties of the structures — principally, how the varied functionality affects cage interactions, solid-state packing, and other properties such as solubility or stability. This is particularly of interest for Janus structures, as the presence of distinct sections or hemispheres within a single structure could have drastic effects on cage-cage interactions, particularly if the two functionalities were disparate in size or structure, e.g., ethyl and crown-ether functionalities on the same cage, as an extreme example. Unfortunately, this goal would be extremely difficult to realise for POCs when using traditional synthetic methods. Taking the scrambled cage mixture described above as an example, the desired $\mathbf{1}^3\mathbf{3}^3$-A structure exists as one of 10 overall products (and one of two $\mathbf{1}^3\mathbf{3}^3$ isomers), all of which cannot be separated from one another in a facile manner. However, use of the functionalised precursor methodology as outlined earlier (Figure 4.8) could allow a direct pathway to Janus POC structures. By using a precursor with a desired functionality and completing the cage synthesis with an amine of differing structure, the desired Janus structure could be realised as the single target of the process. To investigate this concept, in this work part-amide cages were targeted using social self-sorting reactions, utilising an amide-functionalised precursor.

4.2 Designing a suitable POC target for study

To effectively investigate the synthesis of part-amide cages by self-sorting, a suitable target was required for extended study. Inspired by the earlier work of Greenaway *et al*. into organic cage pots,[27] the **CC** series of cages presented as an ideal system for initial study. The prototypical imine cage **CC3** has been the subject of numerous studies since its initial report[39,40] — this understanding provides an excellent control substrate for direct comparison to any formed part-amide analogues. **CC3** is formed by the reaction of 4 equivalents of TFB with 6 equivalents of CHDA to give an octahedral structure. This synthesis could be adapted to use an amide-functionalised triamine representing a single face of the **CC3** structure, resulting in a part-amide **CC3** derivative (**PA-CC3**) where the amide groups are localised to one portion of the cage (Figure 4.10).

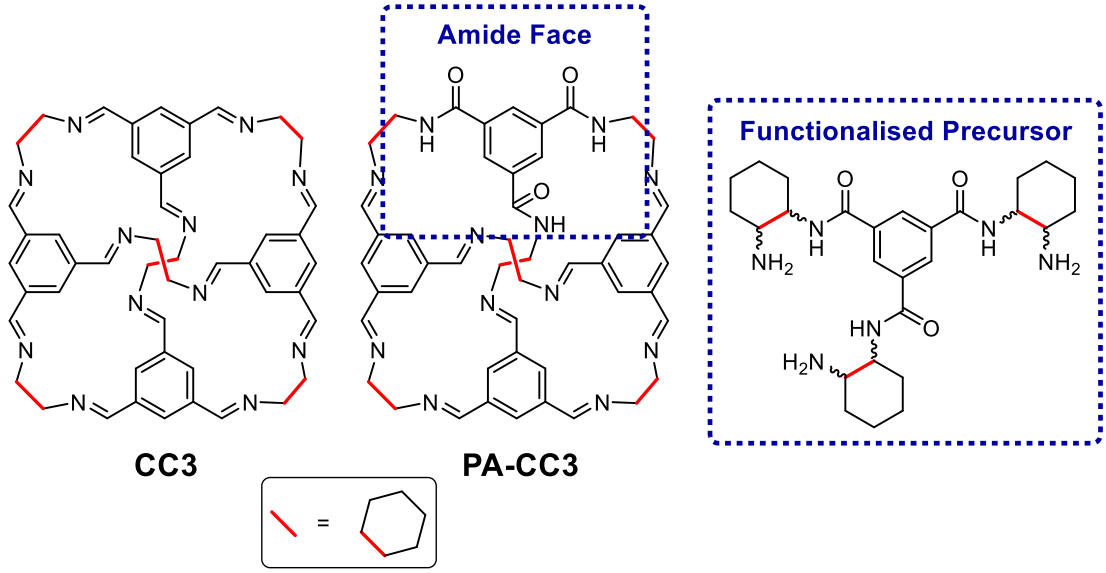

Figure 4.10 – Structural comparison between the proposed part-amide cage, ***PA-CC3****, and the isostructural parent cage,* ***CC3****. Both cages maintain the same geometry and contain cyclohexyl groups at each of the cage vertices.* ***PA-CC3*** *incorporates one amide-containing face, whereas* ***CC3*** *is constructed entirely from imine bonds.*

In previous reported studies of POCs, molecular modelling of potential cages has been utilised as a tool for streamlining their synthesis.[28,41–43] By computationally building cages from selected precursors and calculating their formation energies, the lowest energy topology using a particular set of precursors can be predicted.[44] Insights can then be drawn from the cage model before any experimental studies have been undertaken, for example, an important factor is predicting whether the cage is shape-persistent on desolvation.[45] The low energy conformers of cages that are predicted to collapse *in silico* are likely to do so experimentally, and these collapsed structures are subsequently non-porous, and therefore not POCs. By first investigating the feasibility of cage formation *in silico,* such none shape-persistent cages can be excluded, allowing experimental studies to be conducted more efficiently.

To investigate part-amide derived cages, collaborators within the Jelfs group at Imperial College London (ICL) first modelled the potential part-amide cages *in silico*. **CC3** can be synthesised as either **CC3**-*R* or **CC3**-*S* depending on whether the *R,R* or *S,S* form of CHDA is used, respectively. Similarly, **PA-CC3** would have similar enantiomers based on the chirality of both the triamine and diamine used in the reaction. As such, two functionalised triamines were designed for modelling — *R*-**Tri**

and *S*-**Tri**, synthesised using both the *R,R* and *S,S* enantiomers of their CHDA moieties, respectively . In this system, the functionalised triamines effectively act as a cage hemisphere, whereby the target structure has one amide-containing face, and three imine faces. For cage formation, use of diamine precursors with the same chirality would therefore result in two potential homochiral cages, **PA-CC3**-*R* and **PA-CC3**-*S*, whereas use of the opposite enantiomers would lead to the formation of the heterochiral cages, **PA-CC3**-*RS* and **PA-CC3**-*SR*.[38] To ensure full understanding of the potential formation products, collaborators modelled all four isomer combinations to give a family of four potential part-amide cages (Figure 4.11).

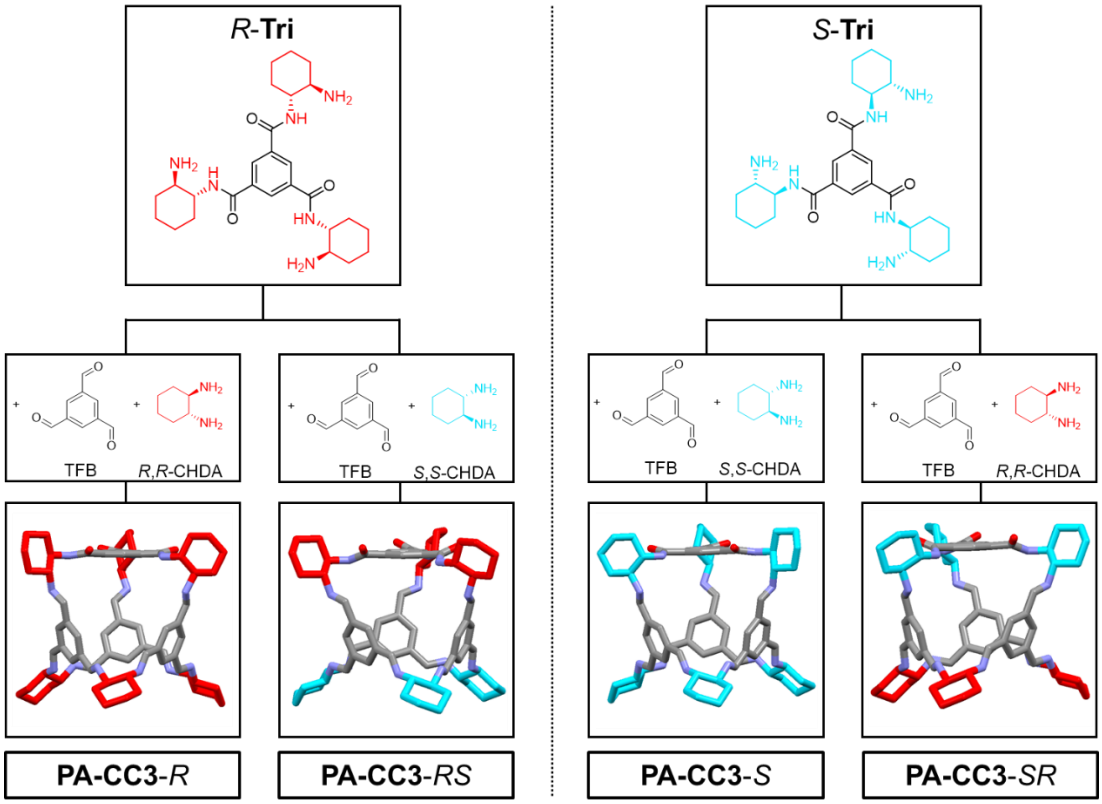

*Figure 4.11 – Schematic to show the design and molecular modelling of a family of part-amide cages based on **CC3**. Using a triamine and diamine of like chirality gives the homochiral cages **PA-CC3**-R and **PA-CC3**-S, whereas using opposite chiralities results in formation of the heterochiral disymmetric cages **PA-CC3**-RS and **PA-CC3**-SR.*

Pleasingly, it was predicted that all four cages should be shape-persistent. The formation energies for the cages were also calculated for the whole series. The calculated formation energy for the homochiral cages **PA-CC3**-*R* and **PA-CC3**-*S* were of -36 kJmol^{-1}; the heterochiral cages **PA-CC3**-*RS* and **PA-CC3**-*SR* differed slightly

with a calculated value of -31 kJmol^{-1}. **CC3** was also modelled in both its -*R* and –*S* forms for comparison, with a calculated formation energy of -50 kJmol^{-1} for each. The similarity between the formation energies suggested that both **PA-CC3** and **CC3** should be formed during the synthesis, which could then potentially be separated to isolate all of the cages. A similar effect was seen for the formation of cage pots as reported by Greenaway *et al.*, where both the cage pots and parent cages were formed, which could then be separated using preparative-HPLC.[27]

In addition, the modelling study outlined several interesting structural motifs in the part-amide cages. Comparison of **CC3**-*R* with the homochiral part-amide cage **PA-CC3**-*R* shows that the structures are nearly identical (Figure 4.12a), although due to the increased flexibility of the amide bond compared to the imine bond, the amide face within the cage exhibits a small amount of twist, causing loss of planarity. However, this did not appear to affect the overall structure of the cage. For the heterochiral cage structure, **PA-CC3**-*SR*, comparison with **CC3**-*R* shows a large amount of twist within one half of the structure, due to the use of the opposite enantiomers in three of the CHDA groups (Figure 4.12b). Again, this does not appear to affect the cage structure, but could have interesting implications in terms of the solid-state packing or crystallisation. In both cases, the presence of the amide groups may influence the polarity of the cage cavity, due to the location of the functionalities.

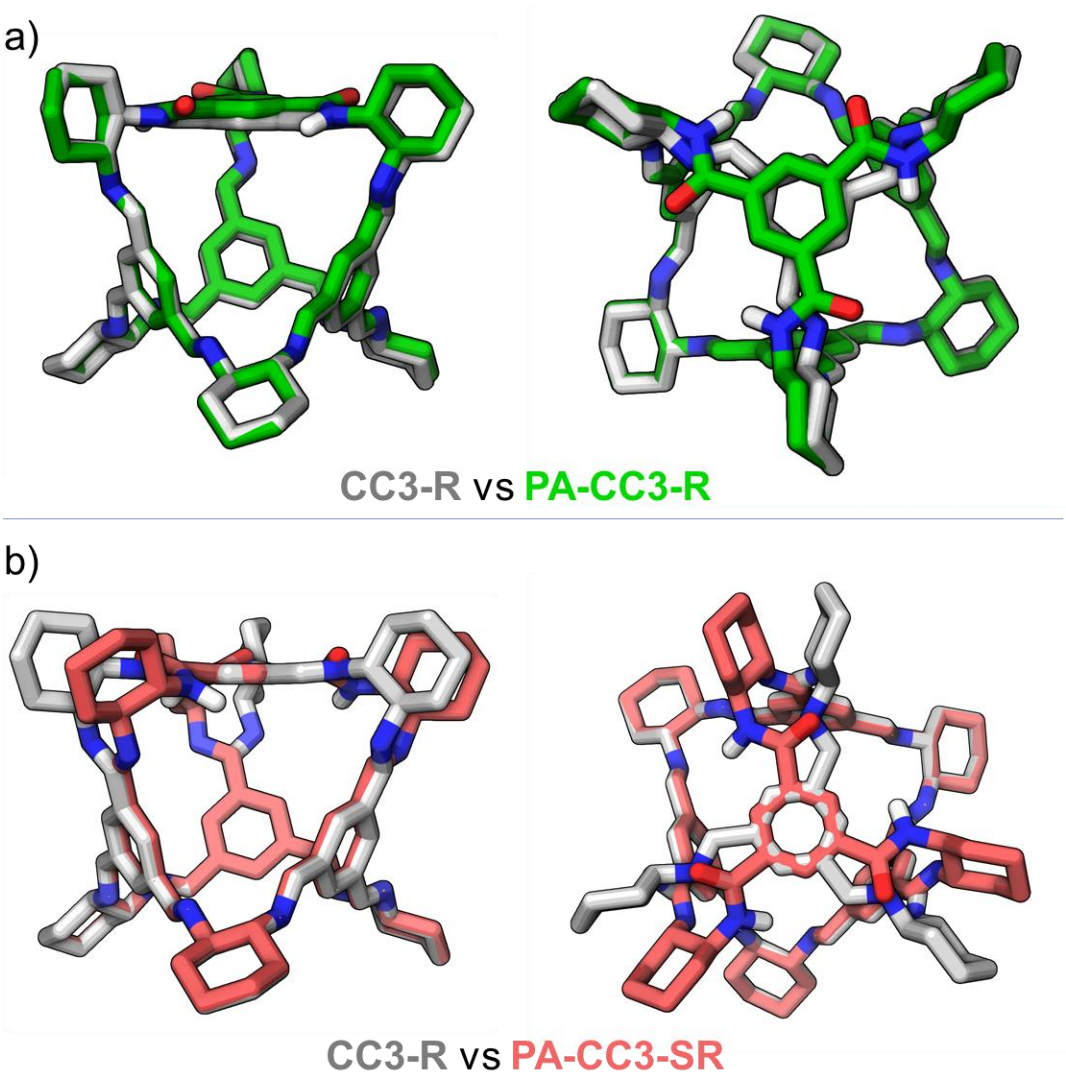

*Figure 4.12 – Molecular modelling of part-amide Janus-type cages in comparison with **CC3**: a) comparison of **CC3**-R (grey) with homochiral **PA-CC3**-R (green); b) comparison of **CC3**-R (grey) with heterochiral **PA-CC3**-SR.*

With the confirmation that the part-amide cages were suitable targets, efforts were focused on developing a suitable synthetic route for precursor and cage formation, and **PA-CC3**-*R* was selected as the target for initial study.

4.3 Synthesis of part-amide cages based on CC3

4.3.1 Synthesis of a suitable amide-functionalised triamine

Initial testing focused on attempts at direct formation of a functionalised triamide precursor by the reaction of benzene-1,3,5-tricarbonyl trichloride in combination with an excess of CHDA, to form the triamine directly as the free base (Figure 4.13). The key limitation of this system was the chance for irreversible polymer formation, although it was hoped that the use of a large excess of diamine would mitigate this, promoting single addition of the CHDA to each acid chloride group. The *R,R*-enantiomer of CHDA was first used, targeting the chiral triamine *R*-**Tri**. Unfortunately, this process was ultimately unsuccessful, producing a complex mixture of products which were difficult to purify and characterise.

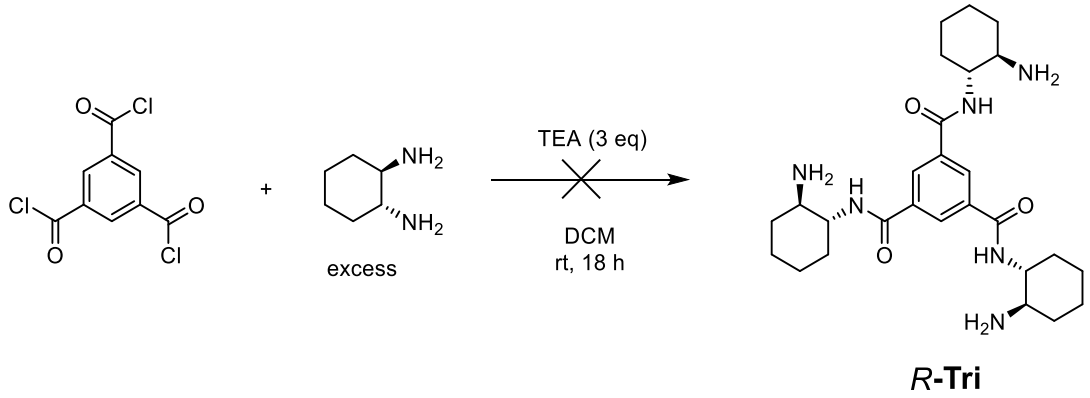

*Figure 4.13 – Attempt to form the functional amide-containing triamine R-**Tri** directly by the condensation of benzene-1,3,5-tricarbonyl trichloride with an excess of R,R-CHDA.*

An alternative method was devised based on inspiration taken in part from work by Roelens and co-workers — this work outlined attempts at receptor and cage formation using pre-formed part-amine structures combined with imine condensations and in situ reduction (Figure 4.14).[46,47] To facilitate precursor formation, they employed the use of mono-protected vicinal diamines which resulted in controlled addition of the diamine to only one equivalent of a tritopic aldehyde, avoiding the formation of unwanted side products including polymeric species. Whilst the desired cage species were not successfully formed, amine addition was controlled, and cage-like receptors were isolated from the reactions. It was hoped that this methodology could be adapted to form the part-amide precursors required for this work.

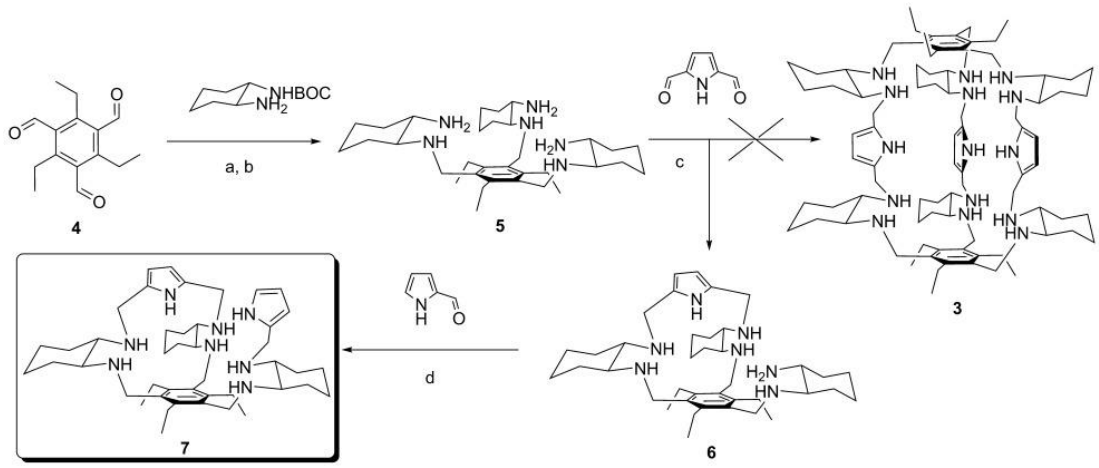

Figure 4.14 – Formation of tripodal receptors as reported Roelens and co-workers, using singly-protected diamines to control addition to a functionalised trialdehyde.[46] *Reaction conditions are as follows: a) tert-butoxycarbonyl-trans-1,2-diaminocyclohexane, $CH_3OH/CHCl_3$ 1:1, 70 °C, 7.5 h, then $NaBH_4$, rt, 1 h, 78 %; b) CF_3COOH, CH_2Cl_2, rt, 1.5 h, 91 %; c) pyrrole-2,5-dicarbaldehyde, $CHCl_3$, 70 °C, 12 h, then $NaBH_4$, CH_3OH, RT, 1 h, 63 %; d) $CHCl_3$, RT, 12 h, then $NaBH_4$, CH_3OH, rt, 1 h, 50 %) (reproduced with permissions from Ref. 46).*

To investigate this, a synthetic route was devised combining benzene-1,3,5-tricarbonyl trichloride with a mono-tert-butoxycarbonyl (Boc) protected analogue of *R*,*R*-CHDA (Figure 4.15a). The Boc-protecting group could then be removed to later yield the desired triamine precursor. The required mono-Boc-protected diamine was available commercially, facilitating a more straightforward synthesis. The starting materials were combined at ambient temperature, in the presence of triethylamine (TEA) as an appropriate base (see experimental section, page 195). Pleasingly, the reaction was a success — the presence of the Boc-protecting group ensured only single addition of each diamine to the acid chloride, with no polymer formation observed. ^{1}H NMR spectroscopic analysis of the crude reaction showed a mixture of products however, likely due to the presence of some unreacted starting material in combination with mono- and di-substitution products. After separation from the formed side-product TEA-hydrochloride salts and isolation, the crude triamine was purified by flash column chromatography (95:5 DCM:MeOH). This resulted in the tri-substituted target species *R*-**Tri-Boc** being isolated in high purity, which was confirmed by mass spectrometry.

For the part-reduced amine analogues described earlier, Roelens and co-workers used the addition of trifluoroacetic acid (TFA) to remove the Boc protecting-groups, yielding the triamine as the free base.[46] Unfortunately, application of this method to the part-amide precursors was unsuccessful, and the free triamine could not be isolated directly. An alternative method was devised using an excess of concentrated hydrochloric acid in place of TFA (Figure 4.15) (see experimental section page 196). This facilitated both deprotection of the Boc-groups, as well as the formation of the triamine hydrochloride salt, *R*-**Tri.3HCl**, which precipitated in THF as a colourless solid that could be easily isolated by vacuum filtration.

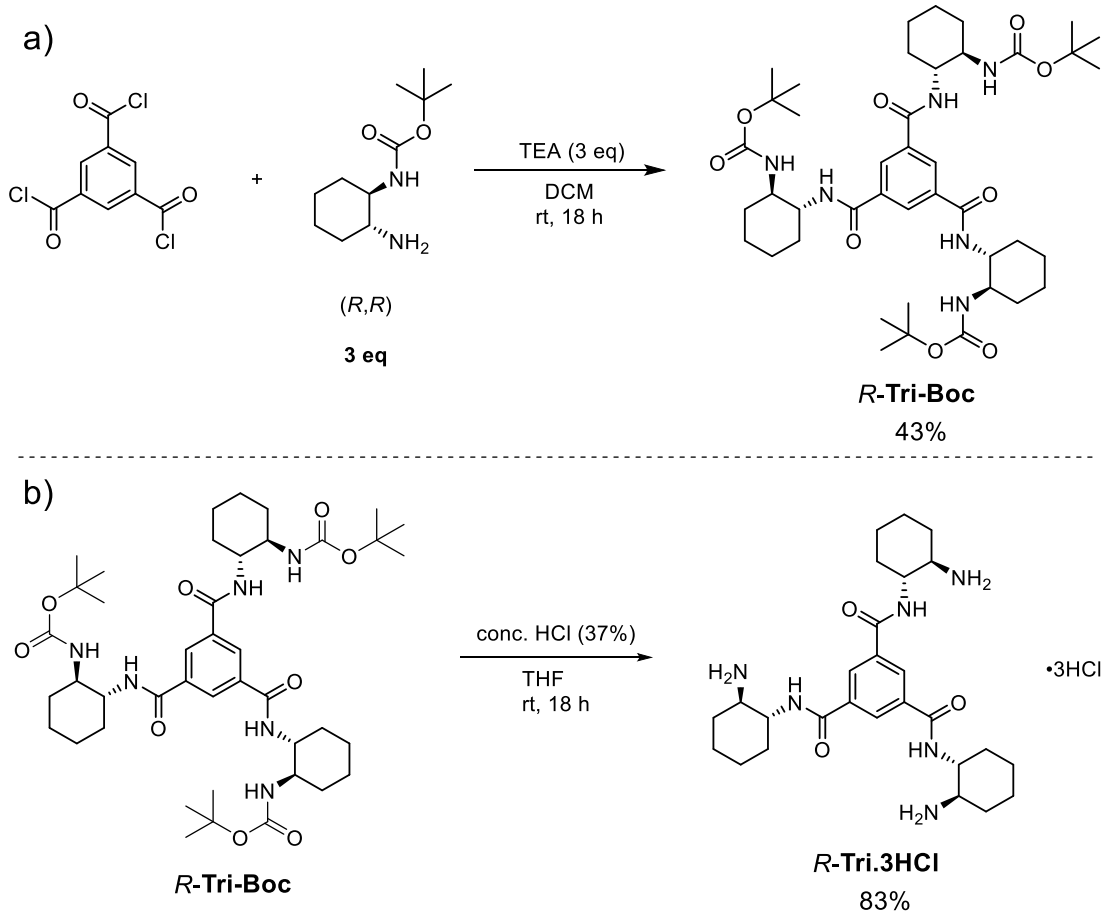

*Figure 4.15 – a) Formation of Boc-protected triamine R-**Tri**-**Boc** by reaction of the singly protected diamine, (1R,2R)-N'-(tert-butoxycarbonyl)-1,2-cyclohexanediamine, with benzene-1,3,5-tricarbonyl trichloride; b) Reaction of R-**Tri-Boc** with concentrated HCl to form the triamine salt R-**Tri.3HCl**. For this initial cage study, the R.R enantiomer of CHDA was used, resulting in the R form of the protected triamine.*

Analysis by ^{1}H NMR spectroscopy confirmed clean formation of the desired triamine salt, *R*-**Tri.3HCl** (Figure 4.16). The structure was further confirmed by mass spectrometry – while the compound appears as the free base due to the ionisation technique, the presence of the triamine, *R*-**Tri**, was confirmed: calculated for $C_{27}H_{42}N_6O_6$ 498.3313, found $[M+H]^+$ 499.3387. Unfortunately, attempts to form the free base of the triamine were unsuccessful, resulting in crude reaction mixtures from which it was difficult to isolate the desired product. As such, further studies were completed using the salt, with the caveat of requiring a suitable base for *in situ* formation of the free triamine when attempting cage formation.

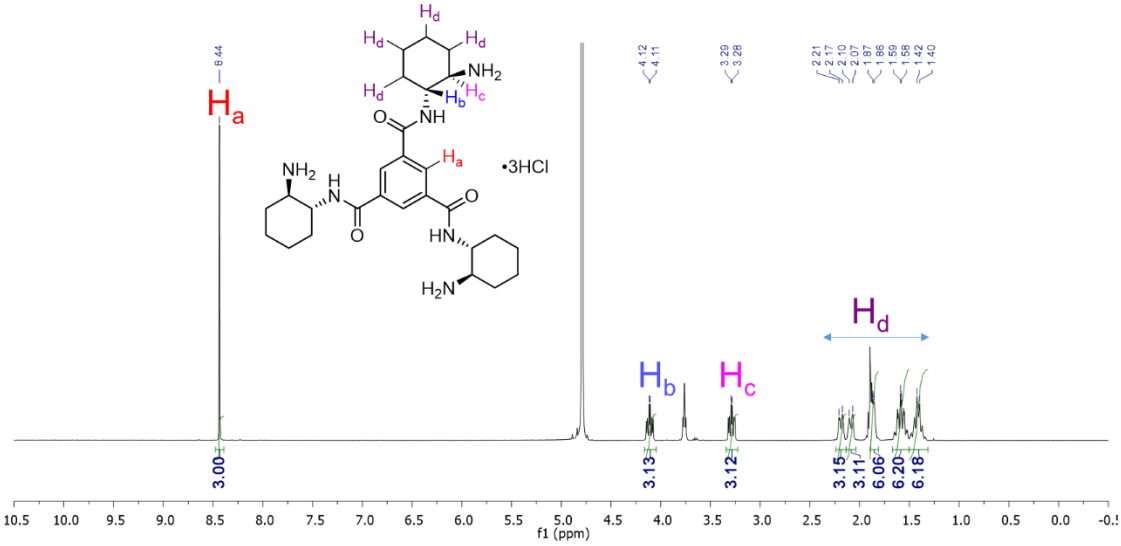

*Figure 4.16 – ^{1}H NMR spectrum (D_2O) of the part-amide precursor R-**Tri.3HCl**.*

4.3.2 Test synthesis of PA-CC3-*R*

With an appropriate amide-functionalised triamine precursor in hand, efforts were shifted to apply self-sorting in the formation of the target cage **PA-CC3**. Methodology was developed using the report of Greenaway *et al*. into the synthesis of organic cage pots.[27] Due to the similarity between the systems, *i.e.*, the reaction of a tritopic amine with TFB and CHDA, the cage pots reaction conditions were employed for this part-amide system (Figure 4.17).

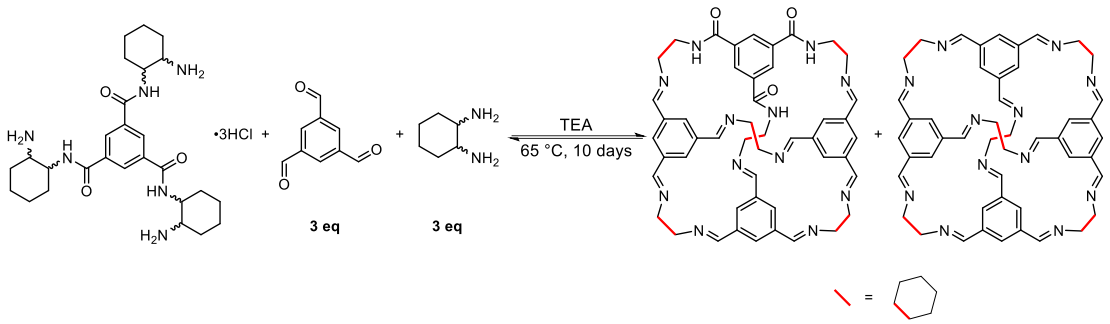

Figure 4.17 – General reaction scheme for the synthesis of a part-amide cage, based on the reaction of an amide-functionalised triamine with TFB and a single enantiomer of CHDA.

For the cage syntheses, a solution of TFB was first prepared, to which separate solutions of both the triamine salt and CHDA enantiomer were added sequentially. As the triamine salt was used, triethylamine (TEA) was added to form the free triamine in solution. To ensure the triamine was completely deprotected, 18 equivalents of TEA were added (6 per amine functionality). As *R*-**Tri.3HCl** was the available triamine, the homochiral cage **PA-CC3**-*R* was initially targeted to ensure the validity of the synthesis (Figure 4.18) (see experimental section page 200).

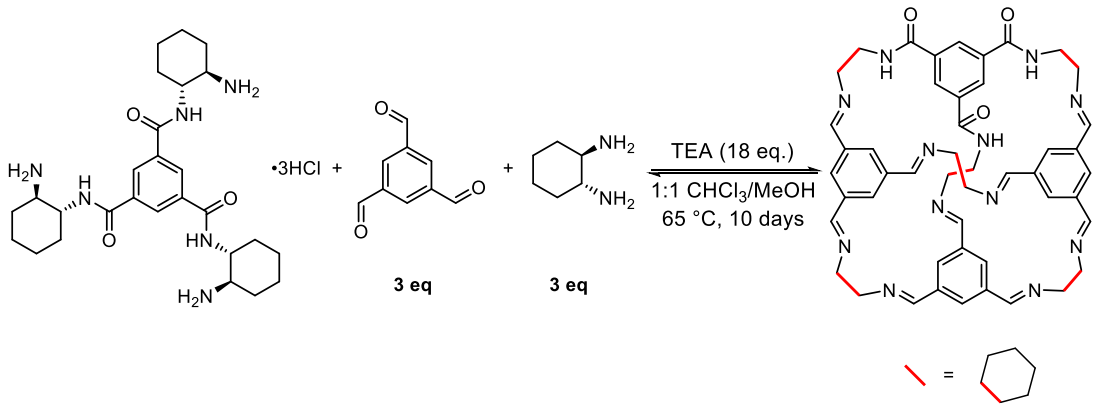

*Figure 4.18 – Synthesis of **PA-CC3**-R by the reaction of R-**Tri.3HCl** with TFB and R,R-CHDA.*

Following heating, the reaction mixture was reduced *in vacuo*, and TEA-HCl salts were obtained by precipitation in THF, removed by filtration, and the resultant solution reduced to dryness. The residue was dissolved in DCM, and addition of n-hexane as an anti-solvent led to immediate precipitation of a solid. This suspension was filtered to give a crude cage product as an off-white solid. Based on the previous cage pots report[27] and the molecular modelling study, this crude product was theorised to

contain both the part-amide cage and parent cage **CC3**. ^{1}H NMR spectroscopy of the crude reaction product showed near complete consumption of the aldehyde species and a complex aromatic region, with a range of peaks which could not be easily distinguished (Figure 4.19). Whilst more proton environments would be expected when compared to **CC3**, the complexity suggested that in addition to any cage products formed, there were likely several cage intermediates and incomplete reaction species present.

In addition to complexities caused by the part-amide cage itself, another key factor to take into account is formation of the parent cage, as the presence of TFB and *R*,*R*-CHDA also allows for the formation of **CC3**-*R* under the applied conditions. This competing reaction had the potential to cause two issues — it could cause an imbalance in the initial ratio of precursors required for the part-amide cage by consuming the required precursor when forming **CC3** by self-sorting, and it could also remain as a contaminant in the product mixture making isolation of **PA-CC3**-*R* difficult. Parent cage formation was expected for a self-sorting reaction of this nature and, as in the examples of cage pots, it was hoped that it could be removed during purification of the part-amide cage. As a contaminant, **CC3** has a varied impact on critically assessing the reaction when using ^{1}H NMR spectroscopy. Upfield regions were impacted due to the similarity and broad nature of groups for the cyclohexyl groups. For the aromatic region, **CC3** impacts less heavily when assessing spectra due to the relative simplicity of the **CC3** spectra (two aromatic singlets) (Figure 4.19). The main difficulty for the **PA-CC3**-*R* crude product mixture was the inherent complexity as outlined earlier and, as a result, the difficulty in clarifying which peaks represent which species (again with slight overlap due to the overall structural similarities between the cages).

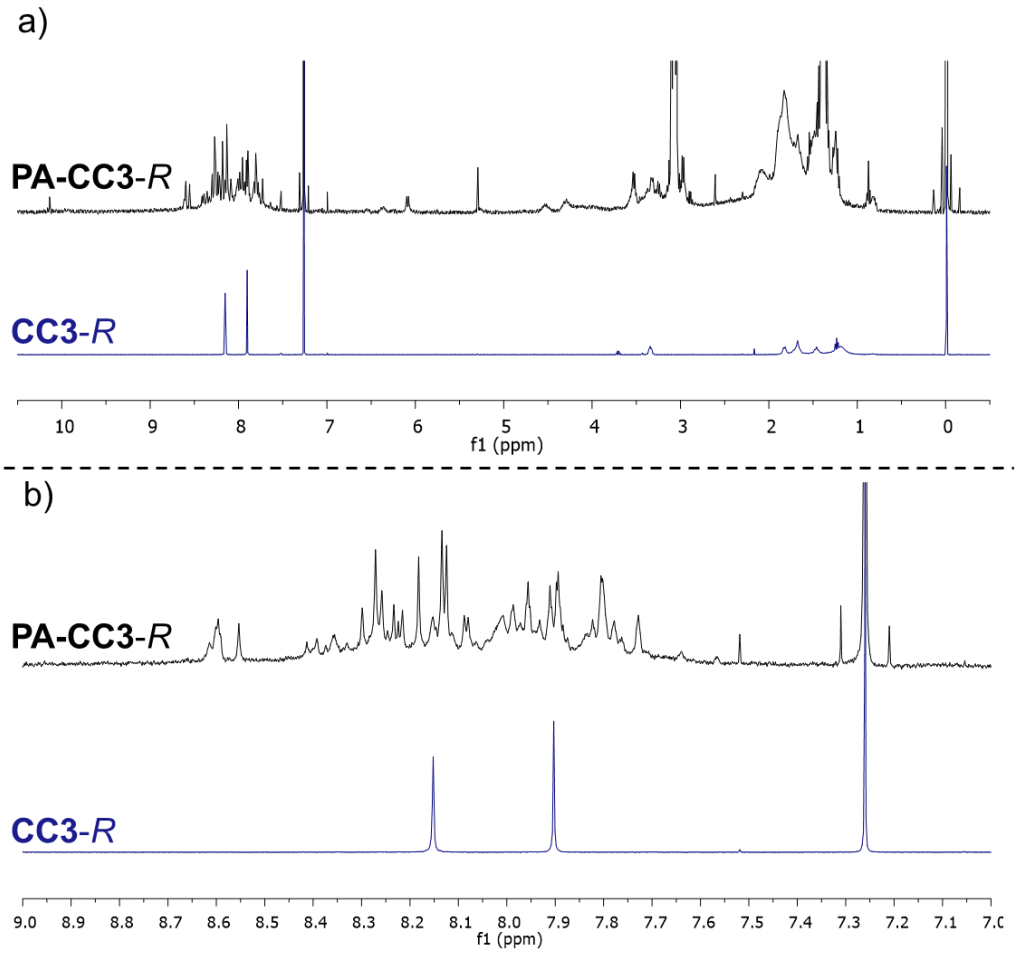

*Figure 4.19 – Stacked ^{1}H NMR ($CDCl_3$) spectra for crude **PA-CC3**-R and parent cage **CC3**-R; a) ^{1}H full spectra **PA-CC3**-R; b) expanded aromatic region of **PA-CC3**-R highlighting the complexity of the spectra compared to that for **CC3**-R; this may be due to the number of potential species present.*

Ultimately, the presence of **PA-CC3**-*R* was confirmed using high-resolution mass spectrometry, where it was present as the singly charged $[M+H]^+$ ion peak (calculated for $C_{72}H_{84}N_{12}O_3$ 1164.6789, found $[M+H]^+$ 1165.8776, Figure 4.20). As expected, **CC3** was also formed as a side-product and is present in the spectrum as the singly charged $[M+H]^+$ species (expected: 1117.7015, found: 1117.8871). Several other species are also present in the spectrum, although it was difficult to assign these additional mass ions to any specific misaligned products.

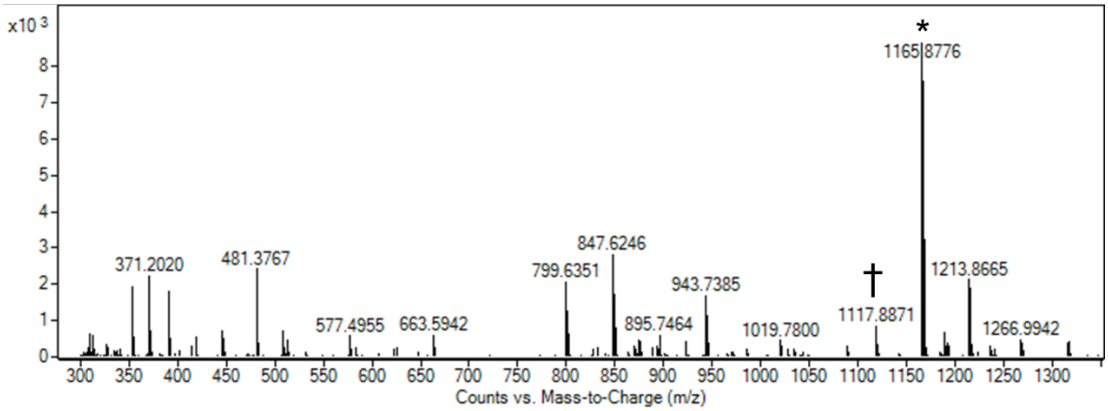

*Figure 4.20 – High-resolution mass spectrum for the crude test reaction attempt at forming **PA-CC3**-R: **PA-CC3**-R is found as the [M+H]⁺ species at 1165.8776, marked by *, and **CC3** is also present as a side-product as the [M+H]⁺ species at 1117.8871, marked by †.*

Whilst the target part-amide cage had not been formed cleanly, the presence of **PA-CC3**-*R* in the mass spectra was very promising. As such, it was decided to apply these conditions to form the series of four part-amide cages as outlined previously (Figure 4.11), with the caveat that further purification would be required further down the line. The reaction conditions were kept the same except for the solvent, as during the test reaction, it was found that while the *R*-**Tri.3HCl** precursor started to dissolve on addition of TEA, the final mixture was a turbid solution which did not change even with additional stirring and sonication. It was therefore thought that this may influence the reaction outcome if less *R*-**Tri.3HCl** was fully dissolved in the solution, leading to less material being available for **PA-CC3**-*R* formation. Additionally, maintaining dissolution of all reaction species was key to avoid premature precipitation of intermediates, as any kinetic formed precipitates may be unable to equilibrate to the target cage.[48] The solvent was therefore changed from neat chloroform to a 50:50 mix of chloroform:methanol, since the addition of methanol facilitated full dissolution of the triamine salts.

Expansion to the full series of cages meant the attempted synthesis of the heterochiral cages **PA-CC3**-*RS* and **PA-CC3**-*SR*. It was thought that the formation of these cage may result in more complex ^{1}H NMR spectra than for the homochiral cage due to the presence of both opposite chiralities, in addition to the existing relative flexibility of the amide groups. Fortunately, a direct comparison was available in the literature — in 2019, Slater *et al.* reported an investigation into **CC3** formation targeting a cheaper

synthetic route by using racemic CHDA rather than a single enantiomer (*i.e., R,R*- or *S,S*-CHDA).[38] Following precipitation and isolation of a poorly soluble **CC3**-*R/S* co-crystal formed after the self-sorting of each enantiomer of CHDA to form **CC3**-*R* and **CC3**-*S*, the reaction filtrate was analysed, revealing the presence of two previously unknown dissymmetric isomers of **CC3**, **CC3**-*RS* and **CC3**-*SR*. These cage isomers are formed from 4 equivalents of TFB with 3 equivalents each of *R*,*R*-CHDA and *S*,*S*-CHDA. The CHDA groups on the vertices are positioned such that **CC3**-RS or **CC3**-SR could be envisioned as having two hemispheres, one with R-functionality, and one with S-functionality. This matched extremely well with the proposed mixed part-amide cage **PA-CC3**-*RS*, providing an ideal structure for comparison (Figure 4.21). The *–RS* and *–SR* labels are swapped between the cages due to the naming convention from this study using the amide-face as the initial chirality, whereas the study by Slater *et al*. uses the window of the cage to determine the first chirality – this distinction does not affect the ability to compare the relative structures of the cages.

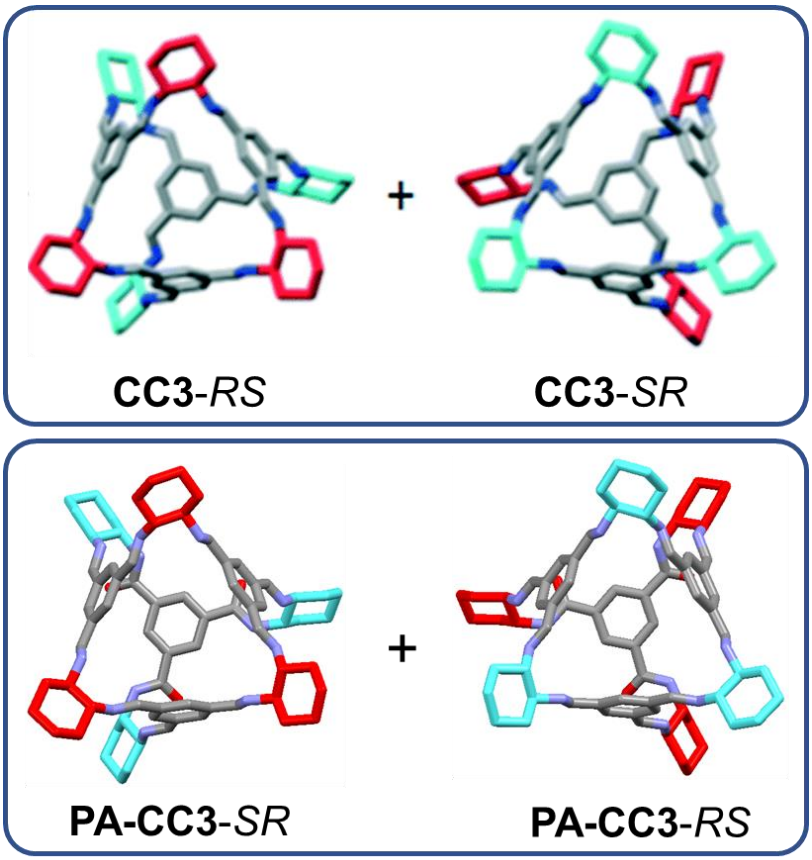

Figure 4.21 – Structural comparison of disymmetric cages: top – dissymmetric cages reported by Slater et al.;[38] bottom: heterochiral part-amide Janus cages as outlined in this study. The –RS and –SR labels are swapped between the cages due to the naming convention from this study using the amide-face as the initial chirality.

Finally, Slater *et al*. note in their study that of all the possible combinations of precursors, only four cages are formed: the two homochiral forms of **CC3**, and the two disymmetric cages described above, indicating a strong preference to form these isomers over a statistical distribution of scrambled species.[38] This highlighted a key benefit of the amide functionalised triamine used for this reaction — due to the inherent stability of the amide C-N bond, substitution or exchange with the free diamine should not occur at these sites; though it is worth noting that exchange with other diamines may be possible in the presence of a suitable catalyst as outlined in chapter 2. As a result, the chirality cannot switch in the *R*-**Tri.3HCl** or *S*-**Tri.3HCl** precursors, which means that for the target heterochiral cages, only the desired *R*,*R*,*R*,*S*,*S*,*S* (**PA-CC3**-*RS*) or *S,S,S,R,R,R* (**PA-CC3**-*SR*) isomers can be formed in the reaction.

4.3.3 Synthesis of part-amide cage series

For the synthesis of the proposed cage series, reaction conditions were maintained as before, though with the change in solvent as outlined previously. For the synthesis of **PA-CC3**-*S* and **PA-CC3**-*SR*, the *S*-enantiomer of the triamine salt (*S*-**Tri.3HCl**) was required. This was synthesised by the same method as previously described, but using mono Boc-protected *S*,*S*-CHDA instead of *R,R*-CHDA (Figure 4.22) (see experimental section pages 196 and 197).

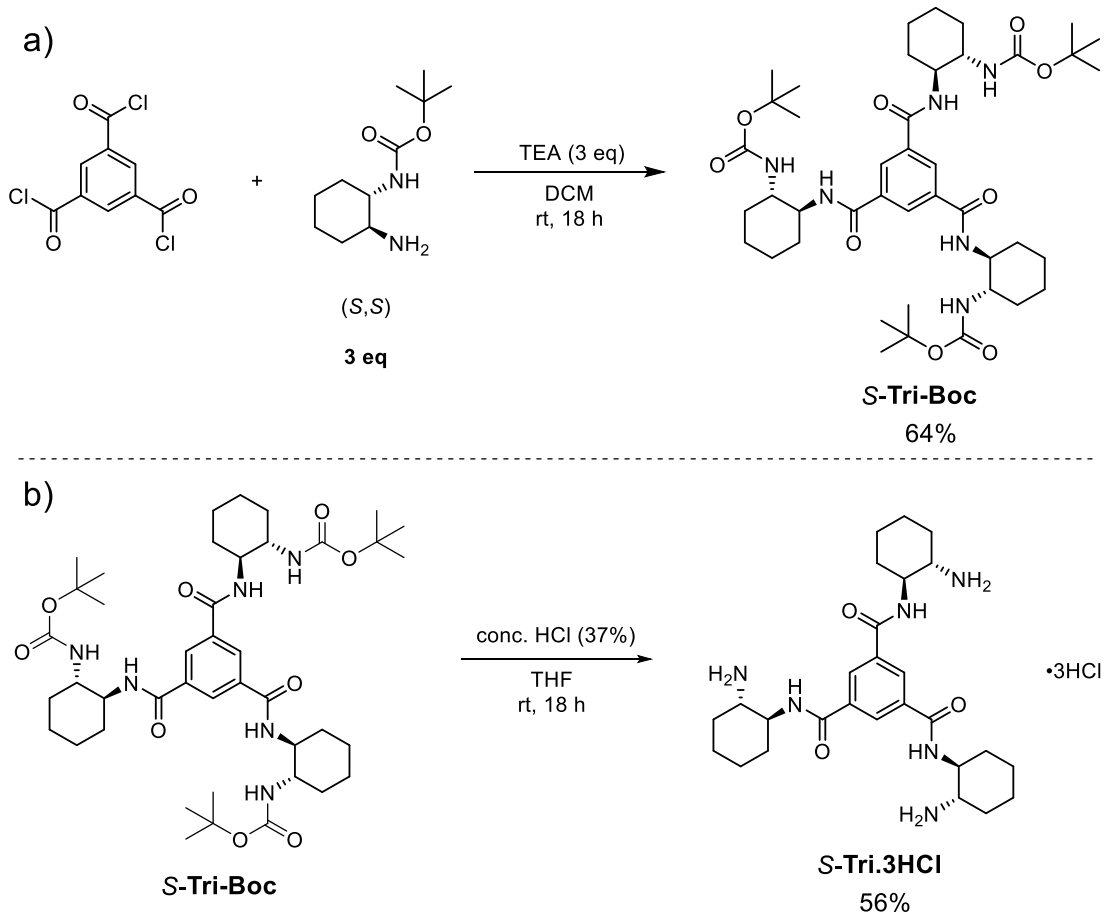

*Figure 4.22 – Synthesis of S-enantiomer functionalised triamine: a) synthesis of S-**Tri-Boc** by the reaction of 1,3,5-benzenetricarbonyl trichloride with mono Boc-protected S,S-CHDA; b) Synthesis of S-**Tri.3HCl** by the treatment of S-**Tri-Boc** with concentrated hydrochloric acid.*

The formation of both *S*-**Tri-Boc** and *S*-**Tri.3HCl** were confirmed initially by ^{1}H NMR spectroscopy, with the spectra for both species in accordance with those recorded previously for the *R*-enantiomers, with mass spectrometry again used for final confirmation. With both amide-derived triamines *R*-**Tri.3HCl** and *S*-**Tri.3HCl** in hand, these were then combined with TFB, and both *R*,*R*- and *S*,*S*-CHDA targeting all four of the desired homochiral and heterochiral part-amide cages (Figure 4.23) (see experimental section page 200). Purification of the reaction was carried out as previously; TEA-HCl salts were first removed, followed by precipitation with an anti-solvent to isolate the four crude cage mixtures.

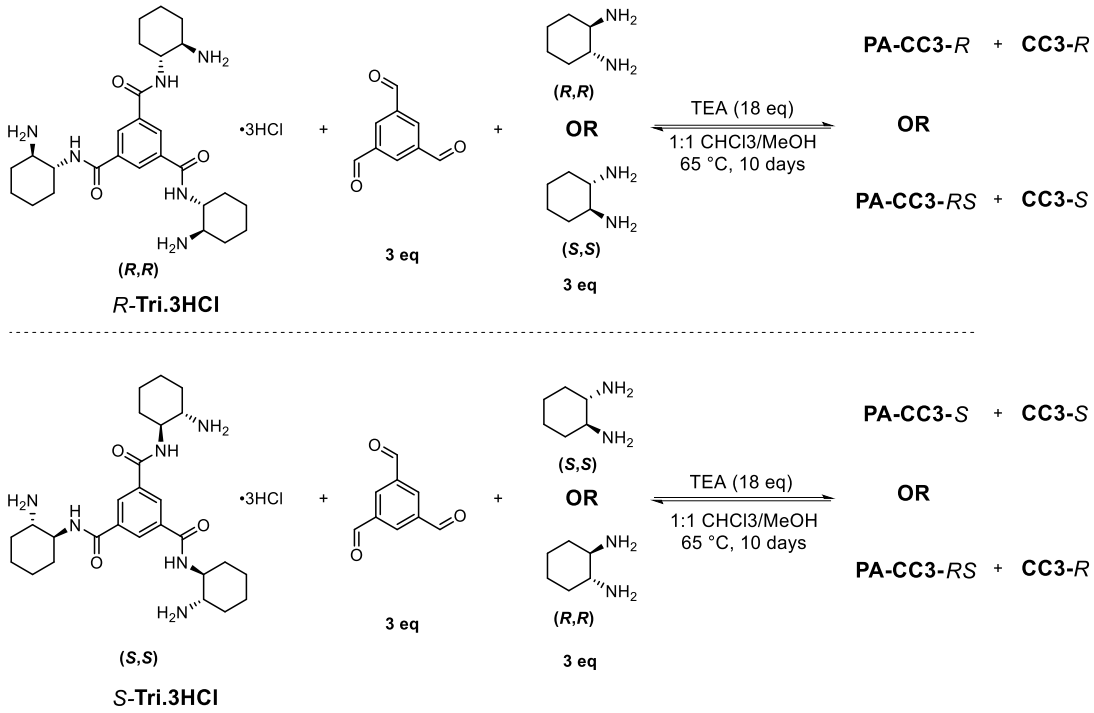

*Figure 4.23 – Overall reaction scheme for the synthesis of a series of part-amide cages based on **CC3**: a) combination of R-**Tri.3HCl** with either enantiomer of CHDA to give **PA-CC3**-R or **PA-CC3**-RS; b) combination of S-**Tri.3HCl** with either enantiomer of CHDA to give **PA-CC3**-S or **PA-CC3**-SR; homochiral cages have like chirality for both triamine and diamine, while heterochiral cages have the opposite chirality.*

Analysis using ^{1}H NMR spectroscopy of the isolated solids for the four attempted cage reactions varied greatly based on the chiralities present (Figure 4.24). Comparison of the crude **PA-CC3**-*R* from this synthesis with the sample from the initial test reaction suggested that the solvent change was beneficial, with a less complex aromatic region for the reaction using 1:1 $CHCl_3$:MeOH. As expected, regions within the spectra still showed complexity; particularly in the upfield regions due to both the broadness of the CHDA signals and the presence of multiple CHDA environments. In addition, there still seemed to be TEA·HCl salts remaining, despite the initial removal by precipitation in THF used during work-up, and based on the aromatic region, it was apparent that the isolated solids contained several products, though there were inherent differences between the four attempted cage syntheses.

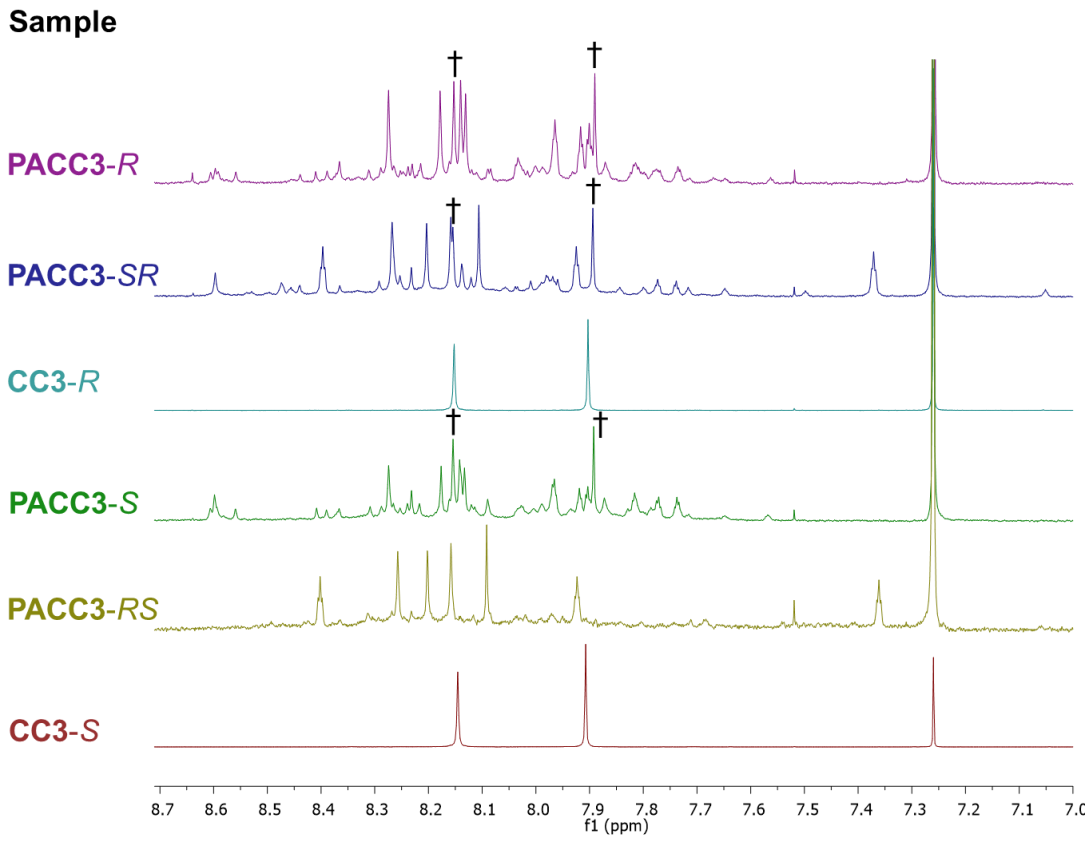

Figure 4.24 - Stacked ^{1}H NMR ($CDCl_3$) spectra of the crude part-amide cages following initial work-up, focused on the aromatic region; ***CC3****-R and* ***CC3****-S parent cages are included for comparison, and the part-amide cages have been grouped in terms of their relative parent cages. Peaks representing* ***CC3*** *present in the PA-CC3 samples are denoted by* †.

The homochiral cages, **PA-CC3**-*R* and **PA-CC3**-*S*, presented similarly to each other with cleaner conversion than the prior test reaction based on their ^{1}H NMR spectra, although the presence of potential oligomeric species was still apparent. Direct comparison to samples of the parent cages **CC3**-*R* and **CC3**-*S*, prepared according to literature methods, enabled partial identification of which signals were related to the part-amide cages. Generally, the ^{1}H NMR spectra for the heterochiral cages appeared cleaner, particularly for **PA-CC3**-*RS* which appeared to contain effectively no **CC3**-*S* or additional oligomeric species. This provided the best spectra of the series and outlined the relevant peaks for **PA-CC3**-*RS*. Additionally, the spectra for these cages matched well with that seen for the isostructural cages reported by Slater *et al*.,[38] though with the presence of additional peaks and some changes in shifts due

to the presence of the amide species and the inherent differences between the cage species.

As all the cages in the series were attempted under identical conditions, it was unclear why **PA-CC3**-*RS* formed much more effectively. As discussed previously, modelling of the cages suggested their formation energies were all very similar, both to each other and the parent **CC3** cages. Therefore, it follows that the ratio of precursors used in the reaction would have an effect on the resulting product distribution, and it is possible that small differences in the amounts of reagent used, *e.g.,* errors when weighing out material, may have directed more towards **PA-CC3**-*RS*.

To aid in the full characterisation and analysis of the part-amide cages, a suitable method for purification was therefore clearly required. The use of preparative-HPLC would be ideal, as with the cage pots and dumbbells reported previously,[16,27] but unfortunately, this method was not available at this stage in the project. In addition, the use of preparative-HPLC is not very scalable when larger amounts of material are required for subsequent analysis of the properties of the part-amide POCs. As such, it was desired to find a straightforward method of purification that could aid in removal of many of the unwanted side-products present in the crude samples, including the parent cage **CC3**. Trituration with THF was therefore first investigated for purification of the part-amide cages, exploiting the relatively poor solubility of **CC3** in THF. Samples of the crude part-amide cages were therefore suspended in small amounts of THF, and the resulting suspension filtered – this was repeated 2-3 times to try and extract as much of the part-amide cage as possible, while leaving **CC3** in the residual solid. This method also had the benefit of helping to remove any remaining TEA·HCl salts, due to it also having poor solubility in THF. The filtrates were subsequently dried under vacuum, and a final precipitation with an anti-solvent was again used to isolate the desired part-amide cages. Unfortunately, the purification was not successful for **PA-CC3**-*R* and **PA-CC3**-*S*, with the former not yielding any material and the latter remaining a complex mixture. The two heterochiral cages **PA-CC3**-*RS* and **PA-CC3**-*SR*, however, both showed an improvement, with a reduction in the impurities apparent, and **PA-CC3**-*SR* also showing a reduction in the quantity of **CC3**-*R* present (Figure 4.25).

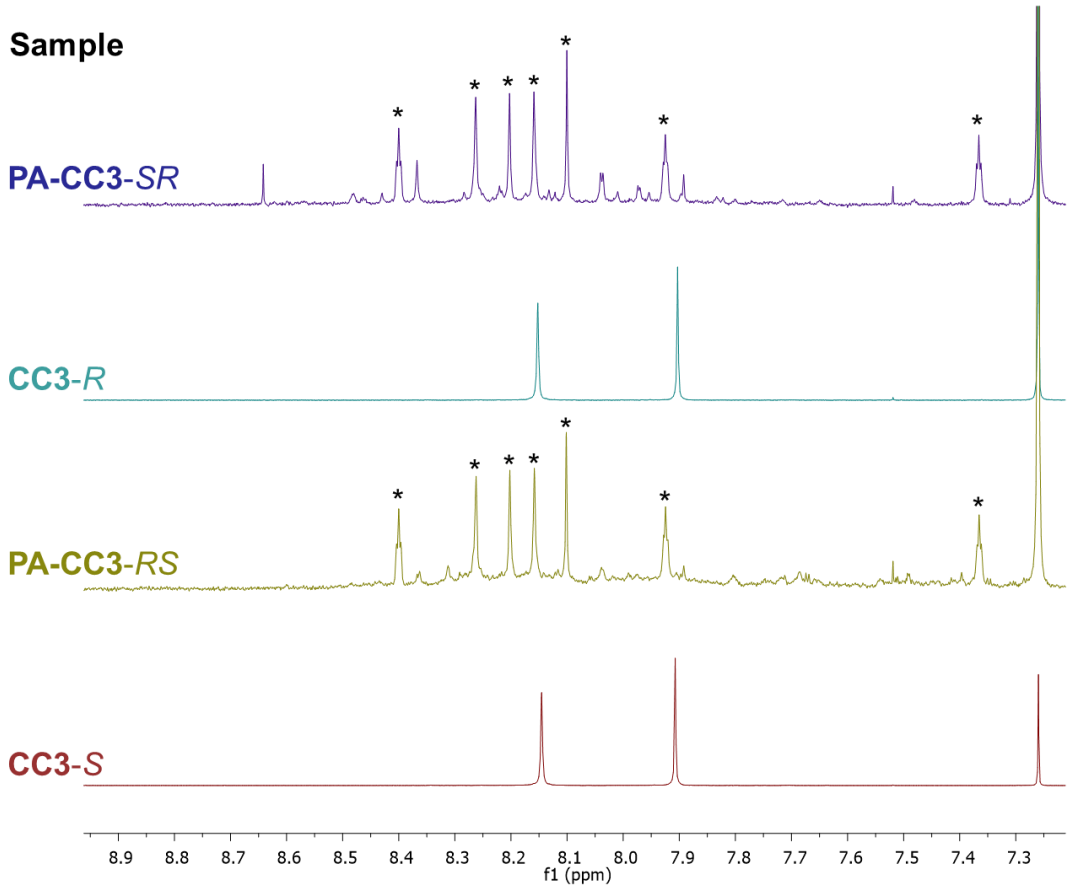

*Figure 4.25 – Stacked ^{1}H NMR ($CDCl_3$) spectra of the heterochiral part-amide cages following trituration with THF, focused on the aromatic region; suspected **PA-CC3** cage peaks are denoted by *.*

In general, while improvements could be seen for the heterochiral part-amide cages, this trituration method did not have the substantive effect it was hoped in terms of purification and elucidation of the spectra for the homochiral cages. However, with a methodology developed for the formation of the target part-amide cages, the reaction process was next investigated as it was still not well understood, for example, how the product distribution was changing over the course of the reaction. Therefore, the synthesis was repeated but focusing on two cages more directly (one homochiral and one heterochiral, **PA-CC3**-*S* and **PA-CC3**-*SR* respectively), with the reaction progress more closely monitored to gain a better understanding into the competitive self-sorting process.

4.4 Further Investigation of PA-CC3-*S* and PA-CC3-*SR*

4.4.1 Monitoring formation of PA-CC3-*S* and PA-CC3-*SR*

The issues with purification outlined previously meant that in-depth study of the cages and their properties was difficult. Of interest was how the product distribution changed over the course of the reaction, *i.e.*, was formation biased towards one cage initially, or more random. To study this further, the process was monitored over the 10-day full reaction period. The syntheses of **PA-CC3**-*S* and **PA-CC3**-*SR* were carried out as per the previous method (Figure 4.23) (see experimental section page 200), and the reactions sampled each day. After the 10-day period, both crude cage products were obtained as off-white solids, with a similar mass recovery (**PA-CC3**-*S*:55%; **PA-CC3**-*SR*:57%).

Considering the difficulties with ^{1}H NMR spectroscopic analysis thus far, HPLC analysis was carried out as an alternative — this gave a much clearer picture of the progress of the reaction (Figure 4.26). Using a reference sample, **CC3** was shown to elute at around 5 minutes under the applied conditions. When determining the possible peak for the part-amide cages, the similarities in structure between **CC3** and the **PA-CC3** cages suggested the part-amide cage may elute similarly to **CC3**, *i.e.*, after initial oligomers and smaller species. As such, the peak at ~3 minutes elution time was deemed to be **PA-CC3**-*S*, and the peak at ~2.7 minutes was assigned as **PA-CC3**-*SR* — this was further confirmed on comparison of the HPLC traces for the isolated **PACC3** solids (Figure 4.26).

During the formation of **PA-CC3**-*S*, both **CC3**-*S* and **PA-CC3**-*S* were present from day one, and comparison of the relative amounts of each cage showed a general trend towards **PA-CC3**-*S* formation (Figure 4.26a). The relative ratio of **PA-CC3**-*S*:**CC3**-*S* increased to 78:22 on isolation of the crude cage mixture. Whilst the relative ratios for the cage species did fluctuate slightly during the full 10 days of reaction, generally the trend suggested that allowing equilibration for the full reaction time was beneficial. It was apparent that the relative ratio of **CC3**-*S* present reduced over time, though it was unclear whether this was because of re-equilibration to the part-amide species. Nevertheless, this gave helpful information on the content of the crude reaction.

The process was also carried out for **PA-CC3**-*SR*, to see if there were any differences in the heterochiral cage synthesis. HPLC analysis for the synthesis of **PA-CC3**-SR suggested a somewhat different process than that seen for **PA-CC3**-*S* —the HPLC

trace for day 1 was very clean, with **PA-CC3**-*SR* observed as the major product in a relative **PA-CC3**-*SR*:**CC3**-*R* ratio of 85:15 (Figure 4.26b). Again, as the reaction time progressed, the relative ratio of the cage species fluctuated slightly, but after 10 days, **PA-CC3**-SR was the favoured species with a final relative ratio of 83:17, and isolation of the crude cage mixture saw a similar ratio of 81:19 (Figure 4.26b).

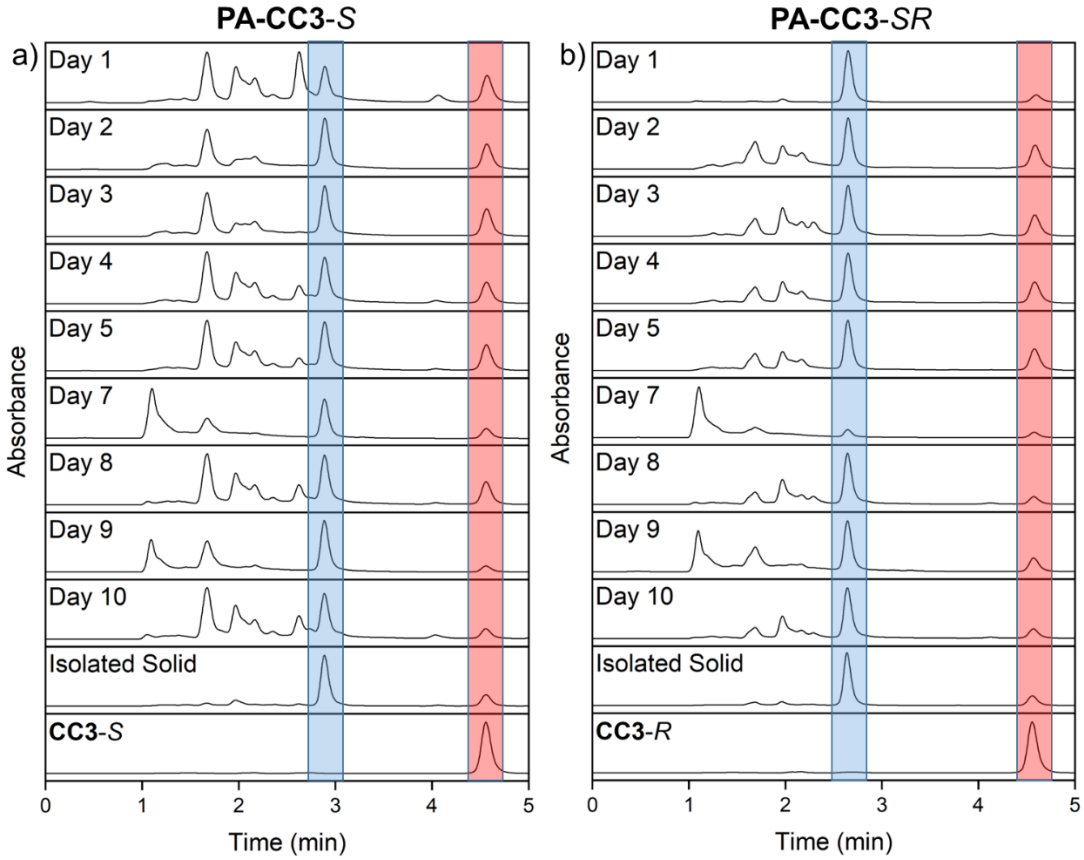

*Figure 4.26 – Stacked HPLC traces for the formation part-amide cages over a 10 day reaction period — pure **CC3** and isolated **PACC3** solids are included for reference; **PACC3** peaks are highlighted by the blue boxes, and **CC3** peaks are highlighted by red boxes: a) synthesis of homochiral **PA-CC3**-S; b) synthesis of heterochiral **PA-CC3**-SR.*

Overall, this suggests that for heterochiral cage formation, extended reaction times may not be required for part-amide cage formation, as after only 1 day of heating, there was clean conversion to a high proportion of the target species. Therefore, it may be beneficial in future studies to halt heterochiral cage synthesis after just a single day to maximise the **PA-CC3**:**CC3** ratio, and potentially aid in purification of the crude product.

4.4.2 Further analysis of crude PA-CC3-*S* and PA-CC3-*SR*

With relatively pure HPLC traces recorded for the isolated crude solids (78:22 **PA-CC3**-*S*:**CC3**-*S*; overall **PA-CC3**-*S* purity 60%; 81:19 **PA-CC3**-*SR*:**CC3**-*R*; overall **PA-CC3**-*RS* purity 69%), ^{1}H NMR spectroscopy was used to assess the crude part-amide cage mixtures further (Figure 4.27). As before, the spectra were compared with the respective **CC3** parent cages. **PA-CC3**-*S* was formed with a higher purity than previously observed, with significantly fewer undesired peaks — as expected, **CC3**-*S* was also present in the sample (77:23 **PA-CC3**-*S*:**CC3**-*S* by ^{1}H NMR; this agrees with the values determined by HPLC). The sample of **PA-CC3**-*SR* also formed with high purity, though with more **CC3**-*R* present than the previously synthesised sample (Figure 4.25). Nevertheless, **PA-CC3**-*SR* was formed as the major species (83:17 **PA-CC3**-*SR*:**CC3**-*R* by ^{1}H NMR; again, this matched well with the values determined by HPLC).

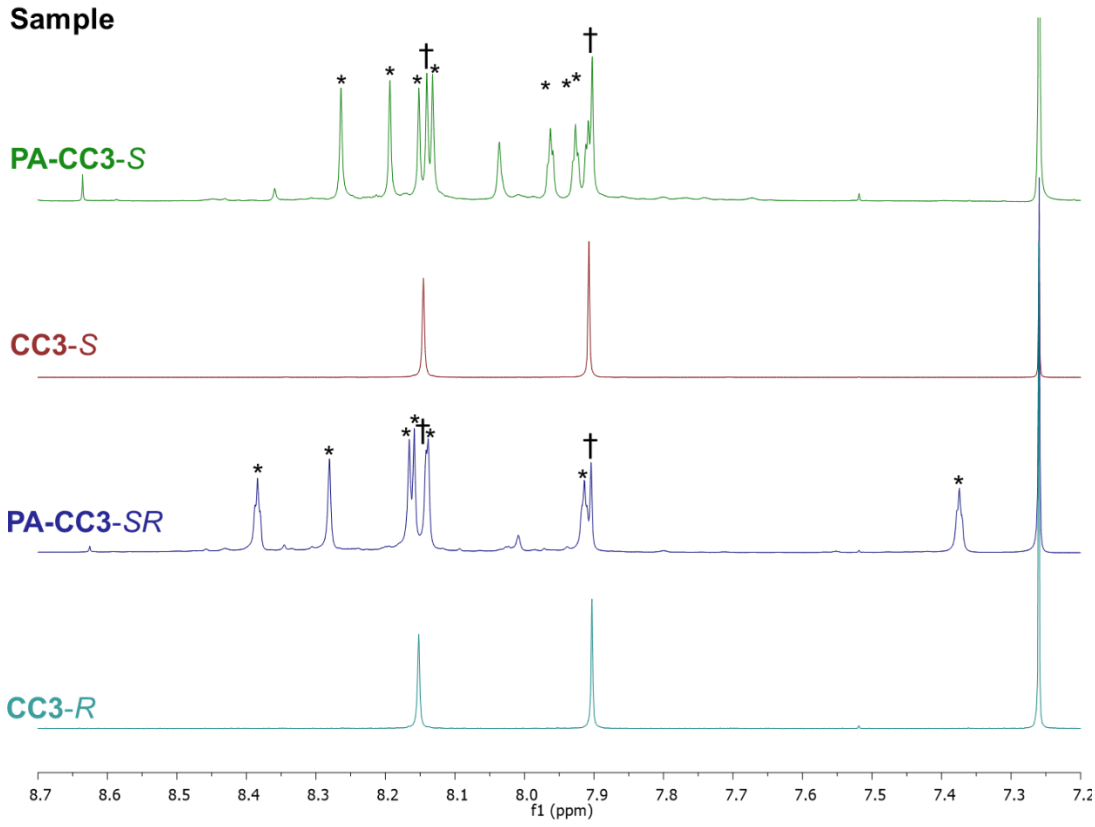

*Figure 4.27 – Stacked ^{1}H NMR ($CDCl_3$) spectra for the isolated samples of **PA-CC3**-S and **PA-CC3**-SR monitored by HPLC and compared to their potential parent **CC3** cages. Potential **PA-CC3** cage peaks denoted cage peaks are denoted by *, **CC3** peaks denoted by †.*

For assignment of the aromatic region of the ^{1}H NMR spectra, the molecular models of **PA-CC3**-*SR* and **PA-CC3**-*SR* were used in conjunction with the spectra to try and gain an insight into the environments present within the two part-amide cages (Figure 4.28). For both cages, the aromatic ring of the amide face presents one proton environment for the aromatic protons of the benzene ring. Assessment of the imine faces suggests three inequivalent imine groups per cage (each representing three protons), due to the imines existing in an up-down arrangement. As such, the three aromatic protons for each face are all inequivalent — this leads to an additional three separate aromatic peaks (each with an expected integration of three) (Figure 4.28). Despite the differences in chirality, the same motifs are seen for both cages — this suggests similar spectra for the two: seven peaks total, with four aromatic peaks (one from amide face, three from the imine face), and three imine peaks, with an expected integration of three for each peak.

Pleasingly, this was reflected in the ^{1}H NMR spectra. Accounting for **CC3**-*S* and an additional contaminant at ~8 ppm, the spectrum for **PA-CC3**-*S* showed 7 peaks in total. The three triplet peaks observed are analogous to what was seen in the ^{1}H NMR spectra observed for the dissymmetric cages reported by Slater *et al.*,[38] and the cage pots reported by Greenaway *et al.*[27] These triplet peaks were found to have *J*-coupling values of 1.4 Hz for each peak. As such, these were assigned as the imine-face aromatic protons. The remaining four singlets were representative of the amide-face aromatic protons, as well as the three imine protons. The singlet at 8.26 ppm was assigned as the amide-face aromatic protons due to its more downfield position, and the chemical equivalency of the protons giving the singlet peak. The remaining singlets were difficult to assign specifically due to their close proximity. All peaks showed the correct integrations, though a slightly higher integration was found where there was overlap with **CC3**-*S* peaks in the spectrum (Figure 4.28b).

For **PA-CC3**-*SR*, the same overall arrangement of peaks was present, with some changes in chemical shift. Three split peaks were again present, with the resolution of peaks sufficient to allow J couplings to be determined for the three peaks. Like the previous study of the homochiral cage, the three triplet peaks were all found to have *J*-coupling values of 1.4 Hz. The remaining singlets were characterised similarly to the homochiral cage, with the most downfield singlet at 8.28 ppm assessed to be the equivalent amide-face aromatic protons. The three imine singlets between 8.2-8.1 ppm were assigned as the imine peaks, with an additional singlet representative of **CC3**-*R*. **CC3**-*R* was assigned as an overlapping peak at 8.14 ppm — comparison of

the integrations of this peak with the known **CC3**-*R* peak at 7.90 ppm showed similar values. Taking this into account leaves the suspected imine peak with an integration matching all other peaks as expected (Figure 4.28c).

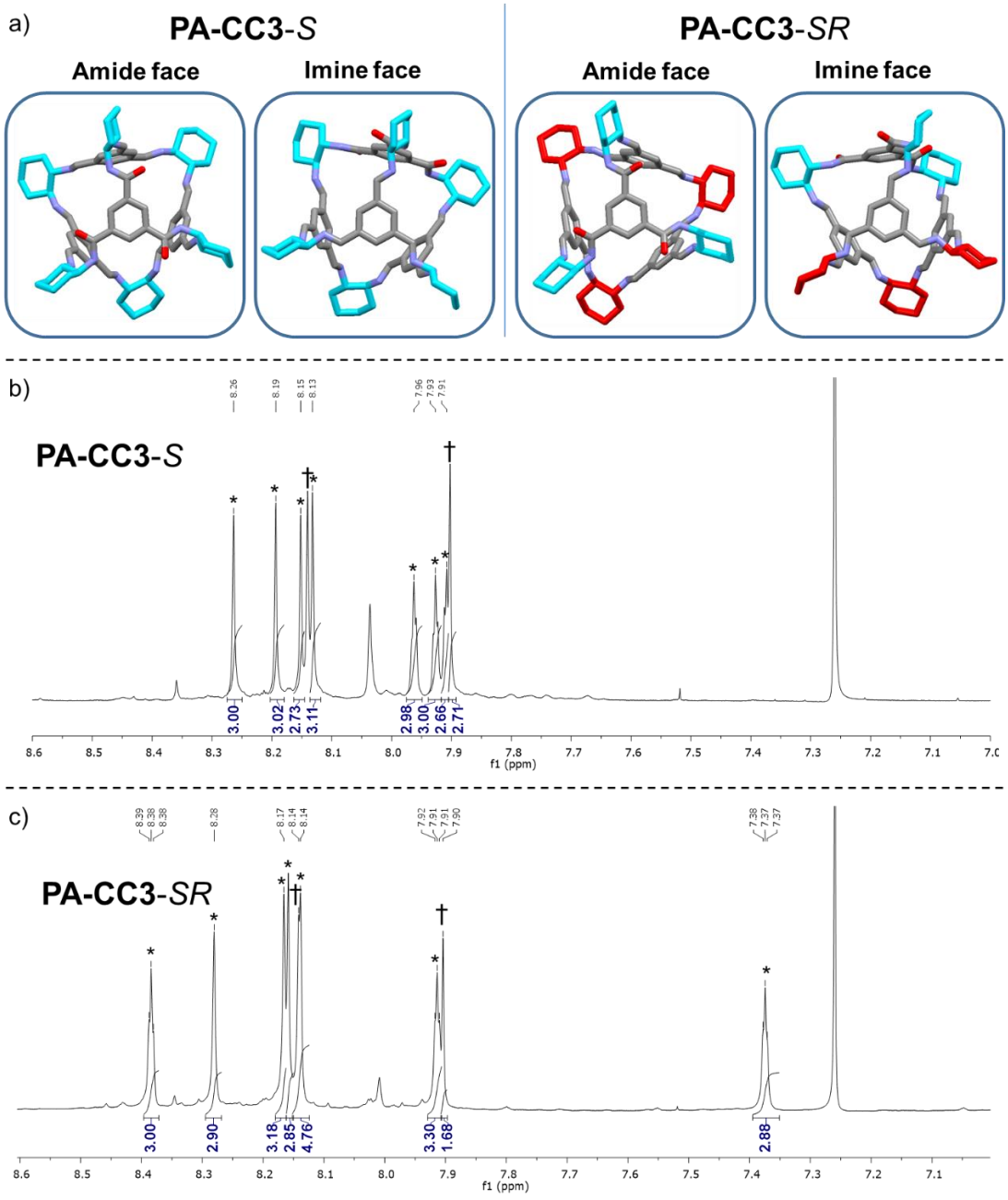

*Figure 4.28 – Further ^{1}H NMR spectroscopy studies for **PA-CC3**-S and **PA-CC3**-SR: a) structural models of the part-amide cages, showing the amide and imine faces — based on these structures it was expected that both cages would display 7 peaks in the aromatic region; b) ^{1}H NMR spectrum of **PA-CC3**-S, focused on the aromatic region; c) ^{1}H NMR spectrum of **PA-CC3**-SR, focused on the aromatic region; **PA-CC3** cage peaks are denoted by *, **CC3** peaks are denoted by †.*

To try and understand these spectra further, correlated spectroscopy (COSY) measurements were also completed for the two part-amide cages. Unfortunately, the COSY spectrum of **PA-CC3**-*S* provided little conclusive data, while analysis of **PA-CC3**-*SR* provided more information. Analysis of the COSY spectrum of **PA-CC3**-*SR* outlined that the three triplet peaks all showed coupling with each other (Figure 4.29a). This in combination with the *J*-coupling values determined previously confirmed assignment of these peaks as the three inequivalent aromatic peaks of the imine face. The COSY spectrum also showed the singlet at 8.28 ppm was isolated, showing no coupling with any other non-equivalent protons (Figure 4.29a) — in combination with the downfield nature of the peak compared to the other singlets present, this confirmed the peak assignment as the amide-face aromatic protons. The remaining three singlets were therefore assigned as the three imine peaks.

Overall, these NMR spectroscopy studies showed the spectra for the homochiral and heterochiral cages were very similar, with the major difference only in the chemical shifts of the imine-face aromatic protons. Whilst more information was obtained about the aromatic region of the spectra, the upfield region would be more difficult due to the difficulty with overlapping **CC3** CHDA peaks with varying chemical shift. In future work, full assignment in the upfield region will be more successful on pure isolated sample of part-amide cages

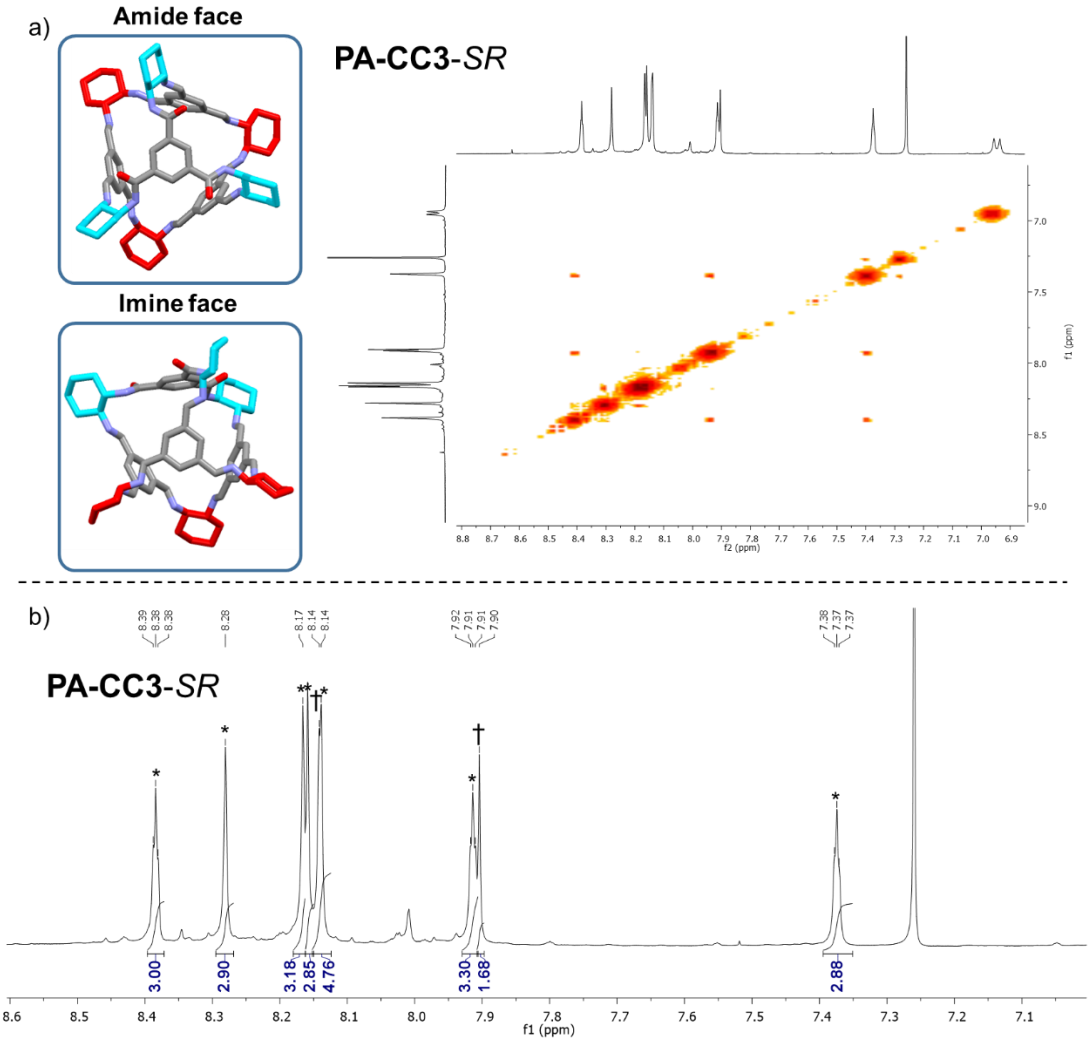

*Figure 4.29 - Further [1]H NMR spectroscopy studies for **PA-CC3**-SR: a) structural models of the part-amide cages, showing the amide and imine faces, with the recorded COSY spectrum; b) [1]H NMR spectrum of **PA-CC3**-SR, focused on the aromatic region; **PA-CC3** cage peaks denoted cage peaks are denoted by *, **CC3** peaks denoted by †.*

The presence of the **PA-CC3** cages was also confirmed by mass spectrometry, with the expected peaks present for both crude cage mixtures (Figure 4.30) — **PA-CC3**: calculated for $C_{72}H_{84}N_{12}O_3$ 1164.6789, **PA-CC3**-S found $[M+H]^+$ 1165.6929; **PA-CC3**-SR found $[M+H]^+$ 1165.6929. As expected, parent cage **CC3** was also present in both samples — **CC3** calculated for $C_{72}H_{84}N_{12}$ 1116.6942, **CC3**-*S* found $[M+H]^+$ 1117.7079; **CC3**-*R* found $[M+H]^+$ 1117.7078.

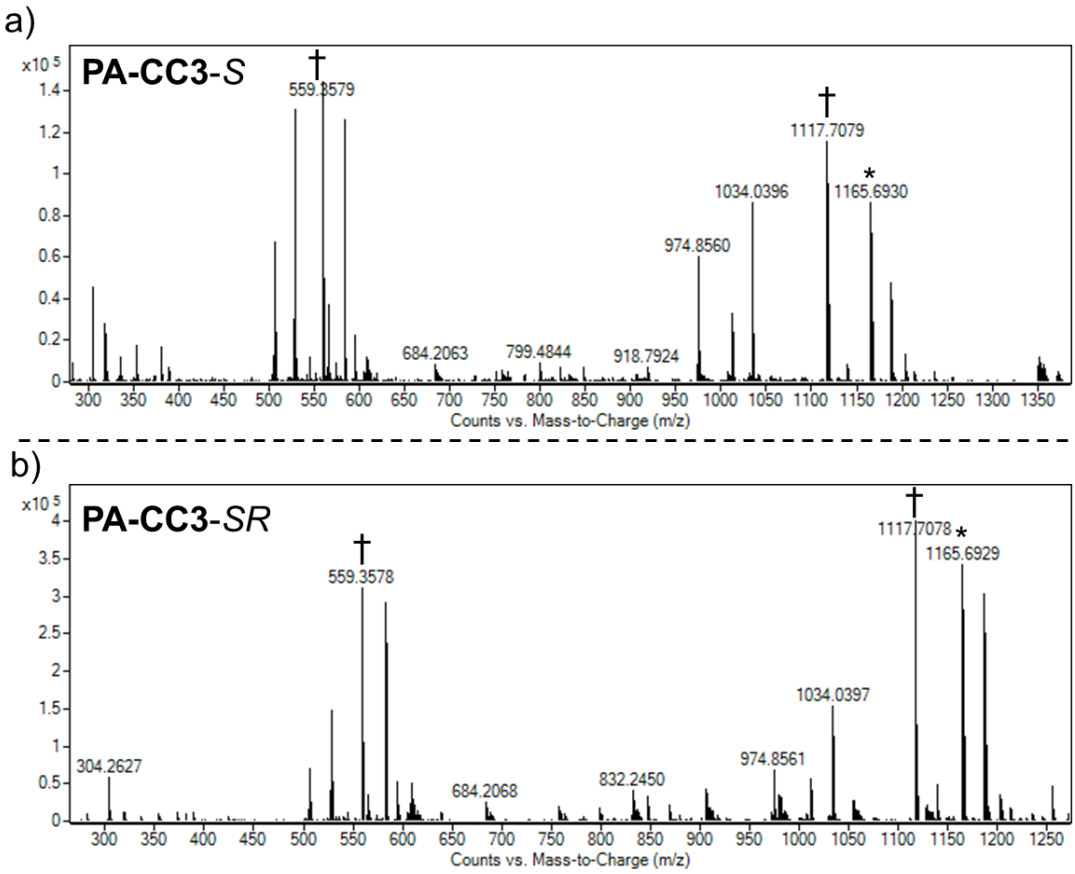

*Figure 4.30 – Mass spectra for the crude samples of **PA-CC3**; a) mass spectrum of crude **PA-CC3**-S calculated for $C_{72}H_{84}N_{12}O_3$ 1164.6789, **PA-CC3**-S found $[M+H]^+$ 1165.6929, **CC3**-S parent cage is also present calculated for $C_{72}H_{84}N_{12}$ 1116.6942, **CC3**-S found $[M+H]^+$ 1117.7079; b) mass spectrum of crude **PA-CC3**-SR calculated for $C_{72}H_{84}N_{12}O_3$ 1164.6789, found $[M+H]^+$ 1165.6929, **CC3**-R parent cage is also present calculated for $C_{72}H_{84}N_{12}$ 1116.6942, found [M+H]+ 1117.7078. PA-CC3 peaks denoted by *, CC3 peaks denoted by †.*

The crude **PA-CC3** cage samples were also studied in the solid-state, first utilising IR spectroscopy. Comparison of the IR spectra showed that the **PA-CC3** cages presented as very similar to the **CC3** parent cages (Figure 4.31). Both **PA-CC3**-*S* and **PA-CC3-***SR* exhibit broadening of a sharp peak at ~1600 cm^{-1} compared to the parent **CC3-***S* and **CC3**-*R* — this could be due to the emergence of a strong C=O amide peak, showing overlap with the existing imine peak. Additionally, both part-amide cages show the emergence of a new peak at ~1500 cm^{-1} — this is representative of the C-N bond present in the part-amide structure, as seen in examples of amide polymers.[49,50]

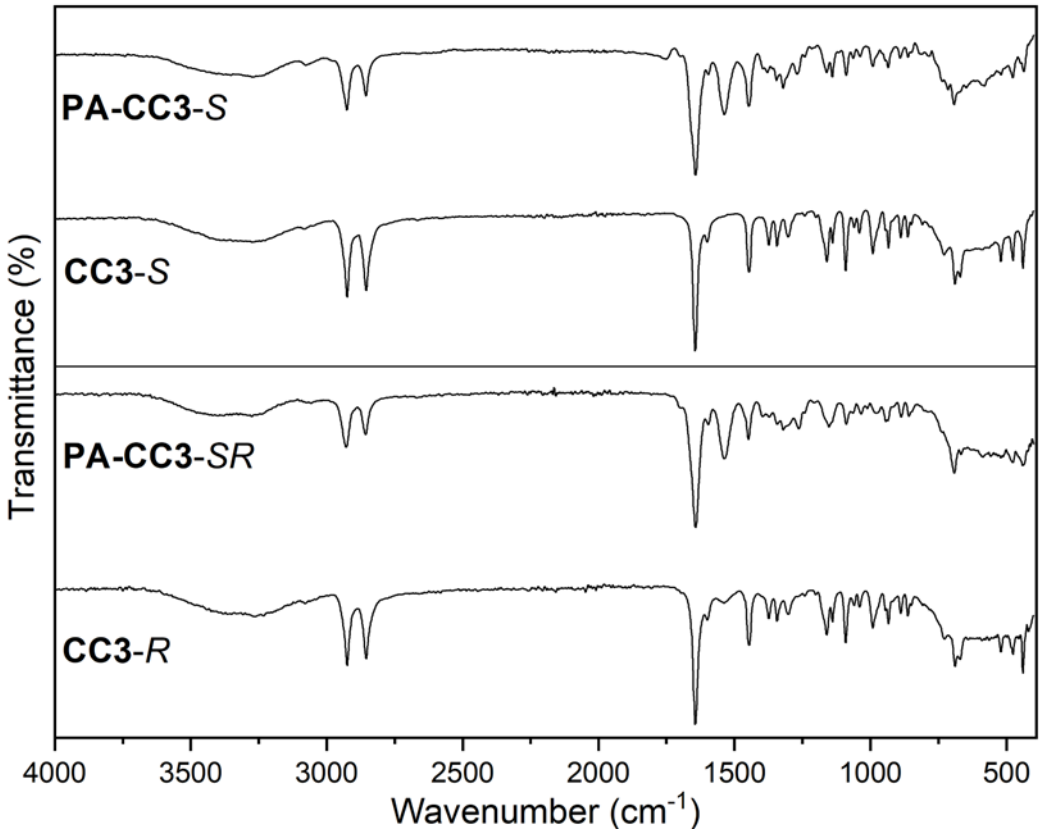

*Figure 4.31 – Stacked IR spectra for the crudes part-amide cage **PA-CC3**-S and **PA-CC3**-R, along with their respective parent cages **CC3**-S and **CC3**-R.*

The part-amide samples were also examined by powder X-ray diffraction (PXRD), again using the parent imine cages for comparison (Figure 4.32). Both part-amide cages presented as less crystalline than the **CC3** parent cages: this is likely in part due to the preparation of the crude cage samples, formed by addition of *n*-hexane to solutions of the crude cages in DCM — this afforded rapid precipitation of the solids. This methodology accounts for the less crystalline PXRD patterns, and the broadening of peaks for **PA-CC3**-*S*; particularly when compared to the method for obtaining the **CC3** samples, which slowly precipitated directly from their respective reaction mixtures over the course of 5 days. The part-amide cage samples still show a small amount of crystalline character, though this was more pronounced for **PA-CC3**-*S* — however, it is unclear whether these small Bragg peaks are due to the part-amide cages themselves, or the presence of the parent cages **CC3**-*S* and **CC3**-*R*.

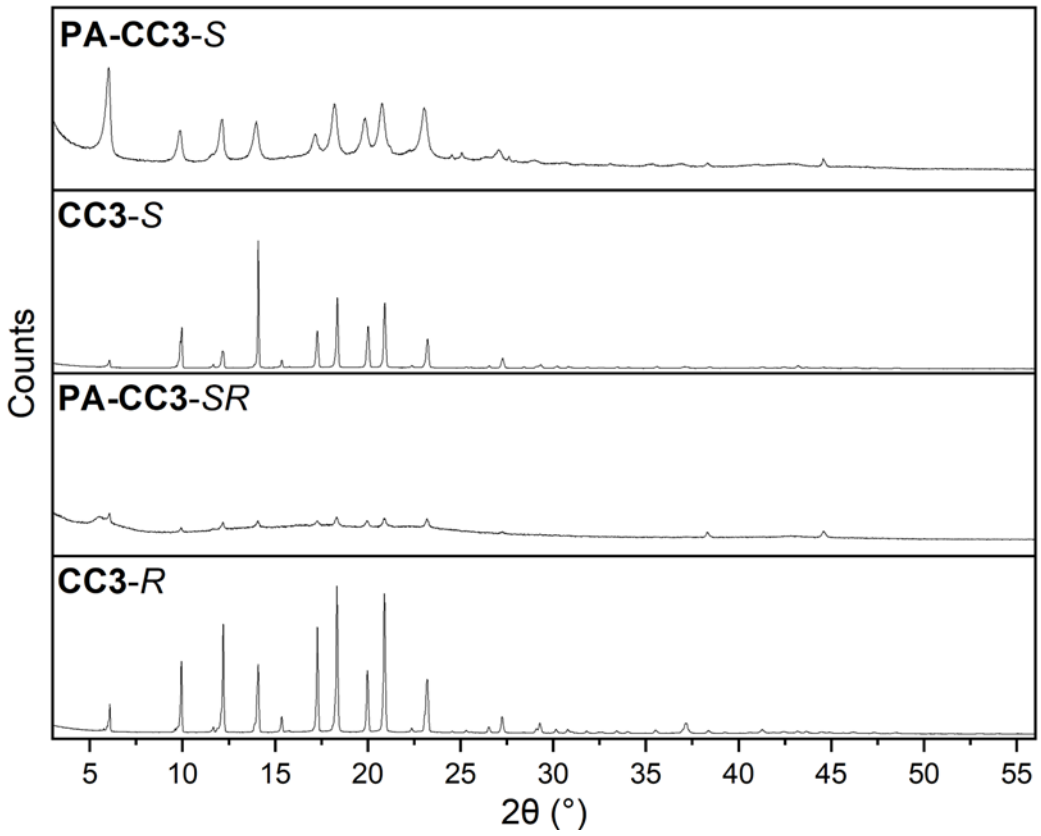

*Figure 4.32 – Stacked PXRD patterns for **PA-CC3**-S and its parent cage **CC3**-S; and **PA-CC3**-SR and its parent cage **CC3**-R.*

In summary, a series of part-amide cages were conceptualised based on the prototypical imine cage **CC3**. These cages were designed to be formed using an amide-functionalised triamine precursor in a social-self sorting reaction with TFB and CHDA — use of alternative chiral forms of CHDA gave four cages: **PA-CC3**-*R,* **PA-CC3**-*RS,* **PA-CC3**-*S,* and **PA-CC3**-*SR*. The use of TFB and CHDA also allowed for formation of parent cage **CC3**. The cages were modelled *in silico* to assess the likelihood of their formation and were calculated to be shape persistent. After optimisation of a synthetic method based on a literature report,[27] the synthesis of the part-amide cages was attempted, and the products were isolated as crude mixtures than contained both the part-amide cages and parent cage **CC3**. Attempts to purify the cages with trituration in THF showed promise, but it was not possible to obtain pure part-amide cage. Fresh samples of **PA-CC3**-*S* and **PA-CC3**-*SR* were formed, monitoring the syntheses by HPLC. The crude mixtures were characterised with HPLC and ^{1}H NMR spectroscopy, finding that the part-amide cages were the major species. Attempts were then made to further analyse the bulk solid, showing a

generally amorphous nature by PXRD (particularly compared to parent cage **CC3**), and similar IR spectra between the target cages and parent cages.

4.5 Conclusions and future work

This chapter has outlined the design and synthesis of a range of part-amide Janus-type porous organic cages based on the prototypical imine cage **CC3**. By controlling the chirality of the amide-derived triamine and diamine precursors used, both homochiral and heterochiral variants of the part-amide cages were initially modelled *in silico* by collaborators to ensure they were synthetically viable and shape-persistent. Following initial optimisation of the reaction conditions, the four cages were targeted using self-sorting reactions. Initial analysis of the crude reaction mixtures was difficult, due to complex ^{1}H NMR spectra, though the presence of the desired cages was confirmed using high resolution mass spectrometry. Ultimately, the biggest issue faced during the study of these cages was one of purification. Literature reports for self-sorting cage reactions typically employ preparative-HPLC for isolation of the desired species — this would've been the ideal method for purification but was not available during the earlier stages of this study.[27] Trituration was instead investigated as a method for removal of the parent cage **CC3** and other contaminants – while this was partially effective, particularly for the heterochiral part-amide cages, pure samples for in-depth study of their properties were not obtained. Clearly a major target moving forward would be the purification and complete study of all cages within the series, with a focus on the effects of the contained amide groups on the properties of the individual cage species and the bulk material properties.

The initial aim of forming part-amide cages was to attempt to impart the positive characteristics of the amide group into cage structures. Chapters 2 and 3 outlined the difficulties of the synthesis of amide cages – here, it was hoped the use of self-sorting reactions would aid in cage synthesis. However, other difficulties in cage formation have also been addressed. As stated previously, control over precursor placement is a key challenge in cage synthesis. The use of functionalised precursors in combination with self-sorting reactions allows for direct control of diamine placement within the **CC**-series of cages, allowing for fine-tuning of cage structures to potentially target specific applications. The functionalised precursors could also be adapted to use amine groups, as seen in literature reports, imparting similar stability as with amides. This also allows for the possibility of fully reduced-and-tied Janus cages, by

using methods seen previously for reduced cages.[51] The part-amide cages discussed here could also be post-synthetically modified to reduce any imine groups to amines. Additionally, the functionalised precursors could be employed in high-throughput studies as a novel tritopic amine, targeting novel cage structures rather than the specific **CC3**-based structures seen in this report.

Whilst this study has focused on **CC3**-type cages, *i.e.*, using CHDA functionalities, the method could also be adapted to use any vicinal diamine, allowing for diversification into large families of cages. For Janus structures, it may be beneficial to target cages with more diverse functionalities around the cage hemispheres, to target greater effects on the properties of the cage, *e.g.*, the use of crown ether-based diamines. The resultant Janus structure would subsequently have larger differences between the cage hemispheres, potentially leading to marked effects on the cage properties as well as avoiding cavity interpenetration, which may occur if using diamines with pendant group functionalities.

To conclude, whilst the specific part-amide targets from this study could not be isolated pure and in bulk, as desired, the methodology used has much wider implications for cage synthesis, allowing for specific targeting of complex, multi-functionality Janus structures. This could allow for the synthesis of more diverse cages, or the tuning of cage properties by carefully controlling the type and placement of the precursors used.

4.6 Experimental

4.6.1 General synthetic methods

Materials: 1,3,5-Triformylbenzene was purchased from Manchester Organics (UK). Other chemicals were purchased from Fluorochem UK, TCI UK or Sigma-Aldrich. Solvents were reagent grade purchased from Fischer Scientific, Sigma-Aldrich or Fluorochem. All materials were used as received unless stated otherwise.

Synthesis: All reactions were stirred magnetically using Teflon-coated stirrer bars. Where heating was required, the reactions were warmed using a stirrer hotplate with heating blocks, with the stated temperature being measured externally to the reaction flask with an attached probe. Removal of solvents was done using a rotary evaporator.

IR Spectra: Infra-red (IR) spectra were recorded on a Bruker Tensor 27 FT-IR using ATR measurements for solids as neat samples.

NMR Spectra: ^{1}H Nuclear magnetic resonance (NMR) were recorded using an internal deuterium lock for the residual protons in $CDCl_3$ (δ = 7.26 ppm), or D_2O (δ = 4.79 ppm) at ambient probe temperature on a Bruker Avance 400 (400MHz).

Data are presented as follows: chemical shift, peak multiplicity (s = singlet, d =doublet, t = triplet, q = quartet, quint = quintet, m = multiplet, br = broad), coupling constants (J / Hz), and integration. Chemical shifts are expressed in ppm on a δ scale relative to δ_{TMS} (0ppm), δ_{CDCl3} (7.26 ppm) or δ_{D2O} (4.89 ppm).

^{13}C NMR Spectra were recorded using an internal deuterium lock using $CDCl_3$ (δ = 77.16 ppm) at ambient probe temperatures on the following instrument: Bruker Avance 400 (101MHz).

HPLC Spectra: HPLC analysis was carried out using an Agilent 1260 LC system with a diode array UV detector using a Syncronis C8 column, 100 x 3 mm, particle size 1.7 µm (part no. 97202-103030, LOT 11232). The mobile phase was isocratic MeOH at a flow rate of 0.5 mL/min for a 5-minute run time, and the column temperature was set to 30 °C, pressure ~275-280 bar. The injection volume was 10 µL and the sample concentration was approximately 1 mg/mL. Detection for UV analysis was conducted at 254 nm.

HRMS spectra: High resolution mass spectrometry (HRMS) was carried out using a 6200 series TOF/6500 series Q-TOF B.09.00 mass spectrometer (fragmentor 120 V) in positive-ion detection mode. The mobile phase was MeOH.

PXRD: Laboratory powder X-ray diffraction (PXRD) data were collected in transmission mode on samples held on a held on thin Mylar film in aluminium well plates on a Panalytical X'Pert PRO MPD equipped with a high-throughput screening (HTS) XYZ stage, X-ray focusing mirror and PIXcel detector, using Ni-filtered Cu Kα radiation. Data were measured over the range 0–56° in ~0.013° steps over 30 minutes.

Molecular modelling: Initial structures were drawn manually in Maestro and high-temperature Molecular Dynamics (MD) simulations were run as an effective way to identify the lowest-energy conformations of the molecules.[44] The simulations were run with the MacroModel package, as part of the Schrödinger Suite (Schrödinger, LLC, New York, NY, 2018-4 release), in the NVE ensemble, with a time step of 1 fs and a total duration of 100 ns with the OPLS3e force field.[52] Structures were sampled every 10 ps and their geometry was optimised following the Polak–Ribière Conjugate Gradient algorithm with a derivative convergence criterion of 0.05 kJ mol−1 Å−1 . This procedure was carried out at both 500 and 1000 K to ensure sampling of the potential energy surface. When the simulations reached convergence, a set of conformers that lay within an energy window of 15 kJ mol−1 was analysed. Redundant conformers were removed with a maximum heavy atom deviation criterion of 0.5 Å and the resulting structures were optimised at the DFT level of theory.

To get a more accurate energetic ranking of the conformations, the structures were optimised with the PBE functionalern with Grimme D3(BJ) dispersion correction.[53] To ensure that true minima were found, frequency calculations were performed and no negative frequencies were found. Next, we performed single point calculations on the PBE-optimised structures using the M06-2X functional.[54] All calculations were performed using the def2-TZVP basis set[55] in Gaussian16.[56] The M06-2X functional was successfully used for formation energy calculations of porous organic cages in the past and does not require additional dispersion corrections, as these are already embedded in the functional.

4.6.2 Synthesis of cage precursors

Tri-*tert*-butyl((1*R*,1'*R*,1''*R*,2*R*,2'*R*,2''*R*)-((benzene-1,3,5 tricarbonyl)tris(azanediyl))tris(cyclohexane-2,1-diyl))tricarbamate (*R*-Tri-Boc)

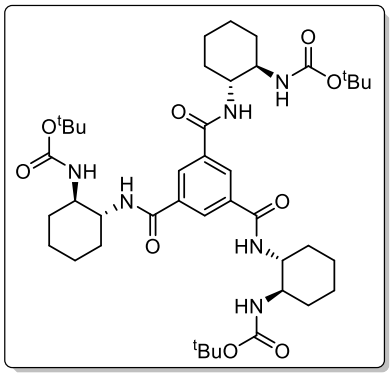

To a solution of (1*R*,2*R*)-*N*-(*tert*-butoxycarbonyl)-1,2-cyclohexanediamine (1.00 g, 4.7 mmol, 3.0 eq.) in DCM (10 mL) was added a stirrer bar and triethylamine (0.65 mL, 4.7 mmol, 3.0 eq.), and the mixture was left to stir for 5 minutes. 1,3,5-Benzenetricarbonyl trichloride (413 mg, 1.6 mmol, 1.0 eq.) was then added portionwise over 1 minute, and the mixture left to stir overnight at ambient temperature. The solvent was removed *in vacuo*, and the residue suspended in THF. The precipitated TEA·HCl salts were removed by filtration, and the resultant filtrate dried *in vacuo*. The residue was re-dissolved in DCM (10 mL), and *n*-hexane (50 mL) was added, affording precipitation of a solid. The volume was reduced *in vacuo*, and the solid formed was collected by vacuum filtration. The crude solid was purified using flash column chromatography (95:5 DCM:MeOH) to give the protected triamine *R*-**Tri-Boc** as a colourless solid (550 mg, 0.69 mmol 43%).

IR (ν_{max}/cm^{-1}): 3308, 2931, 2858, 1652, 1525, 1451, 1451, 1390; **^{1}H NMR** (400 MHz, $CDCl_3$) δ_H 8.44 (s, 3H), 3.89 – 3.76 (m, 3H), 3.60 – 3.46 (m, 3H), 2.23 – 1.97 (m, 6H), 1.84 – 1.72 (m, 6H), 1.32 (m, 12H), 1.25 (s, 27H); **^{13}C NMR**: (101 MHz, $CDCl_3$) δ_C 165.67, 157.05, 134.97, 128.66, 79.84, 55.89, 54.00, 32.77, 32.65, 28.39, 25.19, 24.74.; **HRMS** (ES+) calculated for $C_{42}H_{66}N_6O_9$ 798.4891, found $[M+H]^+$ 799.4963; **Elemental analysis** calculated for $C_{42}H_{66}N_6O_9$ C 63.13, H 8.33, N 10.52, found C 60.39, H 8.26, O 10.36).

N^1,N^3,N^5-tris((1*R*,2*R*)-2-Aminocyclohexyl)benzene-1,3,5-tricarboxamide trihydrochloride (*R*-Tri.3HCl)

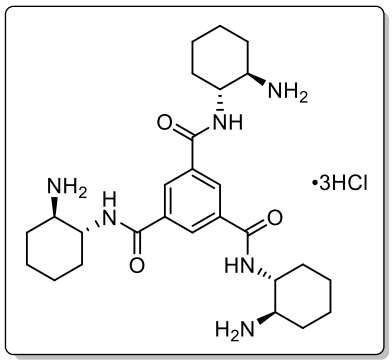

To a solution of *R*-**Tri-Boc** (1.00 g, 1.25 mmol, 1.0 eq) in THF (10 mL) was added a stirrer bar and concentrated hydrochloric acid (37%, 5 mL, excess). The solution was left to stir at ambient temperature overnight, during which time a white precipitate formed. This precipitate was isolated by vacuum filtration, washed with THF, and dried under vacuum to give the desired triamine salt *R*-**Tri.3HCl** as a colourless solid (630 mg, 1.0 mmol, 83%).

IR (ν_{max}/cm^{-1}): 3206, 3040, 2932, 2858, 1666, 1646, 1589, 1448; **^{1}H NMR** (400 MHz, D_2O) δ_H 8.44 (s, 3H), 4.11 (td, *J* = 11.3, 4.3 Hz, 3H), 3.29 (td, *J* = 11.6, 4.2 Hz, 3H), 2.24 – 2.14 (m, *J* = 8.9, 4.1 Hz, 3H), 2.13 – 2.05 (m, 3H), 1.89 – 1.82 (m, *J* = 9.1, 4.0 Hz, 6H), 1.66 – 1.50 (m, 6H), 1.50 – 1.32 (m, 6H); **^{13}C NMR** (101 MHz, D_2O) δ_C 169.03, 134.41, 129.68, 54.56, 51.87, 30.94, 29.57, 23.86, 23.32; **HRMS** (ES+) calculated for $C_{27}H_{42}N_6O_3$ 498.3318, found $[M+H]^+$ 499.3386; **Elemental analysis** calculated for $C_{27}H_{45}Cl_3N_6O_3$ C 53.33, H 7.46, N 13.82; found C 53.21, H 7.70, O 12.50

Tri-*tert*-butyl ((1*S*,1'*S*,1''*S*,2*S*,2'*S*,2''*S*)-((benzene-1,3,5-tricarbonyl)tris(azanediyl))tris(cyclohexane-2,1-diyl))tricarbamate (*S*-Tri-Boc)

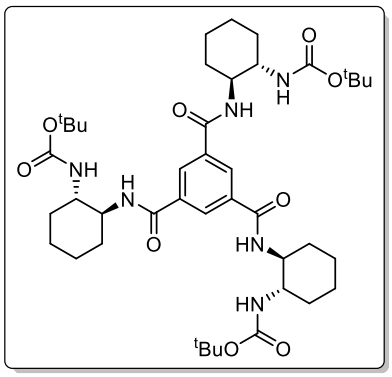

To a solution of (1*S*,2*S*)-*N*-(*tert*-butoxycarbonyl)-1,2-cyclohexanediamine (1.00 g, 4.7 mmol, 3.0 eq.) in DCM (10 mL) was added a stirrer bar and triethylamine (0.65 mL, 4.7 mmol, 3.0 eq.), and the mixture was left to stir for 5 minutes. 1,3,5-Benzenetricarbonyl trichloride (413 mg, 1.6 mmol, 1.0 eq) was then added portionwise over 1 minute, and the mixture left to stir overnight at ambient temperature. The solvent was removed *in vacuo*, and the residue suspended in THF. The precipitated TEA·HCl salts were removed by filtration, and the resultant filtrate dried *in vacuo*. The residue was re-dissolved in DCM (10 mL), and *n*-hexane (50 mL) was added, affording precipitation of solid. The volume was reduced *in vacuo*, and the solid formed was collected by vacuum filtration. The crude solid was purified using

flash column chromatography (95:5 DCM:MeOH)to give the protected triamine *S*-**Tri-Boc** as a colourles solid (820 mg, 1.0 mmol, 64%).

IR (ν_{max}/cm^{-1}): 3317, 2932, 2859, 1653, 1520, 1451, 1391,1366; **^{1}H NMR** (400 MHz, $CDCl_3$) δ_H 8.45 (s, 3H), 3.91 – 3.79 (m, 3H), 3.62 – 3.50 (m, 3H), 2.26 – 2.18 (m, 3H), 2.10 – 2.02 (m, 3H), 1.89 – 1.72 (m, 6H), 1.35 (m, 12H), 1.28 (s, 27H). **^{13}C NMR** (101 MHz, $CDCl_3$) δ_C 165.66, 157.05, 134.97, 128.65, 79.83, 55.91, 54.00, 32.77, 32.65, 28.39, 25.19, 24.74.; **HRMS** (ES+) calculated for $C_{42}H_{66}N_6O_9$ 798.4891, found $[M+H]^+$ 799.4963; **Elemental analysis** calculated for $C_{42}H_{66}N_6O_9$ C 63.13, H 8.33, N 10.52, found C 61.58, H 8.25, N 10.28 .

***N*^{1},*N*^{3},*N*^{5}-tris((1S,2S)-2-Aminocyclohexyl)benzene-1,3,5-tricarboxamide trihydrochloride (*S*-Tri.3HCl)**

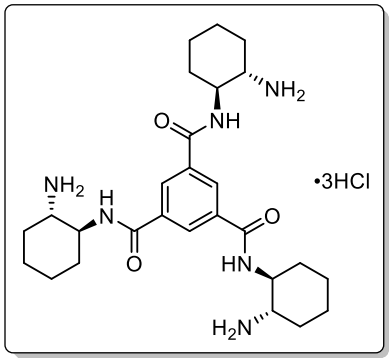

To a solution of *S*-**Tri-Boc** (1.00 g, 1.25 mmol, 1.0 eq.) in THF (10 mL) was added a stirrer bar and concentrated hydrochloric acid (37%, 5 mL, excess). The solution was left to stir at ambient temperature overnight, during which time a white precipitate formed. This precipitate was isolated by vacuum filtration, washed with THF, and dried under vacuum to give the desired triamine salt *S*-**Tri.3HCl** as a colourless solid (430 mg, 0.71 mmol, 56%).

IR (ν_{max}/cm^{-1}): 3206, 3042, 2932, 2859, 1666, 1646, 1589, 1529, 1448; **^{1}H NMR** (400 MHz, D_2O) δ_H 8.44 (s, 1H), 4.11 (td, *J* = 11.3, 4.3 Hz, 3H), 3.30 (td, *J* = 11.5, 4.2 Hz, 3H), 2.25 – 2.14 (m, 3H), 2.14 – 2.04 (m, 6H), 1.89 – 1.79 (m, 6H), 1.67 – 1.51 (m, 6H), 1.51 – 1.32 (m, 6H); **^{13}C NMR** (101 MHz, D_2O) δ_C 169.05, 134.43, 129.64, 54.57, 51.86, 30.92, 29.57, 23.85, 23.32; **HRMS** (ES+) calculated for $C_{27}H_{48}N_6O_3$ 498.3318, found $[M+H]^+$ 499.3394; **Elemental analysis** calculated for $C_{27}H_{45}Cl_3N_6O_3$ C 53.33, H 7.46, N 13.82, found C 53.30, H 7.69, N 12.67.

4.6.3 Synthesis of CC3 reference cages

CC3-*R*

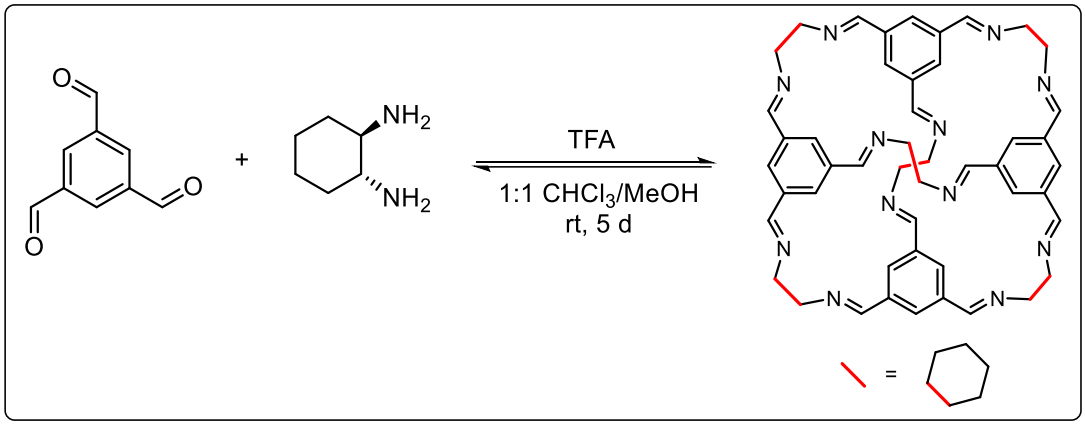

DCM (20 mL) was added slowly onto solid 1,3,5-triformylbenzene (1.0 g, 6.2 mmol, 1 eq.) without stirring at room temperature. Trifluoroacetic acid (100 µL) was added directly to this solution as a catalyst for imine bond formation. Finally, a solution of (*R*,*R*)-1,2-cyclohexyldiamine (1.0 g, 8.7 mmol, 1.4 eq.) in DCM (20 mL) was added. The unmixed reaction was covered and left to stand. Over 5 days, the solid 1,3,5-triformylbenzene was consumed, and **CC3**-*R* precipitated out of the reaction solution. The solid product was removed by filtration and washed with a mixture of 95% ethanol/5% DCM, before being dried under vacuum to give **CC3**-*R* as an off-white solid (750 mg, 0.67 mmol, 44%).

^{1}H NMR (400 MHz, $CDCl_3$) δ_H 8.15 (s, 12H), 7.90 (s, 12H), 3.39 – 3.29 (m, 12H), 1.89 – 1.40 (m, 48H); **^{13}C NMR** (101 MHz, $CDCl_3$) δ_C 159.80, 136.54, 130.01, 74.58, 32.94, 24.35. Data in accordance with literature values.[57]

CC3-*S*

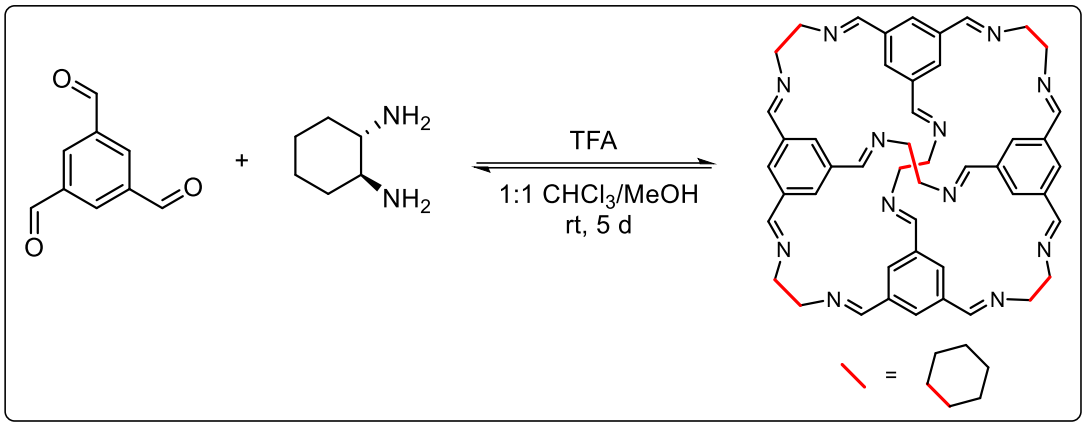

DCM (20 mL) was added slowly onto solid 1,3,5-triformylbenzene (1.0 g, 6.2 mmol, 1 eq.) without stirring at room temperature. Trifluoroacetic acid (100 µL) was added directly to this solution as a catalyst for imine bond formation. Finally, a solution of (*S*,*S*)-1,2-cyclohexyldiamine (1.0 g, 8.7 mmol, 1.4 eq.) in DCM (20 mL) was added. The unmixed reaction was covered and left to stand. Over 5 days, the solid 1,3,5-triformylbenzene was consumed, and **CC3**-*R* precipitated out of the reaction solution. The solid product was removed by filtration and washed with a mixture of 95% ethanol/5% DCM, before being dried under vacuum to give **CC3**-*R* as an off-white solid (730 mg, 0.67 mmol, 43%).

^{1}H NMR (400 MHz, $CDCl_3$) δ_H 8.15 (s, 12H), 7.91 (s, 12H), 3.39 – 3.30 (m, 12H), 1.90 – 1.39 (m, 48H); **^{13}C NMR** (101 MHz, $CDCl_3$) δ_C 159.85, 136.48, 130.03, 74.53, 32.88, 24.30. Data in accordance with literature values.[57]

4.6.4 Synthesis of part-amide cages

Test synthesis of PA-CC3-*R*

To a solution of 1,3,5-triformylbenzene (100 mg, 0.62 mmol, 3.0 eq.) in $CHCl_3$ (100 mL) was added a stirrer bar, a solution of part-amide triamine (128 mg, 0.21 mmol, 1.0 eq.) and triethylamine (0.52 mL, 3.8 mmol, 18 eq) in $CHCl_3$ (33 mL), and a solution of (1R,2R)-(-)-1,2-cyclohexyldiamine (70 mg, 0.62 mmol, 3.0 eq.) in $CHCl_3$ (33 mL). The resulting mixture was heated at 65 °C for 10 days before being allowed to cool to room temperature. The solvent was removed under vacuum, and the resultant solid suspended in THF (50 mL), affording the precipitation of TEA·HCl salts which were removed by filtration. The filtrate was reduced to dryness, and the isolated solid re-dissolved in DCM (10 mL). Hexane (30 mL) was added, resulting in the formation of a colourless precipitate and the volume was reduced under vacuum. The resulting suspension was filtered under vacuum, and the isolated solid dried under vacuum at 70 °C to give the crude cage product mixture as an off-white solid.

General procedure for synthesis of part-amide cage series

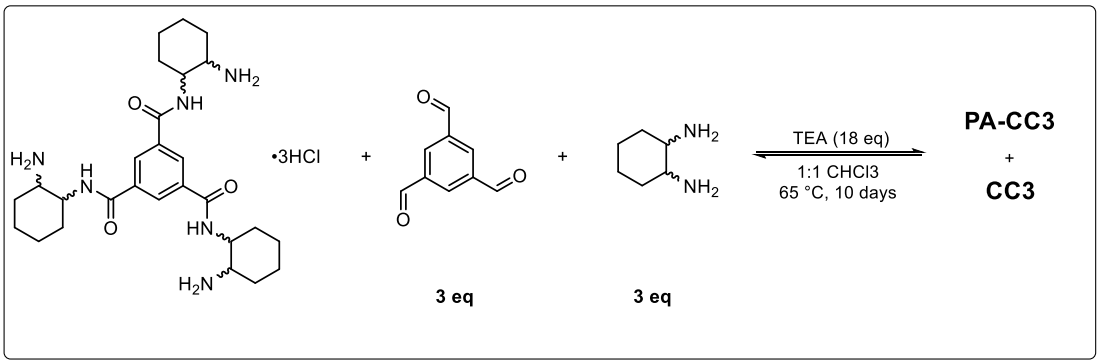

To a solution of 1,3,5-triformylbenzene (100 mg, 0.62 mmol, 3.0 eq.) in 1:1 $CHCl_3$:MeOH (100 mL) was added a stirrer bar, a solution of part-amide triamine (128 mg, 0.21 mmol, 1.0 eq.) and triethylamine (0.52 mL, 3.8 mmol, 18 eq) in 1:1 $CHCl_3$:MeOH (33 mL), and a solution of a selected enantiomer of 1,2-cyclohexyldiamine (70 mg, 0.62 mmol, 3.0 eq.) in 1:1 $CHCl_3$:MeOH (33 mL). The resulting mixture was heated at 65 °C for 10 days before being allowed to cool to room temperature. The solvent was removed under vacuum, and the resultant solid suspended in THF (50 mL), affording the precipitation of TEA·HCl salts which were removed by filtration. The filtrate was reduced to dryness, and the isolated solid re-

dissolved in DCM (10 mL). Hexane (30 mL) was added, resulting in the formation of a colourless precipitate and the volume was reduced under vacuum. The resulting suspension was filtered under vacuum, and the isolated solid dried under vacuum at 70 °C to give the crude cage product as an off-white solid.

Synthesis of **PA-CC3**-*R*:

Prepared using the general procedure for part amide-cage synthesis with:

R-**Tri.3HCl**, TFB and *R*,*R*-CHDA

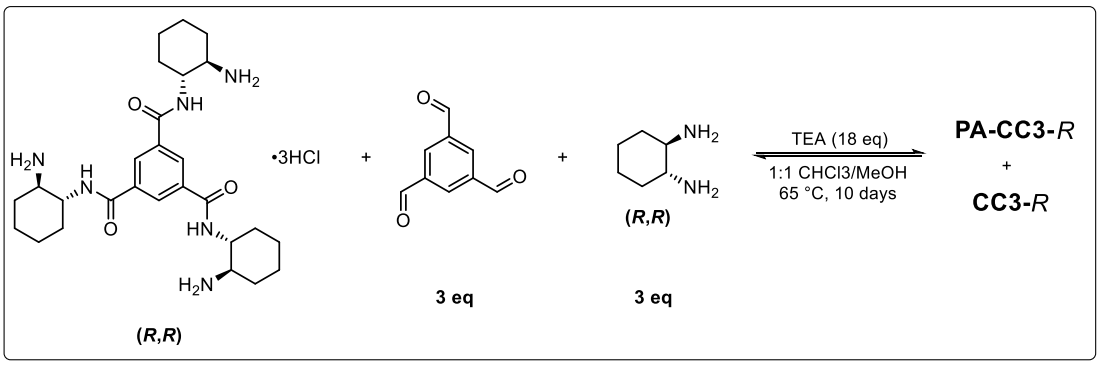

Synthesis of **PA-CC3**-*RS*:

Prepared using the general procedure for part amide-cage synthesis with:

R-**Tri.3HCl**, TFB and *R*,*R*-CHDA

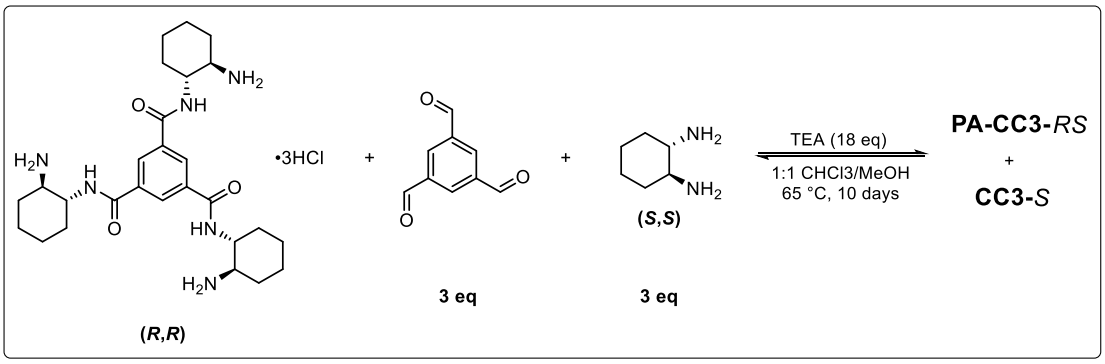

Synthesis of **PA-CC3**-*S*:

Prepared using the general procedure for part amide-cage synthesis with: *S*-**Tri.3HCl**, TFB and *S*,*S*-CHDA

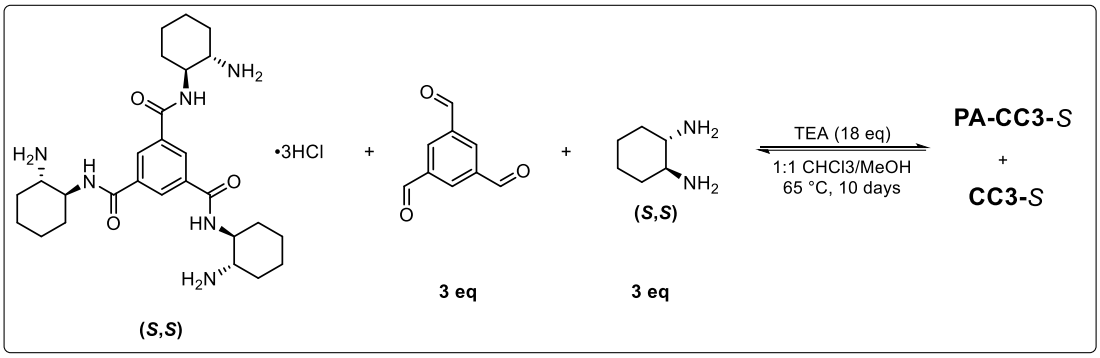

165 mg, mass recovery = 55%

78:22 **PA-CC3**-*S*:**CC3**-*S*; overall **PA-CC3**-*S* purity 60% (HPLC); 78:22 **PA-CC3**-*S*:**CC3**-*S* (^{1}H NMR)

IR (ν_{max}/cm^{-1}): 3272, 2926, 2856, 1643, 1537, 1448, 1321, 1270, 1160, 1141, 1089; **^{1}H NMR** (400 MHz, $CDCl_3$) δ_H 8.26 (s, 3H), 8.19 (s, 3H), 8.15 (s, 3H), 8.13 (s, 3H), 7.96 (t, *J* = 1.4 Hz, 3H), 7.93 (t, *J* = 1.4 Hz, 3H), 7.91 (t, *J* = 1.4 Hz, 3H); **HRMS** (ES+) calculated for $C_{72}H_{84}N_{12}O_3$ 1164.6789, found $[M+H]^+$ 1165.6930

Synthesis of **PA-CC3**-*SR*:

Prepared using the general procedure for part amide-cage synthesis with: *S*-**Tri.3HCl**, TFB and *R*,*R*-CHDA

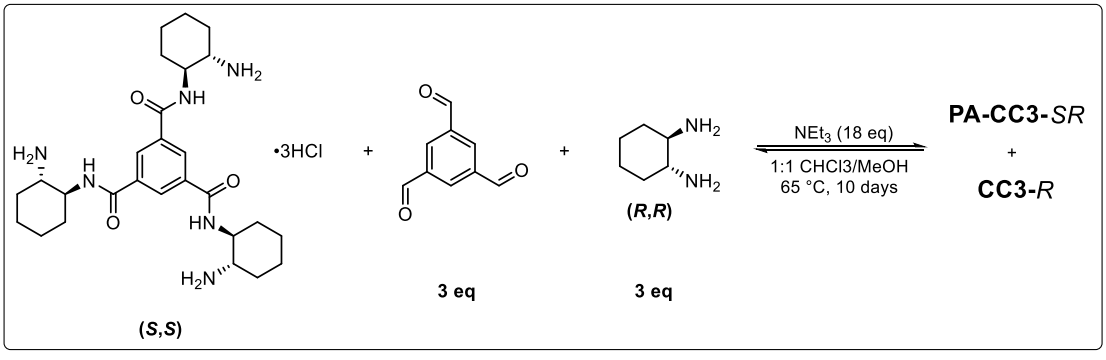

169 mg, mass recovery = 57%

81:19 **PA-CC3**-*SR*:**CC3**-*R*; overall **PA-CC3**-*RS* purity 69% (HPLC); 83:17 **PA-CC3**-*SR*:**CC3**-*R* (^{1}H NMR)

IR (ν_{max}/cm^{-1}): 3397, 3276, 2928, 2857, 1643, 1597, 1538, 1449, 1321, 1264, 1152, 1089; **^{1}H NMR** (400 MHz, $CDCl_3$) δ_H 8.38 (t, *J* = 1.4 Hz, 3H), 8.28 (s, 3H), 8.17 (s, 3H), 8.16 (s, 3H), 8.14 (s, 3H), 7.91 (t, *J* = 1.4 Hz, 3H), 7.37 (t, *J* = 1.4 Hz, 3H); **HRMS** (ES+) calculated for $C_{72}H_{84}N_{12}O_3$ 1164.6789, found $[M+H]^+$ 1165.6929.

4.6.5 Supplementary spectra

Tri-*tert*-butyl((1*R*,1'*R*,1''*R*,2*R*,2'*R*,2''*R*)-((benzene-1,3,5 tricarbonyl)tris(azanediyl))tris(cyclohexane-2,1-diyl))tricarbamate (*R*-Tri-Boc)

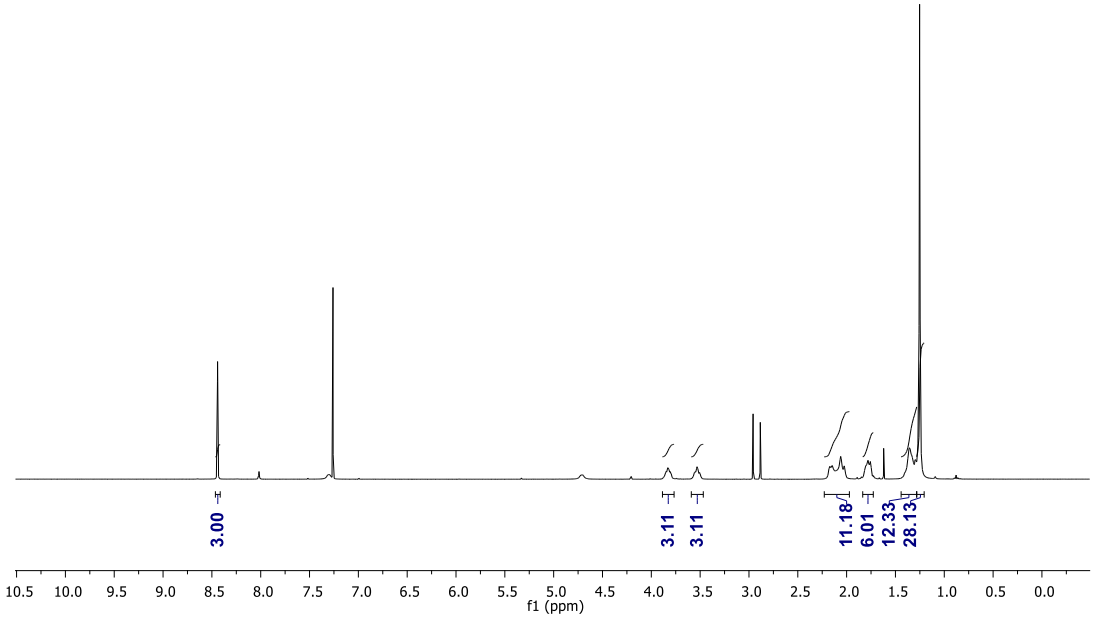

*Figure 4.33 - ^{1}H NMR spectrum of R-**Tri-Boc** (400 MHz, $CDCl_3$).*

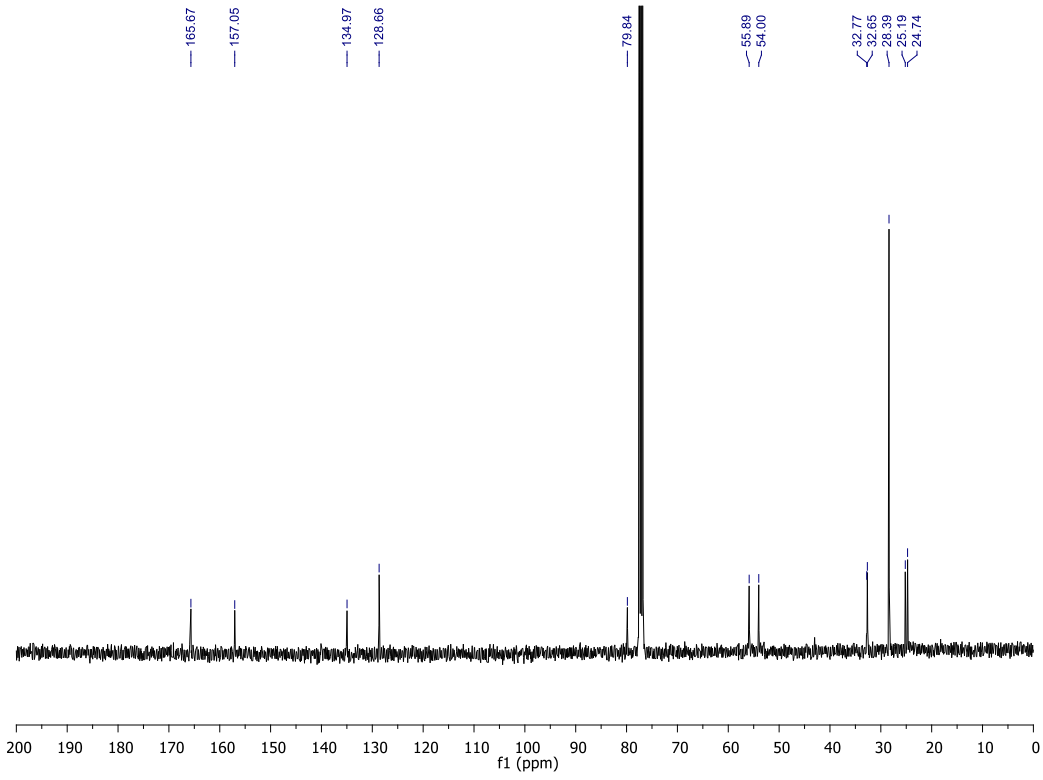

*Figure 4.34 – ^{13}C NMR spectrum of R-**Tri-Boc** (101 MHz, $CDCl_3$).*

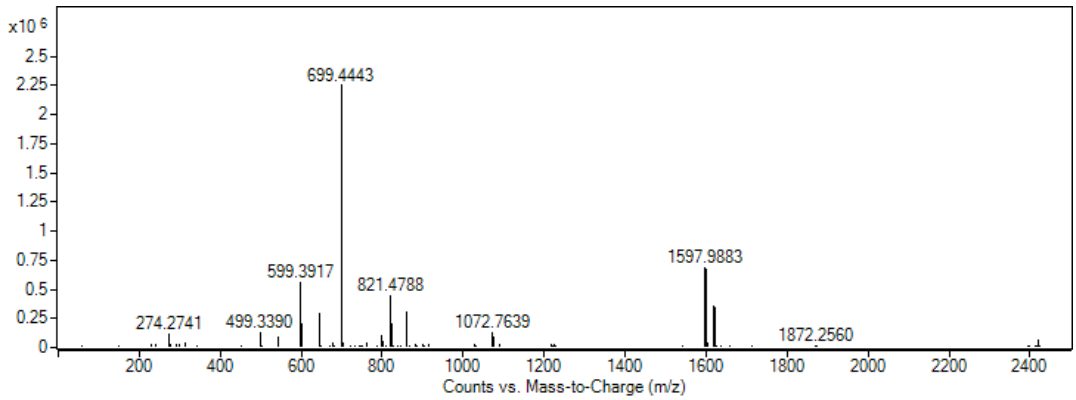

*Figure 4.35 - Mass spectrum (ES+) of R-**Tri-Boc***

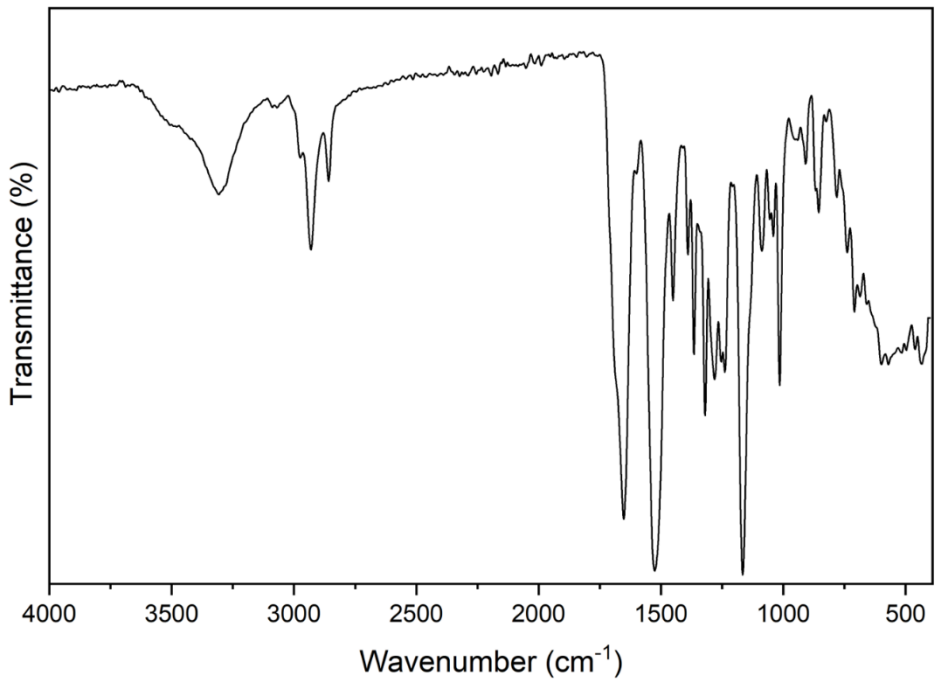

*Figure 4.36 - IR spectra of R-**Tri-Boc***

N^1,N^3,N^5-tris((1*R*,2*R*)-2-aminocyclohexyl)benzene-1,3,5-tricarboxamide trihydrochloride (*R*-Tri.3HCl)

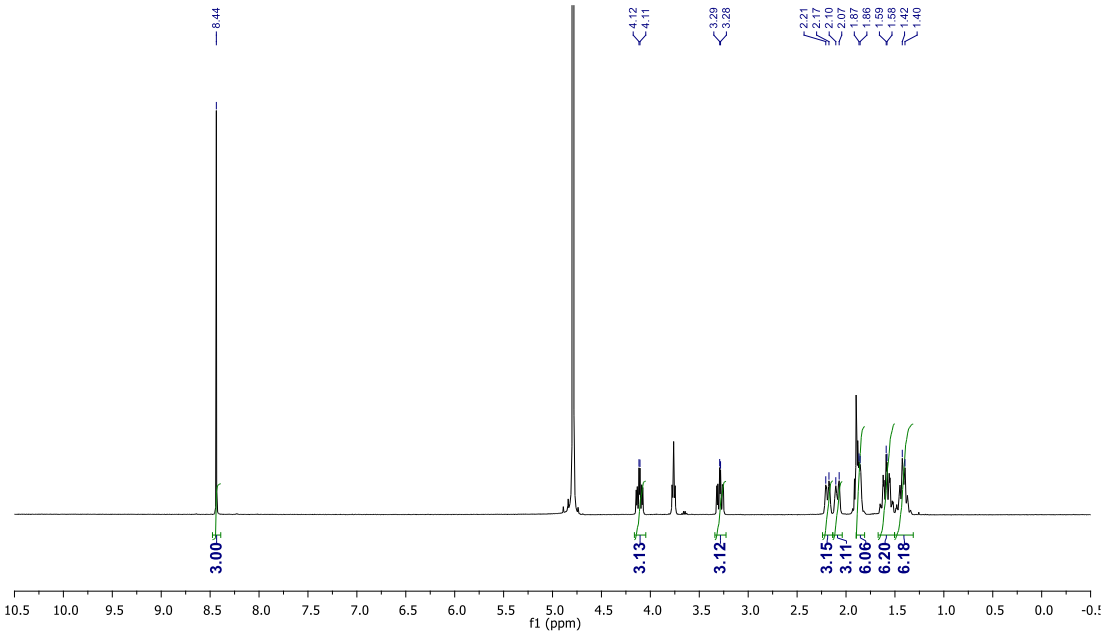

*Figure 4.37 - ^{1}H NMR spectrum of R-**Tri.3HCl** (400 MHz, D_2O).*

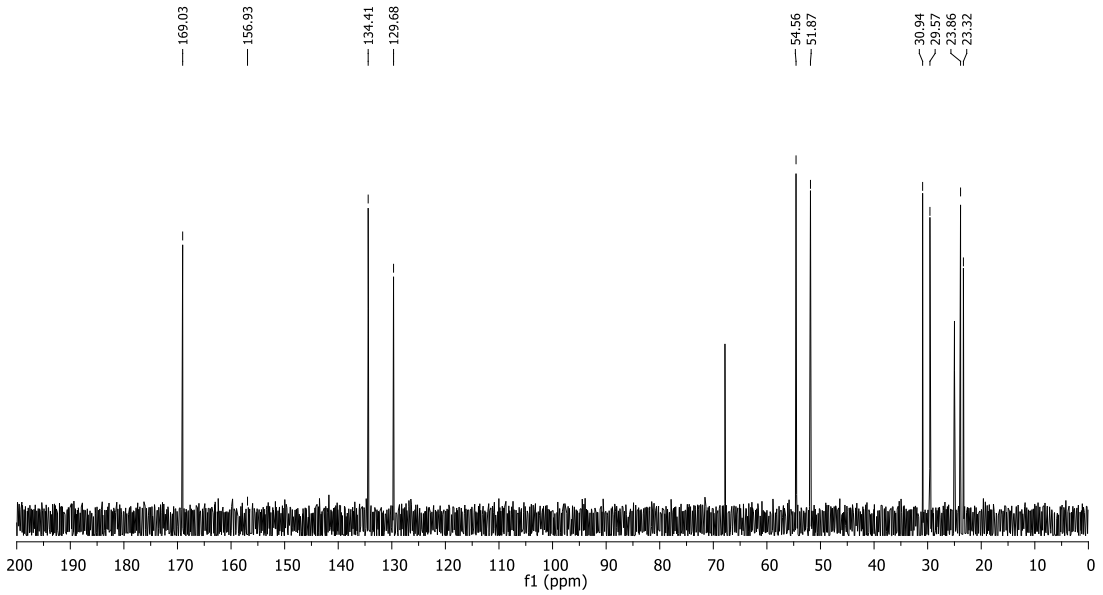

*Figure 4.38 – ^{13}C NMR spectrum of R-**Tri.3HCl** (101 MHz, D_2O).*

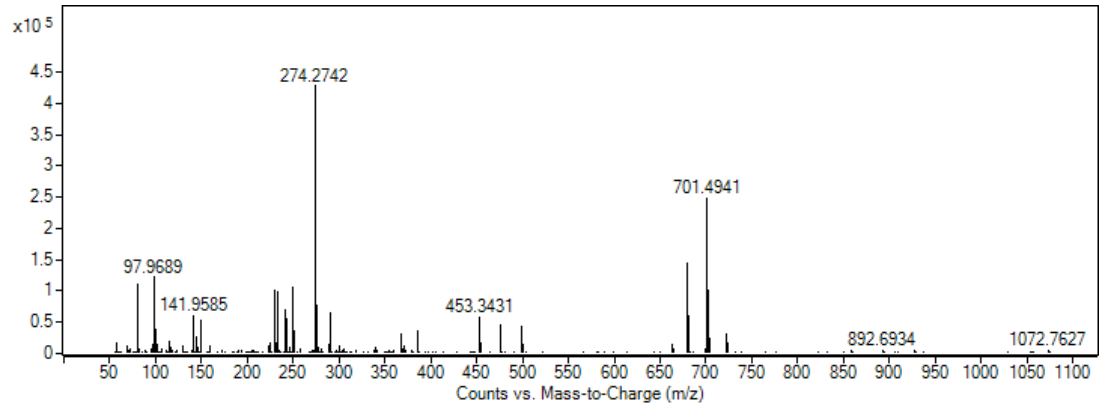

*Figure 4.39 - Mass spectrum (ES+) of R-**Tri.3HCl***

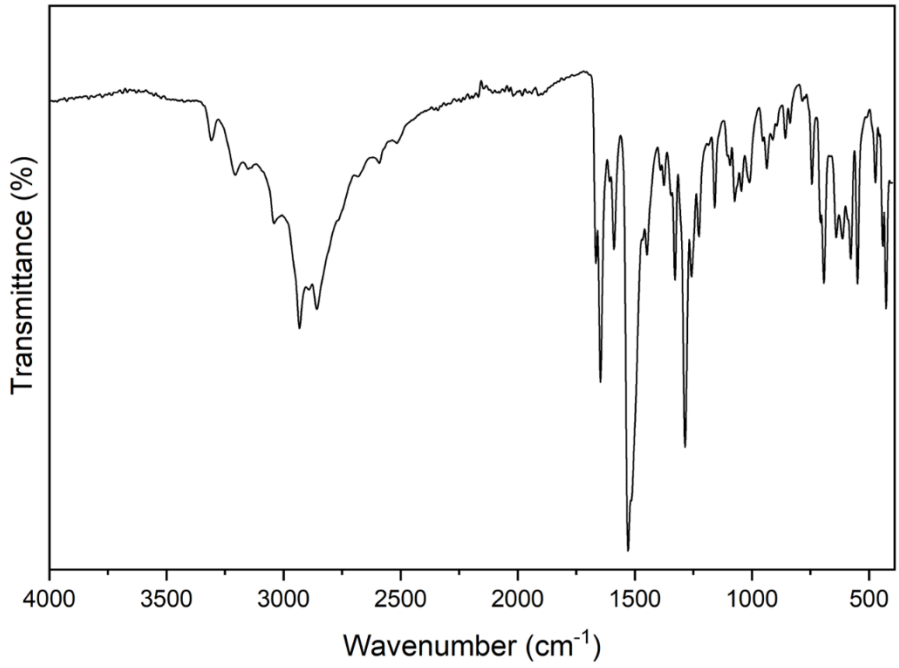

*Figure 4.40 - IR spectrum of R-**Tri.3HCl***

Tri-*tert*-butyl ((1*S*,1'*S*,1''*S*,2*S*,2'*S*,2''*S*)-((benzene-1,3,5-tricarbonyl)tris(azanediyl))tris(cyclohexane-2,1-diyl))tricarbamate (*S*-Tri-Boc)

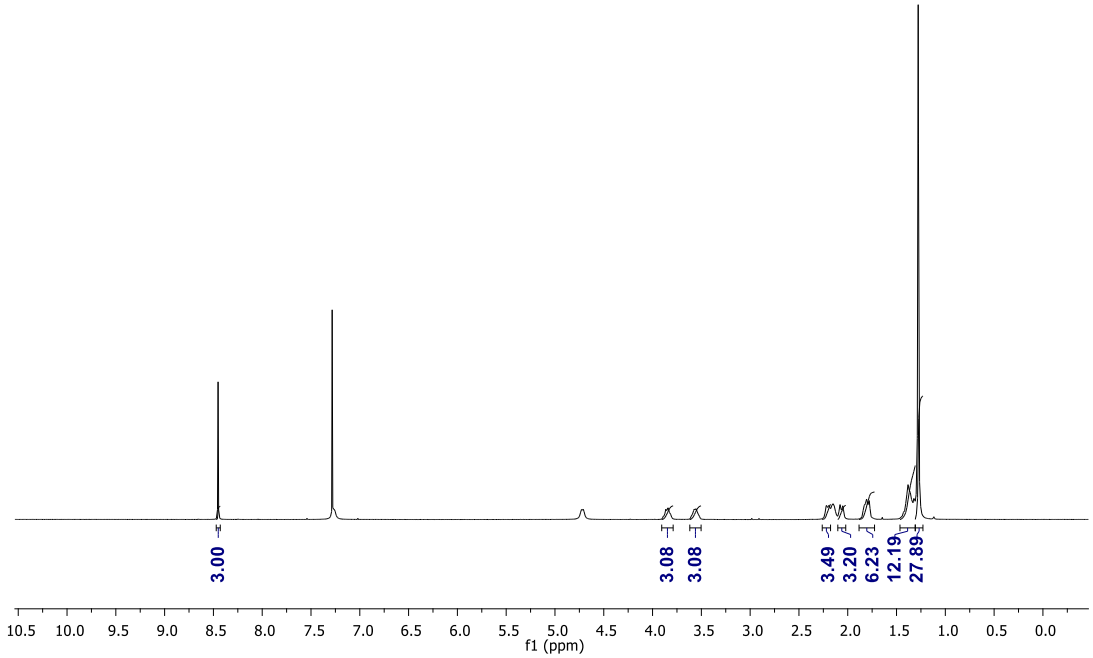

*Figure 4.41 -^{1}H NMR spectrum of S-**Tri-Boc** (400 MHz, $CDCl_3$).*

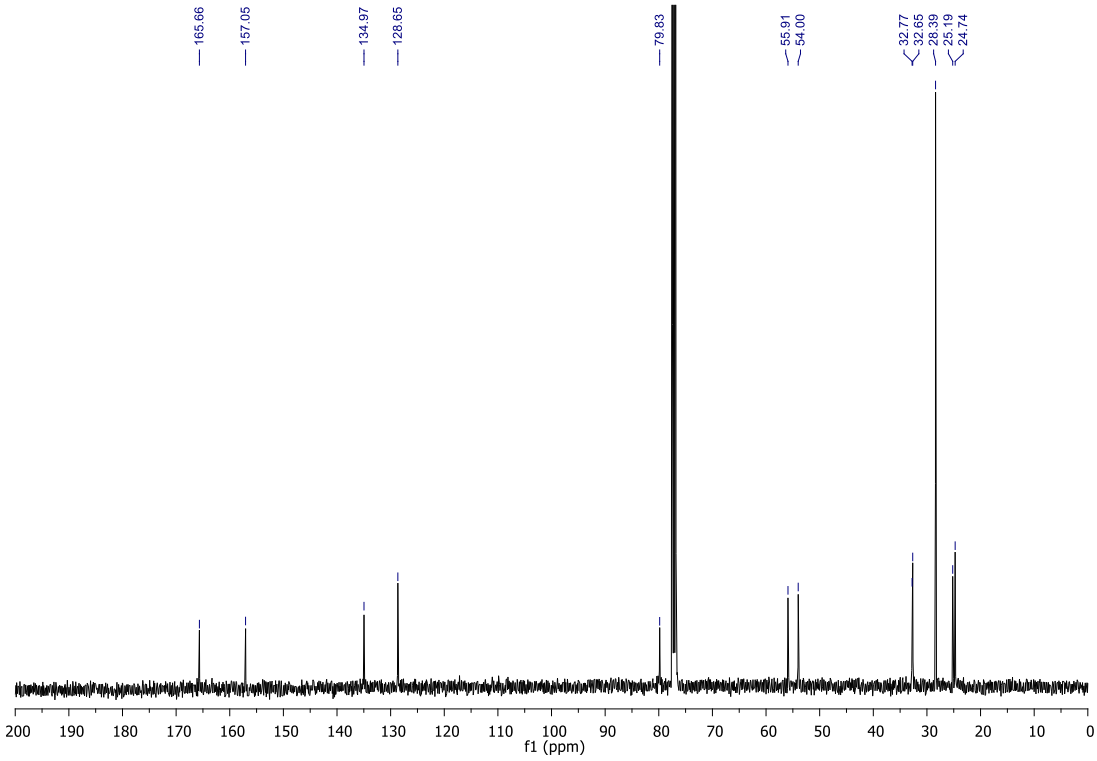

*Figure 4.42 – ^{13}C NMR spectrum of S-**Tri-Boc** (101 MHz, $CDCl_3$)*

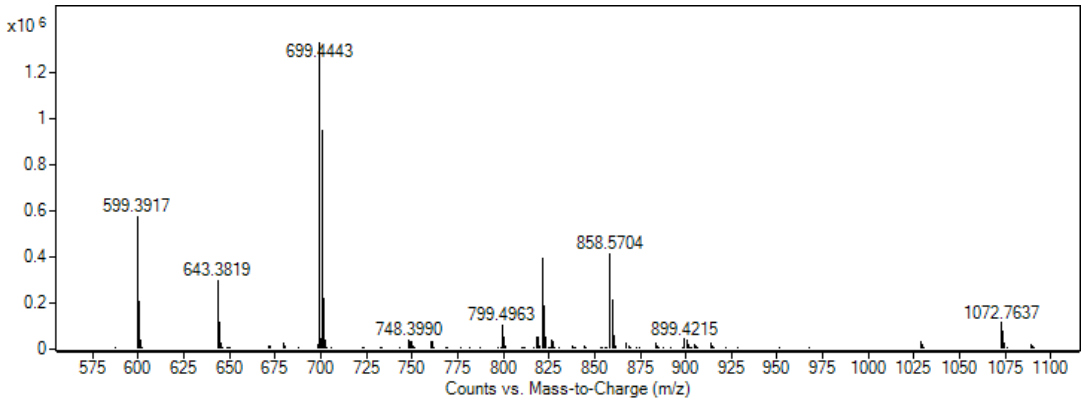

*Figure 4.43 - Mass spectrum (ES+) of S-**Tri-Boc***

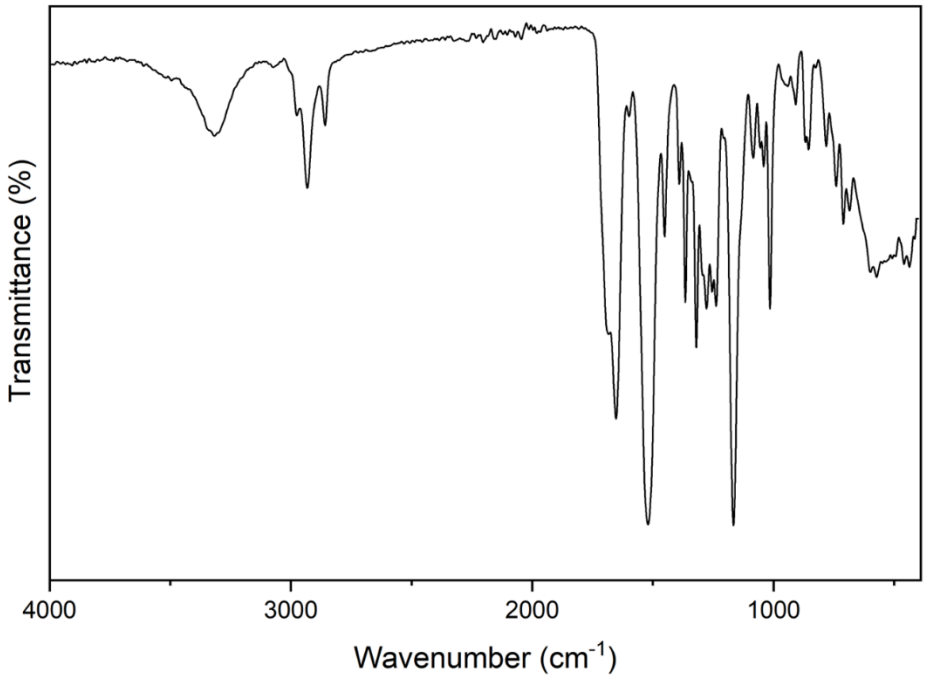

*Figure 4.44 - IR spectrum of S-**Tri-Boc**.*

N^1,N^3,N^5-tris((1*S*,2*S*)-2-aminocyclohexyl)benzene-1,3,5-tricarboxamide trihydrochloride (*S*-Tri.3HCl)

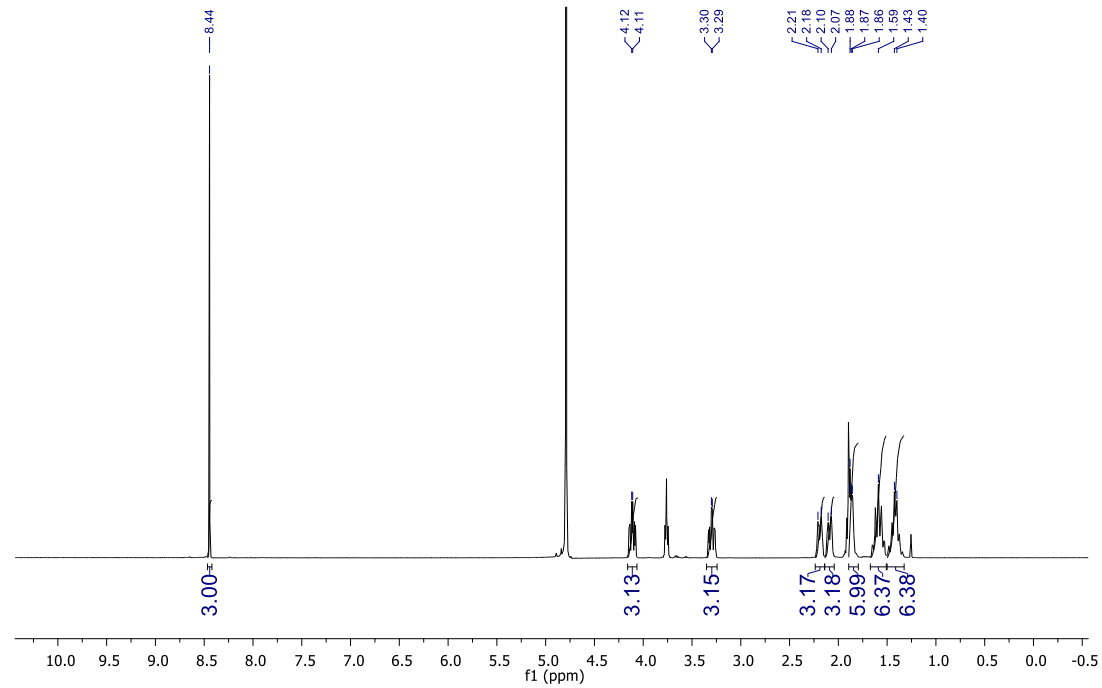

*Figure 4.45 - ^{1}H NMR spectrum of S-**Tri.3HCl** (400 MHz, D_2O).*

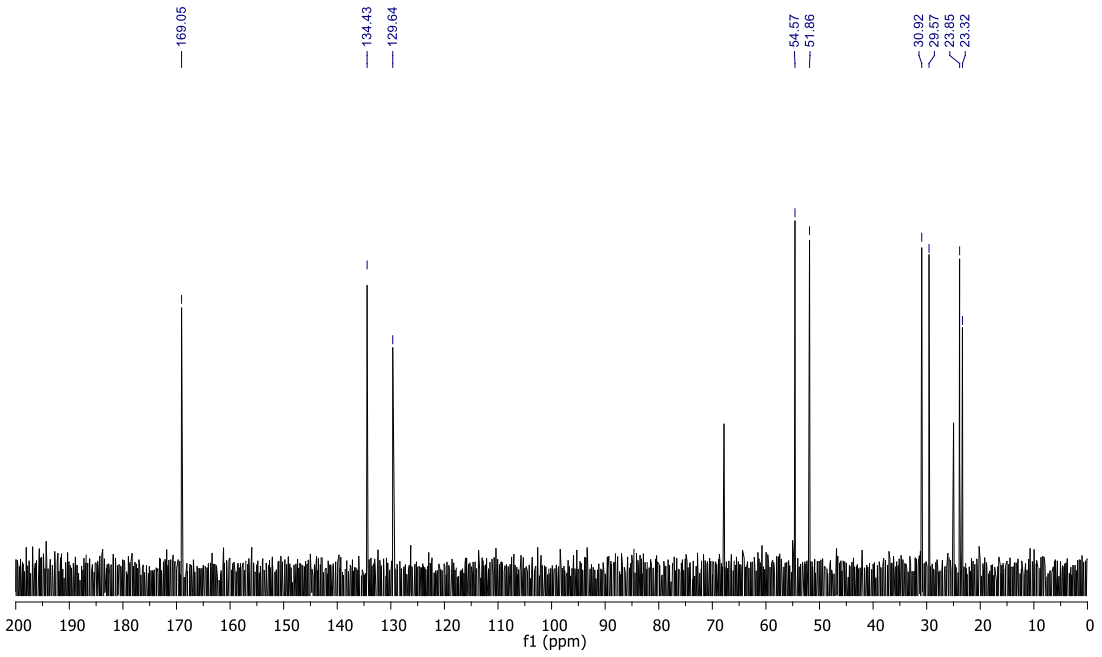

*Figure 4.46 – ^{13}C NMR spectrum of S-**Tri.3HCl** (101 MHz, D_2O).*

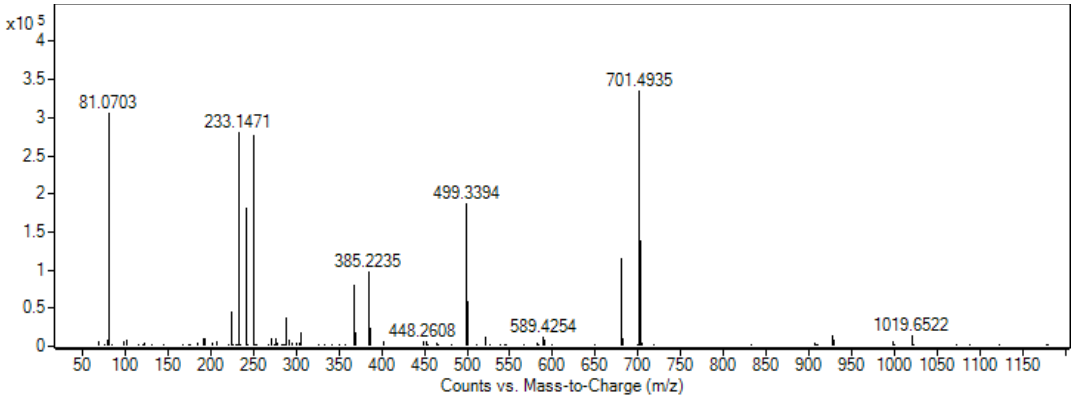

*Figure 4.47 - Mass spectrum of S-**Tri.3HCl**.*

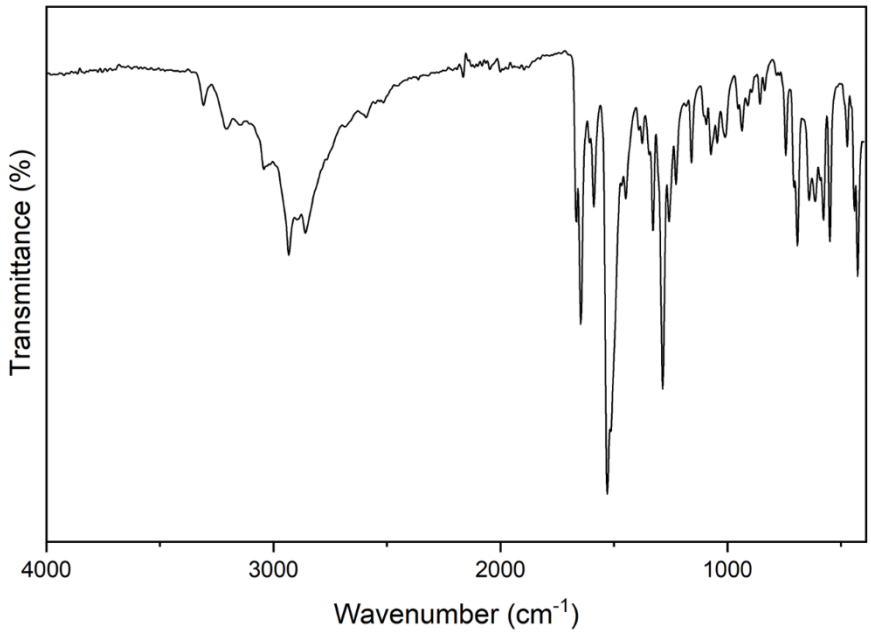

*Figure 4.48 - IR spectrum of S-**Tri.3HCl.***

PA-CC3-*S* crude mixture

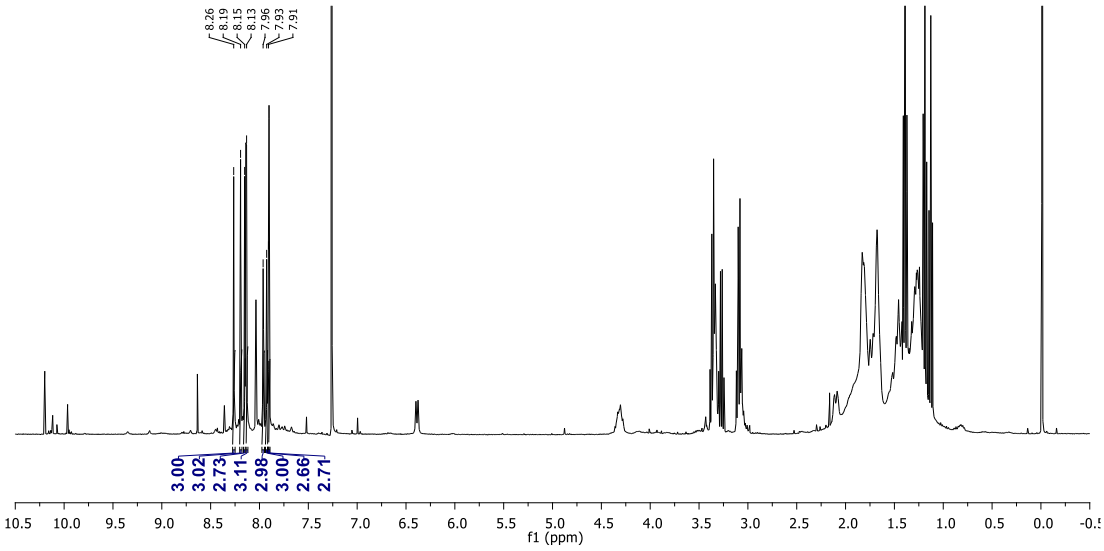

*Figure 4.49 – ^{1}H NMR spectrum ($CDCl_3$) of crude **PA-CC3**-S.*

PA-CC3-*SR* crude mixture

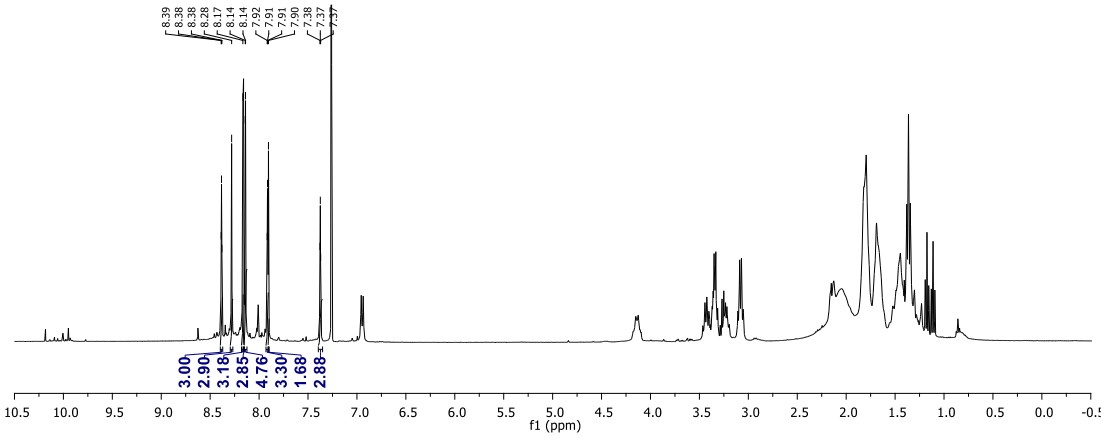

*Figure 4.50 - ^{1}H NMR spectrum ($CDCl_3$) of crude **PA-CC3**-SR.*

4.7 References

1 W. Kiggen and F. Vögtle, *Angew. Chemie Int. Ed. English*, 1984, **23**, 714–715.

2 A. P. Davis and R. S. Wareham, *Angew. Chemie Int. Ed.*, 1998, **37**, 2270–2273.

3 A. S. Bhat, S. M. Elbert, W.-S. Zhang, F. Rominger, M. Dieckmann, R. R. Schröder and M. Mastalerz, *Angew. Chemie Int. Ed.*, 2019, 1–6.

4 I. Martí, J. Rubio, M. Bolte, M. I. Burguete, C. Vicent, R. Quesada, I. Alfonso and S. V. Luis, *Chem. - A Eur. J.*, 2012, **18**, 16728–16741.

5 A. Moure, S. V. Luis and I. Alfonso, *Chem. - A Eur. J.*, 2012, **18**, 5496–5500.

6 H. Li, H. Zhang, A. D. Lammer, M. Wang, X. Li, V. M. Lynch and J. L. Sessler, *Nat. Chem.*, 2015, **7**, 1003–1008.

7 X. Zheng, Y. Zhang, G. Wu, J.-R. Liu, N. Cao, L. Wang, Y. Wang, X. Li, X. Hong, C. Yang and H. Li, *Chem. Commun.*, 2018, **54**, 3138–3141.

8 D. G. Rivera and L. A. Wessjohann, *J. Am. Chem. Soc.*, 2006, **128**, 7122–7123.

9 L. A. Wessjohann, O. Kreye and D. G. Rivera, *Angew. Chemie - Int. Ed.*, 2017, **56**, 3501–3505.

10 Q. H. Ling, J. L. Zhu, Y. Qin and L. Xu, *Mater. Chem. Front.*, 2020, **4**, 3176–3189.

11 S. P. Black, A. R. Stefankiewicz, M. M. J. Smulders, D. Sattler, C. A. Schalley, J. R. Nitschke and J. K. M. Sanders, *Angew. Chemie - Int. Ed.*, 2013, **52**, 5749–5752.

12 K. Mahata, P. D. Frischmann and F. Würthner, *J. Am. Chem. Soc.*, 2013, **135**, 15656–15661.

13 T. K. Ronson, D. A. Roberts, S. P. Black and J. R. Nitschke, *J. Am. Chem. Soc.*, 2015, **137**, 14502–14512.

14 X. Feng, P. Liao, J. Jiang, J. Shi, Z. Ke and J. Zhang, *ChemPhotoChem*, 2019, **3**, 1014–1019.

15 H. H. Huang, K. S. Song, A. Prescimone, A. Aster, G. Cohen, R. Mannancherry, E. Vauthey, A. Coskun and T. Šolomek, *Chem. Sci.*, 2021, **12**, 5275–5285.

16 R. L. Greenaway, V. Santolini, F. T. Szczypiński, M. J. Bennison, M. A. Little, A. Marsh, K. E. Jelfs and A. I. Cooper, *Chem. – A Eur. J.*, 2020, **26**, 3718–3722.

17 F. J. Rizzuto and J. R. Nitschke, *J. Am. Chem. Soc.*, 2020, **142**, 7749–7753.

18 A. W. Markwell-Heys, M. L. Schneider, J. M. L. Madridejos, G. F. Metha and W. M. Bloch, *Chem. Commun.*, 2021, **57**, 2915–2918.

19 R. Kramer, J. M. Lehn and A. Marquis-Rigault, *Proc. Natl. Acad. Sci.*, 1993, **90**, 5394–5398.

20 W. Jiang, H. D. F. Winkler and C. A. Schalley, 2008, 13852–13853.

21 K. Acharyya, S. Mukherjee and P. S. Mukherjee, *J. Am. Chem. Soc.*, 2013, **135**, 554–557.

22 K. Acharyya and P. S. Mukherjee, *Chem. - A Eur. J.*, 2014, **20**, 1646–1657.

23 S. Klotzbach and F. Beuerle, *Angew. Chemie Int. Ed.*, 2015, **54**, 10356–10360.

24 F. Beuerle, S. Klotzbach and A. Dhara, *Synlett*, 2016, **27**, 1133–1138.

25 D. Beaudoin, F. Rominger and M. Mastalerz, *Angew. Chemie - Int. Ed.*, 2017, **56**, 1244–1248.

26 P. Wagner, F. Rominger, W. S. Zhang, J. H. Gross, S. M. Elbert, R. R. Schröder and M. Mastalerz, *Angew. Chemie - Int. Ed.*, 2021, **60**, 8896–8904.

27 R. L. Greenaway, V. Santolini, A. Pulido, M. A. Little, B. M. Alston, M. E.

Briggs, G. M. Day, A. I. Cooper and K. E. Jelfs, *Angew. Chemie*, 2019, **131**, 16421–16427.

28 R. L. Greenaway, V. Santolini, M. J. Bennison, B. M. Alston, C. J. Pugh, M. A. Little, M. Miklitz, E. G. B. Eden-Rump, R. Clowes, A. Shakil, H. J. Cuthbertson, H. Armstrong, M. E. Briggs, K. E. Jelfs and A. I. Cooper, *Nat. Commun.*, 2018, **9**, 1–27.

29 S. Jiang, J. T. A. Jones, T. Hasell, C. E. Blythe, D. J. Adams, A. Trewin and A. I. Cooper, *Nat. Commun.*, 2011, **2**, 207.

30 R. J. Kearsey, B. M. Alston, M. E. Briggs, R. L. Greenaway and A. I. Cooper, *Chem. Sci.*, 2019, **10**, 9454–9465.

31 H. Su, C. A. Hurd Price, L. Jing, Q. Tian, J. Liu and K. Qian, *Mater. Today Bio*, , DOI:10.1016/j.mtbio.2019.100033.

32 S. W. Ng, N. Noor and Z. Zheng, *NPG Asia Mater.*, 2018, **10**, 217–237.

33 L.-T.-C. Tran, S. Lesieur and V. Faivre, *Expert Opin. Drug Deliv.*, 2014, **11**, 1061–1074.

34 A. Blázquez-Moraleja, M. E. Pérez-Ojeda, J. R. Suárez, M. L. Jimeno and J. L. Chiara, *Chem. Commun.*, 2016, **52**, 5792–5795.

35 S. Yadnum, J. Roche, E. Lebraud, P. Négrier, P. Garrigue, D. Bradshaw, C. Warakulwit, J. Limtrakul and A. Kuhn, *Angew. Chemie - Int. Ed.*, 2014, **53**, 4001–4005.

36 C. C. Pattillo and J. S. Moore, *Chem. Sci.*, 2019, **10**, 7043–7048.

37 Y. Lei, Q. Chen, P. Liu, L. Wang, H. Wang, B. Li, X. Lu, Z. Chen, Y. Pan, F. Huang and H. Li, *Angew. Chemie - Int. Ed.*, 2021, **60**, 4705–4711.

38 A. G. Slater, M. A. Little, M. E. Briggs, K. E. Jelfs and A. I. Cooper, *Mol. Syst. Des. Eng.*, 2018, **3**, 223–227.

39 P. Skowronek and J. Gawronski, *Org. Lett.*, 2008, **10**, 4755–4758.

40 T. Tozawa, J. T. A. Jones, S. I. Swamy, S. Jiang, D. J. Adams, S. Shakespeare, R. Clowes, D. Bradshaw, T. Hasell, S. Y. Chong, C. Tang,

S. Thompson, J. Parker, A. Trewin, J. Bacsa, A. M. Z. Slawin, A. Steiner and A. I. Cooper, *Nat. Mater.*, 2009, **8**, 973–978.

41 P. S. Reiss, M. A. Little, V. Santolini, S. Y. Chong, T. Hasell, K. E. Jelfs, M. E. Briggs and A. I. Cooper, *Chem. - A Eur. J.*, 2016, **22**, 16547–16553.

42 M. E. Briggs, K. E. Jelfs, S. Y. Chong, C. Lester, M. Schmidtmann, D. J. Adams and A. I. Cooper, *Cryst. Growth Des.*, 2013, **13**, 4993–5000.

43 K. E. Jelfs, E. G. B. Eden, J. L. Culshaw, S. Shakespeare, E. O. Pyzer-Knapp, H. P. G. Thompson, J. Bacsa, G. M. Day, D. J. Adams and A. I. Cooper, *J. Am. Chem. Soc.*, 2013, **135**, 9307–9310.

44 V. Santolini, M. Miklitz, E. Berardo and K. E. Jelfs, *Nanoscale*, 2017, **9**, 5280–5298.

45 V. Santolini, G. A. Tribello and K. E. Jelfs, *Chem. Commun.*, 2015, **51**, 15542–15545.

46 A. Ardá, C. Vnturi, C. Nativi, O. Francesconi, G. Gabrielli, F. Javier Cañada, J. Jiménez-Barbero and S. Roelens, *Chem. - A Eur. J.*, 2010, **16**, 414–418.

47 C. Nativi, O. Francesconi, G. Gabrielli, A. Vacca and S. Roelens, *Chem. - A Eur. J.*, 2011, **17**, 4814–4820.

48 M. E. Briggs and A. I. Cooper, *Chem. Mater.*, 2017, **29**, 149–157.

49 C. N. Huang, C. M. Wu, H. W. Lo, C. C. Lai, W. F. Teng, L. C. Liu and C. M. Chen, *Polymers (Basel).*, 2019, **11**, 1–13.

50 V. M. Suresh, S. Bonakala, H. S. Atreya, S. Balasubramanian and T. K. Maji, *ACS Appl. Mater. Interfaces*, 2014, **6**, 4630–4637.

51 M. Liu, M. A. Little, K. E. Jelfs, J. T. A. Jones, M. Schmidtmann, S. Y. Chong, T. Hasell and A. I. Cooper, *J. Am. Chem. Soc.*, 2014, **136**, 7583–7586.

52 J. P. Perdew, K. Burke and M. Ernzerhof, *Phys. Rev. Lett.*, 1996, **77**,

3865–3868.

53 S. Grimme, S. Ehrlich and L. Goerigk, *J. Comput. Chem.*, 2011, **32**, 1456–1465.

54 Y. Zhao and D. G. Truhlar, *Theor. Chem. Acc.*, 2008, **120**, 215–241.

55 F. Weigend and R. Ahlrichs, *Phys. Chem. Chem. Phys.*, 2005, **7**, 3297–3305.

56 and D. J. F. M. J. Frisch, G. W. Trucks, H. B. Schlegel, G. E. Scuseria, M. A. Robb, J. R. Cheeseman, G. Scalmani, V. Barone, G. A. Petersson, H. Nakatsuji, X. Li, M. Caricato, A. V. Marenich, J. Bloino, B. G. Janesko, R. Gomperts, B. Mennucci, H. P. Hratchian, J. V., .

57 T. Hasell, S. Y. Chong, K. E. Jelfs, D. J. Adams and A. I. Cooper, *J. Am. Chem. Soc.*, 2012, **134**, 588–598.

Chapter 5

Conclusions and future work

5.1 Conclusions

This thesis has outlined three potential strategies for the formation of amide-derived porous organic cages: direct formation using transamidation, imine oxidation, and the use of functionalised precursors. It was hoped that these methods could give new routes to a range of POCs which did not suffer from the stability issues as seen for other species formed using DCvC methods.

Chapter 2 outlined an investigation into transamidation as a potential route for the formation of amide cages. A model system was first developed based on bifunctional terephthalamide derivatives — this was designed as to allow for analysis of the transamidation progress using ^{1}H NMR spectroscopy, targeting a 50:50 ratio of *N*-benzyl and *N*-*p*-tolyl amides within the crude reaction product. The model system was initially tested using benzoic acid, a known transamidation catalyst.[1] Optimisation of the reaction led to improvements in the degree of transamidation exhibited, though the desired product ratio was not achieved. An extended catalyst study was then carried out testing 55 potential small molecules, with the best-performing candidates taken through for further study. Increasing the catalyst loading from 20 mol% to 60 mol% had the most substantive impact, achieving the desired 50:50 ratio, with 3,5-dibromobenzoic acid selected as the best option for further study. The dynamic nature of the reaction was probed by investigating alternative routes to the same mixed amide product, finding that there was not a significant bias towards either of the target amides. As such, the product distribution could be tuned based on the addition of precursors, and the product ratio was found to be highly dependent on the total amounts of free amine present within the reaction mixture. With the knowledge that there was a dynamic nature to the system, the optimised conditions were used in the attempted synthesis of two amide cages. Unfortunately, analysis of the reaction solutes suggested no presence of the target cages, while the insoluble solids formed in the reaction appeared to be oligomeric or polymeric in nature, with the presence of starting material.

Chapter 3 outlined an investigation into the oxidation of imine cages to their amide analogues, using Pinnick oxidation conditions utilised in previous cage oxidation reports.[2,3] This study focussed on the prototypical imine cage **CC3**,[4] with the hope that the methodology could be applied to the **CC** series to quickly access a new family of amide cages. The attempted oxidation of **CC3** did not progress as hoped, with no clear indication of consumption of the imine bond by ^{1}H NMR spectroscopic analysis. Additionally, peaks matching the aldehyde starting material TFB suggested

degradation of the cage species. After confirming the applied conditions were functioning correctly by use of a suitable model compound, more fundamental testing was completed using a series of monofunctional imines. These were designed to emulate the bonding seen in a verity of cage substrates (including a known oxidation substrate and **CC3**), to investigate how the difference in the imine moieties may have affected the oxidation process. Analysis by ^{1}H NMR spectroscopy showed success for substrates matching that of **IC1**, a known substrate; however, the oxidation attempts for the **CC3** model compound again found the presence of high amounts of both imine and aldehyde groups. Considering the lack of oxidation exhibited for both **CC3** and certain model compounds, no further investigations were continued so that efforts could be focused on alternative projects.

Chapter 4 outlined efforts to form cages using amide-containing triamine precursors in combination with the known cage precursors. The system was designed such that these reagents would combine in a social self-sorting process to form part-amide cages where one face was constructed with amide bonds. It was hoped that this may impart some stability through the amide groups, while the cage-forming step was completed using reversible imine condensation reactions, thereby avoiding the difficulties outlined previously for irreversible bond-formation. This functionalised precursor method also gave rise for the potential to form Janus cages, with distinct regions of functionality around the cage scaffold (in this case amide and imine groups). A series of cages were designed based on the combination of TFB, CHDA and a functionalised precursor to form derivatives of the prototypical cage **CC3**. Use of the different chiral forms of the amines led to 4 potential cages: two homochiral, where the chirality remained the same throughout the cage, and two heterochiral, where the chirality swapped between the two hemispheres of the structure. In silico modelling of the four structures suggested they were all shape persistent, with the structures matching well with parent cage **CC3**, differing only with slight twist for the amide groups, and the heterochiral cages due to multiple chiralities of CHDA.

Following successful synthesis of the triamine precursors, the reaction conditions were optimised using test reaction to form **PACC3**-*R*, the homochiral cage using the -*R* enantiomer of CHDA. Initial conditions were developed using a report of Greenaway *et al.* outlining the synthesis of cage pots via social-self-sorting.[5] Following this reaction, the full series of four cages were targeted, heating for 10 days and isolating as crude mixture. Analysis by ^{1}H NMR spectroscopy showed a complex spectrum, containing the target cage, parent cage **CC3**, and other species from the

reaction. The desired purification technique prep-HPLC was not available, so the crude solids were triturated with THF to remove as much **CC3** as possible. Whilst this technique showed promise, pure samples of **PA-CC3** could not ultimately be obtained. Additionally, solid loss during the multiple purification stages meant there was very little material for further study. As such, fresh samples of two cages, **PACC3**-*S* and **PACC3**-*SR*, were prepared. To avoid the issues seen previously with analysis by ^{1}H NMR spectroscopy, HPLC was used to monitor the progress of the cage synthesis. The reactions were run for the full 10 days as previously, though comparison of the HPLC traces suggested that future attempts may benefit from early isolation of product to maximise the amount of part-amide cage present. Analysis of the isolated crude products found a high proportion of the part amide cages to the parent **CC3** cages, with good overall purity of the part-amide cages.

5.2 Future work

The study outlined in chapter 2 has provided a new methodology for application to the synthesis of amine cages. With an optimised transamidation process, the described conditions could now be applied in the synthesis of new cages. Initially it may be required to limit precursors to the benzylic-amide structures outlined in the model system, though the system could be investigated further with alternative *N*-functionalised precursors. For the transamidation process itself, it may also be useful to investigate recycling of the catalyst mixture to try to mitigate the high loading required for successful transamidation. In terms of materials formation, as the cages **Tri^{4}Di^{6}** and **Tri^{4}Tri^{4}** targeted in this work were not successfully synthesised, it may be beneficial to first target smaller structures such as smaller cages or even macrocycles. However, it may also be necessary to also alter the reaction conditions of the cage formation to use methods seen in irreversible amide cage, *e.g.*, high-dilution or slow addition of precursors. Similarly, further pre-configuration of the precursor could also assist in cage formation, perhaps through the inherent structure of the precursors themselves, or the use of templating. A combined method of dynamic transamidation with techniques from irreversible synthesis may lead to an overall improved methodology compared to each method independently. Ideally, a combined route would show reduced formation of kinetic products and loss of material through polymer/oligomer formation compared to irreversible bond-formation, giving improved yields and more straightforward isolation of target materials.

With the lack of oxidation exhibited for **CC3** as outlined in chapter 2, it is unlikely that application to other **CC** series cages formed from alkyl-derived amines will be successful. It is possible that the lack of oxidation may be due to issues regarding bond angles around the imine as suggested by Bhat,[3] though, considering the lack of reaction seen for **CC3**-mono, it is likely that the functionalities present around the imine bond are a key factor. It may be useful to apply the conditions to **CC** series cages formed using alternative amines.[6] Alternatively, the Pinnick oxidation is not the only know method for imine oxidation; tert-butylhydroperoxide,[7] potassium permanganate,[8] and m-chloroperoxybenzoic acid[9,10] have all been used for imine oxidation. It is possible these routes may be suitable for the alkyl-derived imine groups seen in the **CC** series.

The methodology outlined in chapter 4 presents the most promising route for the formation of new amide derived POCs. The work discussed showed successful formation of part-amide cages by social self-sorting, though unfortunately pure samples of the part-amide cages could not be obtained. This was certainly the key limitation of the study — the original goal was to obtain these cages to assess the effect of the amide face on the overall stability of the cage; without a pure sample of the part-amide cage, a direct comparison of the part-amide cage stability vs wholly imine **CC3** could not be undertaken. For continued study into this area, priority should be given to the isolation of pure part-amide cage samples from the crude cage mixtures, ideally by the use of preparative-HPLC as outlined in analogous literature reports.[5,11] Obtaining pure samples of cage would then allow for more accurate characterisation, but also analysis of the properties — of particular importance would be the thermal stability of the part-amide cages, and how they compare to **CC3**. Additionally, investigating the chemical stability as with existing amide structures[2] would be hugely beneficial — whilst the imine bonds present may not be able to withstand harsh conditions, it would be interesting to see if the presence of the amide face provides an “anchoring” effect as described previously. Following this, investigation of the gas adsorption properties would give an indication on the effect of the amide groups on the cage properties — whilst uptake and BET surface area would be useful, selectivity of CO_2 compared to existing imine cages would be of great interest. Finally, the preparation of single crystals would allow for confirmation of the cage structure, as well as assessing the effect of the amide face on the solid-state packing of the part-amide cages.

With isolation and characterisation of the series of part-amide cages outlined in this thesis, studies could then be shifted to expanding the methodology to other structures. Whilst the use of CHDA moieties provided a prefect structure for comparison with **CC3**, the synthetic route outlined could be very beneficial for more tailored synthesis of porous organic cages. As discussed previously, current reversible methods of cage synthesis do not allow for much control on the placement of precursors around a cage structure when using multiple precursors *e.g.* the statistical mixture of species formed during cage scrambling.[12] The functionalised precursor route outlined in chapter 4 allows for tailored amine placement within the cage scaffold to form Janus cages. This allows for the design and synthesis of cages with specific functionalities on each hemisphere of the cage structure. The use of amide bonds also means the functionalities around the amide face do not readily undergo exchange, ensuring even more complex mixtures of isomers cannot form. To form fully robust cages, the part-amide structures could also be reduced and tied — this could form fully stable cages with varied functionality on the cage scaffold. Additionally, this does not have to be limited to amides — the use of singly-protected amines was imperative for part-amide precursor formation, but this could be adapted to form part-amine structures, thereby more closely matching the insightful route outlined by Roelens and co-workers.[13–15] This could allow for the formation of fully-tied amine cages with varied functionality. Of course, the self-sorting methodology does not have to be used — part-amide/amine precursors could also be included in high-throughput screening to target entirely new cages based on the functionalised triamine and existing aldehyde precursors.

Regardless of the type of stable functionality used, the ability for derivatisation of the Janus cages based on the type of amine included opens countless potential structures for further study. Specific tuning of the precursors to create cages with varied functionality could impact heavily on the properties of the cage, including host-guest interactions or solubility; though of particular interest is how this may affect packing in the solid state. Alternative families of Janus cages could be developed focusing on small changes to the cage scaffold using known diamines, disrupting cage packing or causing different interactions than those seen previously. However, it would also be interesting to target a cage with a large difference in the types of functionality present on each hemisphere, e.g. ethylenediamine,[4] and crown ether-based diamines.[16] The presence of both small and extremely bulky groups on the same cage could have large implications for how the cages interact in the solid-state.

Crown ethers also have the benefit of not interpenetrating into the cavities of neighbouring cages. Of course, the difference in functionalities does not have to be so extreme, but this is an example of how interesting structures could be built using existing building blocks, potentially leading to large impacts on the function of the cages.

5.3 References

1 J. W. Wu, Y. D. Wu, J. J. Dai and H. J. Xu, *Adv. Synth. Catal.*, 2014, **356**, 2429–2436.

2 A. S. Bhat, S. M. Elbert, W.-S. Zhang, F. Rominger, M. Dieckmann, R. R. Schröder and M. Mastalerz, *Angew. Chemie Int. Ed.*, 2019, 1–6.

3 A. S. Bhat, 2021.

4 T. Tozawa, J. T. A. Jones, S. I. Swamy, S. Jiang, D. J. Adams, S. Shakespeare, R. Clowes, D. Bradshaw, T. Hasell, S. Y. Chong, C. Tang, S. Thompson, J. Parker, A. Trewin, J. Bacsa, A. M. Z. Slawin, A. Steiner and A. I. Cooper, *Nat. Mater.*, 2009, **8**, 973–978.

5 R. L. Greenaway, V. Santolini, A. Pulido, M. A. Little, B. M. Alston, M. E. Briggs, G. M. Day, A. I. Cooper and K. E. Jelfs, *Angew. Chemie*, 2019, **131**, 16421–16427.

6 M. J. Bojdys, M. E. Briggs, J. T. A. Jones, D. J. Adams, S. Y. Chong, M. Schmidtmann and A. I. Cooper, *J. Am. Chem. Soc.*, 2011, **133**, 16566–16571.

7 S. Gao, Y. Ma, W. Chen and J. Luo, *Synlett*, 2018, **29**, 2191–2194.

8 J. Larsen, K. A. Jørgensen and D. Christensen, *J. Chem. Soc. Perkin Trans. 1*, 1991, 1187–1190.

9 G. Il An, M. Kim, J. Y. Kim and H. Rhee, *Tetrahedron Lett.*, 2003, **44**, 2183–2186.

10 L. Troisis, M. M. Carrozzo, C. Citti, A. Falcicchio, R. Mansueto, F. Rosato and G. Cannazza, *Synlett*, 2013, **24**, 53–56.

11 R. L. Greenaway, V. Santolini, F. T. Szczypiński, M. J. Bennison, M. A. Little, A. Marsh, K. E. Jelfs and A. I. Cooper, *Chem. – A Eur. J.*, 2020, **26**, 3718–3722.

12 S. Jiang, J. T. A. Jones, T. Hasell, C. E. Blythe, D. J. Adams, A. Trewin and A. I. Cooper, *Nat. Commun.*, 2011, **2**, 207.

13 C. Nativi, O. Francesconi, G. Gabrielli, A. Vacca and S. Roelens, *Chem. - A Eur. J.*, 2011, **17**, 4814–4820.

14 C. Nativi, M. Cacciarini, O. Francesconi, G. Moneti and S. Roelens, *Org. Lett.*,

2007, **9**, 4685–4688.

15 A. Ardá, C. Vnturi, C. Nativi, O. Francesconi, G. Gabrielli, F. Javier Cañada, J. Jiménez-Barbero and S. Roelens, *Chem. - A Eur. J.*, 2010, **16**, 414–418.

16 N. O'Reilly, N. Giri and S. L. James, *Chem. - A Eur. J.*, 2007, **13**, 3020–3025.